UNIVERSITÉ DE STRASBOURG

ÉCOLE DOCTORALE DES SCIENCES DE LA VIE ET DE LA SANTE

Institut de génétique et de biologie moléculaire et cellulaire IGBMC

Unistra- Inserm U1258 / CNRS UMR-7104

THÈSE présentée par :

José Tomás AHUMADA SAAVEDRA

Soutenue le : **24 octobre, 2024**

Pour obtenir le grade de : **Docteur de l'Université de Strasbourg**

Discipline : Sciences de la vie et de la santé

Analyse crâniofaciale des modèles de rongeurs du syndrome de Down

THÈSE dirigée par :

[Mme BLOCH-ZUPAN Agnès] Professeur des Universités, Université de Strasbourg

RAPPORTEURS :

[Mme CHAUSSAIN Catherine] Professeur des Universités, Université Paris Cité

[Mr SANLAVILLE Damien] Professeur des Universités, Université Claude Bernard Lyon 1

EXAMINATEURS :

[Mr LAVERNY Gilles] Chargé de recherche HDR, INSERM, IGBMC, Strasbourg

---

INVITE :

[Mr HERAULT Yann] Directeur de recherche, CNRS, IGBMC, Strasbourg

UNIVERSITÉ DE STRASBOURG

DOCTORAL SCHOOL OF LIFE AND HEALTH SCIENCES

The Institute of Genetics and Molecular and Cellular Biology IGBMC

Unistra- Inserm U1258 / CNRS UMR-7104

THESIS presented by:

José Tomás AHUMADA SAAVEDRA

Defended on: **October 24th, 2024**

To obtain the grade of: **Doctor of University of Strasbourg**

Area: Life and health sciences

Specialty: Molecular and Cellular Aspects of Biology

Craniofacial analysis of Down syndrome rodent models

THESIS directed by:

[Ms. BLOCH-ZUPAN Agnès] Professor, University of Strasbourg

REPORTERS:

[Ms. CHAUSSAIN Catherine] Professor, University of Paris Cité

[Mr. SANLAVILLE Damien] Professor, University Claude Bernard Lyon 1

EXAMINERS:

[Mr. LAVERNY Gilles] Assistant Professor HDR, INSERM, IGBMC, Strasbourg

---

OTHER JURY MEMBERS:

[Mr. HERAULT Yann] Research Director, CNRS, IGBMC, Strasbourg

Remerciements

Je tiens tout d'abord à remercier les membres de mon jury, les Drs Catherine Chaussain, Damien Sanlaville et Gilles Laverny, pour avoir accepté d'évaluer mon travail de thèse.

Je remercie également les membres de mon comité de suivi de thèse, Dr Catherine Chaussain et Dr Manuel Mark, pour les bons conseils qu'ils m'ont donnés tout au long de ma thèse.

Je souhaite exprimer ma profonde reconnaissance envers mes deux co-directeurs de thèse. Je vous dois incontestablement la réussite de ce projet, votre soutien et vos lumières m'ont permis d'avancer et a grandement contribué à mon épanouissement scientifique.

Pr Agnès Bloch-Zupan, merci de m'avoir donné une si belle opportunité, de m'avoir accompagné depuis mon arrivée à Strasbourg et de m'avoir fait confiance sur ce projet. Vos précieux conseils et tout le savoir que vous m'avez transmis m'ont beaucoup apporté, tant sur le plan scientifique que sur le plan humain. Grâce à vous, j'ai également eu la chance de rencontrer des grandes personnes du monde de la recherche. Merci pour votre sympathie et votre écoute, toutes les discussions enrichissantes que nous avons partagées m'ont fait évoluer.

Dr Yann Herault, merci de m'avoir donné la chance d'intégrer cette équipe, ce qui m'a permis de réaliser ce travail dans les meilleures conditions possibles. Votre encadrement et vos enseignements au cours des dernières années m'ont permis d'apprendre beaucoup, notamment à toujours aller plus loin dans mon raisonnement scientifique. Vous m'avez transmis tous les outils théoriques nécessaires à l'accomplissement de mon projet, ainsi qu'à l'évolution de mon travail et de ma démarche scientifique tout au long de ces années.

Je remercie tous les membres actuels et passés de l'équipe « Hérault » que j'ai croisé pendant ces 4 années et même un peu plus.

Claire, j'espère que toutes les personnes qui croiseront ton chemin professionnel se rendront compte de la chance qu'ils ont. Pour ma part c'est chose faite, et au-delà du fait que tu m'aies accompagné tout au long de ma thèse par ton expertise en gestion de lignées, ta bonne humeur apporte une réelle joie de vivre au sein du labo. C'était un véritable plaisir.

Arnaud, Véronique, Elodie et Michel, piliers de cette équipe, vous êtes toujours disponibles et à l'écoute lorsque nous avons besoin d'un conseil, un grand merci.

Marion, c'est toute une aventure de travailler avec les rats et je te remercie mille fois pour tout ce que tu as apporté à ce projet.

JB, Jérémy and Eve, compagnons de galère, je vous suis reconnaissant d'avoir égayé mes journées et vous souhaite tout le meilleur pour la suite de votre brillante carrière de jeunes chercheurs.

Victorine, c'est un plaisir d'avoir pu partager la dernière étape de mon doctorat avec toi. Merci beaucoup pour ton aide désintéressée, qui est très appréciée dans les moments difficiles.

J'ai une pensée particulière pour Pauline, avec qui j'ai passé de supers moments. Merci beaucoup de partager votre humour avec moi, qui m'ont toujours fait beaucoup rire. Surtout ne changes pour rien au monde.

Alexandra, je profite de ces quelques lignes pour t'adresser toute ma gratitude pour l'amitié que nous partageons depuis toutes ces années. Même si un simple merci ne me semble pas suffisant, saches que ta gentillesse, ta bienveillance et ton soutien sans faille sont un réel apaisement pour moi.

Je tiens à remercier l'ensemble des personnes travaillant sur les plateformes de l'IGBMC avec qui j'ai travaillé de près ou de loin.

Merci à Sophie et toutes les personnes qui m'ont accompagné au cours de ces 4 dernières années pour avoir pris soin de mes souris. Merci à Pauline et Loïc pour vos conseils et votre aide lors de mes innombrables ddPCR. Merci David pour ton expertise en Micro-CT qui m'a permis d'obtenir de si jolis résultats. Merci à tous les membres de la zone phénotypage de l'ICS, en particulier Chaouki. Merci à toute l'équipe de microscopie photonique pour votre amour du travail bien fait.

Un merci tout particulier au soutien financier de l'Agence Nationale pour la Recherche et le Développement (ANID, programme de bourses : Doctorado Becas Chile) qui m'a permis de venir étudier en France et de franchir cette nouvelle étape qu'est le doctorat.

Merci à Dr Maria Angelica Torres de la faculté de chirurgie dentaire de l'Université du Chili, pour m'avoir donné l'opportunité de commencer ma carrière dans la recherche et l'enseignement. Pour votre accompagnement lors de cette belle aventure, même à distance.

Ainsi que toutes les personnes qui m'ont permis d'avoir une vie à côté de ma thèse ici à Strasbourg. Josefina, merci pour votre soutien inconditionnel pendant toutes ces années. Levi, Burton, Ivan et Joshua pour votre amitié même si je n'étais pas toujours disponible. À Valentyna, pour son soutien inestimable et vitale au cours des ces derniers mois. Sans oublier mes amis qui sont éparpillés aux quatre coins du globe, Leonardo, Ignacio et Cristobal. Merci.

J'aimerais terminer par remercier ma famille, à mes parents qui m'ont toujours soutenu et encouragé malgré les 12 000 km qui nous séparent, et mon frère Juan Pablo, qui avait toujours un mot d'encouragement pour moi. Sans vous, cela n'aurait pas été possible.

Acknowledgements

First, I would like to thank the members of my jury, Dr Catherine Chaussain, Dr Damien Sanlaville and Dr Gilles Laverny, for agreeing to assess my thesis work.

I would also like to thank the members of my thesis monitoring committee, Dr Catherine Chaussain and Dr Manuel Mark, for the good advice they gave me throughout my thesis.

I would like to express my deepest gratitude to my two thesis co-directors. I undoubtedly owe the success of this project to you; your support and guidance have enabled me to move forward and greatly contributed to my scientific development.

Prof. Agnès Bloch-Zupan, thank you for giving me such a wonderful opportunity, for accompanying me since my arrival in Strasbourg and for trusting me with this project. Your invaluable advice and all the knowledge you have passed on to me have given me a great deal, both scientifically and on a human level. Thanks to you, I have also had the chance to meet some great people from of the research environment. Thank you for your sympathy and your listening skills. All the enriching discussions we have shared have helped me to evolve.

Dr. Yann Herault, thank you for giving me the chance to join this team, which enabled me to carry out this work in the best possible conditions. Your guidance and teaching over the last few years been invaluable and help me in particular to go always further in my scientific reasoning. You have given me all the theoretical tools I needed to complete my project, and to develop my work and my scientific approach over the years.

I would like to thank all past and present members of the « Hérault » team whom I have met over the past 4 years and more.

Claire, I hope that everyone who crosses your professional path realizes how lucky they are. For me, it is a done deal, and over and above the fact that you accompanied me throughout my thesis with your expertise in lineage management, your good humor brought real joie de vivre to the lab. It was a real pleasure.

Arnaud, Véronique, Elodie and Michel, the pillars of this team, you are always available and ready to listen when we need advice, thank you.

Marion, it has been quite an adventure working with the rats, and I would like to thank you a thousand times over for everything you have contributed to this project.

JB, Jérémy and Eve, galley-mates, I am grateful to you for brightening up my days and wish you all the best for the rest of your brilliant careers as young researchers.

Victorine, it has been a pleasure to share the final stage of my PhD. Thank you so much for your selfless help, which is much appreciated in difficult times.

I have a special thought for Pauline, with whom I have had some great times. Thank you so much for sharing your humor with me, which always made me laugh a lot. Never change.

Alexandra, I would like to take this opportunity to express my gratitude for the friendship we have shared over the years. Even if a simple thank you does not seem enough, please know that your kindness, caring and unfailing support are a real comfort to me.

I would like to thank all the people working on the IGBMC platforms with whom I have worked in one way or another.

Thanks to Sophie and all the people who have worked with her over the last 4 years, for taking such good care of my mice. Thanks to Pauline and Loïc for your advice and help with my countless ddPCRs. Thanks to David for your expertise in Micro-CT, which enabled me to obtain such beautiful results. Thanks to all the members of the ICS phenotyping zone, especially Chaouki. Thank you to the entire photonic microscopy team for your love of a job well done.

Special thanks to the financial support of the National Agency for Research and Development (ANID, Doctorado Becas Chile scholarship program), which enabled me to come and study in France and take the next step towards a doctorate.

Thank you to Dr Maria Angelica Torres of the Faculty of Dental Surgery at the University of Chile, for giving me the opportunity to begin my career in research and teaching. For your support during this wonderful adventure, even from a distance.

I extend my gratitude to everyone who has made it possible for me to balance my life in Strasbourg with my thesis. Josefina, thank you for your unconditional support over all these years. Levi, Burton, Ivan and Joshua for your friendship even when I wasn't always available. To

Valentyna, for her invaluable and vital support over the last few months. Of course, without forgetting my friends scattered all over the world, Leonardo, Ignacio and Cristobal. Thank you.

Finally, I would like to thank my family: my parents, who have always supported and encouraged me despite the 12,000 km that separated us, and my brother Juan Pablo, who always had a word of encouragement for me. Without you, this would not have been possible.

Table of contents

List of Figures

Introduction

This doctoral thesis will first present the context of Down syndrome (DS) and its clinical features. It will then examine the characteristic craniofacial phenotype of DS patients and the main murine models, followed by a methodology to study the genes and molecular mechanism underlying this specific phenotype.

1. Down syndrome

1.2. Genetic origin

Down syndrome (DS) is the most common chromosomal disorder and the primary cause of intellectual disability worldwide (Down 1995). In most of the cases, it is due to the presence of a third human chromosome 21 (HSA21). The genetics can be divided in 3 principal types (Figure 1):

- Complete trisomy: This condition occurs in 95% of cases. In this form, an additional complete chromosome 21 (HSA21) is present, and the karyotype has 47 chromosomes. This trisomy affects all cells in the body (Lejeune, Gautier, et Turpin 1959).
- Translocated trisomy: Corresponds to the fusion of two acrocentric chromosomes. This form of trisomy is present in 3 to 5% of DS carriers. In this case, a supernumerary copy of chromosome 21 fuses with another chromosome, usually acrocentric, such as chromosome 14 (Plaiasu 2017).
- Mosaic trisomy impacts 1 to 2% of cases of DS. In this case, the cells are separated into two populations: one that is euploid and the other that has three copies of HSA21. Here, the tissue location of the trisomic cells and the mosaicism percentage determine the clinical characteristics of the trisomy carrier (Plaiasu 2017).

The inability of chromosomes to separate during cell division (non-disjunction) is the root cause of DS, happening during meiosis I or II. If the non-disjunction takes place during meiosis I, the repercussions will be more severe, all the daughter cells in this instance are aneuploid. Additionally, non-disjunction can also occur during mitosis after zygote formation (Antonarakis

et al. 1992). Recently, differences in centromere structure have been hypothesized to play an important role in role in chromosome nondisjunction. Centromeres play an essential role for accurate chromosome segregation during meiosis by promoting the segregation of homologous chromosomes and sister chromatids. In a recent report it was found that DS individuals have shorter chromosome 21 (chr21) centromeres (possibly because of reduced size of the centromeric α-satellite higher-order repeat array) (Mastrorosa et al. 2024).

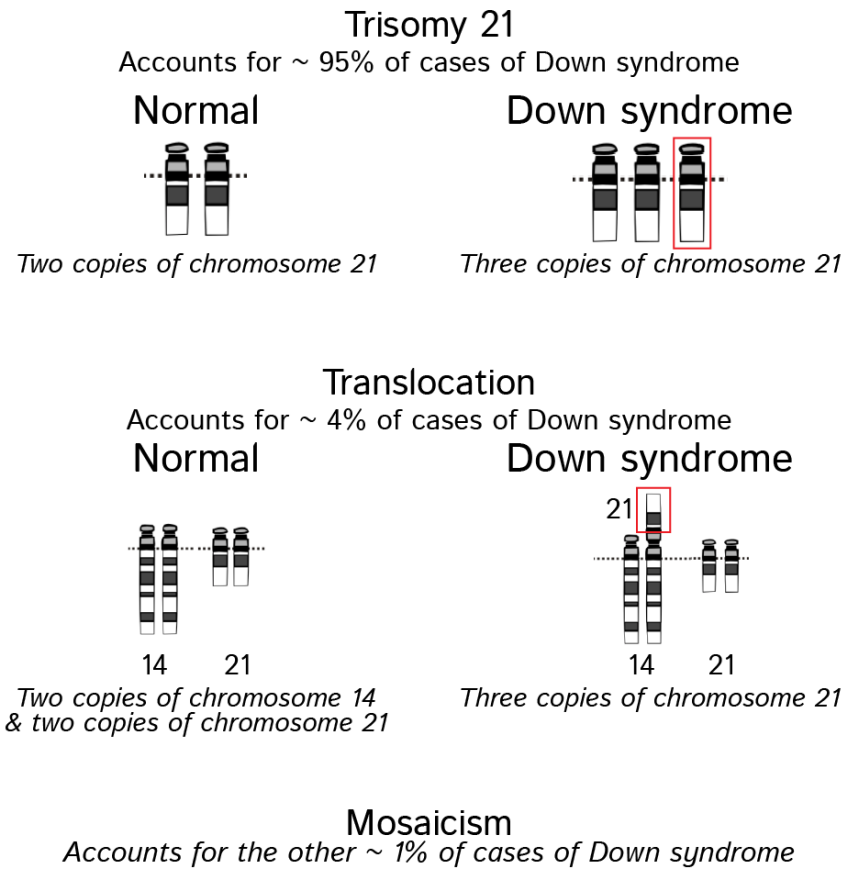

Figure 1. Karyotype for Down syndrome. Complete trisomy, Translocation (Robertsonian 14/21 translocation. The long arm of supernumerary chromosome 21 (21q) is fused to the short arm of chromosome) and Mosaicism. Image modified from the Human Genome Project (Hattori et al. 2000).

1.2. Diagnosis

The diagnosis is clinical either during pregnancy or at birth (American College of Obstetricians and Gynecologists' Committee on Practice Bulletins—Obstetrics, Committee on Genetics, et Society for Maternal-Fetal Medicine 2020).

The prenatal Screening for DS is compound of a blood test looking for serum markers, including free beta–human chorionic gonadotropin (hCG) and pregnancy-associated plasma protein A, collected with a capillary blood sample between 9 and 13 weeks 6 days' gestation (Carlson et Vora 2017). In addition, an ultrasound test (measurement of nuchal translucency) during the first trimester of pregnancy is performed, between 10 and 13 weeks 6 days' gestation. A nuchal translucency of greater than 3 mm is significantly associated with both aneuploidy and structural malformations. 35% of patients with a nuchal translucency measurement greater than 3 mm subsequently had confirmed aneuploidy (Nicolaides et al. 1992; Hyett et al. 1997).

Besides, a combined test (sometimes called an integrated test) is carried out. This approach uses both a blood test and an ultrasound during the first trimester, as well as a second-trimester blood test. Therefore, the health care provider can set up a DS risk rating (Driscoll et Gross 2009).

If the prenatal screening test suggests the likelihood of DS, a diagnostic test can be performed. Diagnostic testing for DS involves removing a sample of genetic material, in this case it would be possible to perform either an amniocentesis, where a sample of amniotic fluid is taken. Chorionic villus sampling in which a sample of cells from the placenta and percutaneous umbilical blood sampling, that use a sample of fetal blood in the umbilical cord through the uterus. All these tests are searching for an extra chromosome and present a risk for the fetus (Carlson et Vora 2017). On the other hand, it is possible to use a non-invasive procedure to analyze the plasma cell-free fetal DNA. This involves extracting fetal cells from the mother's peripheral blood and rare fetal cells from exfoliated cells. The utilization of placental cells circulating in maternal blood for DNA fragment diagnosis technologies has gained widespread acceptance in clinical settings for the detection of common chromosomal aneuploidy (Tang et al. 2022).

Finally, a diagnosis after birth can be done, that is often based initially on physical signs of the syndrome. However, because some individuals with DS may not have these symptoms, a blood sample is taken to confirm the diagnosis. The blood sample is analyzed to confirm by genetic approach (karyotype, sequencing…) the presence of an extra chromosome 21 (Hall 1966).

1.3. Prevalence

The actual prevalence is one out of every 1000 births worldwide. In France, at the end of 2017, the total number of people carrying DS would therefore be between 38,700 and 49,100, giving a prevalence in the total population of 5.5/10,000. (« European Platform on Rare Disease Registration », s. d.). Now in France DS is considered as a rare disease. A disease is defined as rare when it affects less than one in 2,000 people (« Rare Diseases - European Commission » 2024).

The prevalence is also affected by the rise in average maternal age over time that has brought an increase in the number of pregnancies affected by DS. Nonetheless, the growing incidence of prenatal screening and pregnancy termination has generally offset the impact of maternal age and produced a comparatively constant live birth prevalence (Loane et al. 2013) (Figure 2).

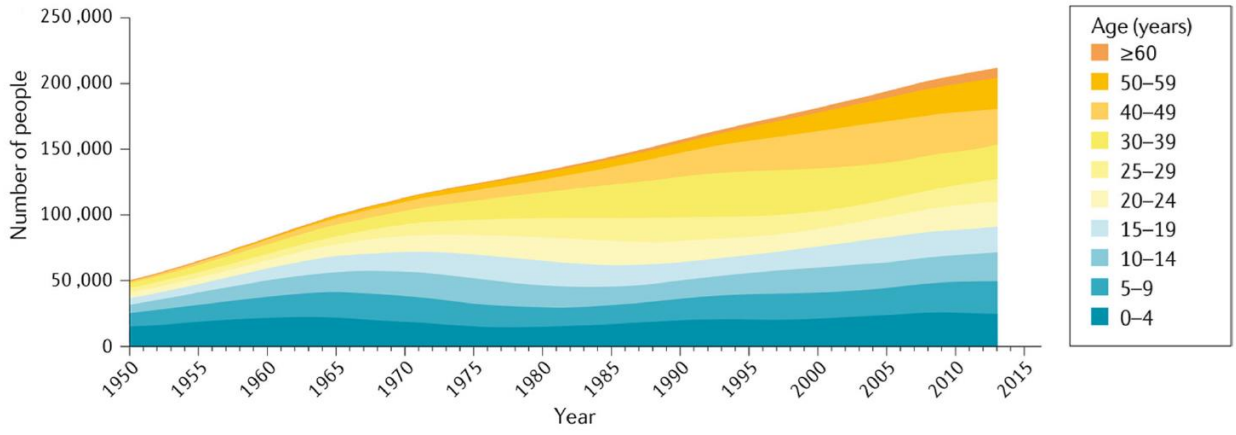

Figure 2. Down syndrome prevalence in US between 1950 and 2023. (Antonarakis et al. 2020).

2. Down syndrome clinical presentation beyond craniofacial changes

The clinical features of DS are complex and variable. Not all alterations are present in the same manner in each affected individual (Hall 1966). These features occur in different degree in every individual with trisomy 21, including craniofacial (CF) dysmorphology, intellectual disability, hypotonia. CF is very frequent with 75% of individuals showing brachycephaly or 60% with epicanthic fold. Some individuals also present congenital heart disease (40%), and higher probability of having leukemia (10-20%) compared to the general population (Antonarakis et al. 2004). Below I will present the two main features and the comorbidities associated with DS. I will present separately the CF features in a dedicated paragraph.

2.1. Intellectual deficiency

Intellectual disability is recognized as the most important feature of DS (Vicari 2006). It is defined as a developmental disability that begins during childhood and is characterized by significant impairment of intellectual functioning and adaptive skills, which causes major limitations to living a normal, independent life (Dierssen, Herault, et Estivill 2009).

When it comes to clinical practice, an intelligence coefficient (IQ) of less than 70 is considered limited in intellectual functioning. The severity of the cognitive impairment and the appearance of other (noncognitive) symptoms vary greatly amongst people with Down syndrome. People with DS often have an IQ between 25 and 55, which is in the severely to moderately retarded range (Vicari et al. 2004; Rueda, Flórez, et Martínez-Cué 2008).

The genetic complexity of Down syndrome accounts for the majority of the IQ variability, and other factors, such as the child's surroundings and the degree of stimulation received from others around him, may also play a role. Furthermore, research on the cognitive deficiencies experienced by DS carriers has shown that as their development advances, their IQ scores decrease. In fact, the average IQ of children with T21 is between 45 and 71, while that of

adolescents and young adults is between 28 and 47, indicating a decrease in IQ with age (Vicari et al. 2004).

A stable set of morphogenetic and functional central nervous system manifestations, including neurological or psychiatric illnesses and brain deformities, are linked to the intellectual disability in DS. Despite being widely utilized, the IQ test lacks specificity and therefore cannot be used to establish a genotype/phenotype correlation. It is important to establish precise diagnostic criteria and use a battery of evaluative tools to record various cognitive abilities such as verbal fluency, abstract reasoning, short- and long-term memory, skill learning, among others (Dierssen, Herault, et Estivill 2009).

Adults with DS present psychiatric disorders as depressive disorder or aggressive behavior (25.6%), which further complicates the situation. Individuals with DS may also have disruptive behavior, attention deficit, hyperactivity disorder (6.1%), conduct/oppositional disorder (5.4%), or aggressive behavior (6.5%) (Roizen et Patterson 2003).

In addition, children with Down syndrome exhibit a significant delay in their developmental skills when compared to other children developing (van Gameren-Oosterom et al. 2011) such as learning to walk, grasping objects or even language skills due to difficulties in articulating the jaw (Melyn et White 1973). The brain's anatomical differences, such as the shrinkage of the cerebellum, frontal lobes, parietal lobes, corpus callosum, and hippocampus, as well as a delay in central and peripheral neuronal myelination, can account for the delay (Alesi et al. 2018).

2.2. Muscular hypotonia

Many deficits, including hypotonia, ligament laxity, decreased muscle strength, insufficient muscular co-contraction, poor postural control, and disrupted proprioception, are found in individuals with Down syndrome. Additionally, DS individuals exhibit balance dysfunctions (Jain et al. 2022).

Hypotonia is caused by tendon laxity affecting the stability of the joint (Malak et al. 2015; Schott, Holfelder, et Mousouli 2014). Besides, insufficient bone density, hypoplasia of cartilage,

failure in sensory integration processes, and muscle weakness cause incorrect muscle contraction (Malak et al. 2015).

Children and adolescents with Down syndrome experience a variety of neuromuscular and musculoskeletal abnormalities as a result of these anatomical modifications (Malak et al. 2015).

2.3. Comorbidities associated with Down syndrome

DS individuals health is associated with different comorbidities as congenital heart defects, gastrointestinal problems, endocrine disorders (hypothyroidism), higher risk for infections, cancer, and obstructive sleep apnea between others (Startin et al. 2020). But also, DS is associated with increased risk for other neurodevelopmental conditions including autism and attention deficit hyperactivity disorder (ADHD) (Naerland et al. 2017).

2.3.1. Congenital Cardiac Defects (CHD)

Congenital cardiac defects are by far the most common and leading cause associated with morbidity and mortality in patients with Down syndrome, especially in the first 2 years of life (Benhaourech, Drighil, et Hammiri 2016). Septal defects are the most prevalent, with atrial septal abnormalities accounting for 32.5% of cases, ventricular septal defects accounting for 20.6% of cases, and atrioventricular septal defects accounting for 17.4% of cases (Heinke et al. 2021).

It is advisable to undergo a fetal echocardiography examination throughout pregnancy. A postnatal cardiology examination should also be conducted, followed by an echocardiography examination within the first month following birth. The management of these defects, including surgical repair, is similar for DS children and the general population. The postoperative mortality rate in children with Down syndrome is comparable to or lower than in the whole population. It is recommended that all individuals with Down syndrome have annual screening throughout their lifetime to detect any evidence of acquired valve disease and heart failure (Antonarakis et al. 2020).

2.3.2. Gastrointestinal abnormalities

Gastrointestinal abnormalities occur in approximately 4 to 10% of individuals (Malt et al. 2013). In longitudinal research spanning 10 years, it was shown that 50.7% of the participants exhibited gastrointestinal issues. The predominant disorders observed were chronic intestinal constipation (49%), intestinal parasites (giardiasis, ascariasis, or enterobiasis—22%), and gastroesophageal reflux disease (14%). 5% of individuals experienced a deformity in their digestive tract (Bermudez et al. 2019).

In a recent systematic study found that DS is connected with a range of prevalence rates of obesity, ranging from 23% to 70%. Possible factors contributing to obesity, along with being shorter in height, included elevated levels of circulating leptin (indicating leptin resistance), decreased expression of adiponectin, following an unhealthy diet, having other medical conditions, experiencing difficulty with walking, and having a lower resting energy expenditure due to poor fitness and low levels of physical activity (Bertapelli et al. 2016).

2.3.3. Immune system-related diseases

DS is commonly linked to immunological dysfunction (Cruz et al. 2009). The presence of these issues in DS patients leads to a reduction in life expectancy due to elevated rates of infections, hematological malignancies, and autoimmunity. Various modifications to the inherent and acquired immune response elements have been proposed as potential explanations for the reported susceptibility of individuals with Down syndrome to autoimmune disorders (Ferrari et Stagi 2021).

Malfunctions are detected in the process of distinguishing B cells, resulting in a notable reduction of switched memory B cells. Dysregulated T cell function, impaired T cell maturation, and abnormal proliferation of memory T cells exist. It has been shown that individuals with DS have CD8+ T cells that produce excessive amounts of cytokines associated with autoimmunity, while their CD4+ T cells have a biased state towards increased production of IL-17A (Araya et al. 2019).

Defects in the Toll-like receptors (TLRs) and interferon (IFN) activity are found. These are important not only for defending against infections but also for preventing damage caused by excessive cytokine production and the resulting autoimmunity. Cytokines may contribute to the harmful effects of inflammation by increasing the levels of both pro-inflammatory (IL-2, IL-1, IL-6, TNF-) and anti-inflammatory cytokines (IL-10, IFN-) at the initial stage and after stimulation (Mattos et al. 2018; Huggard, Doherty, et Molloy 2020).

2.3.4. Sleep Apnea

The occurrence of obstructive sleep apnea is widespread in patients with DS, with an estimated prevalence ranging from 54% to 90%. It is important to do symptom screening at every health check. These symptoms include loud snoring, heavy breathing, restless nights, daytime sleepiness, as well as neurocognitive symptoms like irritability, melancholy, paranoia, cognitive impairment, and behavioral problems (Antonarakis et al. 2020).

Sleep apnea has been attributed to the skeletal and soft-tissue structural alterations that are characteristic of the DS phenotype, predisposing patients with this condition to sleep-disordered breathing and airway obstruction. The particular modifications include adenotonsillar hyperplasia, midfacial and mandibular hypoplasia, hypotonia, macroglossia, choanal atresia, an acute cranial base angle, and tiny upper airways (de Miguel-Díez, Villa-Asensi, et Alvarez-Sala 2003; Goffinski et al. 2015; Ng et al. 2006).

It is advisable to do overnight polysomnography for all children with DS who are under the age of 4, irrespective of any symptoms they may have (Esbensen et al. 2018). Other methods, such as home oximetry, have been proposed to identify persons at risk and decrease the number of children needing comprehensive diagnostic studies. Treatment options for sleep apnea encompass the utilization of continuous positive airway pressure (CPAP), mandibular advancement devices, and weight reduction. While surgical procedures such as tonsillectomy and adenoidectomy can be considered, it is important to note that sleep apnea may still continue even after the surgery (Churchill et al. 2012).

2.3.5. Cancer

While the overall occurrence of cancer is similar between the DS population and the general population, individuals with DS have a lower likelihood of developing solid tumors and a higher likelihood of developing hematological malignancies, specifically acute leukemia. Due to this factor, children with Down syndrome have a notably higher likelihood of acquiring acute leukemia compared to those who do not have DS (Henrik Hasle et al. 2016; H. Hasle, Clemmensen, et Mikkelsen 2000). The cumulative risk of leukemia in children with DS is 2% by 5 years of age and 2.5% by 30 years of age. Leukemia represents 96% of all malignancies, whereas in the general population it is 34% (Baruchel et al. 2023).

2.3.6. Alzheimer's disease

One notable characteristic of DS is an increased risk of developing Alzheimer's disease (AD) between 45 and 65 years of age. Trisomy of chromosome 21, when it occurs in all cells, consistently leads to the formation of amyloid plaques and neurofibrillary tangles in the brain, which are common features of Alzheimer's disease pathology. This often happens by the age of 40, and around two-thirds of people with Down syndrome experience dementia by the age of 60 (Wiseman et al. 2015). Nevertheless, the occurrence of dementia does not reach a 100% incidence, even among older adults, indicating that certain individuals with DS are shielded from the development of AD.

APP, responsible gene for producing amyloid precursor protein is believed to play a crucial role in the development of AD. The presence of an extra copy of the APP may contribute to the progression of AD in individuals with DS by elevating the levels of amyloid-β (Aβ), a protein fragment derived from APP that abnormally folds and builds up in the brain of AD patients (Wiseman et al. 2015).

2.4. Physical Dysmorphisms

Individuals with DS exhibit distinct physical characteristics as a flattened face, especially the bridge of the nose, up slanting almond-shaped eyes, a tongue that tends to stick out of the

mouth, a short neck, small ears, hands, and feet, a single line across the palm of the hand (palmar crease), small pinky fingers, poor muscle tone or loose joints and shorter-than-average height (CDC 2024). Besides, defects in the atlantoaxial joint, which is located between the first and the second vertebrae, are deleted in about 20% of individuals (Alvarez et Rubin 1986)

3. Craniofacial Dysmorphism in Down syndrome

Craniofacial (CF) dysmorphic features are distinctive in individuals with DS (Kisling 1966) although their severity varies from individual to individual (Roper et Reeves 2006). Facial features associated with DS can include epicanthic folds, oblique palpebral fissures, a flattened nasal bridge, an upwardly turned nose, reduced size of the lower and upper jaw, a midface retrusion (hypoplasia), impaired growth of the skull and face, a relatively short face, a tendency to keep the mouth open which may result in a protruding tongue, and various other anatomical alterations (Pueschel 2001). While the face is affected in all people with DS, the degree of anatomical change in craniofacial osseous and soft-tissue induced by trisomy 21 during morphogenesis and subsequent growth varies on a person by person basis (Alio, Lorenzo, et Iglesias 2008).

It is important to understand that those facial features correspond to the expression of the changes in the osseous structure. An overall reduction in head dimensions (microcephaly), brachycephaly (relatively wide neurocranium), small midface, reduced mediolaterally orbital region, reduced bizygomatic breadth, small maxilla, small mandible and increased individual variability are seen (Fink, Madaus, et Walker 1975; Farkas, Kolar, et Munro 1985; Allanson 1993; Frostad, Cleall, et Melosky 1971; Farkas, Posnick, et Hreczko 1991; Richtsmeier, Baxter, et Reeves 2000). Moreover, individuals experience a low bone mass associated with reduced osteoblast activity and bone turnover (McKelvey et al. 2013) (Figure 3).

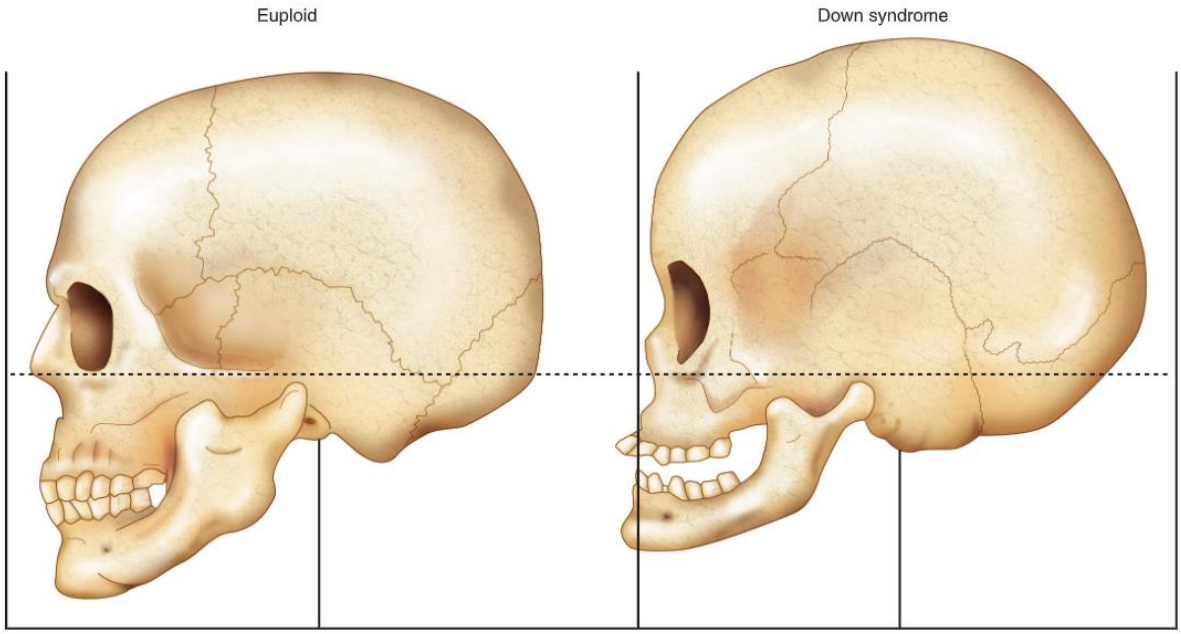

Figure 3. Craniofacial dysmorphism in Down syndrome. Left euploid skull. Right Skull of DS individual, it is possible to observe the characteristic microcephaly and brachycephaly. (Dierssen, Herault, et Estivill 2009).

Initial studies on craniofacial morphology and variability in persons with DS relied on two-dimensional analyses using lateral or frontal cephalograms, which were insufficient in capturing the full range of variation and surface topography in three dimensions. (Frostad, Cleall, et Melosky 1971; Kisling 1966; O'Riordan et Walker 1978). Qualitative labels are useful for identifying and grouping facial features of individuals with DS, but such labels may be poorly defined and are operator dependent. These factors may influence data collection and analysis and could potentially obscure true patterns of anatomical changes associated with DS and their impact on morphogenesis and growth. Several studies aiming to determine the variation in individuals with DS have only utilized a limited number of basic assessments related to the palate, teeth, and dermatoglyphics (Shapiro 1975; Shapiro et al. 1967).

CF cephalometric studies (Figure 4) analyzed different mean dimensions in the CF structure of DS individuals. In the case of the cranial base length, measuring the mean distances between Sella, Nasion and Basion points, it was found that anterior cranial base length was significantly shorter in DS subjects than among control subjects (Jesuino et Valladares-Neto 2013), same

finding for posterior cranial base (Latham 1972); giving in conclusion that the total cranial base length is significantly smaller than in the general population. Upon evaluation of the cranial base angle, it was observed that DS participants exhibited a considerably greater angle compared to the control subjects. In addition, radiographic data of persons with Down syndrome reveals a delay in the fusing of the intra-sphenoidal synchondrosis, which is crucial for the flattening mechanism of the cranial base. The synchondrosis does not fuse until the age of 7, but in the average population, it is completely obliterated by the end of the first year of life (Michejda et Menolascino 1975).

The anteroposterior position of the maxilla to the cranial base, is also significantly shorter in individuals with DS (Jesuino et Valladares-Neto 2013) and the maxillary length was found significantly smaller in DS than control groups, corroborating the existence of maxillary hypoplasia in the sagittal plane (Alio, Lorenzo, et Iglesias 2008). A review of 2020, where seven studies using craniofacial cephalometric were analyzed, shows that the anterior and posterior face height were significantly smaller among individuals with DS. The maxillary hypoplasia in the vertical plane is fundamental for the deficiency in the midface region (Vicente et al. 2020). The mandible in DS individuals is significantly smaller than that of the control subjects at all ages (Fink, Madaus, et Walker 1975; Allanson 1993). In addition, in terms of growth, the maxillary bone has reduced growth in comparison to the mandible (Fink, Madaus, et Walker 1975).

Brachycephaly is found in almost 90% of individuals with DS (Shukla et al. 2014). Brachycephaly results in an abnormally broad head with a high forehead. It occurs when the right and left coronal sutures close prematurely and is often associated with other craniofacial abnormalities. However, the skull grows nearly to the same size as the general adult population (Dierssen, Herault, et Estivill 2009).

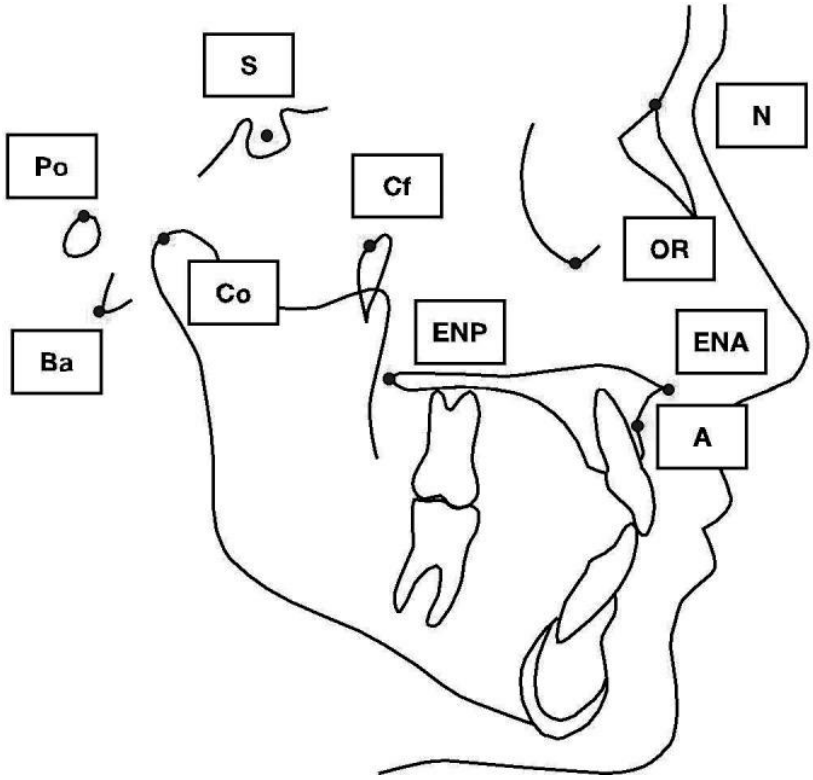

Figure 4. Cephalometry traced with a computerized analysis. Scheme of a lateral cranium radiography traced with the following cephalometric landmarks S (sella), N (nasion), Ba (basion), ANS (anterior nasal spine), PNS (posterior nasal spine), point A, Po (porion), Or (suborbital), CC (pterygomaxillare), and Co (condylion) (Alio, Lorenzo, et Iglesias 2008).

To gain a more comprehensive understanding of craniofacial characteristics related to DS, researchers have begun developing three-dimensional analysis methods. While radiographs can only assess the skeletal structure, anthropometry enables a 3D analysis of the entire craniofacial arrangement without subjecting the individual to potentially harmful procedures (Farkas et al. 2001; Farkas, Katic, et Forrest 2002b; 2002a). Two quantitative noninvasive methods started to be used, collecting soft tissue facial data in three dimensions: conventional anthropometry and digital computerized anthropometry (Allanson 1993; Farkas et al. 2001; Farkas, Katic, et Forrest 2002b; 2002a).

Some of the first quantitative studies performed with conventional anthropometry have analyzed facial dimensions and ratios in North American whites (Farkas, Katic, et Forrest 2002b; Farkas et al. 2001; Farkas, Katic, et Forrest 2002a) and Croatian subjects (Bagić et Verzak 2003)

with Down syndrome, providing a detailed description of the abnormal morphology. The recent discoveries were consistent with the findings documented in previous literature: an underdeveloped middle third of the face with a decreased projection of the nose (resulting in a flatter facial contour in both the horizontal and sagittal planes), and a diminished mandibular area (including a decrease in the angles formed by the soft tissues on both sides of the jaw) (Farkas, Katic, et Forrest 2002a; 2002b; Farkas et al. 2001; Bagić et Verzak 2003; J. T. Richtsmeier, Baxter, et Reeves 2000; Ferrario et al. 2004).

Another initial digital anthropometry study was performed in a group of Italian subjects with DS, and the areas and volumes of several facial structures (nose, lips, eyes, ears) were analyzed (Ferrario et al. 2004). In 2005, the same team (with Italian subjects with DS), using digitalized soft tissue facial landmarks, found smaller facial size and mean z-scores falling outside the normal interval when compared to “normal” sex-, ethnic-, and age-matched controls (Sforza et al. 2005).

At present, the most reliable analysis corresponds to a morphometrics approach, with the quantification and statistical analysis of form in three dimensions (Hallgrimsson et al. 2015). A team in USA (Khurana et al. 2024) utilized Cone Beam Computed Tomography (CBCT) to examine the dental and craniofacial morphology of six individuals with DS (Figure 5). This investigation identified prognathic maxilla in five individuals, prognathic mandible in four patients, and bimaxillary protrusion in two patients, contrasted results with previous reports where retrognathic maxilla, prognathic mandible, and bimaxillary protrusion was found (Korayem et AlKofide 2014). The dental examination revealed the presence of microdontia, enamel hypoplasia, and congenitally missing teeth, with the maxillary and mandibular third molars being the most frequently absent. Additionally, sinus abnormalities, delayed suture closure, and cervical spine deformities were noted. These findings enhance our comprehension of craniofacial traits associated with Down syndrome and align with earlier research. However, it is important to note that studies of this nature involving humans are severely restricted (Khurana et al. 2024).

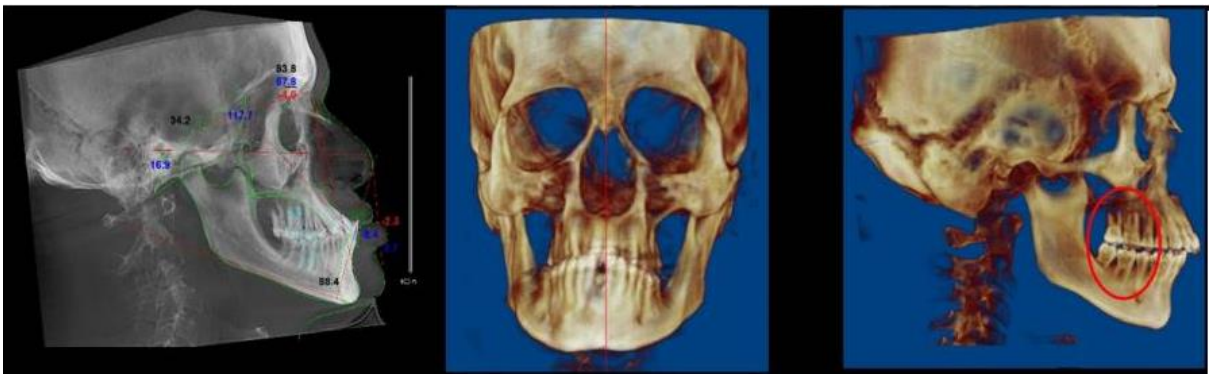

Figure 5. Cone Beam Computed Tomography of a Down syndrome individual. On the Left, lateral cephalometric analysis shows hypodivergent face type, hypoplastic maxilla, proclined anterior teeth, and anterior crossbite. In the middle, a 3D frontal volumetric rendering view shows facial asymmetry; On the right side, a 3D lateral volumetric rendering view shows Class II skeletal pattern (prognathic maxilla and orthognathic mandible) Molar class II full step (red circle) (Khurana et al. 2024).

4. Oral anomalies

DS individuals present several dentofacial anomalies, as fissured tongue, macroglossia, ankyloglossia, angular cheilitis, high arched palate, lack of lip seal, malocclusion, crossbite, open bite, crowding of anterior teeth and many dental anomalies (delayed eruption, microdontia, fractured teeth, retained deciduous teeth, congenitally missing teeth).

4.1. Soft tissues disorders

The most common oral anomaly seen in the individuals with DS is the fissured tongue followed by macroglossia (Bhowate et Dubey 2005). Most of the patients with fissured tongues presented multiple fissures and various fissure patterns on the dorsal surface of the anterior two-thirds of the tongue. The cause of the fissured tongue is possibly developmental (Shukla et al. 2014) and is not associated with sex. The dorsal surface of the tongue, in most cases, was dry because of mouth breathing. The macroglossia in Down syndrome individuals can be defined as a "relative" macroglossia because the tongue that is large relative to the bony elements of the oral cavity but with an absolute volume not greater than that of the normal tongue (Guimaraes et al. 2008). A few individuals also presented with scalloped margins and

imprints of teeth due to abnormal pressure of the enlarged tongue on the teeth (Shukla et al. 2014).

Angular cheilitis and lack of lip seal is also present in DS individuals, this can be the result of the hypotonia of the orbicularis, zygomatic, masseter, and temporalis muscles that leads to mouth breathing and drooling (Wilson 1994).

The high prevalence of high arched palate in this study could be due to midface hypoplasia resulting in a reduction of the length, height, and depth of the palate (Klingel et al. 2017).

4.2. Occlusal disorders

The occlusion, in most cases, corresponds to a class III with prognathy and inverse occlusion (anterior and posterior) (Hennequin, Faulks, et Veyrune 2000). In a study from India, individuals with Down syndrome showed a 93% incidence of definitive malocclusion, primarily of Angle Class III malocclusion (V. Macho et al. 2014). This could be attributed to the underdevelopment of the midface bones, causing a shortened palate in the anteroposterior dimension (Alió et al. 2011). The most frequent occlusal abnormalities stem from variations in vertical and transversal dimensions (anterior open bite, posterior crossbite and reductions in the maxillary arch) (Faulks et al. 2008; Bauer et al. 2012).

Crossbite was found with a prevalence of 31-33% in a group of DS children (Oliveira et al. 2008). Anterior crossbite is primarily attributed to the anteroposterior deficiency of the maxillary arch development, resulting in a crossbite of the mandible, projecting the jawbone arch towards the front of the maxilla (Soares et al. 2009). Anterior open bite is a common occurrence in individuals with Down syndrome. The oral and facial musculature, specifically the tongue and lips, exhibit hypotonia. Tongue thrust and posture may impede proper tooth eruption, leading to an anterior open bite and affecting the form of the dental arch and tooth positioning. Typically, these children exhibit an elevated palate, enlarged tonsils, reduced muscle tone, and nasal blockage, resulting in breathing via the mouth and frequently causing an anterior open bite (Oliveira et al. 2008).

Also, It has been reported in the literature that bruxism prevalence is higher in children with cognitive impairment compared to normal children (Miamoto et al. 2011). DS children have bruxism at a young age and usually it persists throughout life. The factors that are thought to contribute to this phenomenon are that DS children have underdeveloped nervous system, malocclusion, chronic anxiety, temporomandibular joint dysfunction, hypotonicity and laxity of the supporting ligaments (V. Macho et al. 2014).

4.3. Dental anomalies

The prevalence of dental anomalies in Down syndrome patients is about 50.5–95.5%. They are associated with a slow cellular growth rhythm and a reduction in the number of cells that strongly influence tooth development, and they are associated with hypodontia, microdontia, and taurodontism (Desingu, Adapa, et Devi 2019).

4.3.1. Number Anomalies

Tooth number anomalies are 10 times more frequent in DS individuals than the general population (Sixou 2008). Its phenotypic presentation is varied in terms of severity and various terms have been used to describe it - congenitally missing teeth, tooth agenesis, hypodontia, oligodontia and anodontia- (Al-Ani et al. 2017) (Figure 6). Tooth agenesis refers directly to the developmental failure of a tooth. Hypodontia, is more suitable for classifying the type of tooth agenesis present and refers to the developmental failure of six or fewer teeth (Nieminen 2009). Oligodontia and anodontia are used to describe more severe forms of tooth agenesis, typically the absence of more than six teeth and the entire dentition, respectively (Nikopensius et al. 2013).

In DS, the most frequent anomaly corresponds to hypodontia, with a 61.5% of incidence (Andersson et al. 2014). The condition is found more commonly in the maxilla than the mandible. The most common congenitally missing teeth in hypodontia are upper lateral incisors, upper second premolars, lower lateral incisors, and lower second premolars, and they are most prevalent in the female population (Andersson et al. 2014).

True anodontia, often known as congenital tooth absence, can be classified into two types: entire and partial (Desingu, Adapa, et Devi 2019). In DS individuals, the incidence of anodontia is 39.2% (Moraes et al. 2007). The incidence of oligodontia among 63 individuals with Down syndrome was found in 23.8% of the total studied population (Russell et Kjaer 1995).

The prevalence of tooth agenesis in individuals with Down syndrome ranges from 54.6% to 58.5%. It often affects both sides of the mouth and commonly involves the lateral incisors and second premolars in both the upper and lower jaws. Tooth agenesis is a multifaceted and multifactorial characteristic that is highly prevalent in individuals with Down syndrome. It is influenced by both environmental and genetic variables. This condition typically affects the maxillary lateral incisor, mandibular premolar, and mandibular incisors (Desingu, Adapa, et Devi 2019).

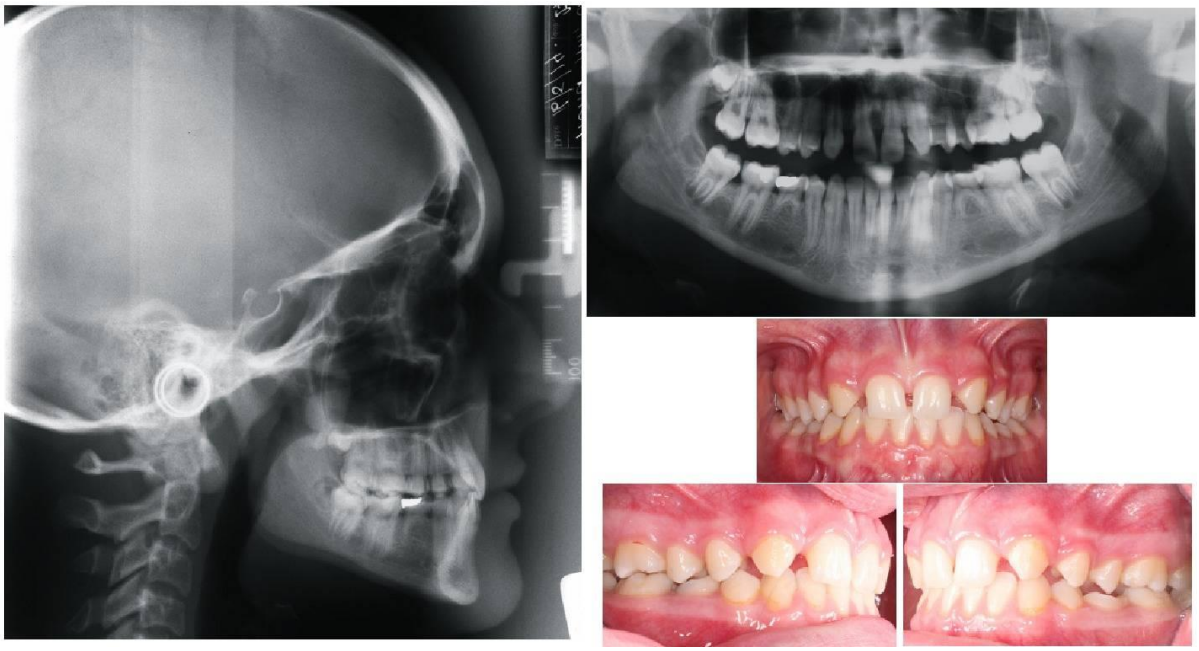

Figure 6. Patient presenting with several features of hypodontia. Agenesis of the maxillary lateral incisors and the second lower premolars, the retained primary mandibular second molars, the generalized spacing, and the deep bite (Al-Ani et al. 2017).

4.3.2. Form and structure anomalies

Taurodontism is the most common form of anomaly seen in DS and corresponds to a dental anomaly only visible on X-rays and characterized by an elongated pulp chamber displaced towards the apical plane of the tooth and by short roots (Sixou 2008). In a study of 49 subjects with DS the incidence of taurodontism was found in 42 individuals with 238 involved teeth (85.7%) (Moraes et al. 2007).

Microdontia refers to teeth that are smaller in size. 35-55% of Down syndrome patients present with microdontia in both the primary and secondary dentition (Desai 1997). In contrast, in 2016, a study assessed a cohort of 105 individuals diagnosed with Down syndrome, and found only that 17 of them (16.2%) exhibited microdontia (Cuoghi et al. 2016), demonstrating that this characteristic has a great variability among DS individuals.

In addition, enamel hypoplasia and hypocalcification are common in DS. Infants show generalized or localized congenital dental malformation ranging from intrinsic discolorations that are smooth to defects that are easily detected by a dental instrument. Hypoplastic defects are frequently the result of significant illnesses or prolonged fevers. Hypocalcified teeth should be under observation for early onset of decay. Depending on the degree of hypoplasia general recommendations would vary from sealants to smooth rough defects to bonding or restorations to full crown coverage. Topical fluoride application should be considered as a preventive measure (Desai 1997).

4.3.3. Eruption anomalies

Tooth eruption may be delayed and may occur in an unusual order in DS. Primary tooth eruption in DS individuals may be delayed up to the 12th month, while the first permanent molar starts to appear around age 8 (Gallo et al. 2019). A study that included 94 children with Down syndrome measured the mean dental maturity score, that expresses the degree of dental development in a child, the score for control children was 30.07 (SD 19.89) and for DS individuals was 15.07 (SD 11.20) (van der Linden et al. 2017).

The eruption movement results from a balance between tissue destruction (bone, connective tissue and epithelium) and tissue formation (bone, periodontal ligament and root). The delay in clinical emergence of teeth within the oral cavity in DS probably finds its origin in the gingival tissue or other factors such as the cellular processes at the apical and occlusal side of the erupting tooth. It is possible that a genetic disturbance in the RANKL/OPG system or the disturbance of *RUNX2* is a cause for the impaired eruption (van der Linden et al. 2017).

4.3.4. Position anomalies

A study in 2000, reveals a high prevalence of impacted maxillary canines, and maxillary canine-premolar transposition in patients with Down syndrome. Canine/premolar transposition is rare, with a prevalence of less than 0.1% in modern populations, nevertheless, among patients with Down syndrome a prevalence of 15% is found. This dental anomaly was present in dentitions that also exhibited either congenitally missing or peg-shaped maxillary laterals. These findings support the existence of a hereditary primary displacement of the tooth germ in the Down syndrome population in addition to the other well-documented dental anomalies (Shapira, Chaushu, et Becker 2000).

4.4. Periodontal disease

Individuals with DS have a high prevalence of periodontal disease, making it the most common oral disease associated with this syndrome (Amano et al. 2001; Sasaki et al. 2004). In 1960, Cohen et al. were the first to report the marked prevalence of periodontitis in young individuals with DS (Cohen et al. 1961). Modern studies have reported a prevalence of between 58% and 96% for DS individuals under 35 years of age (Morgan 2007). Other studies have reported similar results, with prevalence rates ranging from 60% to 95% (Bimstein et al. 2008). Because of this high prevalence, in 1999, The American Association of Periodontology (AAP), agreed upon a new classification of periodontal disease in people with DS, defined as “periodontitis as a manifestation of systemic diseases associated with genetic disorders” (Armitage 1999).

Periodontal disease in patients with trisomy 21 can be detected at an early age. The conditions similar to those of individuals with early-onset periodontitis, including juvenile and prepubertal periodontitis (Cutress 1971; Orner 1976). Early cross-sectional epidemiological studies revealed a significant correlation between age and the prevalence of bone loss in Down syndrome subjects with a mean age of 17.7 (Izumi et al. 1989). These studies suggest that the prevalence of periodontal disease is age-dependent in young adults with Down syndrome. The progression of periodontal disease with age is inevitable in DS, but not all patients are equally exposed to it. Longitudinal studies of these patients have shown that the disease progresses rapidly, although the rate of progression varies from individual to individual (Cichon, Crawford, et Grimm 1998; Saxén, Aula, et Westermarck 1977).

The behavioral pattern of the disease is very peculiar, more severe and aggressive. Periodontal destruction affects primary and permanent teeth, although lesions are most severe around the anteroinferior teeth (Yoshihara et al. 2005). In children, the teeth most affected by the disease are the mandibular incisors and maxillary first molars; canines are the least affected teeth (Modéer, Barr, et Dahllöf 1990). In adults with DS, manifestations of periodontal disease are characterized by marginal gingivitis, necrotizing ulcerative gingivitis, advanced periodontitis, gingival recession and pocket formation. Vertical bone loss with suppuration (5 mm or more in around 70% of DS individuals), mobility of posterior and anterior teeth and frequent tooth loss, particularly in the anterior region of the mandible, are also very common. Children with DS may have a greater tendency to bleeding periodontal tissues and the early onset of gingival inflammation (Carrada et al. 2016). Periodontal disease is an important cause of tooth loss in DS individuals (Reuland-Bosma, van der Reijden, et van Winkelhoff 2001).

On one side, the cause of this severe and exacerbated periodontal disease found in DS, is related to the abnormalities found in the DS immune system as previously described. The polymorphonuclear leucocytes (PMN) activity towards aggregatibacter actinomycetemcomitans (one of the principal bacteria related to periodontitis) is reduced in DS individuals compared to age matched controls (Frydman et Nowzari 2012). On the other side, the number of periodontal pathogens in DS individuals has been found to be higher. Higher amounts of P. Gingivalis, motile organism, Tannerella forsythia and spirochetes have been

reported in different studies. Viruses have also been reported to co-exist with the periodontal pathogens in some DS cases such as Epstein-Barr virus, human cytomegalovirus and herpes virus (Ghaith, Halabi, et Kowash 2017).

4.5. Caries

Regarding dental caries, most of the literature and research studies describe a low prevalence of dental caries in DS children both in the primary and permanent dentition (Macho et al. 2014; Macho et al. 2013; Areias et al. 2013; Jensen, Cleall, et Yip 1973). However, some studies have indicated comparable or higher rates of dental caries between individuals with Down syndrome (DS) and the control group. The inconsistent results may be due to inadequate study designs, insufficient sample size, and the lack of control over variables (Fung, Lawrence, et Allison 2008).

The reduced risk of tooth caries in individuals with DS can be attributed to several factors. These include higher salivary pH, which creates a less acidic environment in the mouth, and higher levels of salivary bicarbonate, which improves the mouth's ability to neutralize acids. DS individuals also tend to have a delayed eruption of teeth, which means they are exposed to caries-causing factors for a shorter period. Additionally, their teeth may be flatter because of early bruxism, making it harder for debris to accumulate and allowing for self-cleansing of the tooth surfaces. Furthermore, due to the intricate nature of their medical condition, the parents of these individuals exhibit a elevated level of worry regarding their oral well-being and proactively seek dental guidance at an early stage (Ghaith, Halabi, et Kowash 2017).

5. Rodent models mimicking the craniofacial phenotype of Down syndrome

The primary goal in comprehending the pathology of DS has been to establish the genotype-phenotype correlation through the examination of individuals with partial T21 (Delabar et al. 1993). The rationale of this approach is that cases of partial trisomy 21 associated with DS features could identify genomic regions associated with specific phenotypes. Because of variable penetrance, only the presence of a particular phenotypic trait is informative for mapping. Investigations into further alterations, such as deletions and translocations that affect HSA21 may also yield insights into the role of HSA21 genes in DS. Initial research postulated that a very limited area of HSA21 would have a significant impact on DS phenotypes, and proposed the concept of a DS critical region (DSCR), region between the genes *KCNJ6* and *DSCR4*, spanning 3.8–6.5 Mb and containing ∼25–50 genes (McCormick et al. 1989; Korenberg et al. 1990; Lyle et al. 2009). However, analysis of further cases indicated that it was more likely that there were critical regions for particular phenotypes and not for the majority of the phenotypes (Korenberg et al. 1994; Lyle et al. 2009).

An extra copy of one or more of the 310 genes presents in HSA21, and the presence of disruptions in protein homeostasis is the current hypothesis to explain different phenotypes in DS (Zhu et al. 2019; Duchon et Herault 2016). Some of these genes are dosage-sensitive; this means that the third copy is expressed and responsible for enhanced activities. Identifying the dosage-sensitive genes responsible for each element of DS phenotype will lead to a better understanding of the molecular mechanisms underlying the various symptoms and will allow better therapeutic options (Antonarakis 2017; Antonarakis et al. 2020). However, studying partial trisomy in humans is overly limiting, because the global population of individuals with incomplete trisomy is extremely small. For this reason, using animal models is crucial for examining the association between genotype and phenotype in DS. Many genes are conserved across mammals, implying that the genetic programs for a specific phenotype may also be conserved. Therefore, this approach can validate the study of animal models to decipher human genetic outcomes (Richtsmeier, Baxter, et Reeves 2000). Also, in the case of the CF

research we have to consider the high correspondence of skull elements between humans and rodents (Figure 7) (Richtsmeier, Baxter, et Reeves 2000).

Several studies in mice and humans have attempted to identify candidate genes that could individually or together explain each clinical feature (Korbel et al. 2009; McCormick et al. 1989). The HSA21 has a conserved synergy with orthologous regions of three murine chromosomes, in mice, the Chr10, Chr16, and Chr17 (Sago et al. 1998; Reeves et al. 1995) and the rapid development of genetic engineering in the last years has made possible the generation of multiple DS mouse models (Dierssen, Herault, et Estivill 2009; Herault et al. 2017).

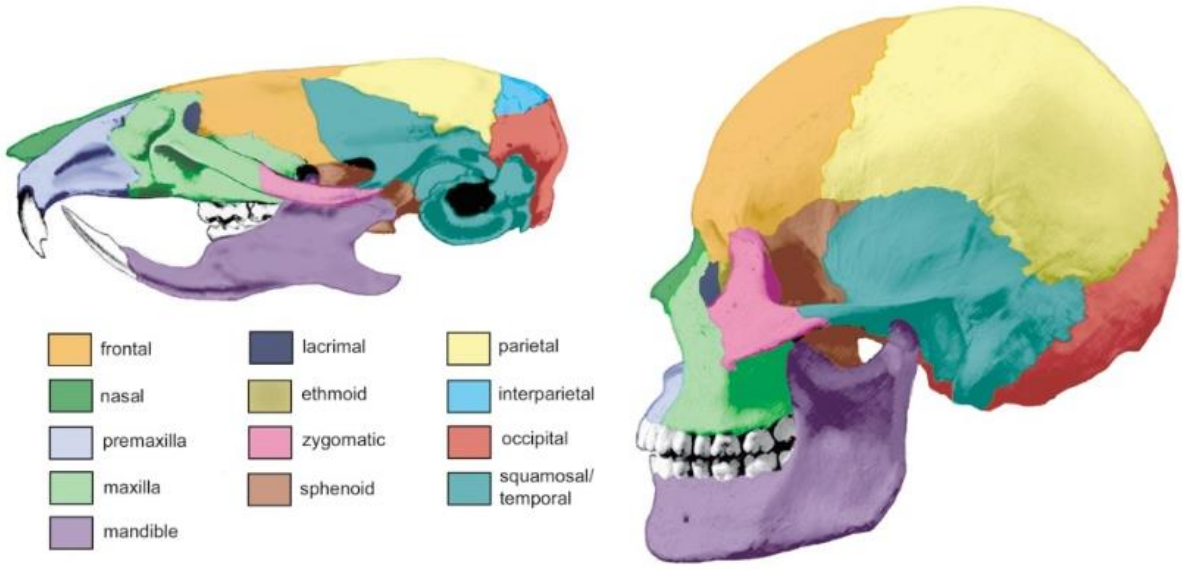

Figure 7. High correspondence of skull elements between humans and rodents. Color-coding shows correspondence of structures between mouse and human skulls. The interparietal bone (bright blue on the mouse skull) is an example of a skull bone that exists in the more primitive (mouse) form, but not in the more derived human skull (Richtsmeier, Baxter, et Reeves 2000).

CF studies were performed in only a few DS mouse models. The most critical DS mouse model, widely used in studies, is the Ts(1716)65Dn, named here Ts65Dn, which displays a variety of phenotypes similar to those found in DS individuals (Olson et al. 2004). This is a strain that carries an extra mini-chromosome with the *mIR155-Zbtb21* region of Mmu16 (abbreviation for Mus musculus Chr 16) translocated downstream of *Pde10a*, close to the centromere of Mmu17.

Thus, Ts65Dn is trisomic for 104 Mmu16 genes orthologs to HSA21 genes between *miR155* and *Zbtb21* (Olson et al. 2004; Gardiner et al. 2003; Muñiz Moreno et al. 2020). The Ts65Dn model presents a low bone mass caused by intrinsic cellular defects in osteoblast differentiation, reducing bone formation. In addition, bone resorption mediated by osteoclasts is also reduced, but it is not enough to overcome the low rate of bone formation (Parsons et al. 2007; Thomas et al. 2021). These animals also show many cognitive and behavioral phenotypes similar to those observed in patients with Down syndrome and characteristic skeletal, craniofacial, cardiovascular, and megakaryocytopoiesis mimicking Down syndrome phenotype (McKelvey et al. 2013). Ts65Dn mouse model presents brachycephaly, reduced facial and cranial vault dimension, reduced cerebellar volume and granule cell density of the dentate gyrus, all features present in human Down syndrome individuals (Figure 8) (Richtsmeier, Baxter, et Reeves 2000). Even more similar CF changes to human features were found in our new Ts(1716)66Yah model, devoid of non-Hsa21 triplicated genes (Duchon et al. 2022), confirming a major contribution of genes from the *mIR155* to *Zbtb21* overdosage to CF phenotypes.

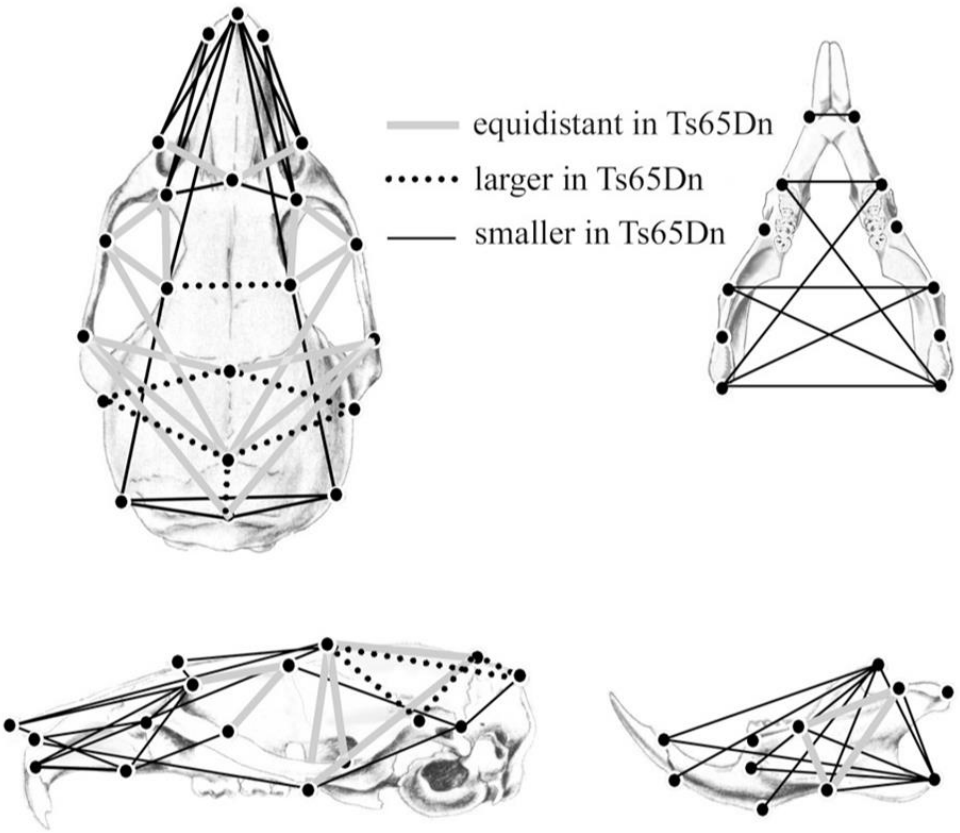

Figure 8. Ts65Dn CF phenotype. Ts65Dn skulls differ significantly from euploid mice in patterns that parallel craniofacial anomalies in DS**.** Indicated measurements are illustrative of some of the statistically significant relationships between Ts65Dn and euploid mice (Richtsmeier, Baxter, et Reeves 2000).

Two other DS models were used to study CF defects. First, The Ts(16C-tel)1Cje (Ts1Cje) model carries a translocation of a shorter region that encompasses 81 genes from *Sod1* to *Mx1*, orthologous to HSA21, to the telomeric part of mouse chromosome 12 (Sago et al. 1998; Huang et al. 1997). This model was used to search for dose-sensitive genes involved in craniofacial changes, as mice models present with a generalized reduction in CF size and additional features (Figure 9) (Richtsmeier et al. 2002). Then, the Dp(16Cbr1-Fam3b)1Rhr (noted here Dp1Rhr), a model trisomic for 33 genes (Olson et al. 2007) exhibited a larger overall size and craniofacial alterations, including a larger and morphologically different mandible than observed in Ts65Dn mice and individuals with DS (Deitz et Roper 2011). Additional studies of Dp1Rhr mice have shown differences in cerebellar and brain size, neuronal long-term potentiation, and in learning and memory (Olson et al. 2007).

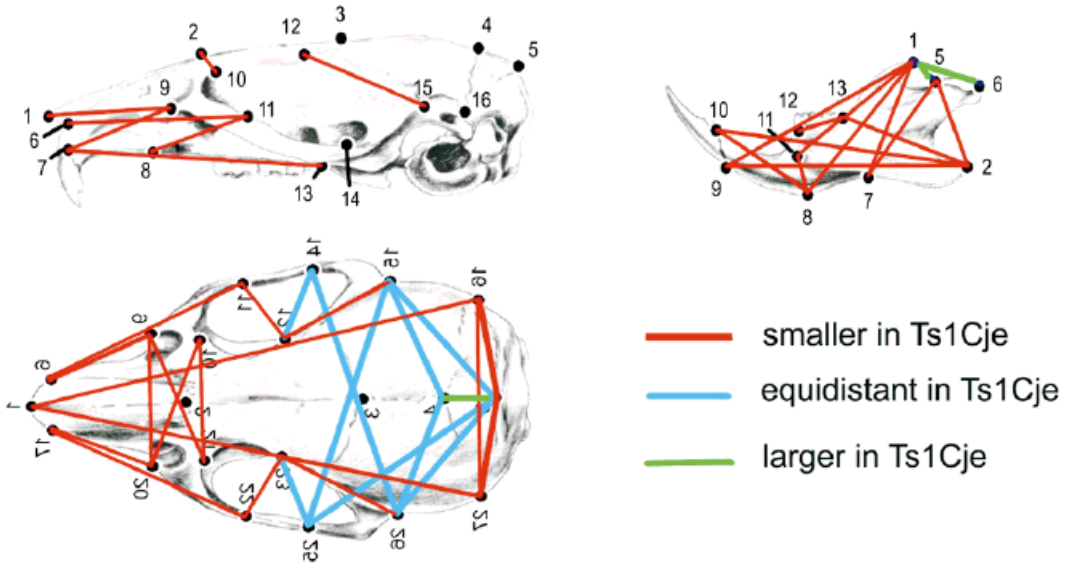

Figure 9. Comparison of normal mouse cranium and mandible with locations of landmarks used in analysis and differences between euploid and aneuploid Ts1Cje. Lines show a subset of those linear distances that are significantly different between Ts1Cje aneuploid and euploid littermates by confidence interval testing (in red and green), as well

as some linear distances that are not affected by aneuploidy (in blue) (Richtsmeier et al. 2002).

The Cre-loxP technology has made engineering more precise duplications of regions orthologous to Hsa21 possible. The Dp(16Lipi-Zbtb21)1Yey (Dp1Yey) is a mouse model with a 22.9 Mb direct duplication of the entire Mmu16 region in conserved synteny with HSA21, containing 118 orthologous protein-coding genes (Li et al. 2007). The CF phenotype corresponds to a reduced dimension of the maxillary and palate, brachycephaly, and reduced mandibular size (Figure 10). The skulls also exhibited increased variance relative to euploid littermates for specific linear distances (Li et al. 2007; Yu et al. 2010; Starbuck et al. 2014).

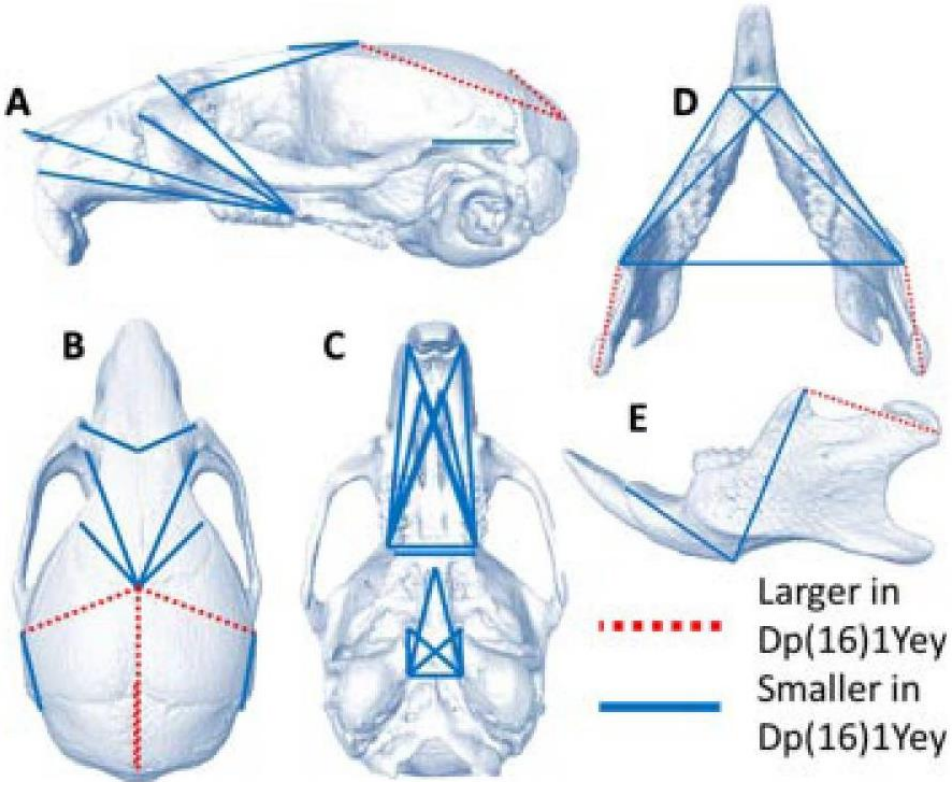

Figure 10. Dp(16)1Yey CF phenotype. Lateral, superior, and inferior views of the mouse cranium and superior and lateral views of the mandible. Linear distances that are significantly smaller (solid) and larger (dashed) in Dp(16)1Yey trisomic mice relative to euploid are depicted (Starbuck et al. 2014).

Another model quite similar to Dp(16)1Yey, but with a slightly different duplicated interval, is the Dp(16*Lipi-Zbtb21*)1TybEmcf or Dp1Tyb, that also presents a DS-like CF phenotype (Lana-Elola et al. 2016). In addition, Dp1Tyb mice display many phenotypic features characteristic of DS in humans, including congenital heart defects, reduced bone density, and deficits in memory, locomotion, hearing, and sleep (Lana-Elola et al. 2011; Watson-Scales 2018; Chang et al. 2020; Thomas et al. 2020).

In 2023, Redhead et al. using morphometrics, did the first genetic mapping taking as reference Dp1Tyb, creating 6 different mouse models (Figure 11). They broke down the region duplicated in Dp1Tyb in three different models, Dp2Tyb, Dp3Tyb and Dp9Tyb. Dp2Tyb and Dp3Tyb presented the same CF changes found in Dp1Tyb, meanwhile Dp9Tyb presented no changes. Later they took the Dp3Tyb region and broke it down again in three different short duplications, Dp4Tyb, Dp5Tyb and Dp6Tyb. No abnormality was seen in Dp4Tyb cranium, while Dp5Tyb and Dp6Tyb cranium were altered in shape but not in size. These results led them to identify four loci causing the DS-CF phenotype found in Dp1Tyb. Furthermore, they crossed mice with a loss-of-function *Dyrk1a* allele (*Dyrk1a*$^{+/-}$) to Dp1Tyb and Dp3Tyb mice to generate Dp1Tyb/*Dyrk1a*KO and Dp3Tyb/*Dyrk1a*KO, achieving a partial rescue of the CF dysmorphology. *Dyrk1a* is therefore one of the genes required in three copies to cause craniofacial dysmorphology in Dp1Tyb mice (Redhead et al. 2023).

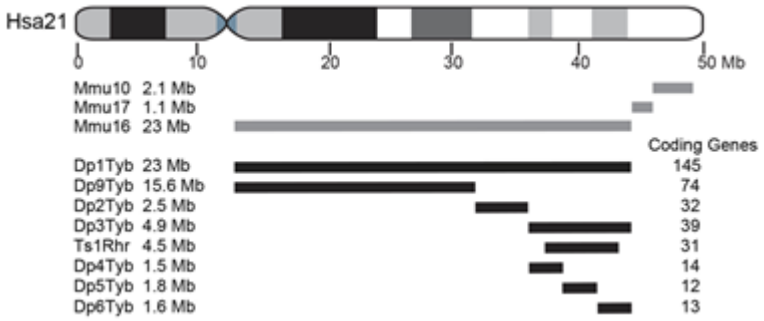

Figure 11. Genetic mapping by Redhead et al. (2023). Black lines represent duplicated regions in each mouse model, showing the number of coding genes within each region (Redhead et al. 2023).

As observed in the different models described, partial trisomy has allowed mapping areas of HSA21 contributing to craniofacial anomalies, but specific genes have not been identified yet (Lyle et al. 2009; Korbel et al. 2009). Even *Dyrk1a* has been implicated in several DS phenotypes, including cognitive impairment, motor function, and craniofacial abnormalities (Hämmerle et al. 2003; Arron et al. 2006; Atas-Ozcan et al. 2021; Redhead et al. 2023). The details of how the dosage imbalance of HSA21 genes affects CF morphogenesis are still poorly understood (Starbuck et al. 2017).

Unraveling the complex genetics and adaptative biological processes involved in forming craniofacial structures is essential. Many genes are conserved across mammals, implying that the genetic programs for a specific phenotype may also be conserved. Therefore, this can validate the study of animal models to decipher human genetic outcomes (Richtsmeier, Baxter, et Reeves 2000). Further, identifying the dosage-sensitive genes responsible for each element of DS phenotype will help us to better understand the molecular mechanisms underlying the various symptoms and will allow us to define better therapeutic options (Antonarakis 2017; Antonarakis et al. 2020).

With this aim, new rodent models have been created in our team headed by Dr. Yann Herault, at the IGBMC with the help of the Institute Clinique de la Souris/ Mouse Clinical Institute (ICS/MCI) - Illkirch, using LoxP/Cre and now CrispR/Cas9 technologies. The models carry duplication of different regions of the rodent chromosomes homologous to human chromosome 21 (Figure 12) (Muñiz Moreno et al. 2020; Duchon et al. 2021; 2022).

For the mouse, seven mouse models have been developed with segmental duplications in the MMU16 homologous to HSA21. Dp(16Samsn1-Cldn17)7Yah [Dp(16)7Yah] with a duplication of the segment compound between *Samsn1* and *Cldn17*. Dp(16*Tiam1-Clic6*))8Yah [Dp(16)8Yah] present a duplication between *Tiam1* and *Clic6*. Dp(16*Cldn17-Brwd1*))9Yah [Dp(16)9Yah] with a duplication in the interval between *Cldn17* and *Brwd1*. Dp(16*Tmprss15-Setd4*)10Yah [Dp(16)10Yah] with the segment between *Tmprss15* and *Setd4* duplicated, similar to Dp(16*Tmprss15-Grik1*)11Yah [Dp(16)11Yah], but this model with a region duplicated until *Grik1*. Dp(16*Tmprss15-Zbtb21*)12Yah [Dp(16)12Yah] has the duplicated region from *Tmprss15*

to *Zfp295*, and Dp(16*Cldn17-Vps26c*(*Dyrk1a*KO))13Yah [Dp(16)13Yah] from *Cldn17* to *Vps26c*, up to the sequence of *Dyrk1a* which is inactivated.

In the case of the rat, thanks to the support of the Jerome Lejeune and Bettencourt-Schueller foundations, new DS rat models have been developed with segmental duplications in the chromosomes 11 and 20 (Birling et al. 2017). In the rat genome, the regions homologous to the HSA21 encompasses 213 genes found on the Rat chromosome 11 (Rno11, Rno for Rattus norvegicus) in the 24.4Mb interval between *Lipi* and *Zbtb21* and on the Rno20 for the most telomeric part of 3.6Mb between *Umodl1* and *Prmt2* (Muñiz Moreno et al. 2020).

We have generated segmental duplication for each interval, Dp(11*Lipi-Zbtb21*)Yahlcs and Dp(20*Umodl1-Prmt2*)Yahlcs, named here Dp(Rno11) and Dp(Rno20). Furthermore, given that *Dyrk1a* is an important candidate gene for the development of the DS-CF phenotype as previously mentioned (Redhead et al. 2023; Johnson et al. 2024), we used other new rat models linked to DS and Mental Retardation autosomal Dominant 7 syndrome (MRD7), Dp(11*Dyrk1a*)6Yah and Del(11*Dyrk1a*)4Yah (Birling et al. 2017).

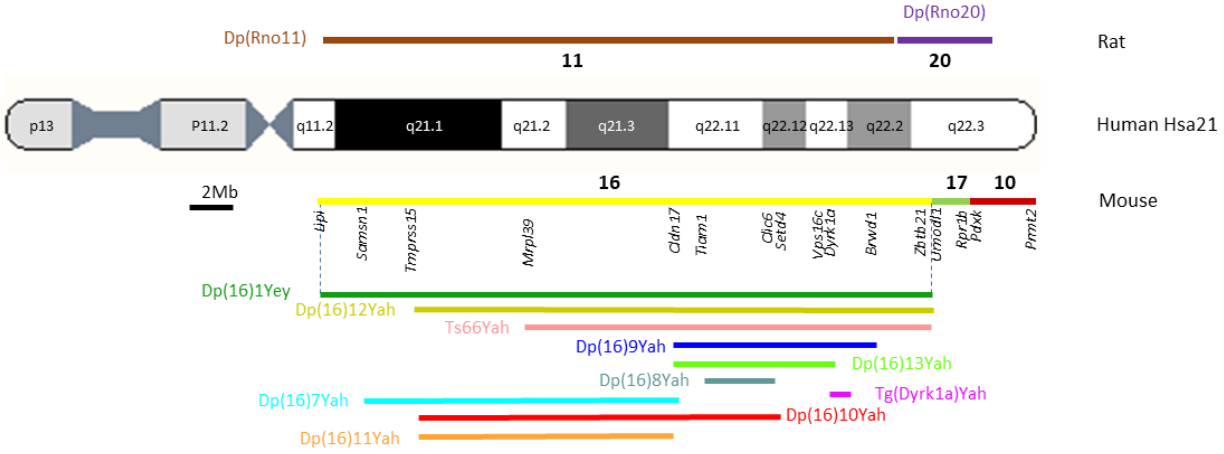

Figure 12. New Down syndrome rodent models. Above human Hsa21, new rat models Dp(RNO11) and Dp(RNO20). In the lower part, new mouse models, in the following order from top to bottom: Dp(16)12Yah, Dp(16)9Yah, Dp(16)13Yah, Dp(16)8Yah, Dp(16)7Yah, Dp(16)10Yah, Dp(16)11Yah and their relative position to the Hsa21 and already know mouse models: Dp(16)1yey, Ts66Yah and Tg(*Dyrk1a*).

In this work, we used these new improved rodent models and existing mouse models to establish correlations between rat, mice, and human phenotypes / genotypes, and to understand the potential craniofacial effect of the duplication/deletion of different chromosomal regions via a morphometric analysis of the animal models. This will lead us to narrow our research to a new chromosomal region and corresponding candidate genes responsible for the DS-CF phenotype.

Objectives

Principal objective

This thesis focuses on deciphering the genetics of craniofacial phenotypes in Down syndrome. For this goal, we aimed to search for CF phenotypes in a set of DS model to narrow the minimal chromosomal regions involved in the craniofacial phenotype; focusing in new and already known DS mouse models with different segmental duplications homologous to HSA21, in order to find dosage-sensitive genes responsible for the CF phenotype.

Specific objectives:

1. **Search for a new chromosomic region and dosage-sensitive genes responsible for the DS-CF phenotype in mouse DS models. Understand the molecular and cellular mechanisms underlying the specific craniofacial phenotype.**

For this aim, using as reference the craniofacial phenotypic changes found in an already known model, Dp(16)1Yey, we expect to dissect and map the chromosomic region with a completely new panel of DS mouse models. We want to define the phenotypes found in every model and identify new candidate genes responsible for the DS-CF features and investigate the molecular and cellular mechanisms underlying the specific craniofacial phenotype. In addition, we want to confirm the role of candidate genes thanks to the creation of a new mouse model (Article #1).

2. **Validate new rat models and define their CF phenotype. Search for a new chromosomic region responsible for the DS-CF phenotypes in the rat.**

Since in mice, the syntenic regions to the Hsa21 are split on 3 different chromosomes (Mmu 10, 16 and 17), it is difficult to create a full trisomic model, even if it's not impossible as shown recently (Li et al. 2021). To overcome this problem, rat models are a good alternative. Indeed, in rats, the syntenic regions to the Hsa21 are split only on 2 different chromosomes, the chromosomes 11 and 20, which make easier the creation of a complete trisomic model. In our lab we have generated different segmental duplication for each interval, Dp(11*Lipi-Zbtb21*)Yahlcs and Dp(20*Umodl1-Prmt2*)Yahlcs. Using these new improved rat models, we expect to define the CF phenotype of every model and reduce the chromosomic region responsible for the DS-CF phenotype (Chapter 2).

Results

Chapter 1: Down syndrome mouse models (Article #1)

Ripply3 overdosage induces mid-face shortening through *Tbx1* downregulation in Down syndrome models

This first chapter contains the publication entitled "*Ripply3* overdosage induces mid-face shortening through *Tbx1* downregulation in Down syndrome models", submitted for publication on September 2024 to the journal scientific eLife (ID#: BIORXIV/2024/612914).

By investigating a new panel of DS mouse models with different segmental duplications on mouse chromosome 16 in the region homologous to human chromosome 21, we managed to identify new regions and new candidate genes for the DS-specific CF phenotype.

We confirmed the role of *Dyrk1a* in the neurocranium brachycephaly. We identified the role of the transcription factor *Ripply3* overdosage in midface shortening through the downregulation of *Tbx1*, another transcription factor involved in DiGeorge syndrome and propose new models for rescuing all aspects of DS-CF phenotypes.

Ripply3 overdosage induces mid-face shortening through *Tbx1* downregulation in Down syndrome models.

José Tomás AHUMADA SAAVEDRA[1]; Claire CHEVALIER[1], Agnes BLOCH ZUPAN[1,2,3,4], and Yann HERAULT[1,*]

Affiliations

[1] Université de Strasbourg, Institut de Génétique et de Biologie Moléculaire et Cellulaire (IGBMC), INSERM U1258, CNRS- UMR7104, Illkirch, France.
[2] Hôpitaux Universitaires de Strasbourg (HUS), Pôle de Médecine et Chirurgie Bucco-dentaires, Centre de Référence des maladies rares orales et dentaires, CRMR-O-Rares, Filière Santé Maladies rares TETE COU & European Reference Network ERN CRANIO, Strasbourg, France
[3] Université de Strasbourg, Faculté de Chirurgie Dentaire, Strasbourg, France
[4] Université de Strasbourg, Institut d'études avancées (USIAS), Strasbourg, France

***Corresponding author**
Yann Herault, Dr.
herault@igbmc.fr

ABSTRACT

The most frequent and unique features of Down syndrome (DS) are learning disability and ucraniofacial (CF) dysmorphism. The DS-specific CF features are an overall reduction in head dimensions (microcephaly), relatively wide neurocranium (brachycephaly), reduced mediolaterally orbital region, reduced bizygomatic breadth, small maxilla, small mandible, and increased individual variability. Until now, the cellular and molecular mechanisms underlying the specific craniofacial phenotype have remained poorly understood. Investigating a new panel of DS mouse models with different segmental duplications on mouse chromosome 16 in the region homologous to human chromosome 21, we identified new regions and the role of two candidate gene for DS-specific CF phenotypes. First, we confirmed the role of *Dyrk1a* in the neurocranium brachycephaly. Then, we identified the role of the transcription factor *Ripply3* overdosage in midface shortening through the downregulation of *Tbx1*, another transcription factor involved in the CF midface phenotype encountered in DiGeorge syndrome. This last effect occurs during branchial arches development through a reduction in cell proliferation. Our findings define a new dosage-sensitive gene responsible for the DS craniofacial features and propose new models for rescuing all aspects of DS CF phenotypes. This data may also provide insights into specific brain and cardiovascular phenotypes observed in DiGeorge and DS models, opening avenues for potential targeted treatment to soften craniofacial dysmorphism in Down syndrome.

INTRODUCTION

Trisomy 21, or Down syndrome (DS), is a pleiotropic disorder with intellectual disability, CF changes, and comorbidities. Somehow, gene dosage effects of one or more of the 671 genes on human chromosome 21 (Hsa21) are responsible for specific pathological features (Zhu et al. 2019; Duchon and Herault 2016). Facial features are characteristic of individuals with DS (Kisling 1966), although their severity varies from one individual to another (Roper and Reeves 2006). DS-related CF dysmorphism includes an overall reduction in head dimensions (microcephaly), relatively wide neurocranium (brachycephaly), small midface, reduced mediolaterally orbital region, reduced bizygomatic breadth, small maxilla, and small mandible (Fink, Madaus, and Walker 1975; Farkas, Kolar, and Munro 1985; Allanson et al. 1993; Baxter et al. 2000). Patients also experience a low bone mass associated with reduced osteoblast activity and high bone turnover (McKelvey et al. 2013).

Studies in rodents and humans have attempted to identify the candidate gene(s) causing DS clinical features (Korbel et al. 2009; McCormick et al. 1989). Using the rapid engineering of the *Mus musculus* (Mmu) genome, multiple DS mouse models have been generated (Dierssen, Herault, and Estivill 2009; Herault et al. 2017) containing extra copies of the Hsa21-orthologous regions of three murine chromosomes: Mmu chromosome 16 (Mmu16), 10 (Mmu10), and 17 (Mmu17) (Reeves et al. 1995; Sago et al. 1998).

DS mouse models have previously been studied for CF phenotypes. The most notable studies have examined the Ts(17^{16})65Dn model, hereafter termed Ts65Dn. This mouse strain carries an extra mini-chromosome with the *mIR155-Zbtb21* region of Mmu16 translocated downstream of *Pde10a,* close to the centromere of Mmu17 (Duchon et al. 2011). Thus, Ts65Dn is trisomic for 104 of the Hsa21 orthologs of the Mmu16 between *miR155 and Zbtb21* (Olson et al. 2004; Gardiner et al. 2003; Muñiz Moreno et al. 2020). The Ts65Dn model displays a variety of phenotypes similar to those found in DS individuals (Olson et al. 2004), including a low bone mass caused by intrinsic cellular defects in osteoblast differentiation, reducing bone formation (Fowler et al. 2012). In addition, bone resorption mediated by osteoclasts is also reduced, but this is not enough to overcome the low rate of bone formation (Parsons et al. 2007; Thomas et al. 2021). These animals also

show many cognitive and behavioral traits as well as characteristic skeletal, craniofacial, cardiovascular features, granule-cell density of the dentate gyrus, and megakaryocytopoiesis mimicking the phenotype encountered in individuals with Down syndrome (Baxter et al. 2000). The CF phenotypes found include brachycephaly, reduced facial and cranial vault dimension, reduced cerebellar volume, and many features present in individuals with DS. CF changes even more similar to those in humans were found in our new Ts(17^{16})66Yah model, devoid of non-Hsa21 triplicated genes (Duchon et al. 2022), confirming a significant contribution of one or more genes found between *mIR155* and *Zbtb21* to the CF phenotypes.

CF defects have also been detected in other DS mouse models. The Ts(16C-tel)1Cje (Ts1Cje) model carries a translocation that encompasses 81 orthologous genes between *Sod1* and *Mx1* (Sago et al. 1998; Huang et al. 1997) and displays a generalized reduction in CF size with additional features (Richtsmeier et al. 2002). By contrast, the Dp(16*Cbr1-Fam3b*)1Rhr (noted here Dp1Rhr), a model trisomic for 33 genes (Olson et al. 2007), exhibited a larger overall size and CF alterations, including more pronounced defects in the mandible than observed in Ts65Dn mice and individuals with DS (Deitz and Roper 2011).

The Dp(16*Lipi-Zbtb21*)1Yey mouse model (Dp1Yey) is a larger model with a 22.9 Mb direct duplication of the entire Mmu16 region in conserved synteny with Hsa21, containing 118 orthologous protein-coding genes (Li et al. 2007). The CF phenotype corresponds to brachycephaly, a reduced dimension of the maxillary and palate, and reduced mandibular size. The skulls also exhibited increased variance relative to euploid littermates for specific linear distances (Li et al. 2007; Yu et al. 2010; Starbuck et al. 2014).

Another model quite similar to Dp(16)1Yey, but with a slightly different duplicated interval, is the Dp(16*Lipi-Zbtb21*)1TybEmcf, or Dp(16)1Tyb (Lana-Elola et al. 2016). In 2023, using morphometric analysis of the Dp1Tyb mouse model of DS and an associated mouse genetic mapping panel, Redhead et al. (Redhead et al. 2023) showed that *Dyrk1a* is required in three copies to cause CF dysmorphology in Dp(16)1Tyb mice. In addition, Dp(16)1Tyb mice display many phenotypic features characteristic of DS in humans, including congenital heart defects, reduced bone density, and deficits in memory, locomotion, hearing, and sleep

(Chang et al. 2020; Lana-Elola et al. 2011; 2016; Thomas et al. 2020; Watson-Scales 2018). Taken together, the candidate genes responsible for craniofacial phenotypes found in DS models include *Dyrk1a*, *Rcan1* (*Dscr1*), and *Ets2*. *Dyrk1a* has been implicated in several DS phenotypes, including cognitive impairment, motor function, and craniofacial abnormalities (Hämmerle et al. 2003; Arron et al. 2006; Atas-Ozcan et al. 2021). Jhonson et al. in 2024, showed that a decreased in *Dyrk1a* in Xenopus resulted in craniofacial malformations, altered expression of critical craniofacial regulators as *Pax3* and *Sox9* fundamental for cranial neural crest development, and presented altered retinoic acid, hedgehog, nuclear factor of activated T cells (*NFAT*), *Notch* and *WNT* signaling pathways. These results indicate that DYRK1A function is critical for early craniofacial development and must properly regulate the expression of specific craniofacial regulators in the branchial arches (Johnson et al. 2024).

Disruption of *Tbx1* expression is a common aspect of CF dysmorphias. *Tbx1* Is the first dosage-sensitive gene identified in the DiGeorge syndrome (DGS)/velocardiofacial syndrome (VCFS), a congenital disorder characterized by neural-crest-related developmental defects. In humans, *TBX1* haploinsufficiency causes craniofacial anomalies (Lindsay et al. 2001). In the mouse model for DiGeorge syndrome the phenotype observed in the mutant mice for the T-box gene, $Tbx1^{+/-}$, encompasses abnormal development of the skeletal structures derived from the first and second pharyngeal arches, with reduced dimension of the midface (Jerome and Papaioannou 2001); a similar situation found in the DS mouse models.

However, the details of how the dosage imbalance of Hsa21 genes affects CF morphogenesis are still poorly understood (Starbuck et al. 2017). Unraveling the complex genetics and adaptative biological processes involved in forming craniofacial structures is essential. Many genes are conserved across mammals, implying that the genetic programs for a specific phenotype may also be conserved. Therefore, this can validate the study of animal models to decipher human genetic outcomes (Richtsmeier, Baxter, and Reeves 2000).

As observed in different models, human partial trisomy has allowed mapping areas of Hsa21 to contribute to craniofacial anomalies, but a specific region has not yet been identified (Lyle et al. 2009; Korbel et al. 2009). Identifying the dosage-sensitive genes responsible for each element of the DS phenotype will help us better understand the molecular mechanisms underlying the various symptoms and will allow us to define therapeutic options better (Antonarakis 2017; Antonarakis et al. 2020).

The Cre-LoxP technology has enabled the engineering of more precise duplications (Hérault et al. 2010; Ruf et al. 2011). Applying this technology, we generated mouse models carrying different segmental duplications of regions located on the Mmu16 homologous to Hsa21. In this study, we used these new DS models and two already known models, Dp(16)1Yey and Tg(Dyrk1a), to establish correlations between human-related CF phenotype and genotype and to understand the potential craniofacial effect of the duplication of different chromosomal regions via a morphometric analysis of the animal models. This led us to narrow our research to find new Mmu16 regions involved in CF and identify corresponding candidate genes responsible for the DS-CF phenotype.

MATERIALS AND METHODS

Previously reported rodent models used

The Dp(16)1Yey and Tg(*Dyrk1a*) (official name Tg(*Dyrk1a*)189N3Yah) models (Li et al. 2007; Guedj et al. 2012) were maintained on the C57BL/6J genetic background. We also used the SD:CRL Dp (11Lipi-Zbtb21)1Yah (short name Dp(Rno11)) rat model generated in the lab (Birling et al. 2017) that carries a duplication of the *Lipi-Zbtb21*, an interval similar to the mouse Dp(16)1Yey, found on rat chromosome 11.

Generation of the new DS mouse strains

These new lines were generated via an *in vivo* chromosomal recombination technique, which combines a transposon system (Ruf et al. 2011) and a meiotic recombination system Cre-LoxP (Hérault et al. 1998). The transposon system consists of the transposase enzyme

and its substrate, the transposon. The enzyme recognizes specific repeat sequences (ITR) flanked on either side of a given DNA sequence (in this case, a vector containing a specific *loxP* site) (Ruf et al. 2011). Once a region of interest is bounded by two *loxP* sites, a transgene expressing the Cre recombinase is brought into the same individual by successive crosses. In this animal, the Cre enzyme recombines the sequences of the *loxP* sites to produce a duplication (or partial trisomy) of the region of interest (Hérault et al. 1998; Hérault et al. 2010).

The new mouse models have been developed with the following segmental duplications in the Mmu16. For Dp(16*Samsn1-Cldn17*)7Yah (Dp(16)7Yah) we duplicated the segment between *Samsn1* and *Cldn17*. Dp(16*Tiam1-Clic6*))8Yah (Dp(16)8Yah) presents a duplication between *Tiam1* and *Clic6*. Dp(16*Cldn17-Brwd1*))9Yah (Dp(16)9Yah) displays a duplication in the interval between *Cldn17* and *Brwd1*. Dp(16*Tmprss15-Setd4*)10Yah (Dp(16)10Yah) has the segment between *Tmprss15* and *Setd4* duplicated, similar to Dp(16*Tmprss15-Grik1*)11Yah (Dp(16)11Yah), but this model presents a region duplicated until *Grik1*. Dp(16*Tmprss15-Zbtb21*)12Yah (Dp(16)12Yah) has the duplicated region from *Tmprss15* to *Zfp295*, and Dp(16*Cldn17-Vps26c*(*Dyrk1a*KO))13Yah (Dp(16)13Yah) from *Cldn17* to *Vps26c*, up to the sequence of *Dyrk1a* which is inactivated. All lines were maintained on C57BL/6J genetic background (Fig. 2A).

Adult cohorts generated

Mice were housed under specific pathogen-free (SPF) conditions and were treated in compliance with the animal welfare policies of the French Ministry of Agriculture (law 87 848). As a major genotype effect compared to sex was previously described elsewhere independently (Redhead et al. 2023), we decided to use females. For each mouse line, about ten littermates by each genotype, DS, and wild-type (WT) were collected (n = 180). We tried to have balanced males and females in the cohorts. For example, For the Dp(16)1Yey line, six females plus five males for the dup carrier and six males plus three females for control were used. Nevertheless, this was not the case in all the other lines, with sometimes more female individuals collected than males, because males were used to breed the lines.

Micro-computed tomography scan of the skull of mutant and control mouse lines

Animals were euthanized with the standard procedure at 14 weeks old. Briefly, the mouse heads were dissected apart from the body. A polystyrene section was interposed between the mandible and maxilla to separate the jaws. After dissection, samples were fixed in a 4% paraformaldehyde solution (PFA), washed with water, and stored in 70% ethanol. The mouse heads were scanned using the Quantum FX micro-computed tomography imaging system (Caliper Life Sciences, Hopkinton, MA, USA) to evaluate the morphology of the skull and mandible. The images obtained were delivered in DICOM format. The scan parameters used to carry out the scanning of the samples correspond to 2 scans of every sample, anterior part, and posterior part using the mode Scan Technique Fine of 2 minutes, with a field of view (FOV) of 40 mm, the voltage 90 kV, CT 160 µA, resolution pixel size 10 µm and the capture size for live mode viewing in small, live current 80kV.

Imaging Processing

For each sample, two scans were obtained, one from the anterior area of the skull and one from the posterior region. FIJI software was used to unite these two scans and create a single file, performing the plugin "Stitching" and making one file in TIFF format. This format can be opened using different image processors. Stratovan Checkpoint software (Stratovan Corporation, Sacramento, USA, Version 2018.08.07. Aug 07, 2018.) was used to place the landmarks (Table S1 and S2, supplementary information), extract the 3D coordinates, create Procrustes average models, and perform the voxel analysis. 3dMD Vultus® software (3dMD LLC, Atlanta, GA, USA) generated heat maps.

Morphometrics analysis

Morphometrics is the quantification and statistical analysis of form. Form is the combination of size and shape of a geometric object in an arbitrary orientation and location (shape is what remains of the geometry of such an object once it is standardized for size). Various approaches can be employed when conducting morphometric analysis. The method of interest in this study is the landmark-based method, which is a conventional approach that relies on phenotypic measurements such as linear distances, angles, weights, and

areas. In this case, we used 61 landmarks, 39 in the skull and 22 in the mandible, to obtain the 3D coordinates of the structure (Hallgrimsson et al. 2015).

Based on 3D coordinates, Euclidean Distance Matrix Analysis (EDMA) is one of the principal tools for analyzing landmark-based morphometric data (Lele and Richtsmeier 2001). This method builds a matrix of linear distances between all possible pairs of landmarks for each specimen (Lele et Richtsmeier 1991). Morphological differences between groups can be pinpointed to specific linear distances on an object through pairwise comparisons of mean form or shape matrices, followed by bootstrapping to estimate the significance of these differences (Lele and Richtsmeier 2001). In this study, two tests were done for each group of samples, first to analyze the form of the skull and mandibles with form difference matrix (FDM) and then the shape with the shape difference matrix (SDM).

In addition, to track the landmarks associated with a significant change and understand where they are located in the CF structures, "EDMA FORM or SHAPE Influence landmark analysis" was performed (Cole and Richtsmeier 1998). The purpose of this test is to search which landmarks present a Relative Euclidean distance (RED) > 1.05 or < 0.95 (outside of the confidence interval 97,8%), meaning, which landmarks show a bigger difference in linear distances between every landmark and in what direction.

Another way to handle landmark-based data is using a multivariate statistical analysis of form, geometric morphometric. This method relies on the superimposition of landmark coordinate data to place individuals into a common morpho-space. The most used superimposition form is the Generalized Procrustes (GP) method and Principal Component Analysis (PCA). This method places multiple individual specimens into the same shape space by scaling, translating, and rotating the landmark coordinates around the centroid of every sample (Rohlf and Slice 1990). As an alternative, we took advantage of Stratovan Checkpoint (Stratovan Corporation, Sacramento, USA) to create population average models and perform a voxel-based analysis, where we can observe directly in 3D models the changes between populations.

Finally, using the 3dMD Vultus® software, we created Procrustes average models created in Checkpoint to perform a landmarking calculation.

Whole-Mount Skeletal Staining

DS individuals also experience a low bone mass associated with reduced osteoblast activity and bone turnover (McKelvey et al. 2013). To study these defects in ossification, we performed a skeletal/cartilage staining with alizarin red and alcian blue in a representative DS mouse model, Dp(16)1Yey.

Whole-mount skeletal staining permits the evaluation of the shapes and sizes of skeletal elements. Thus, it is the principal method for detecting changes in skeletal patterning and ossification. Because cartilage and bone can be distinguished by differential staining, this technique is also a powerful means to assess the pace of skeletal maturation.

We collected n=20 specimens, ten samples (5 WT vs 5 Dp(16)1yey) for the embryonic stage (E) 18.5 and 10 samples (5 WT vs 5 Dp(16)1yey) for P2 (2 days after birth), and were prepared by removing skin, organs, and brown fat. Then, they were dehydrated and fixed in 95 % ethanol for four days. To further remove fatty tissue and tissue permeabilization, specimens were exposed to acetone for one day. Consecutively, samples were transferred to Alcian blue and Alizarin red staining solutions. Later, they were exposed to potassium hydroxide (KOH) for three days, leading to tissue transparency. Finally, they were preserved in Glycerol 87%. The procedure can be adjusted depending on the size/age of the specimens (Rigueur and Lyons 2014).

Dissection of branchial arches during development, RNA extraction, and RT-Digital Droplet™ PCR (RT-ddPCR)

To study the level of expression of different genes triplicated on the DS mouse models, we performed RT-ddPCR (BioRad, Hercules, USA), a digital PCR used for absolute quantification that allows the partitioning of the cDNA samples obtained from the RT procedure up to 20,000 droplets of water-oil emulsions in which the amplification was performed (Lindner, Cayrou, Jacquot, et al. 2021).

For this, we collected the embryos of four pregnant females, Dp(16)1yey at E11.5 and four pregnant females of Dp(RNO11) (DS rat model with a complete duplication of chromosome 11) at E12.5. We obtained 20 embryos for each line (10 WT vs. 10 DS model, n=40) and dissected the frontonasal process, maxillary process, mandibular process, lateral and medial nasal process, and first pharyngeal arch. The dissected tissues are placed in cryogenic storage vials and quickly transferred to liquid nitrogen to avoid RNA decomposition. RNA extraction was performed using the RNeasy Plus Mini Kit (QIAGEN, Hilden, Germany), and RNA quality and concentration were assessed using Nanodrop (Thermo Fisher Scientific, Illkirh, France). cDNA synthesis was performed using the SuperScript™ VILO™ cDNA synthesis kit (Invitrogen), the final reaction is diluted five times and stored at −20 °C until use.

For the PCR reaction, 2 µL of the diluted cDNA samples are supplemented with 10 µL of Supermix 2X ddPCR (without dUTP, Bio-Rad, #1863024), 1 µl of target probe (ZEN™ FAM)/primers mix (final concentration of 750 nM of each primer and 250 nM of probe) and 1 µl of reference probe (ZEN™ HEX)/primer mix (final concentration of 750 nM of each primer and 250 nM of probe) obtaining a total volume of 20 µl. Once prepared, the samples are fractionated into droplets using the QX200 droplet generator (Bio-Rad). The PCR reaction can then be performed by transferring 40 µL of the samples to a 96-well plate. The fluorescence intensity of each droplet is then measured with the QX200 reader (Bio-Rad). Data are analyzed using QuantasoftTM Analysis Pro software (Version 1.0.596). More detailed protocol can be found in Lindner et al. 2021 (Lindner, Cayrou, Jacquot, et al. 2021).

Primers marked with specific fluorescent probes were designed using the PrimerQuest online web interface from IDT (https://www.idtdna.com/Primerquest/Home/Index) to target the genes of interest plus the housekeeping gene. Primers are blasted on the target gene map to verify that they span the exon/exon boundaries on the RNA. For mice and rats, the target genes were *Ripply3, Tbx1*, and *Dyrk1a*. The housekeeping gene for mice was *Tbp,* and for the rats, *Hprt1*. The primers are described below.

The primers used for mice were for *Ripply3* (ENSMUSG00000022941.9), forward AACGTCCGTGTGAGTCTTG, Reverse CTTTACTTACCCGTTTCAAAGCG, Probe ACACACATCGGGATCAAAGGGAGC (HEX); *Tbx1* (ENSMUSG00000009097.11), forward CTGTGGGACGAGTTCAATCA, reverse ACTACATGCTGCTCATGGAC, probe TCACCAAGGCAGGCAGACGAAT (FAM); *Dyrk1a* (ENSMUSG00000022897.16), forward GCAACTGCTCCTCTGAGAAA, reverse AACCTTCCGCTCCTTCTTATG, probe AAGAAGCGAAGACACCAACAGGGC (HEX); and housekeeping gene *Tbp* (ENSG00000112592.15), forward AAGAAAGGGAGAATCATGGACC, reverse GAGTAAGTCCTGTGCCGTAAG, probe CCTGAGCATAAGGTGGAAGGCT (FAM/HEX).

For the rat samples, primers were for *Ripply3* (ENSRNOG00000001684.7), forward GCTGATCTGACCAGAACTGAA, Reverse CGCTTTGAAATGGGCAAGTAA, Probe TTGGGAGGACCAACAAACCTTGGG (HEX); *Tbx1* (ENSRNOG00000001892.6), forward CAGTGGATGAAGCAGATCGTAT, reverse GGTATCTGTGCATGGAGTTAAGA, probe TCGTCCAGCAGGTTATTGGTGAGC (FAM); *Dyrk1a* (ENSRNOG00000001662.8), forward ACAGTTCCCATCATCACCAC, reverse TCCTGGGTAGAGGAGCTATTT, probe AATTGTAGACCCTTGGCCTGGTCC (HEX); and housekeeping gene *Hprt1* (ENSRNOG00000031367), forward TTTCCTTGGTCAAGCAGTACA, reverse TGGCCTGTATCCAACACTTC, probe ACCAGCAAGCTTGCAACCTTAACC (FAM/HEX).

EdU Labeling

Depending on their capacity to proliferate, cells in the organism can be divided into three categories: proliferating cells, non-proliferating cells that have left the cell cycle, and quiescent cells capable of entering the cell cycle if necessary (Leblond 1964). Proliferating cells continue to progress through the different phases of the cell cycle (G1-> S-> G2->M). Daughter cells from a previous division immediately enter the next cell cycle. There are several specific markers for each phase of the cell cycle. For example, Phosphohistone 3 (PH3) corresponds to phosphorylated histone 3 and is found in mitotic cells. EdU is a thymidine analog that can be incorporated into DNA during replication (S phase of the cell

cycle). We can define the percentage of proliferating cells and cell cycle progression using these two markers.

First, pregnant females Dp(16)1Yey at E8.5 stage were injected intraperitoneally with EdU (SIGMA, ref. E9386; diluted in NaCl 0.9%, final concentration 7.5µg/µL; volume injected: 41ug for each milligram of animal weight). Then, embryos were collected 24 hours after EdU injection (E9.5). After, embryos were fixed with 4% paraformaldehyde and embedded in Shandon Cryomatrix Frozen Embedding Medium (Thermo Scientific™). Frozen sagittal sections (14 µm) were cut using a Leica CM3050 S cryostat and placed on Superfrost Plus™ slides for immunohistochemistry.

The immunohistochemistry for EdU was performed following the protocol described in the Kit de cellular proliferation EdU Click-iT™ for imaging, Alexa Fluor™ 555 (REF: C10338). For PH3 we used as primary antibody the Anti-phospho-Histone H3 (Ser10) Antibody, Mitosis Marker (Merck Millipore, REF: 06-570, 1:500) and secondary antibody the Donkey anti-Rabbit IgG (H+L), Alexa Fluor™ 647 (Invitrogen, REF: A-31573, 1:500). For the nuclear marker we used Hoechst nucleic acid stain (Invitrogen, REF: H3570, 1:2000). Quantitative analyses comparing wild-type and mutant embryos. The percentage of EdU-positive cells determined the proliferation index (the number of proliferating cells relative to the total number of cells, labeled with Hoechst) in the area of interest. In addition, the ratio of EdU-positive/PH3-positive cells allow to assess how many proliferating cells have progressed from S phase to G2/M phase (mitotic cells), thus defining the mitotic index.

RESULTS

Contribution of *Lipi-Zbtb21* region to DS craniofacial features in Dp(16)1Yey mouse model

In individuals with DS, sexual dimorphism is observed since early age, with higher measurements in males than in females, but the growth rate remains unchanged. However, in the studies where cephalometric superimposition variables were analyzed, these differences did not appear. This might be because of the low magnitude of the superimposition measurements; making it difficult to determine significant differences (Alio, Lorenzo, and Iglesias 2008; Vicente et al. 2020).

Previous studies in mice have shown no sex differences in the shape of the cranium and only a subtle difference in the shape of the mandible (Toussaint et al. 2021). Importantly, for both the cranium and mandible, the effect of genotype was stronger than sex for Dp1Tyb mice and the other strains (Redhead et al. 2023). Considering this information, we decided to verify this observation and used both sexes together in the CF analysis of Dp(16)1Yey.

First we analyzed the Dp(16)1Yey DS mouse models to compare them with the other DS model Dp(16)1Tyb (Redhead et al. 2023). Then, we performed morphometric analysis of Dp(16)1Yey on adult samples. We observed significant changes in form and shape difference matrix that can be understood as an overall reduction of dimensions (microcephaly) and smaller mandible (Fig S1). For a more detailed investigation of the patterns of displacements of landmarks and their dimensionality, we used principal component analysis (PCA). In the skull and mandible, the PCA of Dp(16)1Yey showed significant differences in the dimensionality versus the WT group (Figure 1A).

To track the landmarks associated with a significant change and understand where they are located in the CF structures, “EDMA FORM or SHAPE Influence landmark analysis” was performed (Cole et Richtsmeier 1998). The purpose of this test is to search which landmarks present a Relative Euclidean distance (RED) > 1.05 or < 0.95 (outside of the confidence interval 97,8%), meaning which landmarks show a bigger difference in linear distances between every landmark and in what direction. On one side, the most influential landmarks with decreased dimensions corresponded to the ones from the maxillary bones, mandible, premaxilla, frontal, temporal (with the squamosal portion), and occipital bone. On the other side, landmarks with a significant increase of dimensions were in the cranial vault, the parietal bone, and the intraparietal bone (Fig. S1).

For a more detailed investigation of the patterns of displacements of landmarks and their dimensionality, we used PCA. In skull and mandible, the PCA of Dp(16)1Yey showed significant differences in the dimensionality versus the WT group (Figure 1A). Also, using Procrustes average models of the different populations to perform a voxel analysis, we found that the key aspects of the Dp(16)1Yey phenotype correspond to a decrease in the

dimensions of the midface, defining a midface hypoplasia and a short nasal region. In the neurocranium, an increase of dimensions in the lateral width was found, with a reduction in the occipital bone, leading to a shortening of the anteroposterior axis (brachycephaly). In the case of the mandible, we found a decrease in the width of the ramus, body, incisor alveolus, and molar alveolus and increased lateral dimension in coronoid and condylar process (expected by the skull brachycephaly; Figure 1A).

Besides, individuals with DS also experience a low bone mass associated with reduced osteoblast activity and bone turnover (McKelvey et al. 2013). Knowing this, plus the information obtained in the craniofacial analysis, we proposed that these significant changes could affect bone ossification during development. To address this, we performed a skeletal/cartilage staining with alizarin red and alcian blue in Dp(16)1Yey in embryonic stage (E) 18.5 and P2. At E18.5, mutant embryos exhibit a defect in the mineralization in the parietal bones, intraparietal, nasal bone, and atlas compared to WT (Figure 1B-C). Interestingly, no more phenotype was observed at P2 (Figure 1D). Altogether, the origin of the CF morphological changes in the Dp(16)1Yey are similar to Dp(16)1Tyb (Toussaint et al. 2021) and probably originate during pre-natal development in the mouse.

Dissection of CF phenotype: Mapping the location of dosage-sensitive genes inside *Lipi-Zbtb21,* that cause the craniofacial dysmorphology using a new panel of mouse models.

To elucidate the location of dosage-sensitive genes that are predominantly involved in the craniofacial dysmorphology of Dp(16)1Yey mice, we took advantage of a new panel of 7 mouse models with shorter segmental duplications covering the Mmu16: Dp(16)7Yah, Dp(16)8Yah, Dp(16)9Yah, Dp(16)10Yah, Dp(16)11Yah, Dp(16)12Yah and Dp(16)13Yah. We analyzed their CF morphology and compared duplication versus their control wild-type (WT) littermates (Fig. 2A).

Performing the identical craniometric analysis as previously described, we found significant skull changes in form and shape in all the models except Dp(16)8Yah (Fig. S2). Multivariable analysis using PCAs showed changes in the same direction along principal component 1 as seen in Dp(16)1Yey mice (Fig. 2B). A major contribution of the principal component 1 (PC1)

for Dp(16)12Yah, Tg(*Dyrk1a)*, was found as in Dp(16)1Yey, then Dp(16)7Yah and Dp(16)9Yah.

Similar changes in shape and form in the skull, with an overall reduction in midface region and a strong brachycephaly, were observed in Dp(16)1Yey, Dp(16)9Yah and Dp(16)12Yah (Fig. 2B). The Dp(16)13Yah model also presented a reduction in the midface region. Still, the premaxilla and nasal region were not reduced, and the brachycephaly was not seen (Fig 2B). The Tg(*Dyrk1a)* model, overexpressing *Dyrk1a* alone, showed strong brachycephaly and reduced premaxilla and nasal bone.

In contrast, we found an inverse phenotype in Dp(16)7Yah compared to Dp(16)1Yey. We scored increased dimensions in the midface and decreased dimensions in the neurocranium; similar changes were found in Dp(16)11Yah but were less significant. Dp(16)10Yah presented an overall reduction of head dimensions, partially observed in the Dp(16)8Yah with a larger midface part. Still, an increase in premaxilla and occipital bone size, resulting in an elongation of the anteroposterior axis in Dp(16)10Yah also observed in Dp(16)13Yah (Fig. 2B). The PCAs showed changes in the inversion direction along principal component 1 as seen in Dp(16)1Yey mice (Fig. 2B).

For the mandibles, as in the skull, significant changes in form and shape were found in all the lines (Fig S3). Here, the changes were different, although the most important changes were found in the same DS models, namely Dp(16)9Yah, Dp(16)13Yah, Dp(16)12Yah, and Dp(16)7Yah. In Dp(16)9Yah and Dp(16)12Yah, a reduction in the lateral width on the body of the mandible, ramus, molar and incisor alveoli, but an increase in the dimension in the condylar process (coincident with the brachycephaly found in the neurocranium) were detected; these changes were similar to the ones found in Dp(16)1Yey (Fig S3). In the case of Dp(16)13Yah, this model also presented a similar phenotype but with increased dimensions in the ramus (apart from the condylar process) (Fig. S3). Dp(16)7Yah had increased dimensions in the body of the mandible, ramus, molar alveolus, and condylar process but maintained the reduced dimensions of the incisor alveolus. A similar phenotype is found in Dp(16)11Yah, but dimensions decrease in the angular process. Also, in

Dp(16)10Yah, significant changes were found in the condylar process, presenting a reduction in the lateral width (Fig. 2B).

The analysis of this new mouse panel allows us 1) to dissect the contribution of several Mmu16 region overdosages to CF phenotypes in DS and 2) to show the differences in their contribution to the cranium and mandible CF phenotypes.

Candidate genes for CF DS phenotype in DS rodent models.

We focused on a new chromosomal region selected from the previous morphometric analysis, encompassing 15 genes between *Setd4 –Dyrk1a* genes (Fig 3A). Inside this region, based on scientific literature and a data set from the FaceBase Consortium (Hong Li 2017), we isolated a set of candidate genes. Among these genes, *Dyrk1a* (Dual Specificity Tyrosine Phosphorylation Regulated Kinase 1A) and *Ripply3* (Ripply Transcriptional Repressor 3) seemed promising targets for CF in DS.

To explore this hypothesis, we analyzed the expression levels of *Dyrk1a, Ripply3*, and *Tbx1* via Droplet digital polymerase chain reaction (RT-ddPCR) in Dp(16)1Yey branchial arches and frontal process at E11.5. The stage is just after the neural crest-derived mesenchymal cells are differentiated into different bones in the facial region (Everson et al. 2018). In the Dp(16)1Yey samples, an overexpression of *Dyrk1a* and *Ripply3* is detected in the craniofacial precursor tissues in mutant versus wild-type. Concomitantly, *Tbx1* was downregulated in trisomic model versus control.

We also did similar expression studies in the Dp(RNO11) rat model with complete duplication of *Lipi-Zbtb21* region in the rat chromosome 11 (Birling et al. 2017) at embryonic stage E12.5 (homologous to the mouse stage). Similar results were found in the rat DS models with overexpression of *Dyrk1a* and *Ripply3* and down-regulation of *Tbx1* (Figure 4B). Overall, the *Ripply3* overexpression due to the triplication of the gene has the same consequence with a reduced expression of *Tbx1* in the branchial arches.

Role of *Dyrk1a* overdosage in the increased dimensions in neurocranium (brachycephaly) on DS mouse models.

Dyrk1a has been implicated in several DS phenotypes and craniofacial abnormalities (Guedj et al. 2012; McElyea et al. 2016; Redhead et al. 2023; Starbuck et al. 2021) and in the last decade has become one of the top candidate gene in DS for therapeutic intervention (De la Torre et al. 2014; Atas-Ozcan et al. 2021). Here we took advantage of Tg(*Dyrk1a*) - a model with 3 copies of *Dyrk1a* (Guedj et al. 2012) - and compared with the results of the new model Dp(16)13Yah where Dyrk1a is not overexpressed, to confirm the role of *Dyrk1a* in the development of the DS CF phenotype. Brachycephaly and higher dimensions in the neurocranium were present in Tg(*Dyrk1a*), but also a reduction in the midface region, a phenotype very similar to the one observed in Dp(16)1Yey (Fig. 2). In Dp(16)13Yah, a reduction in the midface region was also seen but focussed in the maxillary bones, the premaxilla and nasal region were not reduced and the strong brachycephaly was absent. Overall, this comparison confirmed the hypothesis and the role of *Dyrk1a* overdosage in inducing the brachycephaly.

Dyrk1a and _Ripply3_ overdosages affect the proliferation and mitosis of the NCC derivates in the first branchial arch during craniofacial development.

In Tg(Dyrk1a) and in the new panel of mouse models (specifically in Dp(16)9Yah, Dp(16)12Yah and Dp(16)13Yah), significant changes were observed in the midface region, in structures that share the same embryonic origin, the neural crest cells (NCC) (Richtsmeier and Flaherty 2013). These findings, considering the relation of *Dyrk1a* with an altered expression of critical craniofacial regulators fundamental for cranial neural crest development (Johnson et al. 2024) allows us to postulate that *Dyrk1a* and probably *Ripply3* overdosages could affect the proliferation of the NCC derivates during craniofacial development.

To demonstrate this, we monitored the proliferation of NCC with 5-Ethynyl-2'- deoxyuridine (EdU) a thymidine analogue incorporated into the DNA during replication (Tucker et al. 2010). Compared to controls, immunohistological analysis was used to detect the proliferation of NCC derivates in the first branchial arch of the Dp(16)1Yey embryos. In addition, quantitative analyses defined the proliferation and mitotic index (Harris et al.

2018). A reduced proliferation and mitotic index in the first branchial arch were detected (Fig. 3C). Thus, overexpression of triplicated genes from Dp(16)1Yey, including *Dyrk1a* and *Ripply3*, lead to the reduced proliferation of mesenchyme cells from the branchial arches.

Confirmed role of *Ripply3* overdosage during midface development in DS mouse models.

To confirm the role of *Ripply3* in midface hypoplasia, we crossed mice with a loss-of-function allele (*Ripply3*$^{tm1b/+}$) obtained from the IMPC initiative (www.mousephenotype.org) with the Dp(16)1Yey line. We obtained Dp(16)1Yey/*Ripply3*^{tm1b} males carrying a trisomy of all the genes present in Mmu16 but with only two functional copies of *Ripply3*, this to rescue the midface hypoplasia of Dp(16)1Yey. Morphometric analysis of Dp(16)1Yey/*Ripply3*^{tm1b} showed significant shape changes in the skull and mandibles compared to Dp(16)1Yey. In the SDM influence landmarks analysis, we can observe that the most influence landmarks leading to increased dimensions are located in the midface (Fig. 4C). The skull voxel analysis showed the expected result with a similar change in the neurocranium to that present in Dp(16)1Yey. We noticed a phenotypical shape rescue in the midface, with increased dimension in maxillary bones, alveolar process, and premaxilla. The mandible presented the same changes found in Dp(16)1yey (Fig. 4D). To confirm this result and obtain further details, we mapped the surface differences in 3dMD Vultus® software. Using the average model of each population, Dp(16)1Yey average model vs Dp(16)1Yey/*Ripply3*^{tm1b} average model, we performed a superimposition of the 3D models employing landmarks to have an exact matching (Fig 4E). Once the comparison was made, we obtained a histogram of every distance evaluated (in this case more than 1.238.684 points) and a 3D heatmap with the surface differences. In the heat map, we could observe the increased dimensions in all the bones corresponding to the red regions' midface. In light blue, the structures that did not present significant changes (Fig. 4E).

Integrative multivariate analysis of the craniofacial studies unravels four different subgroups of DS models

So far, after doing separate analyses of the DS models with their mutant and control littermates, we decided to combine all the data and see whether we could discriminate different contributions. As shown in Fig. 5, all the wild-type controls clustered together for the cranium and the mandible, with a higher variation, probably due to the altered position of some landmarks.

Focusing on the skull, the DS models were separated into four main groups according to the first two dimensions. One is composed of the Dp(16)1Yey, Dp(16)1Yey/*Ripply3*^{tm1b}, a second of Dp(16)12Yah and Dp(16)9Yah, a third with Dp(16)10Yah, Dp(16)13Yah and Dp(16)8Yah, and the Dp(16)11Yah mixed with the wild-type while the Ts66Yah, the Tg(Dyrk1a) are on the same side of the DS models and the Dp(16)7Yah stayed apart from the other on PC1. Somehow this distribution of models reflected the complexity of genetic interactions for the cranium phenotypes with at least 3 minimal Mmu16 regions: CF1 from *Setd4* to *Brwd1,* involving notably *Dyrk1a* and *Ripply3*, a second CF2 mapping to *Tiam1-Clic6*, and a third CF3 *Samsn1-Tmprss15* responsible for the Dp(16)7Yah phenotypes.

For the mandible, the graph showed another complexity with a main group of 5 models closed to the wild-type (Dp(16)11Yah, Dp(16)7Yah, Dp(16)10Yah, Dp(16)8Yah, Tg(Dyrk1a)) then two branches separated on PC2 with on one side the Dp(16)1Yey, Dp(16)1Yey/*Ripply3*^{tm1b}, linked to the wt-like group with Dp(16)13Yah, and on the other side Dp(16)12Yah and Dp(16)9Yah. The Ts66Yah being kept alone. Interestingly the Dp(16)1Yey, Dp(16)1Yey/*Ripply3*^{tm1b}, Dp(16)12Yah and Dp(16)9Yah, are closer for cranium changes, but they are well-separated for the mandibular phenotypes. These differences could come from various interacting regions contributing to the cranium and mandibular phenotypes.

DISCUSSION

In DS individuals, craniofacial dysmorphism is almost 100% penetrant, but the contributive genetic and developmental factors were unclear. The DS CF phenotype typically encompasses microcephaly, a small midface, a reduced mediolateral orbital region,

reduced bizygomatic breadth, a small maxilla, brachycephaly (a relatively wide neurocranium), and a small mandible (Olson et al. 2004).

We used Dp(16)1Yey to study this characteristic phenotype. This model carries a complete duplication of Mmu16 (Li et al. 2007) and a previously well-described DS-like craniofacial phenotype (Starbuck et al. 2014). Our results reproduce the same findings using a standard craniofacial analysis plus a new voxel analysis, where we could observe the principal changes in the skull and mandibles in 3D. We found that the changes were correlated with the human DS CF phenotype, making Dp(16)1Yey the appropriate model to study DS CF phenotype. Besides, we performed skeletal staining where we could identify a defect in intramembranous ossification, the results obtained at different embryonic stages allowed us to postulate that the changes observed at E18.5 did correspond to a delay and not to a continuous defect in intramembranous ossification. This defect could be related to a problem in the differentiation of mesenchymal cells into osteoblasts or in osteoblast proliferation with a subsequent attenuated osteoblast function (Thomas et al. 2021).

Here we demonstrated that the craniofacial dysmorphism found in Dp(16)1Yey, correlated with the human DS CF phenotype, and we mapped three distinct chromosomic regions of Mmu16. Using a new panel of DS mouse models with specific CF phenotypes (Table 1), we could now identify new dosage-sensitive regions and genes responsible for DS CF phenotype. Saying this, the Ts66Yah behaved independently according to dosage effects in CF phenotypes compared to lines with segmental duplication. This may reflect a unique contribution of the minichromosome on the CF severity while the gene content is close to Dp(16)9Yah. Further experiments with new models will help to confirm the role of the segregating chromosome in CF DS phenotypes (Xing et al. 2023).

This report excludes the *Tmprss15-Grik1* regions, triplicated in Dp(16)11Yah alone, with almost no effect on CF form and shape. This agrees with the Dp(16)9Tyb lack of CF phenotype (Redhead et al. 2023). On one hand, two of the three CF regions defined here, CF1 and CF3, settled the telomeric regions described by Redhead et al. (2023). Nevertheless, we found the contribution of the most centromeric part CF3 involved in cranium

enlargement as new. It could be slightly artificial as this effect was not seen in the Dp(16)1Yey, but could also be due to an effect specific to this region while not triplicated with CF2 and CF3. Only more detailed investigations with new models would allow us to discriminate the genetic interaction of the 3 CF regions. On the other hand, while the overdosage of *Dyrk1a* was crucial for the Dp(16)1Tyb phenotypes (Redhead et al. 2023), the sole overexpression of *Dyrk1a* in the Tg(Dyrk1a) line only replicated well the skull phenotype, more precisely the brachycephaly. Conversely, using PCA, transgenic individuals were closer to the WT group for the lower jaw. Recently, *Dyrk1a* has been identified as one of the genes required in three copies to cause CF dysmorphology in mouse models of DS, and the use of DYRK1A inhibitors or genetic knockout of DYRK1A has been shown to rescue the skull and jaw malformations (McElyea et al. 2016; Redhead et al. 2023). However, Johnson et al. in 2024, showed that a decrease in *Dyrk1a* in Xenopus resulted in craniofacial malformations, altered expression of critical craniofacial regulators as *Pax3* and *Sox9* fundamental for cranial neural crest development, and presented altered retinoic acid, hedgehog, nuclear factor of activated T cells (*NFAT*), *Notch* and *WNT* signaling pathways. These results indicate that DYRK1A function is critical for early craniofacial development and must properly regulate the expression of specific craniofacial regulators in the branchial arches (Johnson et al. 2024). We achieved to demonstrate, thanks to the analysis in Tg(*Dyrk1a*) and Dp(16)13Yah, that 3 copies of *Dyrk1a* are necessary to induce the brachycephaly found in DS. Thus, *Dyrk1a* overdosage is essential and sufficient for brachycephaly, but other genes are responsible for the mandibular phenotypes observed in DS.

Our other candidate gene*, Ripply3*, is a transcriptional corepressor, acting as a negative regulator of the transcriptional activity of *Tbx1* and playing a role in the development of the pharyngeal apparatus and derivatives (Okubo et al. 2011). *Tbx1* Is the first dosage-sensitive gene identified in the DiGeorge syndrome (DGS)/velocardiofacial syndrome (VCFS), a congenital disorder characterized by neural-crest-related developmental defects. In human and DGS models, *TBX1* haploinsufficiency causes craniofacial anomalies (Lindsay et al. 2001) and contributes to heart defects (Merscher et al. 2001). More precisely, the phenotype

observed in the mutant mice for the T-box gene, *Tbx1*$^{+/-}$, encompasses abnormal development of the skeletal structures derived from the first and second pharyngeal arches, with reduced dimension of the midface (Jerome and Papaioannou 2001); a similar situation found in the DS mouse models. In Dp(16)1Yey at an early stage (E11.5), *Ripply3* is overexpressed, and consecutively, *Tbx1* is downregulated in the midface precursor tissues. Still, we also detected a defect in cell proliferation of the NCC derivates in the first branchial arch, which also demonstrated a contribution to the midface shortening. In addition, our new model Dp(16)1Yey/*Ripply3*^{tm1b} demonstrated an increased shape dimension in the structures corresponding to the midface compared to Dp(16)1Yey. Also, in some DS brain models, such as Ts1Rhr and Ts1Cje, the expression of the *Tbx1* gene was found to be significantly downregulated, and it might be involved in delayed fetal brain development and postnatal psychiatric phenotypes observed in DS (Shimizu et al. 2021). Considering this information, we postulated that the overexpression of *Ripply3* in DS mouse models will lead to a downregulation of *Tbx1*, in other DS organs and tissues, leading to additional changes. As such, some DS heart defects, such as the tetralogy of Fallot observed in some individuals, may be related to *Ripply3*-dependent downregulation of *Tbx1*, while in DGS, they are caused by the direct *Tbx1* haploinsufficiency (Merscher et al. 2001). Consequently, investigating treatment for DGS to reestablish a normal TBX1 function will also be of interest for Down syndrome, not only for the craniofacial but also for the brain and the heart function.

Author contributions

Conceptualization: JTAS, ABZ, YH

Data Curation: JTAS, ABZ, YH

Formal Analysis: JTAS, CC, YH

Funding Acquisition: JTAS, ABZ, YH

Investigation: JTAS, CC, ABZ, YH

Methodology: JTAS, CC, YH

Project Administration: ABZ, YH

Supervision: JTAS, ABZ, YH

Validation: JTAS, ABZ, YH

Visualization: JTAS, ABZ, YH

Writing – Original Draft Preparation: JTAS, ABZ, YH

Writing – Review & Editing All

Conflict of interest statement

The authors declare no competing interests.

Funding

This work of the Interdisciplinary Thematic Institute IMCBio, as part of the ITI 2021-2028 program of the University of Strasbourg, CNRS and Inserm, was supported by IdEx Unistra (ANR-10-IDEX-0002), SFRI-STRAT'US project (ANR 20-SFRI-0012), INBS PHENOMIN (ANR-10-INBS-07) and EUR IMCBio (ANR-17-EURE-0023) under the framework of the French Investments for the Future Program. JT A received funding from the National Agency for Research and Development (ANID)/Scholarship Program/DOCTORADO BECAS CHILE/2020-72210028.

Acknowledgments

We thank the Mouse Clinical Institute (PHENOMIN-ICS) for helping maintain the mutant mouse models. Special thanks to Loïc Lindner and Pauline Cayrou for helping with ddPCR design and training, to Sophie Brignon, Charley Pinault, and Aurélie Eisenmann at PHENOMIN-ICS and the IGBMC animal facility for their services, and to Patrick Reilly for proof-reading the manuscript.

Data availability

The morphological data are deposited in Zenodo under the doi: 10.5281/zenodo.13639386

REFERENCES

Alio, Juan J., Jose Lorenzo, and Carmen Iglesias. 2008. "Cranial Base Growth in Patients with Down Syndrome: A Longitudinal Study." *American Journal of Orthodontics and Dentofacial Orthopedics* 133 (5): 729–37. https://doi.org/10.1016/j.ajodo.2006.03.036.

Allanson, J. E., P. O'Hara, L. G. Farkas, and R. C. Nair. 1993. "Anthropometric Craniofacial Pattern Profiles in Down Syndrome." *American Journal of Medical Genetics* 47 (5): 748–52. https://doi.org/10.1002/ajmg.1320470530.

Antonarakis, Stylianos E. 2017. "Down Syndrome and the Complexity of Genome Dosage Imbalance." *Nature Reviews. Genetics* 18 (3): 147–63. https://doi.org/10.1038/nrg.2016.154.

Antonarakis, Stylianos E., Brian G. Skotko, Michael S. Rafii, Andre Strydom, Sarah E. Pape, Diana W. Bianchi, Stephanie L. Sherman, and Roger H. Reeves. 2020. "Down Syndrome." *Nature Reviews. Disease Primers* 6 (1): 9. https://doi.org/10.1038/s41572-019-0143-7.

Arron, Joseph R., Monte M. Winslow, Alberto Polleri, Ching-Pin Chang, Hai Wu, Xin Gao, Joel R. Neilson, et al. 2006. "NFAT Dysregulation by Increased Dosage of DSCR1 and DYRK1A on Chromosome 21." *Nature* 441 (7093): 595–600. https://doi.org/10.1038/nature04678.

Atas-Ozcan, Helin, Véronique Brault, Arnaud Duchon, and Yann Herault. 2021. "Dyrk1a from Gene Function in Development and Physiology to Dosage Correction across Life Span in Down Syndrome." *Genes* 12 (11): 1833. https://doi.org/10.3390/genes12111833.

Baxter, L. L., T. H. Moran, J. T. Richtsmeier, J. Troncoso, and R. H. Reeves. 2000. "Discovery and Genetic Localization of Down Syndrome Cerebellar Phenotypes Using the Ts65Dn Mouse." *Human Molecular Genetics* 9 (2): 195–202. https://doi.org/10.1093/hmg/9.2.195.

Birling, Marie-Christine, Laurence Schaeffer, Philippe André, Loic Lindner, Damien Maréchal, Abdel Ayadi, Tania Sorg, Guillaume Pavlovic, and Yann Hérault. 2017. "Efficient and Rapid Generation of Large Genomic Variants in Rats and Mice Using CRISMERE." *Scientific Reports* 7 (1): 43331. https://doi.org/10.1038/srep43331.

Chang, Pishan, Daniel Bush, Stephanie Schorge, Mark Good, Tara Canonica, Nathanael Shing, Suzanna Noy, et al. 2020. "Altered Hippocampal-Prefrontal Neural Dynamics in Mouse Models of Down Syndrome." *Cell Reports* 30 (4): 1152-1163.e4. https://doi.org/10.1016/j.celrep.2019.12.065.

Cole, T. M., and J. T. Richtsmeier. 1998. "A Simple Method for Visualization of Influential Landmarks When Using Euclidean Distance Matrix Analysis." *American Journal of Physical Anthropology* 107 (3): 273–83. https://doi.org/10.1002/(SICI)1096-8644(199811)107:3<273::AID-AJPA4>3.0.CO;2-1.

De la Torre, Rafael, Susana De Sola, Meritxell Pons, Arnaud Duchon, María Martínez de Lagran, Magí Farré, Montserrat Fitó, et al. 2014. "Epigallocatechin-3-Gallate, a DYRK1A Inhibitor, Rescues Cognitive Deficits in Down Syndrome Mouse Models and in Humans." *Molecular Nutrition & Food Research* 58 (2): 278–88. https://doi.org/10.1002/mnfr.201300325.

Deitz, Samantha L., and Randall J. Roper. 2011. "Trisomic and Allelic Differences Influence Phenotypic Variability during Development of Down Syndrome Mice." *Genetics* 189 (4): 1487–95. https://doi.org/10.1534/genetics.111.131391.

Dierssen, Mara, Yann Herault, and Xavier Estivill. 2009. "Aneuploidy: From a Physiological Mechanism of Variance to Down Syndrome." *Physiological Reviews* 89 (3): 887–920. https://doi.org/10.1152/physrev.00032.2007.

Duchon, Arnaud, and Yann Herault. 2016. "DYRK1A, a Dosage-Sensitive Gene Involved in Neurodevelopmental Disorders, Is a Target for Drug Development in Down Syndrome." *Frontiers in Behavioral Neuroscience* 10:104. https://doi.org/10.3389/fnbeh.2016.00104.

Duchon, Arnaud, Maria del Mar Muñiz Moreno, Claire Chevalier, Valérie Nalesso, Philippe Andre, Marta Fructuoso-Castellar, Mary Mondino, et al. 2022. "Ts66Yah, a Mouse Model of Down Syndrome with Improved Construct and Face Validity." *Disease Models & Mechanisms* 15 (12): dmm049721. https://doi.org/10.1242/dmm.049721.

Duchon, Arnaud, Matthieu Raveau, Claire Chevalier, Valérie Nalesso, Andrew J. Sharp, and Yann Herault. 2011. "Identification of the Translocation Breakpoints in the Ts65Dn and Ts1Cje Mouse Lines: Relevance for Modeling Down Syndrome." *Mammalian Genome: Official Journal of the International Mammalian Genome Society* 22 (11–12): 674–84. https://doi.org/10.1007/s00335-011-9356-0.

Everson, Joshua L., Dustin M. Fink, Hannah M. Chung, Miranda R. Sun, and Robert J. Lipinski. 2018. "Identification of Sonic Hedgehog-Regulated Genes and Biological Processes in the Cranial Neural Crest Mesenchyme by Comparative Transcriptomics." *BMC Genomics* 19 (1): 497. https://doi.org/10.1186/s12864-018-4885-5.

Farkas, Leslie G., John C. Kolar, and Ian R. Munro. 1985. "Craniofacial Disproportions in Apert's Syndrome: An Anthropometric Study." *The Cleft Palate Journal* 22 (4): 253–65.

Fink, G. B., W. K. Madaus, and G. F. Walker. 1975. "A Quantitative Study of the Face in Down's Syndrome." *American Journal of Orthodontics* 67 (5): 540–53. https://doi.org/10.1016/0002-9416(75)90299-7.

Fowler, Tristan W., Kent D. McKelvey, Nisreen S. Akel, Jaclyn Vander Schilden, Anthony W. Bacon, John W. Bracey, Timothy Sowder, et al. 2012. "Low Bone Turnover and Low BMD in Down Syndrome: Effect of Intermittent PTH Treatment." *PLoS ONE* 7 (8): e42967. https://doi.org/10.1371/journal.pone.0042967.

Gardiner, Katheleen, Andrew Fortna, Lawrence Bechtel, and Muriel T. Davisson. 2003. "Mouse Models of Down Syndrome: How Useful Can They Be? Comparison of the Gene Content of Human Chromosome 21 with Orthologous Mouse Genomic Regions." *Gene* 318 (October):137–47. https://doi.org/10.1016/s0378-1119(03)00769-8.

Guedj, Fayçal, Patricia Lopes Pereira, Sonia Najas, Maria-Jose Barallobre, Caroline Chabert, Benoit Souchet, Catherine Sebrie, et al. 2012. "DYRK1A: A Master Regulatory Protein Controlling Brain Growth." *Neurobiology of Disease* 46 (1): 190–203. https://doi.org/10.1016/j.nbd.2012.01.007.

Hallgrimsson, Benedikt, Christopher J. Percival, Rebecca Green, Nathan M. Young, Washington Mio, and Ralph Marcucio. 2015. "Chapter Twenty - Morphometrics, 3D Imaging, and Craniofacial Development." In *Current Topics in Developmental Biology*, edited by Yang Chai, 115:561–97. Craniofacial Development. Academic Press. https://doi.org/10.1016/bs.ctdb.2015.09.003.

Hämmerle, B., C. Elizalde, J. Galceran, W. Becker, and F. J. Tejedor. 2003. "The MNB/DYRK1A Protein Kinase: Neurobiological Functions and Down Syndrome Implications." *Journal of Neural Transmission. Supplementum*, no. 67, 129–37. https://doi.org/10.1007/978-3-7091-6721-2_11.

Harris, Lachlan, Oressia Zalucki, Sabrina Oishi, Thomas H. Burne, Dhanisha J. Jhaveri, and Michael Piper. 2018. "A Morphology Independent Approach for Identifying Dividing Adult Neural Stem Cells in the Mouse Hippocampus." *Developmental Dynamics: An Official Publication of the American Association of Anatomists* 247 (1): 194–200. https://doi.org/10.1002/dvdy.24545.

Hérault, Y., M. Rassoulzadegan, F. Cuzin, and D. Duboule. 1998. "Engineering Chromosomes in Mice through Targeted Meiotic Recombination (TAMERE)." *Nature Genetics* 20 (4): 381–84. https://doi.org/10.1038/3861.

Herault, Yann, Jean M. Delabar, Elizabeth M. C. Fisher, Victor L. J. Tybulewicz, Eugene Yu, and Veronique Brault. 2017. "Rodent Models in Down Syndrome Research: Impact and Future Opportunities." *Disease Models & Mechanisms* 10 (10): 1165–86. https://doi.org/10.1242/dmm.029728.

Hérault, Yann, Arnaud Duchon, Damien Maréchal, Matthieu Raveau, Patricia L. Pereira, Emilie Dalloneau, and Véronique Brault. 2010. "Controlled Somatic and Germline Copy Number Variation in the Mouse Model." *Current Genomics* 11 (6): 470–80. https://doi.org/10.2174/138920210793176038.

Hong Li, Kenneth Jones., Joan Hooper, Trevor Williams. 2017. "Temporal Analysis of Ectoderm and Mesenchyme Gene Expression in the Developing Mouse Facial Prominences." *FaceBase Consortium*. https://doi.org/10.25550/TJA.

Huang, T. T., M. Yasunami, E. J. Carlson, A. M. Gillespie, A. G. Reaume, E. K. Hoffman, P. H. Chan, R. W. Scott, and C. J. Epstein. 1997. "Superoxide-Mediated Cytotoxicity in Superoxide Dismutase-Deficient Fetal Fibroblasts." *Archives of Biochemistry and Biophysics* 344 (2): 424–32. https://doi.org/10.1006/abbi.1997.0237.

Jerome, L. A., and V. E. Papaioannou. 2001. "DiGeorge Syndrome Phenotype in Mice Mutant for the T-Box Gene, Tbx1." *Nature Genetics* 27 (3): 286–91. https://doi.org/10.1038/85845.

Johnson, H. Katherine, Stacey E. Wahl, Fatmata Sesay, Larisa Litovchick, and Amanda JG. Dickinson. 2024. "Dyrk1a Is Required for Craniofacial Development in *Xenopus Laevis*." *Developmental Biology*, April. https://doi.org/10.1016/j.ydbio.2024.04.004.

Kisling, Erik. 1966. *Cranial Morphology in Down's Syndrome: A Comparative Roentgenencephalometric Study in Adult Males*. Munksgaard.

Korbel, Jan O., Tal Tirosh-Wagner, Alexander Eckehart Urban, Xiao-Ning Chen, Maya Kasowski, Li Dai, Fabian Grubert, et al. 2009. "The Genetic Architecture of Down Syndrome Phenotypes Revealed by High-Resolution Analysis of Human Segmental Trisomies." *Proceedings of the National Academy of Sciences of the United States of America* 106 (29): 12031–36. https://doi.org/10.1073/pnas.0813248106.

Lana-Elola, Eva, Sheona D. Watson-Scales, Elizabeth M. C. Fisher, and Victor L. J. Tybulewicz. 2011. "Down Syndrome: Searching for the Genetic Culprits." *Disease Models & Mechanisms* 4 (5): 586–95. https://doi.org/10.1242/dmm.008078.

Lana-Elola, Eva, Sheona Watson-Scales, Amy Slender, Dorota Gibbins, Alexandrine Martineau, Charlotte Douglas, Timothy Mohun, Elizabeth MC Fisher, and Victor LJ Tybulewicz. 2016. "Genetic Dissection of Down Syndrome-Associated Congenital Heart Defects Using a New Mouse Mapping Panel." Edited by Margaret Buckingham. *eLife* 5 (January):e11614. https://doi.org/10.7554/eLife.11614.

Leblond, C. P. 1964. "CLASSIFICATION OF CELL POPULATIONS ON THE BASIS OF THEIR PROLIFERATIVE BEHAVIOR." *National Cancer Institute Monograph* 14 (May):119–50.

Lele, Subhash R., and Joan T. Richtsmeier. 2001. *An Invariant Approach to Statistical Analysis of Shapes*. CRC Press.

Li, Zhongyou, Tao Yu, Masae Morishima, Annie Pao, Jeffrey LaDuca, Jeffrey Conroy, Norma Nowak, Sei-Ichi Matsui, Isao Shiraishi, and Y. Eugene Yu. 2007. "Duplication of the Entire 22.9 Mb Human Chromosome 21 Syntenic Region on Mouse Chromosome 16 Causes Cardiovascular and Gastrointestinal Abnormalities." *Human Molecular Genetics* 16 (11): 1359–66. https://doi.org/10.1093/hmg/ddm086.

Lindner, Loic, Pauline Cayrou, Sylvie Jacquot, Marie-Christine Birling, Yann Herault, and Guillaume Pavlovic. 2021. "Reliable and Robust Droplet Digital PCR (ddPCR) and RT-ddPCR Protocols for Mouse Studies." *Methods (San Diego, Calif.)* 191 (July):95–106. https://doi.org/10.1016/j.ymeth.2020.07.004.

Lindner, Loic, Pauline Cayrou, Thomas W. Rosahl, Heather H. Zhou, Marie-Christine Birling, Yann Herault, and Guillaume Pavlovic. 2021. "Droplet Digital PCR or Quantitative PCR for In-Depth Genomic and Functional Validation of Genetically Altered Rodents." *Methods*, Methods of genome engineering and model validation, 191 (July):107–19. https://doi.org/10.1016/j.ymeth.2021.04.001.

Lindsay, Elizabeth A., Francesca Vitelli, Hong Su, Masae Morishima, Tuong Huynh, Tiziano Pramparo, Vesna Jurecic, et al. 2001. "Tbx1 Haploinsufficiency in the DiGeorge Syndrome Region Causes Aortic Arch Defects in Mice." *Nature* 410 (6824): 97–101. https://doi.org/10.1038/35065105.

Lyle, Robert, Frédérique Béna, Sarantis Gagos, Corinne Gehrig, Gipsy Lopez, Albert Schinzel, James Lespinasse, et al. 2009. "Genotype-Phenotype Correlations in Down Syndrome Identified by Array CGH in 30 Cases of Partial Trisomy and Partial Monosomy Chromosome 21." *European Journal of Human Genetics: EJHG* 17 (4): 454–66. https://doi.org/10.1038/ejhg.2008.214.

McCormick, Mary Kay, Albert Schinzel, Michael B. Petersen, Gail Stetten, Daniel J. Driscoll, Eduardo S. Cantu, Lisbeth Tranebjaerg, Margareta Mikkelsen, Paul C. Watkins, and Stylianos E. Antonarakis. 1989. "Molecular Genetic Approach to the Characterization of the 'Down Syndrome Region' of Chromosome 21." *Genomics* 5 (2): 325–31. https://doi.org/10.1016/0888-7543(89)90065-7.

McElyea, Samantha D., John M. Starbuck, Danika M. Tumbleson-Brink, Emily Harrington, Joshua D. Blazek, Ahmed Ghoneima, Katherine Kula, and Randall J. Roper. 2016. "Influence of Prenatal EGCG Treatment and Dyrk1a Dosage Reduction on Craniofacial Features Associated with Down Syndrome." *Human Molecular Genetics* 25 (22): 4856–69. https://doi.org/10.1093/hmg/ddw309.

McKelvey, K. D., T. W. Fowler, N. S. Akel, J. A. Kelsay, D. Gaddy, G. R. Wenger, and L. J. Suva. 2013. "Low Bone Turnover and Low Bone Density in a Cohort of Adults with Down Syndrome." *Osteoporosis International : A Journal Established as Result of Cooperation between the European Foundation for Osteoporosis and the National Osteoporosis Foundation of the USA* 24 (4): 1333–38. https://doi.org/10.1007/s00198-012-2109-4.

Merscher, S., B. Funke, J. A. Epstein, J. Heyer, A. Puech, M. M. Lu, R. J. Xavier, et al. 2001. "TBX1 Is Responsible for Cardiovascular Defects in Velo-Cardio-Facial/DiGeorge Syndrome." *Cell* 104 (4): 619–29. https://doi.org/10.1016/s0092-8674(01)00247-1.

Muñiz Moreno, Maria Del Mar, Véronique Brault, Marie-Christine Birling, Guillaume Pavlovic, and Yann Herault. 2020. "Modeling Down Syndrome in Animals from the Early Stage to the 4.0 Models and Next." *Progress in Brain Research* 251:91–143. https://doi.org/10.1016/bs.pbr.2019.08.001.

Okubo, Tadashi, Akinori Kawamura, Jun Takahashi, Hisato Yagi, Masae Morishima, Rumiko Matsuoka, and Shinji Takada. 2011. "Ripply3, a Tbx1 Repressor, Is Required for Development of the Pharyngeal Apparatus and Its Derivatives in Mice." *Development* 138 (2): 339–48. https://doi.org/10.1242/dev.054056.

Olson, L, Joan Richtsmeier, J Leszl, and Roger Reeves. 2004. "Olson, LE, Richtsmeier, JT, Leszl, J and Reeves, RH. A Chromosome 21 Critical Region Does Not Cause Specific Down Syndrome Phenotypes. Science 306: 687-690." *Science (New York, N.Y.)* 306 (November):687–90. https://doi.org/10.1126/science.1098992.

Olson, Lisa E., Randall J. Roper, Crystal L. Sengstaken, Elizabeth A. Peterson, Veronica Aquino, Zygmunt Galdzicki, Richard Siarey, Mikhail Pletnikov, Timothy H. Moran, and Roger H. Reeves. 2007. "Trisomy for the Down Syndrome 'critical Region' Is Necessary but Not

Sufficient for Brain Phenotypes of Trisomic Mice." *Human Molecular Genetics* 16 (7): 774–82. https://doi.org/10.1093/hmg/ddm022.

Parsons, Trish, Timothy M. Ryan, Roger H. Reeves, and Joan T. Richtsmeier. 2007. "Microstructure of Trabecular Bone in a Mouse Model for down Syndrome." *The Anatomical Record* 290 (4): 414–21. https://doi.org/10.1002/ar.20494.

Redhead, Yushi, Dorota Gibbins, Eva Lana-Elola, Sheona Watson-Scales, Lisa Dobson, Matthias Krause, Karen J. Liu, Elizabeth M. C. Fisher, Jeremy B. A. Green, and Victor L. J. Tybulewicz. 2023. "Craniofacial Dysmorphology in Down Syndrome Is Caused by Increased Dosage of Dyrk1a and at Least Three Other Genes." *Development* 150 (8): dev201077. https://doi.org/10.1242/dev.201077.

Reeves, R. H., N. G. Irving, T. H. Moran, A. Wohn, C. Kitt, S. S. Sisodia, C. Schmidt, R. T. Bronson, and M. T. Davisson. 1995. "A Mouse Model for Down Syndrome Exhibits Learning and Behaviour Deficits." *Nature Genetics* 11 (2): 177–84. https://doi.org/10.1038/ng1095-177.

Richtsmeier, Joan T., Laura L. Baxter, and Roger H. Reeves. 2000. "Parallels of Craniofacial Maldevelopment in down Syndrome and Ts65Dn Mice." *Developmental Dynamics* 217 (2): 137–45. https://doi.org/10.1002/(SICI)1097-0177(200002)217:2<137::AID-DVDY1>3.0.CO;2-N.

Richtsmeier, Joan T., and Kevin Flaherty. 2013. "Hand in Glove: Brain and Skull in Development and Dysmorphogenesis." *Acta Neuropathologica* 125 (4): 469–89. https://doi.org/10.1007/s00401-013-1104-y.

Richtsmeier, Joan T., Ann Zumwalt, Elaine J. Carlson, Charles J. Epstein, and Roger H. Reeves. 2002. "Craniofacial Phenotypes in Segmentally Trisomic Mouse Models for Down Syndrome." *American Journal of Medical Genetics* 107 (4): 317–24. https://doi.org/10.1002/ajmg.10175.

Rigueur, Diana, and Karen M. Lyons. 2014. "Whole-Mount Skeletal Staining." *Methods in Molecular Biology (Clifton, N.J.)* 1130:113–21. https://doi.org/10.1007/978-1-62703-989-5_9.

Rohlf, F. James, and Dennis Slice. 1990. "Extensions of the Procrustes Method for the Optimal Superimposition of Landmarks." *Systematic Biology* 39 (1): 40–59. https://doi.org/10.2307/2992207.

Roper, Randall J., and Roger H. Reeves. 2006. "Understanding the Basis for Down Syndrome Phenotypes." *PLoS Genetics* 2 (3): e50. https://doi.org/10.1371/journal.pgen.0020050.

Ruf, Sandra, Orsolya Symmons, Veli Vural Uslu, Dirk Dolle, Chloé Hot, Laurence Ettwiller, and François Spitz. 2011. "Large-Scale Analysis of the Regulatory Architecture of the Mouse Genome with a Transposon-Associated Sensor." *Nature Genetics* 43 (4): 379–86. https://doi.org/10.1038/ng.790.

Sago, Haruhiko, Elaine J. Carlson, Desmond J. Smith, Joshua Kilbridge, Edward M. Rubin, William C. Mobley, Charles J. Epstein, and Ting-Ting Huang. 1998. "Ts1Cje, a Partial Trisomy 16 Mouse Model for Down Syndrome, Exhibits Learning and Behavioral Abnormalities." *Proceedings of the National Academy of Sciences of the United States of America* 95 (11): 6256–61.

Shimizu, Ryohei, Keiichi Ishihara, Eri Kawashita, Haruhiko Sago, Kazuhiro Yamakawa, Ken-Ichi Mizutani, and Satoshi Akiba. 2021. "Decrease in the T-Box1 Gene Expression in Embryonic Brain and Adult Hippocampus of down Syndrome Mouse Models." *Biochemical and Biophysical Research Communications* 535 (January):87–92. https://doi.org/10.1016/j.bbrc.2020.12.026.

Starbuck, John M., Theodore M. Cole, Roger H. Reeves, and Joan T. Richtsmeier. 2017. "The Influence of Trisomy 21 on Facial Form and Variability." *American Journal of Medical Genetics. Part A* 173 (11): 2861–72. https://doi.org/10.1002/ajmg.a.38464.

Starbuck, John M., Tara Dutka, Tabetha S. Ratliff, Roger H. Reeves, and Joan T. Richtsmeier. 2014. "Overlapping Trisomies for Human Chromosome 21 Orthologs Produce Similar Effects on Skull and Brain Morphology of Dp(16)1Yey and Ts65Dn Mice." *American Journal of Medical Genetics. Part A* 164 (8): 1981–90. https://doi.org/10.1002/ajmg.a.36594.

Starbuck, John M., Sergi Llambrich, Rubèn Gonzàlez, Julia Albaigès, Anna Sarlé, Jens Wouters, Alejandro González, et al. 2021. "Green Tea Extracts Containing Epigallocatechin-3-Gallate Modulate Facial Development in Down Syndrome." *Scientific Reports* 11 (1): 4715. https://doi.org/10.1038/s41598-021-83757-1.

Thomas, Jared R., Kourtney Sloan, Kelsey Cave, Joseph M. Wallace, and Randall J. Roper. 2021. "Skeletal Deficits in Male and Female down Syndrome Model Mice Arise Independent of Normalized Dyrk1a Expression in Osteoblasts." *Genes* 12 (11): 1729. https://doi.org/10.3390/genes12111729.

Thomas, Michael S. C., Olatz Ojinaga Alfageme, Hana D'Souza, Prachi A. Patkee, Mary A. Rutherford, Kin Y. Mok, John Hardy, Annette Karmiloff-Smith, and LonDownS Consortium. 2020. "A Multi-Level Developmental Approach to Exploring Individual Differences in Down Syndrome: Genes, Brain, Behaviour, and Environment." *Research in Developmental Disabilities* 104 (September):103638. https://doi.org/10.1016/j.ridd.2020.103638.

Toussaint, Nicolas, Yushi Redhead, Marta Vidal-García, Lucas Lo Vercio, Wei Liu, Elizabeth M. C. Fisher, Benedikt Hallgrímsson, Victor L. J. Tybulewicz, Julia A. Schnabel, and Jeremy B. A. Green. 2021. "A Landmark-Free Morphometrics Pipeline for High-Resolution Phenotyping: Application to a Mouse Model of Down Syndrome." *Development (Cambridge, England)* 148 (18): dev188631. https://doi.org/10.1242/dev.188631.

Tucker, Eric S., Maria K. Lehtinen, Tom Maynard, Mariela Zirlinger, Catherine Dulac, Nancy Rawson, Larysa Pevny, and Anthony-Samuel Lamantia. 2010. "Proliferative and Transcriptional Identity of Distinct Classes of Neural Precursors in the Mammalian Olfactory Epithelium." *Development (Cambridge, England)* 137 (15): 2471–81. https://doi.org/10.1242/dev.049718.

Vicente, Ascensión, Luis-Alberto Bravo-González, Ana López-Romero, Clara Serna Muñoz, and Julio Sánchez-Meca. 2020. "Craniofacial Morphology in down Syndrome: A Systematic Review and Meta-Analysis." *Scientific Reports* 10 (1): 19895. https://doi.org/10.1038/s41598-020-76984-5.

Watson-Scales, Sheona. 2018. "Analysis of Motor Dysfunction in Down Syndrome Reveals Motor Neuron Degeneration.," May.

Xing, Zhuo, Yichen Li, Eduardo Cortes-Gomez, Xiaoling Jiang, Shuang Gao, Annie Pao, Jidong Shan, et al. 2023. "Dissection of a Down Syndrome-Associated Trisomy to Separate the Gene Dosage-Dependent and -Independent Effects of an Extra Chromosome." *Human Molecular Genetics* 32 (13): 2205–18. https://doi.org/10.1093/hmg/ddad056.

Yu, Tao, Zhongyou Li, Zhengping Jia, Steven J. Clapcote, Chunhong Liu, Shaomin Li, Suhail Asrar, et al. 2010. "A Mouse Model of Down Syndrome Trisomic for All Human Chromosome 21 Syntenic Regions." *Human Molecular Genetics* 19 (14): 2780–91. https://doi.org/10.1093/hmg/ddq179.

Zhu, Ping Jun, Sanjeev Khatiwada, Ya Cui, Lucas C. Reineke, Sean W. Dooling, Jean J. Kim, Wei Li, Peter Walter, and Mauro Costa-Mattioli. 2019. "Activation of the ISR Mediates the Behavioral and Neurophysiological Abnormalities in Down Syndrome." *Science (New York, N.Y.)* 366 (6467): 843–49. https://doi.org/10.1126/science.aaw5185.

TABLES

	Skull - Cranium		Lower jaw - Mandible	
	Shape	Form	Shape	Form
Dp(16)1Yey	Strong	Strong	Strong	Strong
Dp(16)1Yey/Ripply3 +/-	Mild	Mild	Mild	Strong
Tg(Dyrk1a)	Strong	Strong	Mild	NS
Dp(16)9Yah	Strong	Strong	Strong	Strong
Dp(16)12Yah	Strong	Strong	Strong	Strong
Dp(16)8Yah	Mild	NS	Mild	NS
Dp(16)10Yah	Mild	Strong	Mild	Strong
Dp(16)13Yah	Mild	Mild	Strong	NS
Dp(16)7Yah	Strong (Inverse)	Mild	Mild	Mild
Dp(16)11Yah	Mild (Inverse)	Mild	Mild	Mild

Table 1: Summary of the CF phenotypes observed in DS models.

LEGEND TO FIGURES

Figure 1. Alteration of DS craniofacial features in Dp(16)1Yey is observed during late development. (A) Morphometric analysis of the cranium and mandible of adult Dp(16)1Yey vs control. WT is in light blue and Dp(16)1Yey in yellow. PCA (first two components) of general Procrustes analysis of aligned cranium shapes, using data from females (red circle) and males (green circle) mice. The percentage of variance in PC1 corresponds to 39.2%. In the figure WT vs Dp(16)1Yey shape difference warping, with in blue the bones with decreased dimensions in Dp(16)1Yey (midface hypoplasia and mandible), and in yellow, the bones with increased dimensions (neurocranium). **(B-D)** Skeletal staining with alizarin red and alcian blue. Comparison WT vs Dp(16)1yey E18.5 whole body, upper (top) and lower (bottom) magnification of the skull showing less mineralization in temporal, parietal, intraparietal, and occipital bones. **(C)** Magnification of lateral view of skeletal staining, WT vs Dp(16)1Yey at E18.5 (2 individuals). Red arrows showing less mineralization in nasal bones, neurocranium, and form defect in atlas vertebrae. **(D)** Lateral view of skeletal staining of two WT vs Dp(16)1Yey individuals showing normal ossification pattern at P2.

Figure 2. New DS mouse model panel to identify genetic regions whose overdosage causes the craniofacial dysmorphology of Dp(16)1Yey. (A) Summary table of a new panel of DS mouse model and their segmental duplication of the genetic interval. **(B)** Morphometric analysis of the cranium of the new panel of DS mouse models, plus Tg(Dyrk1a). Shape difference warping highlighted, in blue, the bones with decreased dimensions in DS models, and in red, the bones with increased dimensions. PCA (first two components) of general

Procrustes analysis of aligned cranium shapes for every model with the percentage of variance graphic in PC1.

Figure 3. Genetic mapping identifies a new chromosomic region and dosage-sensitive genes for the DS craniofacial phenotype. (A) Scheme of the relative position of the new mouse and rat models in HSA21, and the new chromosomic region of interest for DS CF phenotype (red square). **(B)** RT-ddPCR results graphics for Mouse model Dp(16)1Yey E11.5 in the left, the gene expression ratio shows statistically significant overexpression of the triplicated *Dyrk1a* (***, p<0.000*)* and *Ripply3* (***, p<0.000) and a downregulation of *Tbx1* (**, p<0.005*)*. In the right, the graph for the Rat model Dp(RNO11) E12.5. The gene expression ratio shows statistically significant overexpression of the triplicated *Dyrk1a* (***, p<0.000*)* and *Ripply3* (*, p< 0,02) and a downregulation of *Tbx1* (**, p<0.01*)*. **(C)** Edu, PH3, and Hoechst unrevealed defects in the proliferation and mitosis of the NCC derivates in the 1st branchial arch during craniofacial development in Dp(16)1Yey. In the right graphic, the proliferation (***, p<0.000) and mitotic (***, p<0.000) indexes were significantly reduced in Dp(16)1Yey.

Figure 4. Shape rescue in the midface phenotype in the Dp(16)1Yey/ *Ripply3^{tm1b}* compound mutant. (A) Shape difference matrix based on Dp(16)1Yey vs Dp(16)1Yey/ *Ripply3^{tm1b}* comparison. Confidence interval and Frequency Bootstrap graphics with 10.000 resamplings showed significant shape changes (Z statistics = 0,045, CI = [0.06065 / -0.06202]). Influence landmarks analysis to show the most influential landmarks (red circle) that lead to significant changes in Dp(16)1Yey/ Ripply3^{tm1b} vs Dp(16)1Yey in **(B)** with their position **(C)** located in the midface. **(D)** Shape difference warping of Dp(16)1Yey vs Dp(16)1Yey/ *Ripply3^{tm1b}*. Dp(16)1yey is displayed in yellow and Dp(16)1Yey/ *Ripply3^{tm1b}* in orange. The bones with increased dimensions are in orange in the cranium figure of Dp(16)1Yey vs Dp(16)1Yey/*Ripply3^{tm1b}* warping. Maxillary bone, premaxilla, alveolar process and neurocranium are similar to that found in Dp(16)1Yey). In yellow, the bones with decreased dimensions (nasal bone and skull base). In the mandible of Dp(16)1Yey vs Dp(16)1Yey/ *Ripply3^{tm1b}* warping, the mandible presented the same changes found in Dp(16)1yey. PCA (first three components) of general Procrustes analysis of aligned cranium shapes. Showing significant changes in PC1/PC2, PC3/PC1 and PC3/PC2. **(E)** Comparison of Dp(16)1Yey average model vs Dp(16)1Yey/Ripply3^{tm1b} average model with a 3D heatmap from 3dMD Vultus ® software analysis. Pink/red shows increased shape dimensions in all the structures corresponding to the midface. In light blue, the structures with no significant changes. On the left, the histogram of every point distance evaluated (in this case, more than 1.238.684 points) and the surface differences with the color code for the increase-decrease dimensions (Red to green).

Figure 5. Integrative multivariate analysis of the craniofacial studies. (A) Schematic representation of DS models and their relative position to HSA21, showing the 3 new CF regions (red squares) involved in the DS CF phenotype located on Mmu16. **(B)** Integrative

multivariate analysis of all the models used in this study, plus Ts66Yah vs wild-type. The PCAs correspond to a canonical variate analysis (Procrustes Distance Multiple Permutations tests at 1000 iterations). DS strains show significant differences compared with their wild-type controls. DS models were separated into four main groups with the cranium PCA graph, whereas for the mandible, the graph showed a prominent group of 5 models close to the wild-type and two branches separated on PC2.

Figure 1.

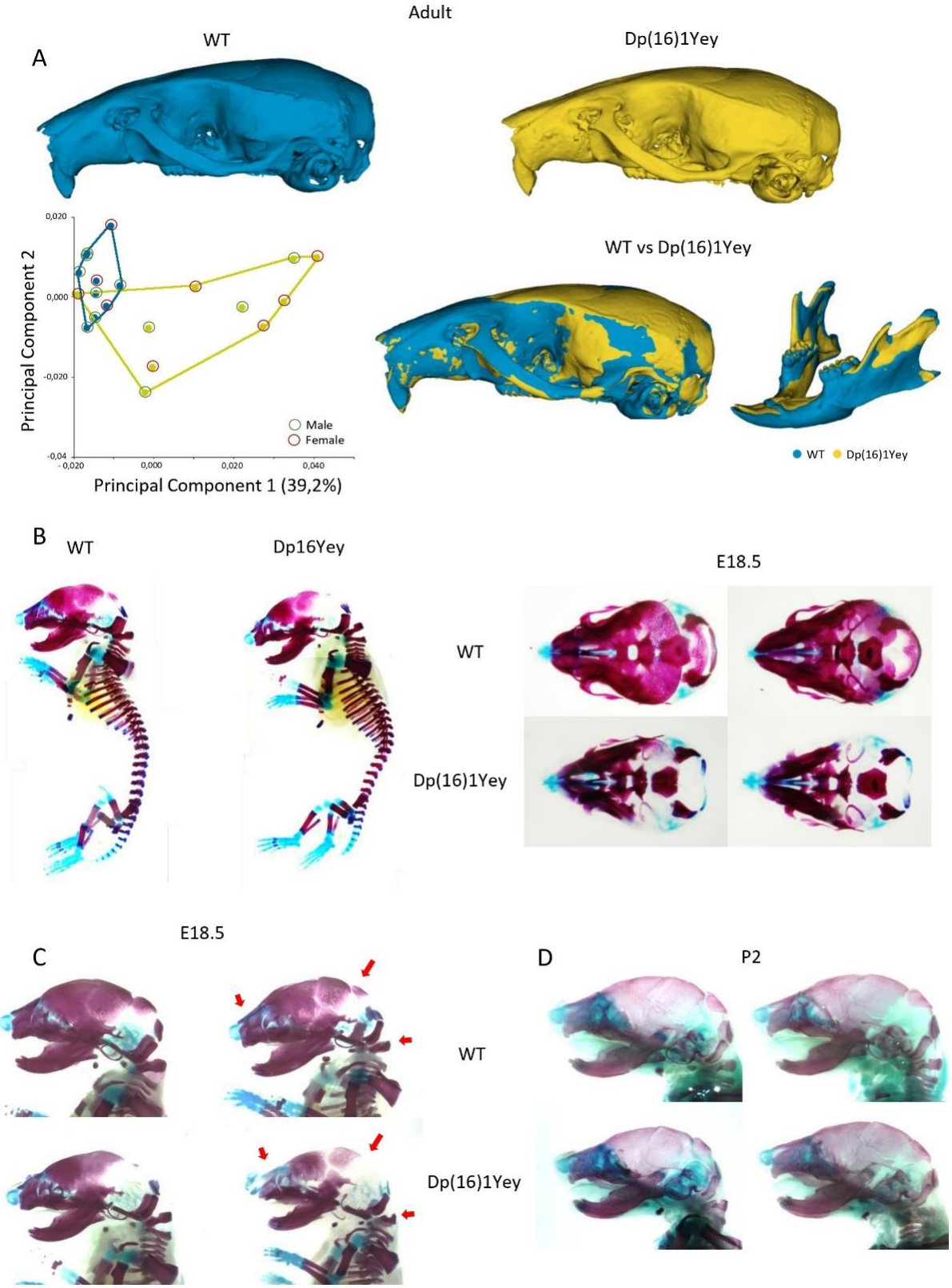
Adult
A
WT
Dp(16)1Yey
WT vs Dp(16)1Yey
Principal Component 2
Principal Component 1 (39,2%)
Male
Female
WT
Dp(16)1Yey
B
WT
Dp16Yey
E18.5
WT
Dp(16)1Yey
C
E18.5
WT
Dp(16)1Yey
D
P2

Figure 2.

A

Short name	Official name	Notes	Reference
Dp(16)1Yey	Dp(16*Lipi-Zbtb21*)1Yey	Segmental duplication	(Li et al 2007)
Dp(16)7Yah	Dp(16*Samsn1-Cldn17*)7Yah	Segmental duplication	This publication
Dp(16)8Yah	Dp(16*Tiam1-Clic6*))8Yah	Segmental duplication	This publication
Dp(16)9Yah	Dp(16*Cldn17-Brwd1*))9Yah	Segmental duplication	This publication
Dp(16)10Yah	Dp(16*Tmprss15-Setd4*)10Yah	Segmental duplication	This publication
Dp(16)11Yah	Dp(16*Tmprss15-Grik1*)11Yah	Segmental duplication	This publication
Dp(16)12Yah	Dp(16*Tmprss15-Zbtb21*)12Yah	Segmental duplication	This publication
Dp(16)13Yah	Dp(16*Cldn17-Vps26c*(*Dyrk1a*KO))13Yah	Segmental duplication with *Dyrk1a* inactivated	This publication
Tg(Dyrk1a)	*Tg(Dyrk1a)189N3Yah*	Bac transgenic	(Guedj et al. 2012)

B

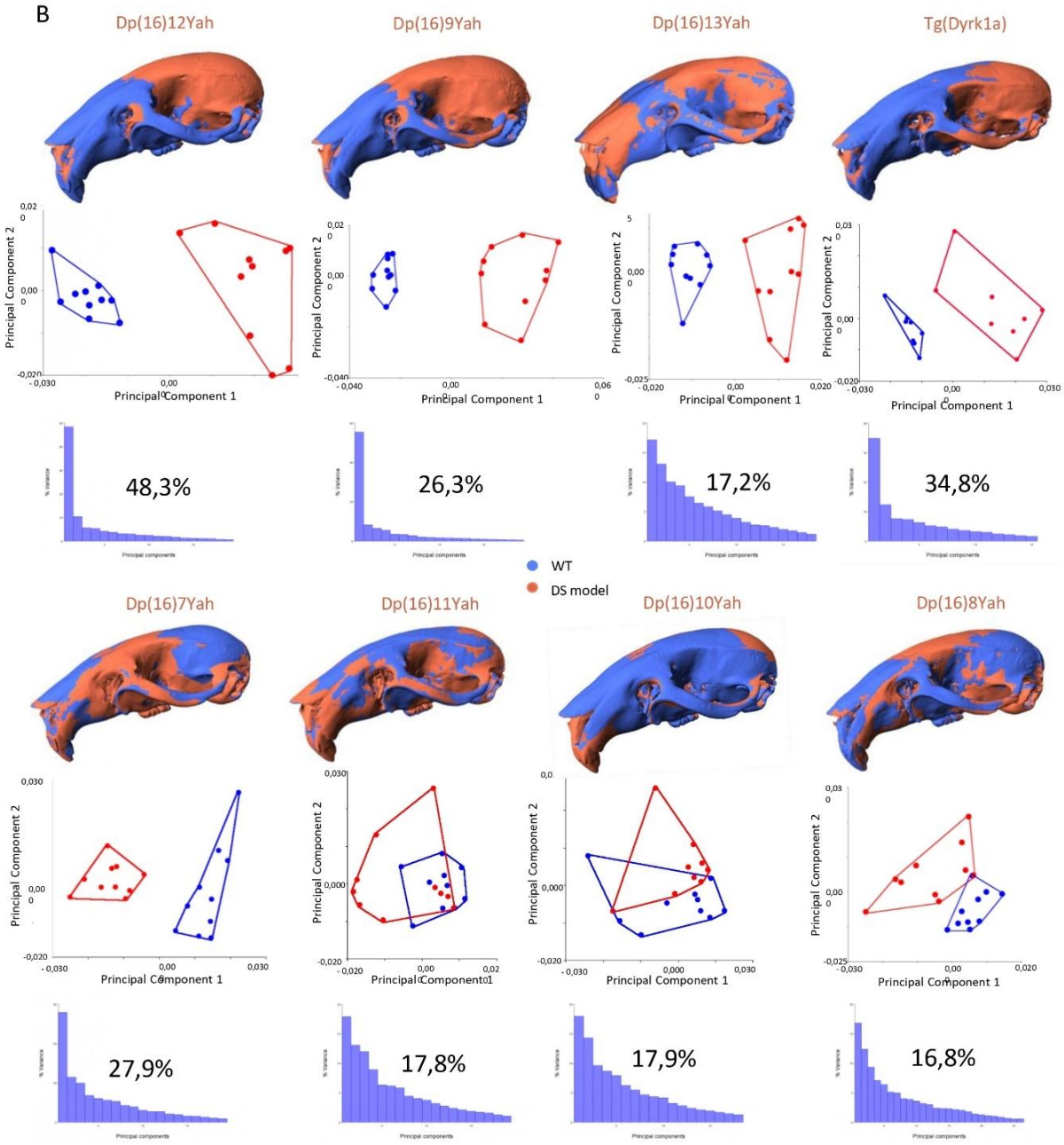

Figure 3.

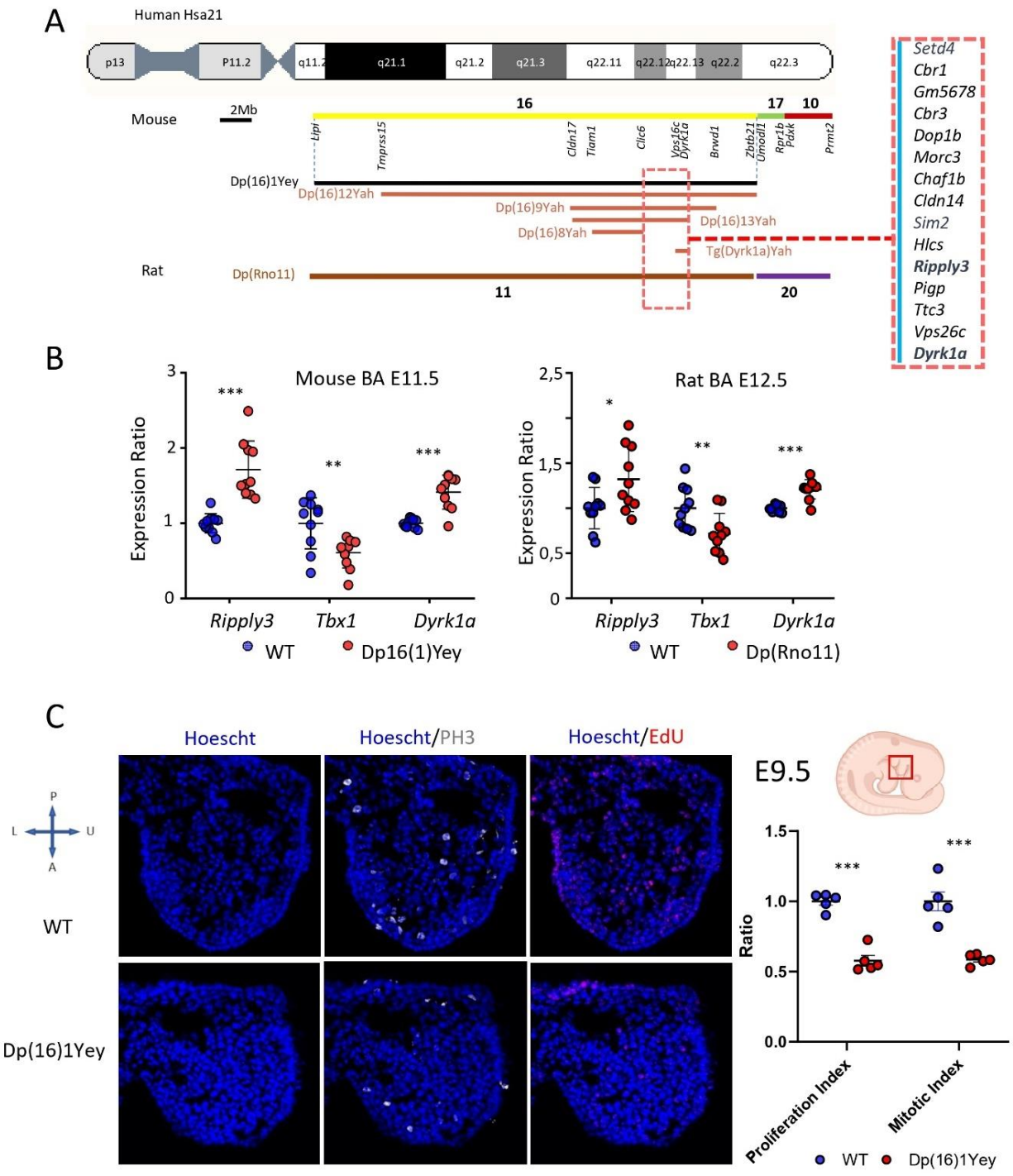
A
Human Hsa21
p13
P11.2
q11.2
q21.1
q21.2
q21.3
q22.11
q22.12
q22.13
q22.2
q22.3
Mouse
2Mb
16
17
10
Lipi
Tmprss15
Cldn17
Tiam1
Clic6
Vps16c
Dyrk1a
Brwd1
Zbtb21
Umodl1
Rpr1b
Pdxk
Prmt2
Dp(16)1Yey
Dp(16)12Yah
Dp(16)9Yah
Dp(16)13Yah
Dp(16)8Yah
Tg(Dyrk1a)Yah
Rat
Dp(Rno11)
11
20
Setd4
Cbr1
Gm5678
Cbr3
Dop1b
Morc3
Chaf1b
Cldn14
Sim2
Hlcs
Ripply3
Pigp
Ttc3
Vps26c
Dyrk1a
B
Mouse BA E11.5
Expression Ratio
Ripply3
Tbx1
Dyrk1a
WT
Dp16(1)Yey
Rat BA E12.5
Dp(Rno11)
C
Hoescht
Hoescht/PH3
Hoescht/EdU
P
L
U
A
WT
Dp(16)1Yey
E9.5
Ratio
Proliferation Index
Mitotic Index

Figure 4.

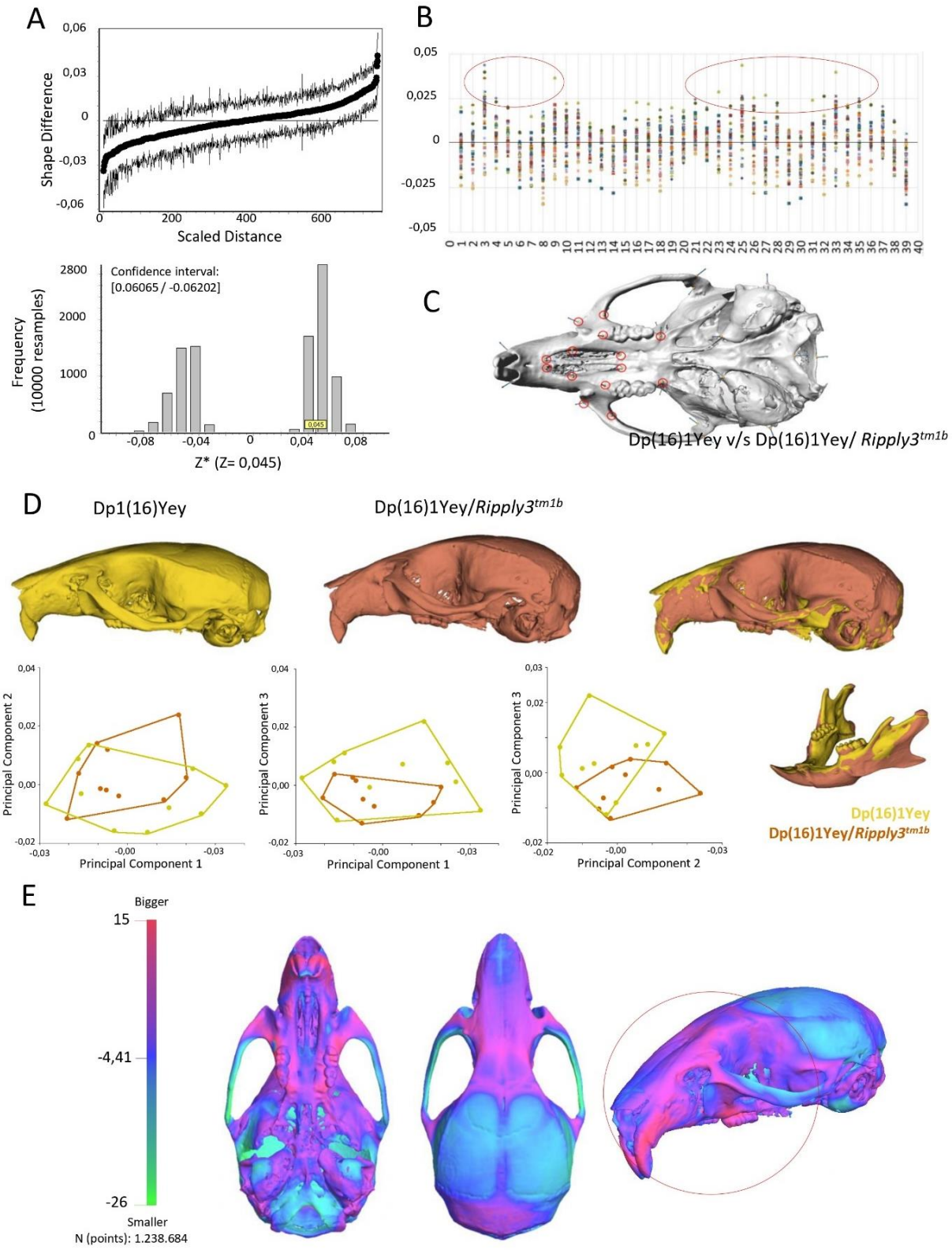
A
Shape Difference
Scaled Distance
Confidence interval:
[0.06065 / -0.06202]
Frequency
(10000 resamples)
Z* (Z= 0,045)
B
C
Dp(16)1Yey v/s Dp(16)1Yey/ Ripply3tm1b
D
Dp1(16)Yey
Dp(16)1Yey/Ripply3tm1b
Principal Component 1
Principal Component 2
Principal Component 3
Dp(16)1Yey
Dp(16)1Yey/Ripply3tm1b
E
Bigger
15
-4,41
-26
Smaller
N (points): 1.238.684

Figure 5.

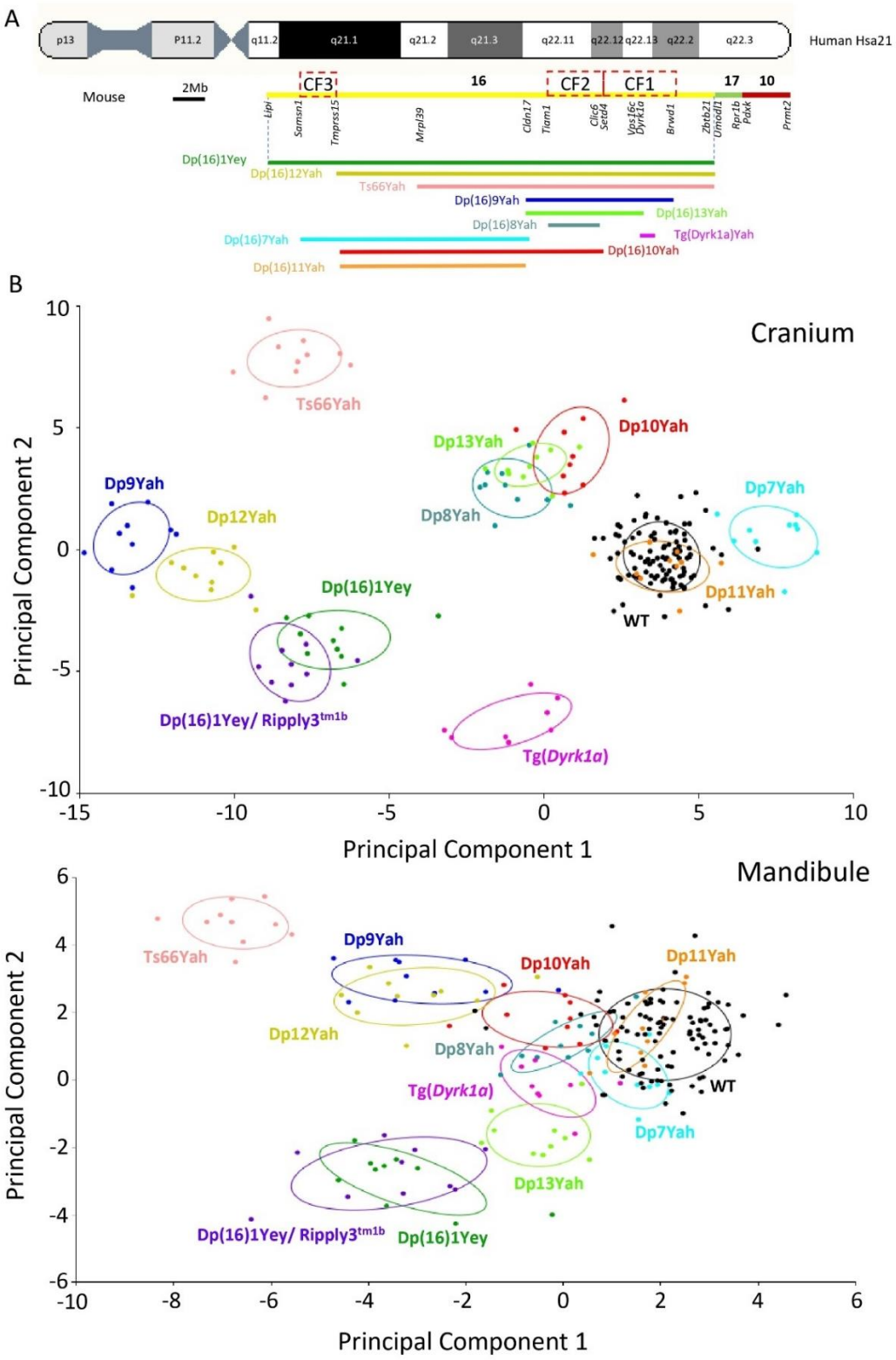
A
p13
P11.2
q11.2
q21.1
q21.2
q21.3
q22.11
q22.12
q22.13
q22.2
q22.3
Human Hsa21
Mouse
2Mb
CF3
16
CF2
CF1
17
10
Lipi
Samsn1
Tmprss15
Mrpl39
Cldn17
Tiam1
Cbs
Setd4
Vps16a
Dyrk1b
Brwd1
Zbtb21
Umodl1
Rpr1b
Pdxk
Prmt2
Dp(16)1Yey
Dp(16)12Yah
Ts66Yah
Dp(16)9Yah
Dp(16)13Yah
Dp(16)8Yah
Tg(Dyrk1a)Yah
Dp(16)7Yah
Dp(16)10Yah
Dp(16)11Yah
B
Cranium
Principal Component 2
Principal Component 1
Ts66Yah
Dp10Yah
Dp13Yah
Dp9Yah
Dp7Yah
Dp12Yah
Dp8Yah
Dp(16)1Yey
Dp11Yah
WT
Dp(16)1Yey/ Ripply3tm1b
Tg(Dyrk1a)
Mandibule
Principal Component 2
Principal Component 1
Ts66Yah
Dp9Yah
Dp10Yah
Dp11Yah
Dp12Yah
Dp8Yah
Tg(Dyrk1a)
WT
Dp7Yah
Dp13Yah
Dp(16)1Yey/ Ripply3tm1b
Dp(16)1Yey

SUPPLEMENTARY INFORMATIONS

Ripply3 overdosage induces mid-face shortening through *Tbx1* downregulation in Down syndrome models.

José Tomás AHUMADA SAAVEDRA[1]; Claire CHEVALIER[1], Agnes BLOCH ZUPAN[1,2,3,4], and Yann HERAULT[1,*]

Affiliations

[1] Université de Strasbourg, Institut de Génétique et de Biologie Moléculaire et Cellulaire (IGBMC), INSERM U1258, CNRS- UMR7104, Illkirch, France.
[2] Hôpitaux Universitaires de Strasbourg (HUS), Pôle de Médecine et Chirurgie Bucco-dentaires, Centre de Référence des maladies rares orales et dentaires, CRMR-O-Rares, Filière Santé Maladies rares TETE COU & European Reference Network ERN CRANIO, Strasbourg, France
[3] Université de Strasbourg, Faculté de Chirurgie Dentaire, Strasbourg, France
[4] Université de Strasbourg, Institut d'études avancées (USIAS), Strasbourg, France

***Corresponding author**
Yann Herault, Dr.
herault@igbmc.fr

SUPPLEMENTARY TABLES

	Landmarks Cranium
1	Nasale: Intersection of nasal bones, rostral point
2	Nasion: Intersection of nasal bones, caudal point
3	Bregma: intersection of frontal bones and parietal bones at midline
4	Intersection of parietal bones with anterior aspect of interparietal bone at midline
5	Intersection of interparietal bones with squamous portion of occipital bone at midline
6	Opisthion, midsagittal point on the posterior margin of the foramen magnum
7	Center of alveolar ridge over maxillary incisor, right side
8	Anterior Intersection of frontal process of maxilla with frontal bone, right side.
9	Anterior notch on frontal process lateral to infraorbital fissure, right side
10	Intersection of frontal process of maxilla with frontal and lacrimal bones, right side
11	Frontal-squasmosal intersection at temporal crest, right side
12	Intersection of zygoma (jugal) with zygomatic process of temporal, superior aspect, left side
13	Intersection of zygoma (jugal) with zygomatic process of temporal, inferior aspect, left side
14	Most posteroinferior point on the superior portion of the tympanic ring, right side

15	Center of alveolar ridge over maxillary incisor, left side
16	Anterior Intersection of frontal process of maxilla with frontal bone, left side.
17	Anterior notch on frontal process lateral to infraorbital fissure, left side
18	Intersection of frontal process of maxilla with frontal and lacrimal bones, left side
19	Frontal-squasmosal intersection at temporal crest, left side
20	Intersection of zygoma (jugal) with zygomatic process of temporal, superior aspect, right side
21	Intersection of zygoma (jugal) with zygomatic process of temporal, inferior aspect, right side
22	Most poteroinferior point on the superior portion of the tympanic ring, left side
23	Most anterior point of the anterior palatine foramen, right side
24	Most posterior point of the anterior palatine foramen, right side
25	Most infero lateral point on premaxilla-maxilla suture, right side
26	The anterior most point on the central ant/post axis of the right molar alveolus
27	Intersection of zygomatic process of maxilla with zygoma (jugal), inferior surface, right side
28	Lateral intersection of maxilla and palatine bone posterior to the third molar, right side
29	Joining of squasmosal body to zygomatic process of squasmosal, right side
30	Most inferior aspect of posterior tip of medial pterygoid process, right side
31	Most anterior point of the anterior palatine foramen, left side
32	Most posterior point of the anterior palatine foramen, left side
33	Most infero lateral point on premaxilla-maxilla suture, left side
34	The anterio most point on the central ant/post axis of the left molar alveolus
35	Intersection of zygomatic process of maxilla with zygoma (jugal), inferior surface, left side
36	Lateral intersection of maxilla and palatine bone posterior to the third molar, left side
37	Joining of squasmosal body to zygomatic process of squasmosal, left side
38	Most inferior aspect of posterior tip of medial pterygoid process, left side
39	Basion, midsagittal point on the anterior margin of the foramen magnum

Table S1: 39 cranium Landmarks.

Landmarks Mandible	
1	Apex of coronoid process, Right side
2	Intersection of molar alveolar rim and base of coronoid process, Right side
3	Anterior edge of alveolar process where first molar hits alveolus at the midline, Right side
4	Superior-most point on incisor alveolar rim at midline (at bone-tooth junctions), Right side
5	Inferior-most point on incisor alveolar rim at midline (at bone-tooth junction), Right side
6	Inferior point on mandibular symphysis, Right side
7	Anterior edge of the coalescence of curve of masseteric ridge with post-symphyseal rugged area, Right side
8	Tip of mandibular angle, Right side

9	Posterior midline point on condyle, Right side
10	Anterior midline point on condyle, Right side
11	Anterior edge of the mental foramen, Right side
12	Apex of the coronoid process, left side
13	Intersection of molar alveolar rim and base of coronoid process, left side
14	Anterior edge of alveolar process where first molar hits alveolus at the midline, left side
15	Superior-most point on incisor alveolar rim at midline (at bone-tooth junctions), left side
16	Inferior-most point on incisor alveolar rim at midline (at bone-tooth junction), left side
17	Inferior point on mandibular symphysis, left side
18	Anterior edge of the coalescence of curve of masseteric ridge with post-symphyseal rugged area, left side
19	Tip of mandibular angle, left side
20	Posterior midline point on condyle, left side
21	Anterior midline point on condyle, left side
22	Anterior edge of the mental foramen, left side

Table S2: 22 mandible Landmarks.

SUPPLEMENTARY FIGURES

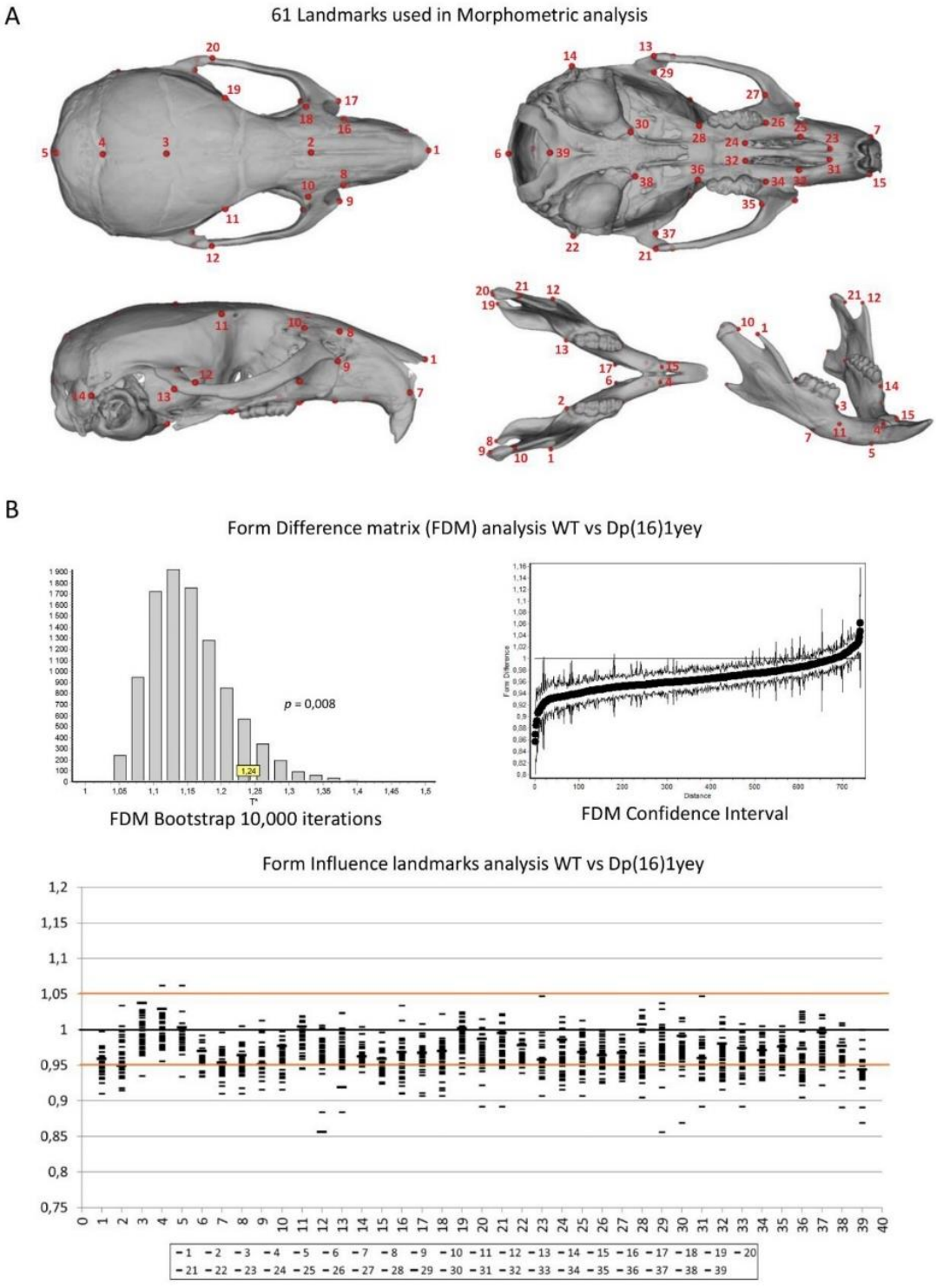

Figure S1. Landmark detailed analysis of the cranium and mandibular phenotypes in Dp(16)1Yey. **(A)** 61 Landmarks used in the CF analysis of Dp(16)1Yey (and in all the other DS models). 39 in the cranium and 22 in the mandible. **(B)** Form difference matrix analysis: FDM Bootstrap with 10,000 iterations showing significant changes in Form (p=0.008). The FDM confidence interval graph shows a decrease of more than 90% of the distances measured. Form Influence landmarks graphic,

showing the landmarks that present a relative Euclidean distance > 1.05 or < 0.95 (outside of the confidence interval 97,8%, red lines) and a general reduction of all dimensions.

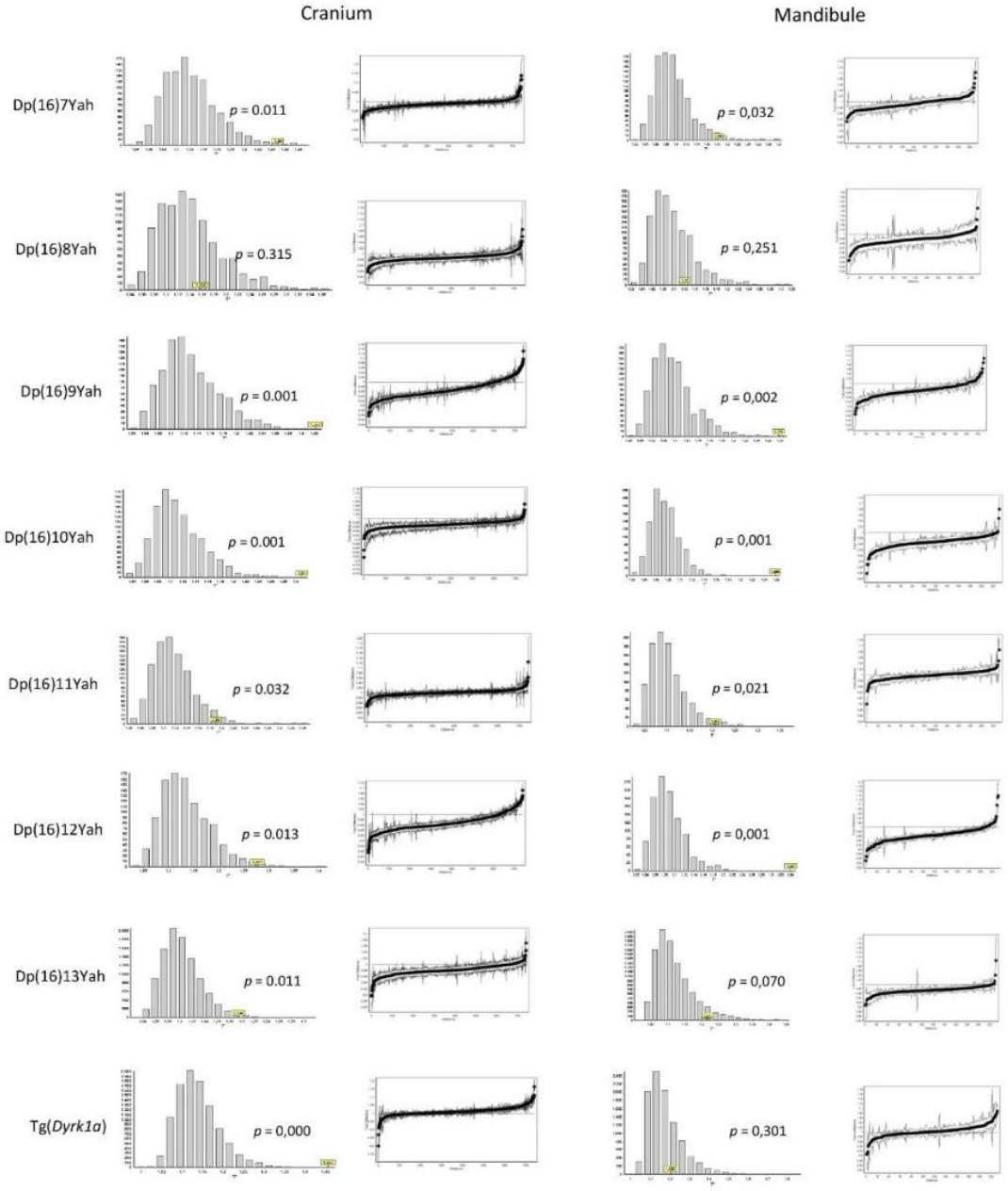

Figure S2. Form difference matrix analysis of the new panel of mouse models, plus Tg(Dyrk1a). On the left, Cranium analysis with from difference matrix (FDM) tested for with Bootstrap (graph) showing significant changes in form for all the models with form difference interval graph, except Dp(16)8Yah (p=0.315). On the right, the same graphs for the mandible show significant changes in form for all the models except Dp(16)8Yah (p=0.215). On the right, the FDM confidence interval graph shows the ratio of the distances measured.

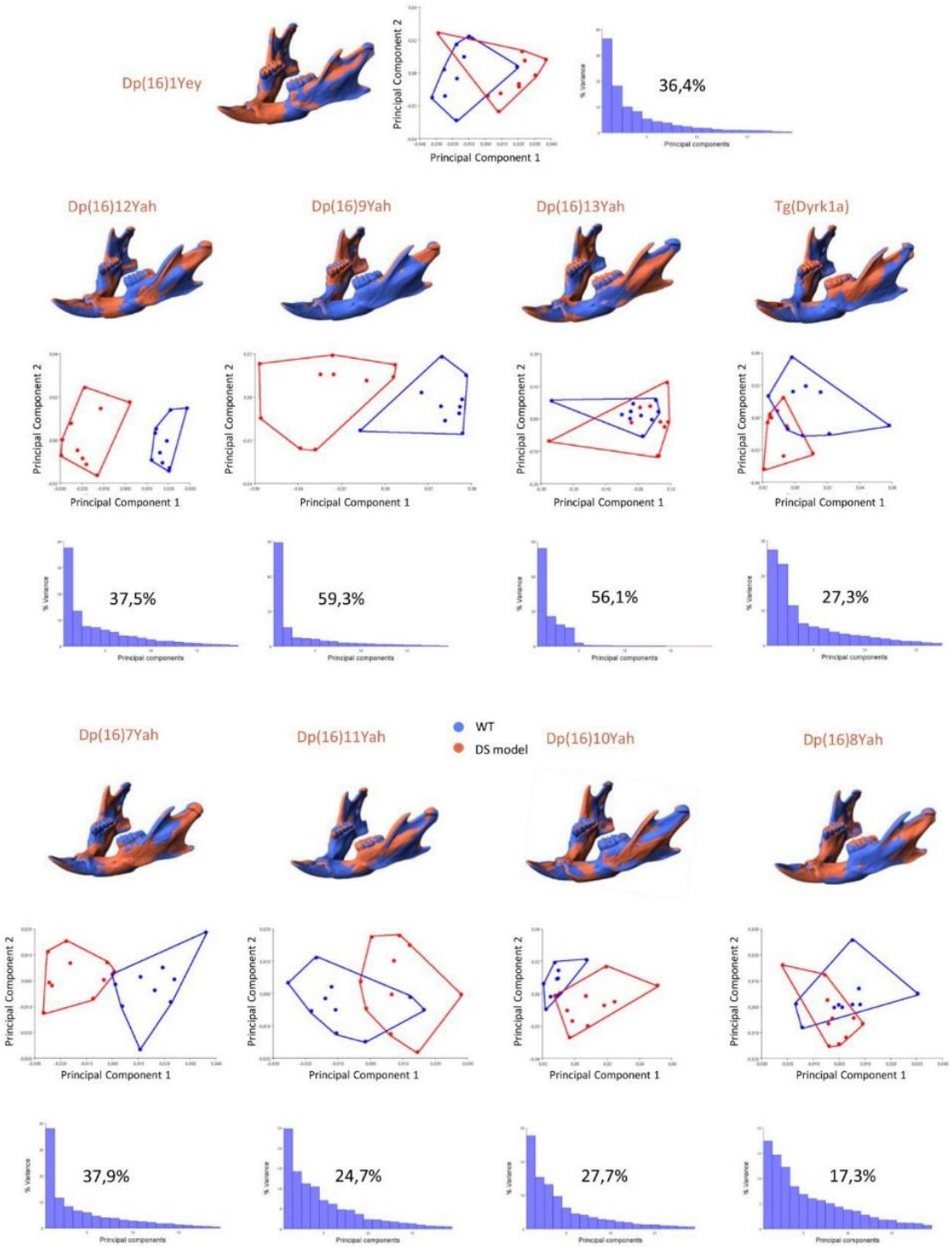

Figure S3. New DS mouse models mapping the location of dosage-sensitive genes that cause the craniofacial dysmorphology of Dp(16)1Yey (Mandibles). Morphometric analysis of the mandibles of the new panel of DS mouse models, plus Tg(Dyrk1a) and Dp(16)1yey. Shape difference warping to display the mandible parts with decreased dimensions in DS models (in blue), and with increased dimensions (in red). PCA (first two components) of general Procrustes analysis of aligned mandible shapes for every model with the contribution to the explained variance for each dimension.

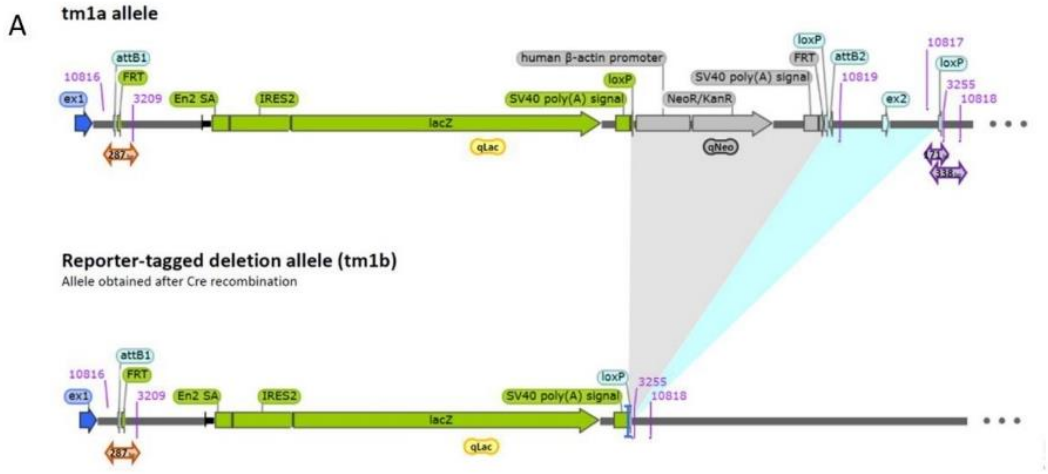

Figure S4. Schematic representation of the *Ripply3*^{tm1b} knock-out model derived from *Ripply3*^{tm1a}.

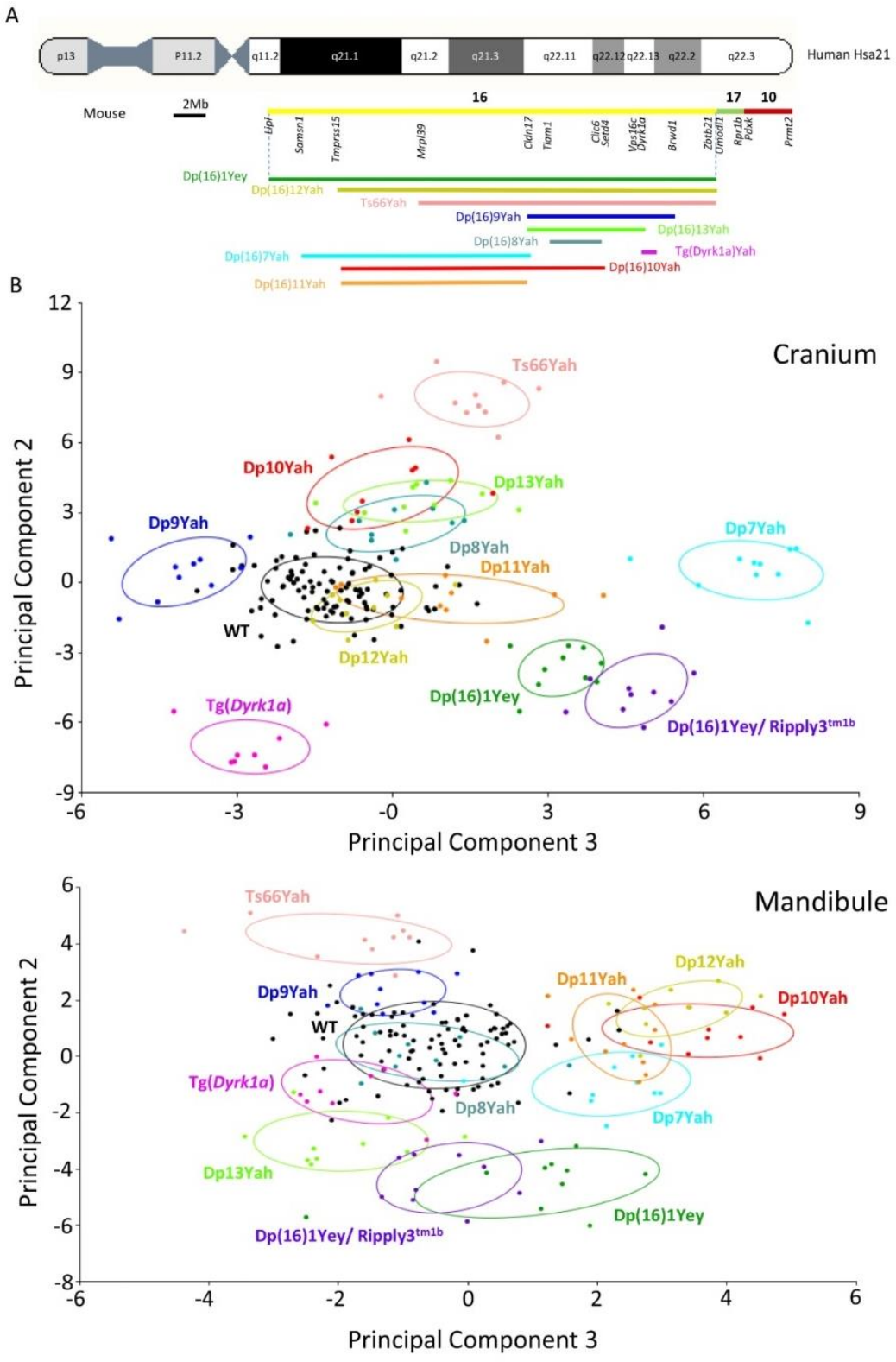

Figure S5. PC2 and PC3 projection of the CF analysis discriminate the genotypes of DS models. (A) Schematic representation of DS models and their relative position to HSA21. **(B)** PC2 and PC3 graphs for the cranium and mandible. Integrative multivariate analysis of all the models used in this study,

plus Ts66Yah, vs wild-type. The PCAs (PC2 vs PC3) correspond to a canonical variate analysis (Procrustes Distance Multiple Permutations test at 1000 iterations). DS strains show significant differences compared with their wild-type controls. DS models were separated into four main groups in the cranium graph, as in PC1, but with different distributions. For the mandible, the graph showed a primary group of 5 models close to the wild-type and two branches separated on PC2, as observed in PC1 vs PC2.

Chapter 2: New Down syndrome rat models

New Down syndrome rat models

In this second chapter, I will describe the results found in the morphometric analysis of new rat models (Figure 13). These models will make up part of two bigger publications (in preparation) to validate these models in different aspects of DS.

We studied the rat models with segmental duplication for each interval in chromosome 11 and 20, Dp(11*Lipi-Zbtb21*)Yahlcs and Dp(20*Umodl1-Prmt2*)Yahlcs, and the cross between them. We analysed also, another new rat models linked to DS and Mental Retardation autosomal Dominant 7 syndrome (MRD7), Dp(11*Dyrk1a*)6Yah and Del(11*Dyrk1a*)4Yah (Birling et al. 2017).

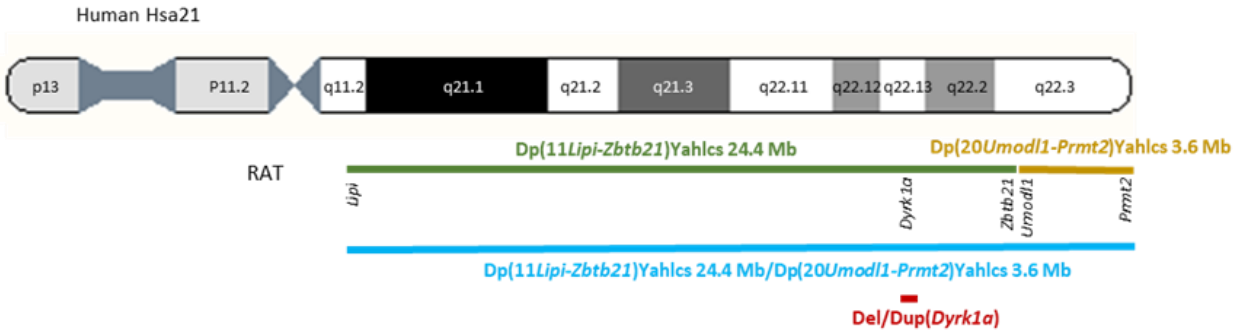

Figure 13. New rat models and their schematic position in Hsa21. In green Dup(RNO11), in Yellow Dup(RNO20), in Light Blue Dup(RNO11-20) and in Red Del(11*Dyrk1a*)4Yah and Dp(11*Dyrk1a*)6Yah noted as Del/Dup(*Dyrk1a*).

Dup(Rno11), Dup(Rno20) and Dup(Rno11-20)

Thanks to the support of the foundation Jerome Lejeune and foundation Bettencourt-Schueller, new DS rat models have been developed with segmental duplications in the chromosomes 11 and 20 (Birling et al. 2017). In the rat genome, the regions homologous to the HSA21 encompasses 213 genes found on the Rat chromosome 11 (Rno11, Rno for Rattus norvegicus) in the 24.4Mb interval between *Lipi* and *Zbtb21* and on the Rno20 for the most telomeric part of 3.6Mb between *Umodl1* and *Prmt2* (Muñiz Moreno et al. 2020). We have generated segmental duplication for each interval, Dp(11*Lipi-Zbtb21*)Yahlcs and Dp(20*Umodl1-Prmt2*)Yahlcs, named here Dup(Rno11), Dup(Rno20) and Dup(Rno11-20).

The results presented below focus only on the morphometric craniofacial analysis of these models, using the same morphometric analysis method presented in Chapter 1. These results will be added in a larger scale publication for their validation as new models of Down syndrome.

Euclidean Distance Matrix Analysis (EDMA)

We performed morphometrics analysis (Hallgrimsson et al. 2015) with a landmark-based method (Lele et Richtsmeier 1991; Lele et Richtsmeier 2001), in three rat models with the following different genotypes: Dup(RNO11), Dup(RNO20) and the last with both duplications Dup(RNO11-20), versus their control wild-type (WT) littermates. n = 120, 60 females and 60 males 14-week-old. We manually placed 61 landmarks, 39 in the cranium and 22 in the mandible to obtain 3D coordinates of each sample.

Significant changes in FDM and SDM were found in the models carrying a duplication of the chromosome 11, this can be understood as the presence of a smaller cranium and mandible (microcephaly). Dup(Rno20) doesn't present significant changes (Figure 14). The Influence landmark analysis showed that in Dup(Rno11), the most influent landmarks corresponded to the ones in maxillary bones, temporal bones (with the squamosal portion) and mandible, while in addition to those changes, landmarks located in premaxilla and frontal bones were also influent in the model with both duplications Dup(Rno11-20) (Figure 15).

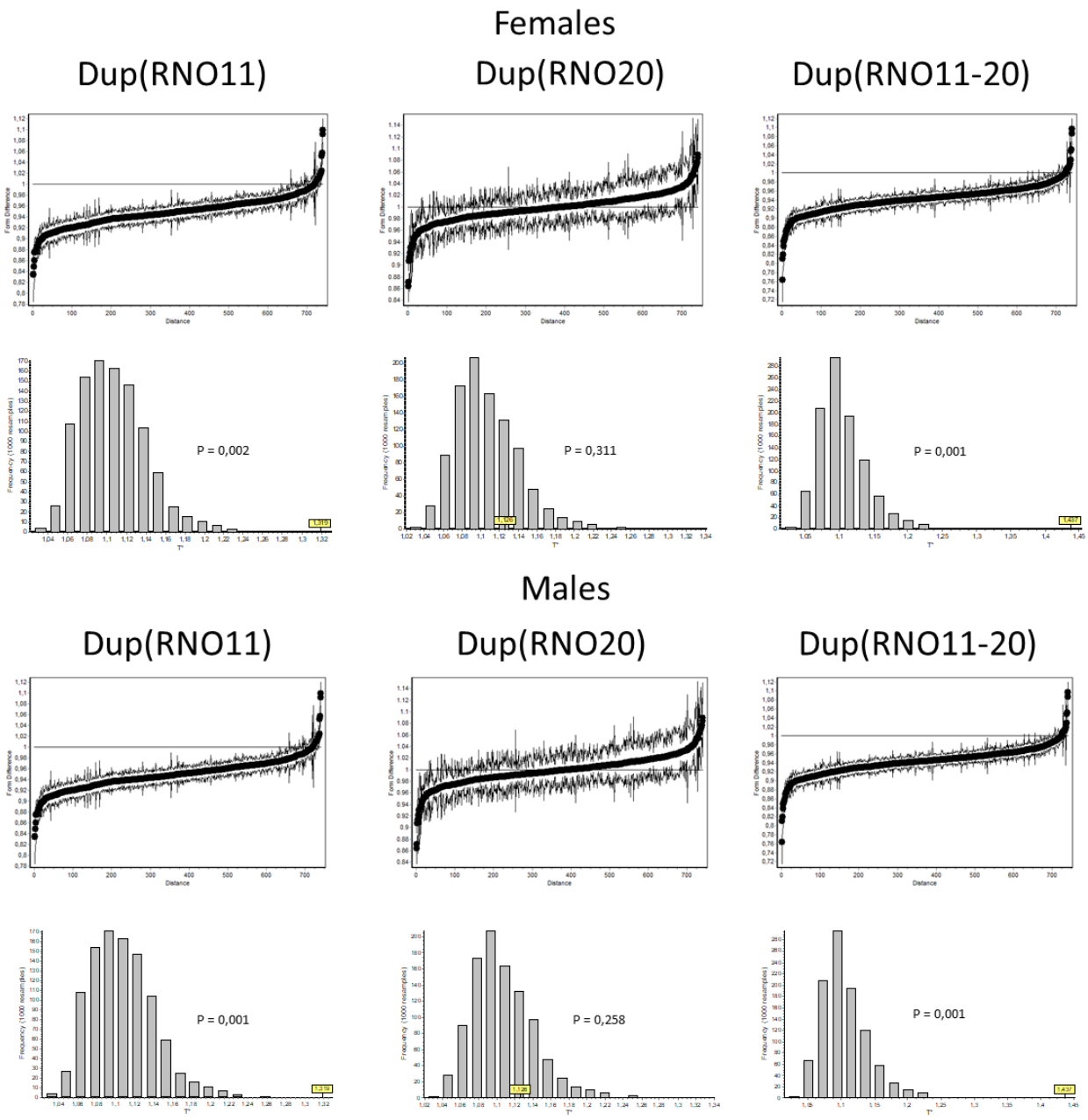

Figure 14. FDM Dp(11Lipi-Zbtb21)Yahlcs [Dp(Rno11)], Dp(20Umodl1-Prmt2)Yahlcs [Dp(Rno20)] and Dp(11Lipi-Zbtb21)Yahlcs/Dp(20Umodl1-Prmt2)Yahlcs [Dup(Rno11-20)] lines, females and males. Females, confidence interval showing a decrease of the ratio in Dup(Rno11) and Dup(Rno11-20). Bootstrap distribution, showing significant differences in Dup(Rno11) (***, p>0.002) and Dup(Rno11-20) (***, p>0.001). Males, confidence interval showing a decrease of the ratio in Dup(Rno11) and Dup(Rno11-20). Bootstrap distribution showing significant differences in Dup(Rno11) (***, p>0.001) and Dup(Rno11-20) (***, p>0.001).

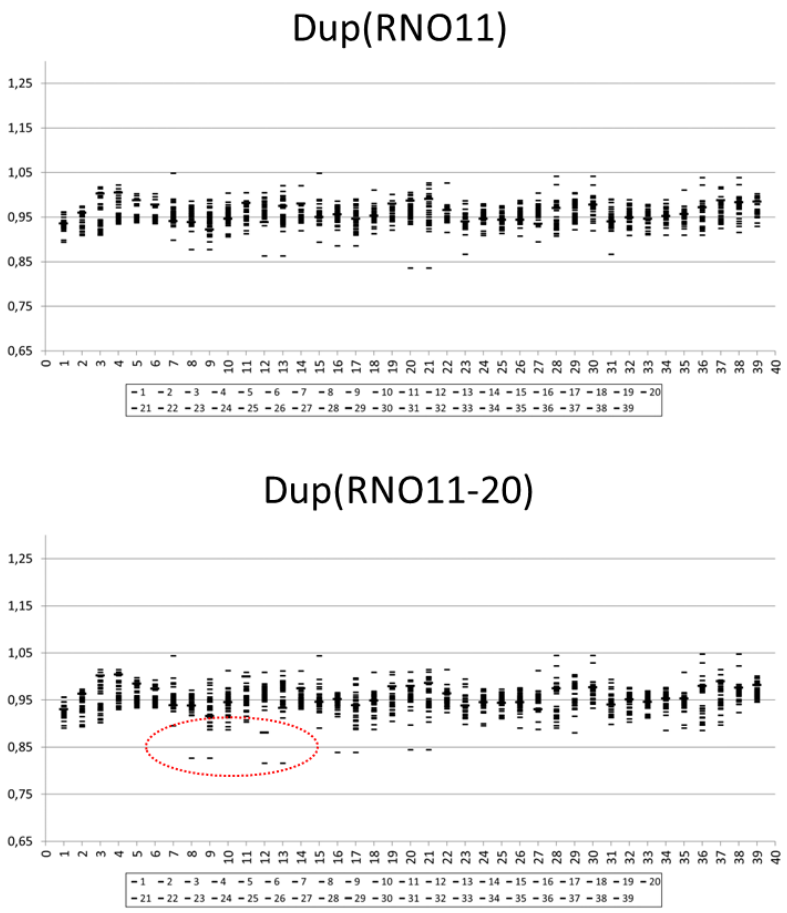

Figure 15. Influence landmarks analysis Dup(Rno11) and Dup(Rno11-20). Landmarks with a relative Euclidean distance (RED) > 1.05 or < 0.95 (confidence interval 97,8%). Red circle, extra landmarks associated to the double duplication [Dup(Rno11-20)], located in premaxilla and frontal bones.

General Procrustes and Principal component analysis

For a more detailed investigation of the patterns of displacements of landmarks and their dimensionality, we used principal component analysis PCA. In skull and mandible, PCA between WT and Dup (RNO20) does not show significant differences. However, concerning Dup(RNO11) and Dup(RNO11-20) a significant difference in PC1 versus the WT group was observed, with a variance between 30-50% (Figure 16). Same findings in mandibles, with a variance around 30% (Figure 17).

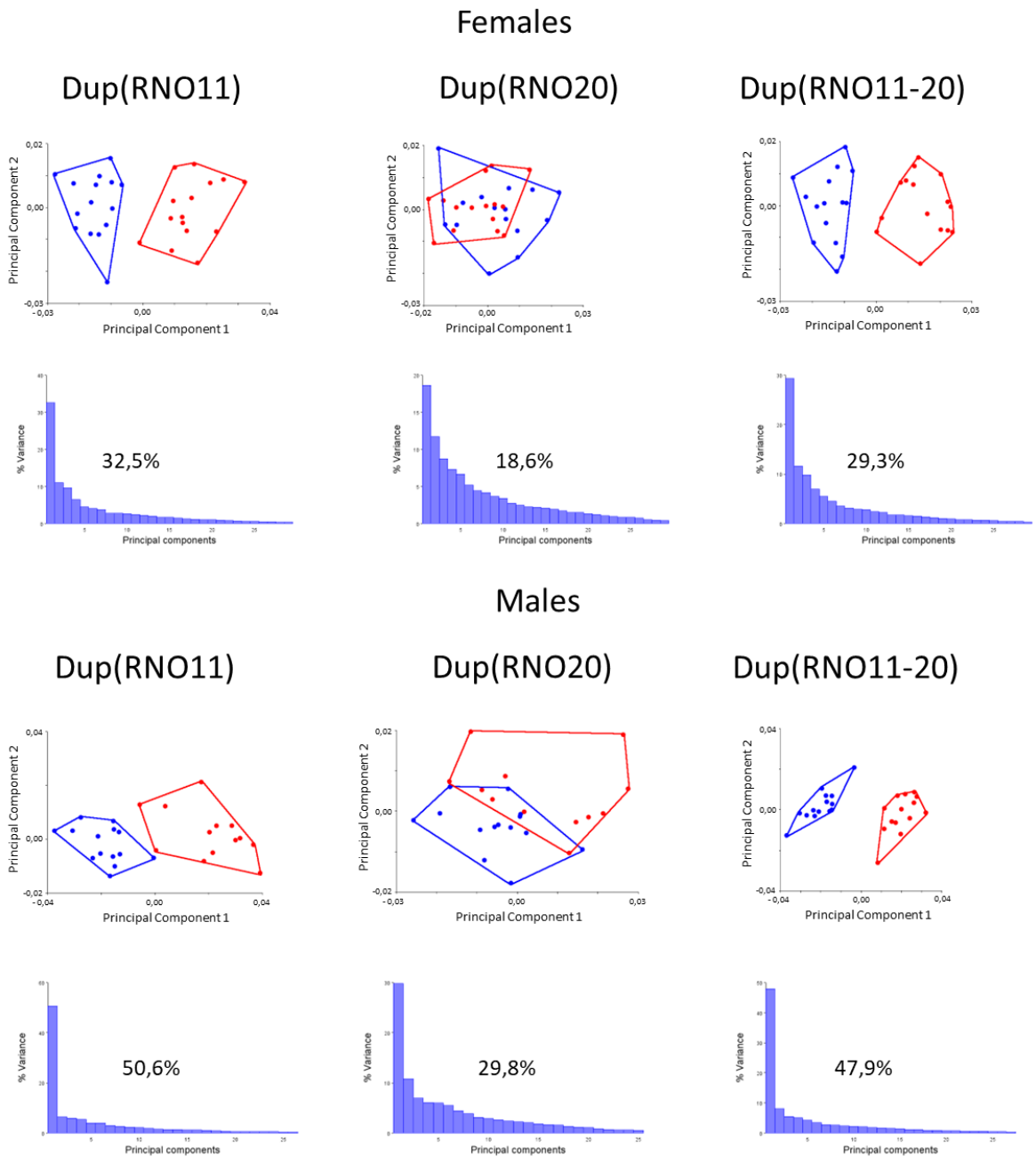

Figure 16. Cranium Principal component analysis of Dup(Rno11), Dup(Rno20) and Dup(Rno11-20) lines. For females and males, PCA and percentage of variance graphics. PCA, in Blue WT controls, in Red DS models. The distribution shows no difference between WT and Dup(Rno20) and significant differences in Dup(Rno11) and Dup(Rno11-20).

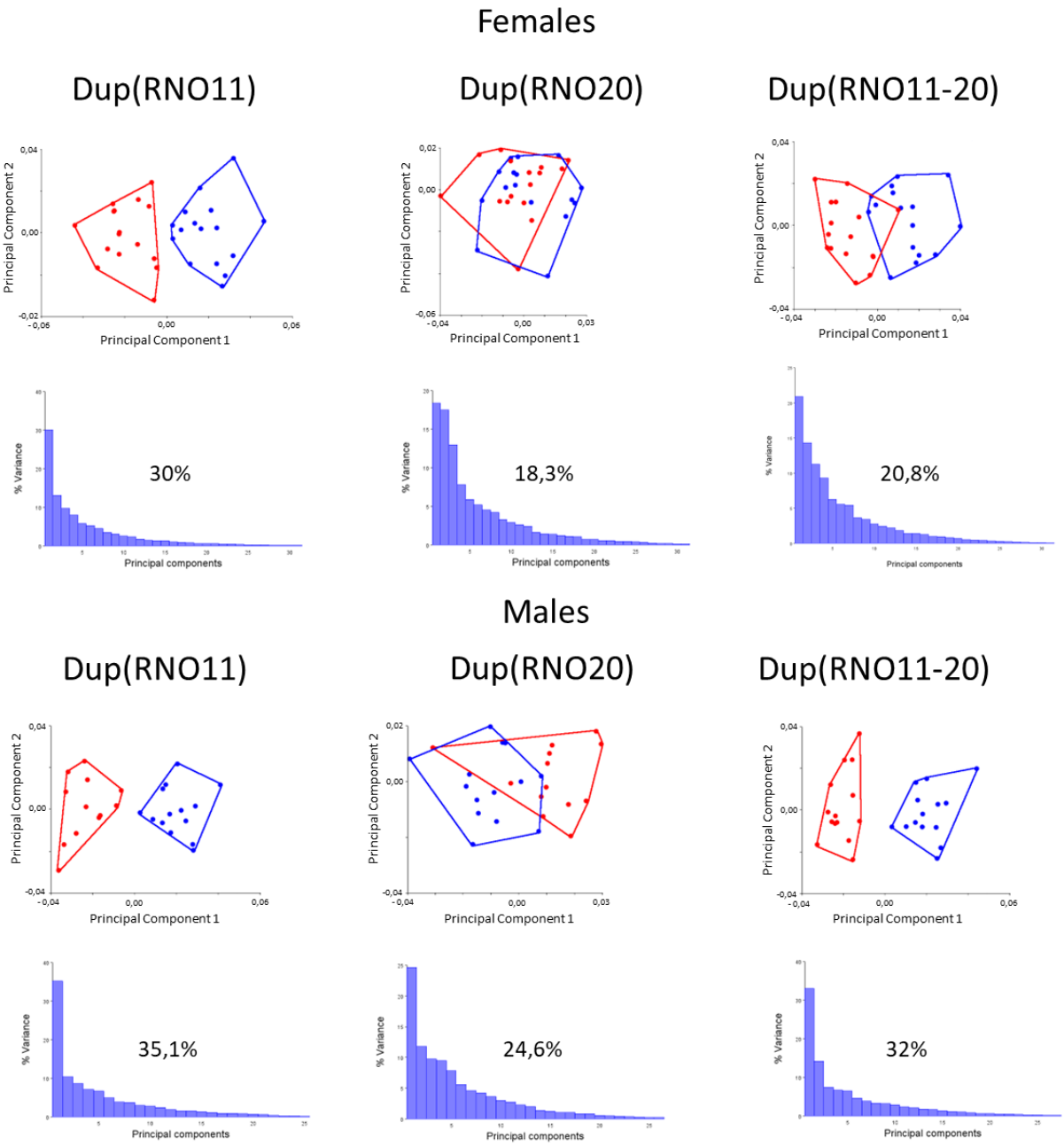

Figure 17. Mandibles Principal component analysis of Dup(Rno11), Dup(Rno20) and Dup(Rno11-20) lines. For females and males, PCA and percentage of variance graphics. PCA, in Blue WT controls, in Red DS model. The distribution shows no difference between WT and Dup(Rno20) and significant differences in Dup(Rno11) and Dup(Rno11-20).

Voxel analysis

The voxel analysis of average population models revealed the shape differences and affected bones. The models that are carrying the duplication of the chromosome 11, present dysmorphic traits such as microcephaly, small midface, smaller mandibles and brachycephaly, but also an effect of the dosage of the Rno20 region is reinforcing the phenotypes, outcome also found in the other DS phenotypes (Figure 18). In the case of the mandible, we found a decrease in the width of the ramus, body, incisor alveolus, molar alveolus and dimension in coronoid and condylar process (Figure 19).

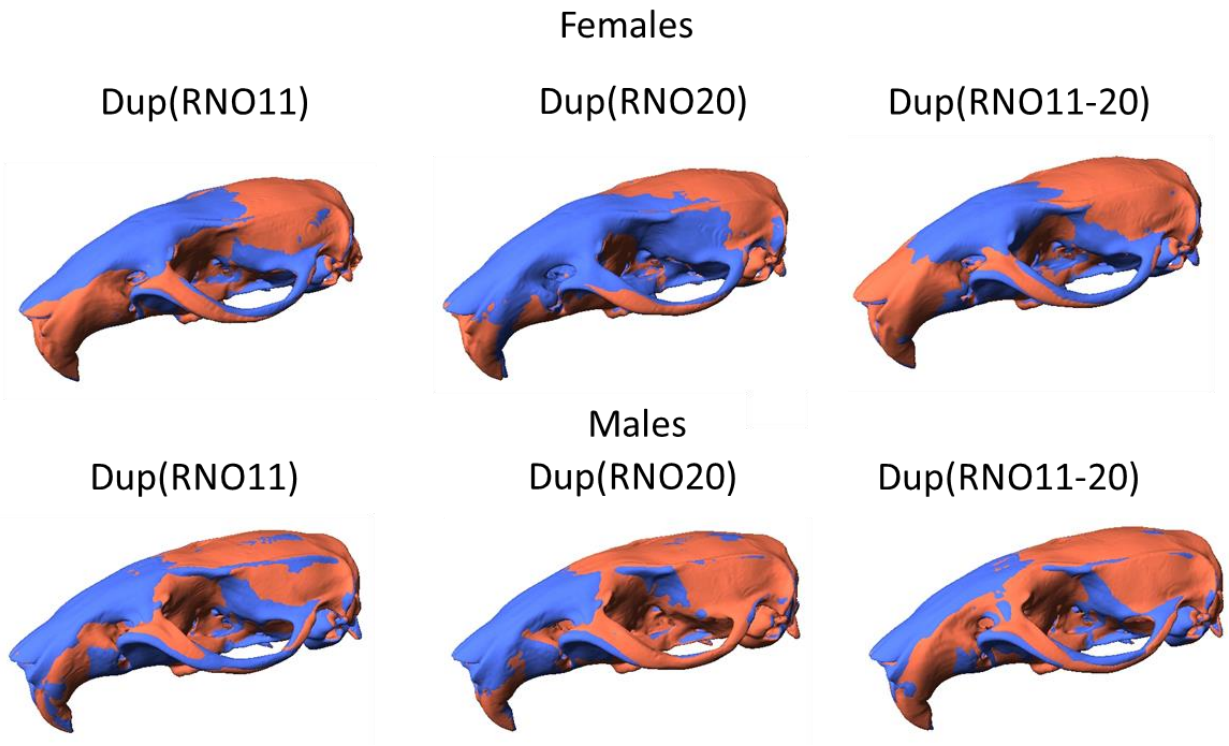

Figure 18. Cranium Voxel analysis of Dup(Rno11), Dup(Rno20) and Dup(Rno11-20) lines. In Blue WT controls. In Red DS models. Voxel shape difference analysis of using average population models. In the models Dup(Rno11) and Dup(Rno11-20) in both sexes, is possible to observe significant changes, showing a decrease in the dimension related to the midface and an increase in the dimensions related to the cranial vault. The changes observed in Dup(Rno20) are not statistically significant.

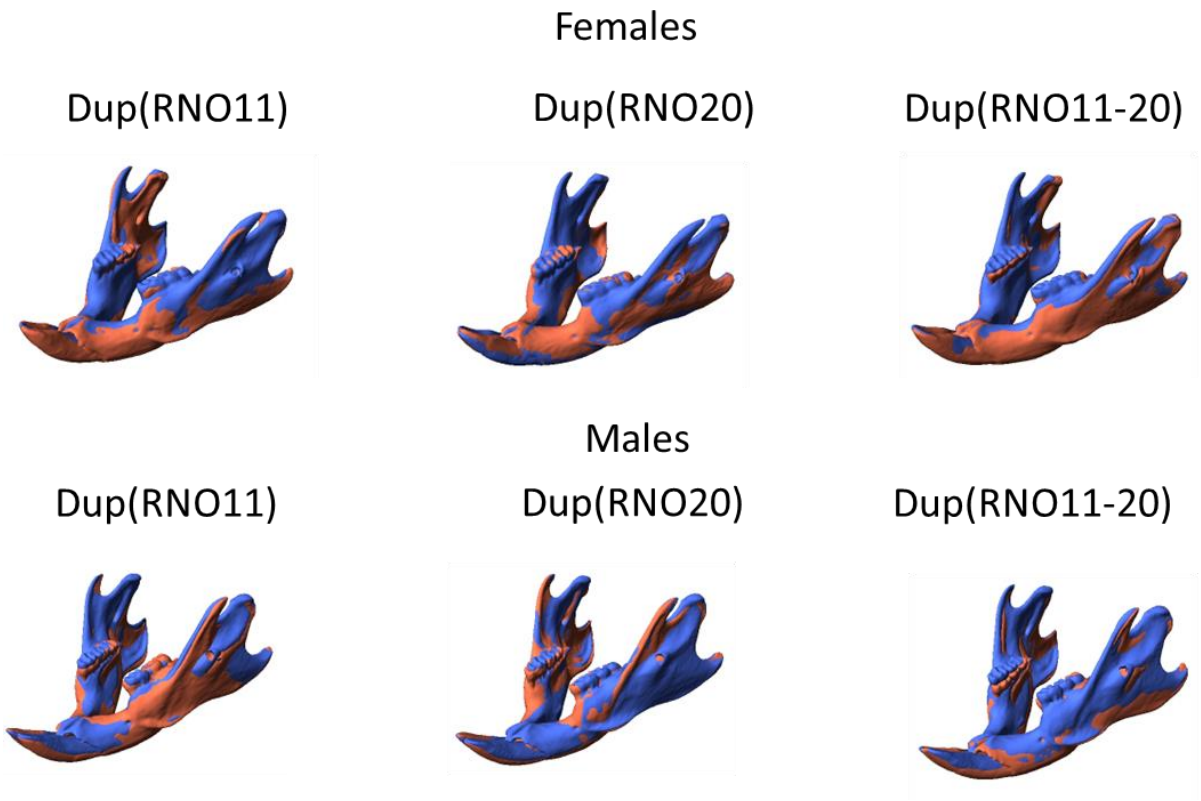

Figure 19. Mandibles Voxel analysis of Dup(Rno11), Dup(Rno20) and Dup(Rno11-20) lines. In Blue WT controls. In Red DS models. Voxel shape difference analysis of using average population models. In Dup(Rno11) and Dup(Rno11-20) models in both sexes, is possible to observe significant changes, showing a decrease in the anteroposterior dimension and less width in ramus, body, coronoid process and condylar process. The changes observed in Dup(Rno20) are not statistically significant.

Integrative multivariate analysis

We performed an integrative multivariate analysis of the craniofacial phenotypes, using the Procrustes distance multiple permutations test at 10.000 iterations in MorphoJ software (Klingenberg 2011). This with the aim of visualizing the statistical significance of shape differences and distribution of the different DS models vs the WT controls. The results show the existence of two well defined groups, one with Dup(Rno11) and Dup(Rno11-20), that correspond to the models with the most significant changes and DS-like phenotype (% of variance 91,5% in PC1). On the contrary, we discovered a second group that had no significant alterations and included Dup(Rno20) and WT controls. These results can be observed in Figure 20.

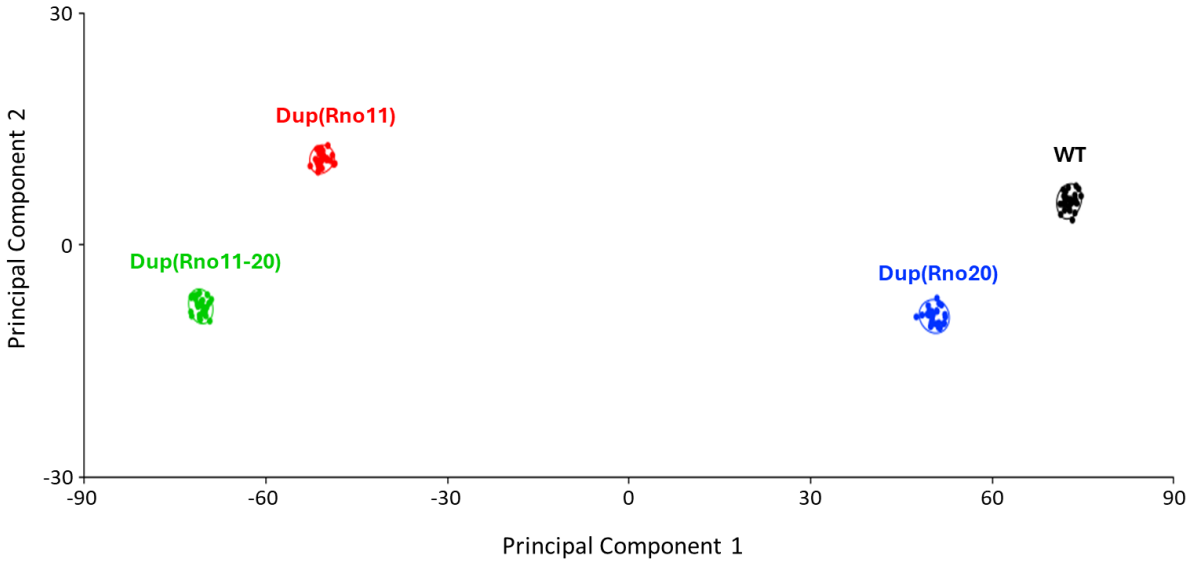

Figure 20. Integrative multivariate analysis of Dup(Rno11-20) lines. In Black WT controls, in Red Dup(Rno11), in Blue Dup(Rno20) and in green Dup(Rno11-20). The samples are distributed in two mains groups in PC1. Dup(Rno11) + Dup(Rno11-20) and WT + Dup(Rno20). It is possible to observe that there is no difference related to sex between genotypes.

The discussion of these results can be found in the "Discussion, conclusion and perspectives" section of this thesis manuscript, on page 155.

Del(11*Dyrk1a*)4Yah and Dp(11*Dyrk1a*)6Yah

Dyrk1a is an important candidate gene for the development of the DS-CF phenotype (Redhead et al. 2023; Johnson et al. 2024), therefore, we analyzed two new rat models, one linked to DS and the other to the Autosomal Dominant Mental Retardation 7 (MDR7). The first with a duplication of *Dyrk1a* [Dp(11*Dyrk1a*)6Yah] and the second with a deletion of *Dyrk1a* [Del(11*Dyrk1a*)4Yah]. These models were generated using the "CRISpr-Mediated Rearrangement mechanism" (CRISMERE) strategy. For Del(11*Dyrk1a*)4Yah pairs of gRNA located around position 34,842,454-34,963,976 of chr11 (rat genome RGSC 6.0/rn6) for an interval of 121.7 kb were used. For Dp(11*Dyrk1a*)6Yah two other sgRNA pairs (upstream and downstream of *Dyrk1a*) were used to duplicate a 219 kb region containing the entire genetic region located between *Dscr3* and *Kcnj6* with the interval at position chr11:34,791,993-35,011,015 (Birling et al. 2017).

Using the same morphometric approach as the previous models, craniofacial analysis was performed. These results are detailed below in the publication in preparation titled "Changes in *DYRK1A* copy number in rat models induce phenotypes related to Mental retardation disease 7 and Down syndrome."

A more detailed discussion of these results can be found in the "Discussion, conclusion and perspectives" section of this thesis manuscript, on page 155.

Changes in *DYRK1A* copy number in rat models induce phenotypes related to Mental retardation disease 7 and Down syndrome.

Helin Atas-Özcan[1], Damien Maréchal[2], José Tomás Ahumada Saavedra[1], Michel Roux[1], Maria del Mar Muniz Moreno[1], Julien Dairou[3], Marie-Christine Birling[4], Véronique Brault[1], Yann Hérault[1,4]

[1]Institut de Génétique Biologie Moléculaire et Cellulaire, Translational Medicine and Neurogenetics program, IGBMC, CNRS, INSERM, Université de Strasbourg, UMR7104, UMR964, 1 rue Laurent Fries, 67404 Illkirch, France.

[2]Neuroscience Initiative, Advanced Science Research Center, CUNY, New York City, New York, USA.

[3]UMR 8601 CNRS, Laboratoire de Chimie et Biochimie Pharmacologiques et Toxicologiques, Université Paris Descartes-Sorbonne Paris Cité, 75270, Paris, France.

[4] Institut Clinique de la Souris (ICS), CELPHEDIA, PHENOMIN, CNRS, INSERM, University of Strasbourg, 1 rue Laurent Fries, F-67404 Illkirch-Graffenstaden, France.

Institut de Génétique et de Biologie Moléculaire et Cellulaire, Illkirch, France.

***Corresponding author:** Yann Hérault

Institut de Génétique Biologie Moléculaire et Cellulaire, Translational medicine and Neuroscience program, IGBMC, CNRS, INSERM, Université de Strasbourg, UMR7104, U964, 1 rue Laurent Fries, 67404 Illkirch, France.

Tel: +33 388655657

Fax: +33 238 25 5450

Email: herault@igbmc.fr

Keywords: Mental Retardation autosomal Dominant 7, Down syndrome, DYRK1A, mental retardation, rat model.

ABSTRACT (229 words)

The *DYRK1A* gene, part of the DYRK family, plays a critical role in neurodevelopment and cognitive function. It is involved in various biological processes, including cell cycle regulation, neuronal differentiation, and synaptic signalling. Alterations in DYRK1A dosage are linked to several neurological disorders, including Down syndrome (DS) and autosomal dominant mental retardation 7 (MRD7). DYRK1A haploinsufficiency, as seen in MRD7, causes cognitive deficits, microcephaly, and autism spectrum disorders. Overexpression, associated with DS, leads to intellectual disability and synaptic plasticity defects.

Mouse models have been pivotal in understanding the role of DYRK1A, showing that both overdosage and deletion result in cognitive impairments. However, results from these models have had limited translation to human treatments. Recently developed rat models with either deletion or duplication of DYRK1A offer new insights. Rats, with their physiology and behaviour closer to humans, display phenotypes that better reflect human conditions. *Dyrk1a* haploinsufficient rats mirror features of MRD7, such as hypoactivity and memory impairments. Conversely, rats with *Dyrk1a* overexpression show defects in short-term memory and spatial learning, reflecting aspects of DS. These models provide a better platform for studying cognitive deficits and testing therapeutic approaches, including DYRK1A inhibitors. The findings suggest that *DYRK1A* dosage affects synaptic signalling pathways and cognition, offering the potential for targeted therapies in DS and MRD7. The use of rats complements existing mouse models, enhancing the relevance of preclinical studies to human conditions.

Introduction

The Dual-specificity tyrosine-regulated kinases 1A (DYRK1A) is one member of the mammalian DYRK subfamily belonging to the CMCG kinase group which are highly conserved among organisms. DYRK1A kinase, like other DYRK family members, catalyzes its autophosphorylation – on tyrosine residue localized in the kinase domain (Tyr321) – and the phosphorylation of serine/threonine residues on exogenous substrates (Leder et al. 1999; Himpel et al. 2001; Soundararajan et al. 2013). Many proteins involved in various signaling pathways are interacting or phosphorylated by DYRK1A (Duchon et Herault 2016; Atas-Ozcan et al. 2021). As such, DYRK1A is involved in many biological processes such as the cell cycle, differentiation and

arborization of neuronal cells, vesicle trafficking and neurotransmission (Hämmerle et al. 2011; Park et al. 2012; Grau et al. 2014; Soppa et al. 2014; Ori-McKenney et al. 2016; Dang et al. 2018).

The importance of DYRK1A dosage was first demonstrated in Drosophila melanogaster by studying the homologous minibrain gene (*mnb*). Indeed, the mutation *mnb* leads to a decrease in the production of neuroblastic cells resulting in the volume increases of the adult optic lobes and central brain hemispheres (Tejedor et al. 1995). The essential role of DYRK1A which is further demonstrated by the generation of a knock-out mouse model for *Dyrk1a*, *Dyrk1a*$^{+/-}$ animals presents a 30% decrease in brain size compared to control mice as well as cognitive deficits in recognition memory and spatial learning memory, and hypoactivity (Vassiliki Fotaki et al. 2002; V. Fotaki et al. 2004; Arqué et al. 2008). While *Dyrk1a*$^{+/-}$ mice show a reduction in viability, homozygous *Dyrk1a*$^{-/-}$ mice die during organogenesis (Vassiliki Fotaki et al. 2002). In humans, haploinsufficiency of DYRK1A was found associated with " Mental Retardation autosomal Dominant 7" syndrome, hereafter MRD7 (Møller, Rubolini, et Lehikoinen 2008; Courraud et al. 2021). This syndrome is characterized by microcephaly, mental retardation, impaired language development, epilepsy, anxiety behavior problems, and autism spectrum disorder (Bronicki et al. 2015; Earl et al. 2017; Ji et al. 2015; Luco et al. 2016; van Bon et al. 2011; Courraud et al. 2021). Phenotypes observed by DYRK1A haploinsufficiency in MRD7 highlight the crucial role of DYRK1A in a dose-dependent manner in neurocognitive development.

In human, the *DYRK1A* gene is located on the long arm of chromosome 21 (Hsa21) at 21q22.13 and extends over about 150 kb. The overdosage of DYRK1A was linked to some of the phenotypes observed in Down syndrome (DS), like cognitive impairments, due to the trisomy of Hsa21 (X. Altafaj et al. 2001; Ahn et al. 2006; Souchet et al. 2014). In mouse, the *Dyrk1a* gene maps to chromosome 16, in the syntenic region to the Hsa21 (Song, Chung, et Kurnit 1997). The Dp(16)1Yey mouse model which presents a trisomy of the Mmu16 syntenic region to Hsa21, has a delay in learning abilities, a deficit in spatial memory, an alteration of memory associated with context, an alteration of working memory and object recognition memory (Li et al. 2007; Duchon et al. 2021). These mice exhibit synaptic plasticity defects with decreased long-term potentiation (Yu et al. 2010). Transgenic mice with three copies of murin *Dyrk1a* highlight the role of *Dyrk1a* in causing the cognitive deficit observed in DS. Indeed, this mouse model presents a deficit in working memory as well as impaired learning and long-term spatial

memory and cognitive flexibility evaluated in the Morris water maze (MWM) test (Souchet et al. 2014). In addition, an increase of dendritic spines density in the cortex leading to disturbances in the synaptic activity of the prefrontal cortex of *Dyrk1a* transgenic mice are pointed out (Thomazeau et al. 2014). Furthermore, the normalization of gene *Dyrk1a* dosage in the brain of DS mice allows the correction of cognitive deficit (Xavier Altafaj et al. 2013; García-Cerro et al. 2017; Brault et al. 2021). Rescue of cognitive functions is also observed after DYRK1A kinase activity normalization using pharmacologic inhibitors on DS mouse models (Souchet et al. 2014; Nguyen et al. 2018). These results reflect the major role played by DYRK1A gene dosage and in particular its kinase activity which can be used for therapeutical purposes in improving cognitive functions of people with DS

Mouse models have been crucial for deciphering basic biological mechanisms that underlie DS and MRD7 syndromes. However, treatment protocols targeting the overdosage of DYRK1A and successfully tested on those models, had more mitigated results in human (Cieuta-Walti et al. 2022). As an alternative to mice, rats have several advantages such as its physiology and behavior closer to human. Rats are also more social; they show higher levels of strategy and more stable performance in cognitive tests, making them a better model for translation to humans and increasing the relevance of preclinical studies. All the knowledge accumulated using various mouse models highlights the importance of *Dyrk1a* dosage in cognitive deficits associated with MRD7 and DS. However, the use of different animal models would allow a better translation to humans to further understand the disturbed mechanisms and the development of therapeutic strategies. Another animal model often used is the rat which has many advantages over the mouse model. Indeed, the genetics, physiology, and behavior of rats are closer to humans. Rats' behavior and in particular their sociability are closer to humans, the rat is therefore a solid model for studying intellectual disability syndromes such as DS and MRD7 (Drummond et Wisniewski 2017; Do Carmo et Cuello 2013). However, rat models were not used until the last years because of the lack of a genetic manipulation system, but the discovery of CRISPR/Cas9 genome editing strategy allows the generation of desired genetic mutations (Jinek et al. 2012).

Here we report new rat models with either a deletion or a duplication of the *Dyrk1a* gene to complement the studies already done in mouse models. The phenotypic effects of the deletion or the duplication of *Dyrk1a* in rats will be presented, providing evidence on the importance of *Dyrk1a* gene dosage in the onset of cognitive deficits as observed in DS and MRD7.

Materials and methods

Animals

The Del(11*Dyrk1a*)4Yah, Dp(11*Dyrk1a*)5Yah, Dp(11*Dyrk1a*)6Yah rat lines, (noted also Del4, Dp5 and Dp6 here), were generated in the Sprague Dawley outbred background with the CRISpr-Mediated Rearrangement (CRISMERE) strategy (Birling et al. 2017). The Del4 and Dp4 were generated with pairs of gRNA located around chr11 position 34,842,454-34,963,976 (rat genome RGSC 6.0/rn6) for a 121.7 kb interval. Two other pairs of sgRNA, one located upstream and the other downstream of *Dyrk1a*, were used to duplicate a region of 219 kb containing the whole genetic region located between *Dscr3* and *Kcnj6,* but not containing these genes, with the interval at position chr11:34,791,993-35,011,015. The sgRNA used are presented in **Table S1** and were validated in vitro using Sureguide kit (Agilent Technologies #5190-7716). Injection condition are Cas9 mRNA 50-60 ng/µL and 40-60 sgRNA ng/µL (see (Birling et al. 2017) for more information).

During the behavioral testing phase, the rats were housed in groups of two individuals in disposable plastic cages (Innocage® #R-BTM-H, Innovive, Paris, France) of dimensions 43.2x34x19.8 cm placed on ventilated racks. Rats had *ad libitum* access to water and food and were in a controlled environment with a light/dark cycle of 12 hours (light from 7:00 am to 7:00pm) and a temperature of 23±1°C. The experiments implemented in this project complied with ethical standards of the French Ministry of Agriculture (law 87 848). In addition, these projects was validated by our local ethical committee (Com'Eth, n°17) under two authorization numbers: one for the Del(*Dyrk1a*)1 and Dp(*Dyrk1a*)5 lines (APAFIS no. #31362) and the other for the Dp(*Dyrk1a*)6 line (APAFIS no. #18895).

Genotyping

For the Del(11*Dyrk1a*)4 and Dp(11*Dyrk1a*)5 lines the genotype was determined using the following protocol. DNA was extracted using the DNA Extract All Reagents kit (Applied BiosystemsTM, Thermo Fisher Scientific) using 50 µL of lysis buffer and further incubation at 95 ° C for 10 min. Then, 50 µL of neutralizing solution was added for the DNA extract. Polymerase chain reaction (PCR) reaction was done with 50 ng of DNA extract, 7.5 µL FastStart 2X PCR Master (Roche, Basel, Swiss), 100 µM primers in a total volume of 15 µL. Primers used for

Del(Dyrk1a)4genotyping were Ef[2] (5'- CTGTCGTCGAGGTGCAGCATC -3') and Wr (5'- GGGGTGATGATCAGAAACTGAGG -3') for the wild type allele and Ef (5'- GGCAAAATTCGTGAGTCAGTGACTC -3') and Er (5'- CTGCCACTCATACCCAGCACAAC -3') for the deleted allele. Primers used for Dp(11Dyrk1a)5 genotyping are Ef[2] (5'- CCTGTCGTCGAGGTGCAGCATC -3') and Er (5'- CTGCCACTCATACCCAGCACAAC -3'), these primers allow to discriminate wild type allele than the duplicated allele. The PCR reaction carried out was a thermocycler according to the following conditions: 95°C for the 4 min followed by 34 cycles of 94°C for 30s, 62°C for 30s and 72°C for 1 min and a final elongation step for 7 min at 72°C.

For Dp(11*Dyrk1a*)6 genotyping, we used another protocol in which tissue DNA was digested in 100µL of lysis buffer (Direct PCR Lysis Reagent, Viagen #102-T) with 10 µL of proteinase K 10mg/mL (#P6556-1G, Sigma-Aldrich). After incubation at 56 °C over night, the samples are moved at 95 ° C for 30 min to inactivate proteinase K. After centrifugation for 5 min at 13,000 rpm (rotations per minute), the supernatant was used for PCR with the Phusion Hot Start II High-Fidelity DNA polymerase kit (Thermo Fisher Scientific, Strasbourg, France). About 100 ng DNA is added to the Polymerase Chain Reaction (PCR) mix: 4 µL Phusion HF buffer (1x), 0.4 µL dNTP (10 mM, Thermo Scientific), 0.1 µL primers (100 µM), 0.2 µL Phusion Hot Start II polymerase (10 µM) and 14.2 µL H_2O. Primer's sequence used to detect Dp(11Dyrk1a)6allele were: F6 (5'- GACAGCAAGAAGATGAGAGTCAGG -3') and the R1 primers (5'- CCTCTGTAGGATGAGACAATAGCT -3'). The PCR reaction was first denaturation 98°C for the 30s followed by 30 cycles of 98°C for 8s, 55-65°C for 10s and 72°C for 1 min and a final elongation step for 5 min at 72°C.

All PCR products were separated by electrophoresis (30 min to 130V) according to their size on a 2% agarose gel with ethidium bromide (0.5 µM, Euromedex #EU0070). For the Del(11Dyrk1a)4 model, the deleted allele corresponds to a fragment of 234 bp, and the wild type allele has a size of 274 bp. For the Dp(Dyrk1a)5 model, a fragment of 1449 bp size is obtained for the duplicated allele and a fragment of 442 bp for the type allele. Dp(11Dyrk1a)5 model genotyping presents a fragment of 443 bp for the duplicated allele.

Quantification of gene copy number

Gene copy number quantification were performed on Del(11*Dyrk1a*)4, Dp(11*Dyrk1a*)5 and Dp(11*Dyrk1a*)6 rats using the digital droplet PCR technology (ddPCR). For the Del(11Dyrk1a)4

the analysis was performed on three individuals from the F1 generation. Similarly, we used for Dp(11Dyrk1a)5 allele, also with 3 individuals, while for Dp(11Dyrk1a)6, we used 13 individuals. DNA was extracted using the DNA Extract All Reagents kit (Applied BiosystemsTM, Thermo Fisher Scientific) from Tail samples by adding 50 µL of lysis buffer. They were then incubated at 95 ° C for 10 min. Once the biopsies werre digested, 50 µL of neutralizing solution were added. The samples were then diluted 20 times for ddPCR (Lindner et al. 2021). The PCR reaction was carried out from 2 µL of samples diluted to the twentieth, to which 10 µL of the Supermix ddPCR 2x (without dUTP, #1863024, Bio-Rad), 250 nM of the probe coupled to a fluorophore (FAM or HEX), 750 nM of the primers (Table S2 for primers and probes) were added for a final volume of 20 µL for each sample (Lindner et al. 2021). The samples prepared were fractionated into droplets using the QX200 droplet generator (Bio-Rad). The PCR reaction was performed by depositing 40 µL of the samples on a 96-well plate. The DNA contained in the droplets was amplified according to the following conditions: 95 ° C for 10 min, followed by 40 cycles from 20s to 95 ° C, followed by a hybridization gradient between 53 and 63 ° C for 1 min, then 10 min at 98 ° C for a deactivation step. The PCR products were analyzed using the QX200 reader (Bio-Rad) to measure the fluorescence intensity of each droplet. The data was analyzed with QuantasoftTM Analysis Pro software (Version 1.0.596).

Targeted gene expression analysis

For *Dscr3* and *Kcnj6* levels, PCR was realized with TaqMan® Universal Master Mix II and pre-optimized TaqMan® Gene Expression assays (Applied Biosystems, Waltham, Massachusetts, USA). mRNA expression profiles were analyzed by real-time quantitative PCR using TaqMan TM universal master mix II with UNG in a realplex II master cycler Eppendorf (Hambourg, Germany). The complete reactions were subjected to the following program of thermal cycling: 1 cycle of 2 minutes at 50°C, cycle of 10 minutes at 95°C, 40 cycles of 15 seconds at 95°C and 1 minute at 60°C. Efficiencies of the TaqMan assays were checked using cDNA dilution series from extracts of hippocampal samples. Normalization was performed by carrying out in parallel the amplification of three housekeeping genes (*Gnas, Pgk1* and *Atp5b*) coupled to the GeNorm procedure to correct the variations of the amount of source RNA in the starting material. All the samples were tested in triplicate (Lindner et al. 2021) . The analysis of *Dyrk1a* level was performed using the ddPCR technology which is more precise than classical qPCR. The experimental procedure is the same as the gene expression assay. For *Dyrk1a* primers used

were forward 5'- GCCATGGACTGTGAGACACATA -3' and reverse 5'- GCCATGGACTGTGAGACACATA -3'. The probe used for *Dyrk1a* analysis was derived from a Universal Probe Library System, which corresponds to a short hydrolysis probe (labeled at the 5' end with fluorescein (FAM) and at the 3' end with a dark quencher dye) substituted with Locked Nucleic Acids. For normalization the *Hprt* gene expression was determined with the primers: forward 5'- CCCCAAAATGGTTAAGGTTGC -3' and reverse 5'- AACAAAGTCTGGCCTGTATCC -3'. Probe used was a ZEN™ probe with double-quenched probes labelled with a specific fluorochrome (HEX): 5'- CTTGCTGGTGAAAAGGACCTCTCGAA -3'.

Protein level analysis

Hippocampal tissues were isolated by decapitation/dissection of 3-month-old rats and flash-frozen in liquid nitrogen. Samples were lysed in ice-cold sonication buffer supplemented with Complete™ Protease Inhibitor Cocktail (Roche, #11873580001). Samples were disaggregated, centrifuged at 4°C for 30 minutes at 14000 rpm, diluted in 5X loading buffer (Pierce Lane Marker Thermo Scientific™, #39001) containing β-mercaptoethanol and incubated at 95 °C for 5 min. Protein concentration was determined by Pierce™ BCA Protein Assay Kit (Thermo Fisher Scientific, #23225). Per well, 30 µg of protein was loaded onto a polyacrylamide gel composed of Tris-Glycine-SDS (25 nM Tris, 192 nM Glycine, 0.1% SDS). Proteins were transferred to nitrocellulose membranes by Trans-Blot® Turbo™ Transfer System (BioRad, France) using the MIXED MW Bio-Rad Pre-programmed Protocol. Then, blots were incubated overnight at 4°C with the blocking solution: 5% milk, 1X Tris-buffered saline, 0.1% Tween 20 (TBS-T), and incubated with primary antibody diluted in blocking solution overnight at 4°C. Blots were washed in TBS-T and incubated with 1:10.000 HRP conjugated Goat anti-mouse secondary antibody (#PO447 Dako, France, 1:10.000) diluted in blocking TBS-T for 1 hour at room temperature. Proteins were visualized with Amersham™ Imager 600 and signals were quantified using ImageJ and the statistical analysis with GraphPad. Primary antibodies used: mouse monoclonal anti-DYRK1A C-terminal (#H00001859-M01, Thermo Fisher, 1:1.000), mouse monoclonal anti-β-actin–peroxidase antibody (#A3854 Sigma, 1:150.000) and a mouse monoclonal anti-GAPDH antibody (#MA5-15738 ThermoFisher, 1:5.000). Relative amount of DYRK1A protein was measured as the ratio of the signal detected for DYRK1A compared to the β-actin or GAPDH signal detected and normalized by the mean signal of the wild type samples.

Protein kinase assay

The proteins were extracted from frozen half-brains of rats of Del(Dyrk1a) 4 and Dp(11Dyrk1a)6 models. Proteins were first extracted in the following lysis buffer: 60 mM β-glycerophosphate, 15 mM p-nitrophenyl phosphate, 25 mM Mops (pH 7.2), 15 mM EGTA, 15 mM MgCl2, 2 mM dithiothreitol, 1 mM sodium orthovanadate, 1 mM sodium fluoride, 1 mM phenyl phosphate disodium and protease inhibitors (Roche, #11873580001). The proteins were then dosed with the Pierce BCA protein assay kit (Thermo Fisher #23225). DYRK1A catalytic activity dosage was determined as described in Bui et al. (Bui et al. 2014). Assays were performed in a 96-well ELISA plate in a total volume of 50 µL consisting of kinase buffer (50 mM Tris–HCl, 10 mM DTT and 5 mM MgCl2), ATP (up to 1000 µM), FAM–peptide substrate (up to 60 µM), and brain extracts (100 µg total protein extract). Briefly, samples containing the enzyme were preincubated with peptide substrate at 37 °C for 1 min and the reaction was started by the addition of ATP. At different time points (up to 30 min), 50 µl of HClO4 (15% in water) was added to stop the reaction, and 20 µl was automatically injected into the HPLC column. The kinetic parameters for two-substrate kinetics were determined by fitting the data iteratively to the equation $V_i = V_{max}[S_A][S_B]/(K_{AB} + K_{mB}[S_B] + K_{mA}[S_B] + [S_A][S_B])$ using the program Prism 5 (GraphPad Software).

Behavioral pipeline

From the mouse work, no sex effect was detected when analyzing models for DYRK1A (Brault et al. 2021). Thus, a battery of behavioral experiments was performed only on rat males to follow the 3'R, with an age range from 9-12 weeks.

The tests were performed with three cohorts for the behavioral analysis of Del(11Dyrk1a)4. A first cohort of 15 Del(11Dyrk1a)4 rats and 15 control disomic rats was tested with: Novel Object Place (NOP) with 5 min of retention, Novel Object Preference (NOR) with 1 hour of retention, NOP with 24 hours of retention with 2 objects, social interaction and the Morris Water Maze (MWM). The second cohort of 8 Del(11Dyrk1a)4 rats and 8 control rats performed the following tests: Y-maze, circadian activity, open field, NOP with 5 min of retention and NOP with 24 hours of retention, and NOR with 3 objects. The last cohort of Del(11Dyrk1a)4 rats with 4 Del(Dyrk1a) 4 and 2 control rats realized the NOP with 5 min of retention and NOP with 24 hours of retention and 3 novel-objects. A unique cohort with 16 individuals per genotype was generated

for Dp(Dyrk1a)5 rat model and analysed for body weight, open fiel activities, NOR with 1h and 24h retention and Morris water maze .

A single cohort of Dp(11*Dyrk1a*)6 rats consisting of 15 rats trisomic for *the Dyrk1a* gene and 15 control rats was generated for phenotypic analysis: open field, NOP with 1 or 24 hours of retention and 2 objects, and MWM. Three cohorts of Dp(11*Dyrk1a*)6 rats were generated for behavioral analysis. The first two cohorts were composed of 11 rats per group and performed the following tests in the order listed: circadian activity, Y-maze, open field, NOP with 5 min retention, NOP with 24 hours of retention and 3 objects, and MWM. The third cohort was used only for the NOP test (n = 7 Dp(11*Dyrk1a*)6 and n = 7 disomic rats).

The behavioral tests are presented in the order in which they were carried out. Behavioral experimenters were blinded concerning the genotype of rats. On each day of the test, rats were transferred to the experimental room 30 min before the beginning of the experiment. All experiments were realized between 8:00 am and 4:00 pm except for the circadian activity test, which was for 46 hours (start at 11:00 am).

To assay the general locomotor and circadian activity, rats were housed in individual activity cages from 11:00 am for 46 hours (22 hours for light and 24 hours for dark phase) with water and food *ab libitum*. Locomotor activity cages (Tecniplast™) are transparent with dimensions of 33x20x19cm and placed in a sound-attenuated chamber. The device comprises 4 bars of infrared sensors for each cage, allowing it to record locomotor activity and the number of rears. The device is connected to a computer that extracts different variables using the POLY_PLUS software (Imetronic®, Marcheprime, France). The activity was evaluated in intervals of 1 hour, the first 3 hours of the test corresponding to the habituation phase.

Short-term memory was measured by recording spontaneous alternation in the Y-maze test (Kraeuter, Guest, et Sarnyai 2019). The spontaneous alternation behavior (SAB) evaluates the preference of animals to explore an arm that has not been previously explored at a frequency superior to 50%. The maze, which has a Y shape, was made of three plastic arms, each with a different pattern to encourage SAB. Animals were placed in one arm, facing away the wall of the arm and arms were cleaned between each rat with 50° ethanol. The starting arm was alternated randomly for each rat to prevent bias. Animals were allowed to explore arms during 8 minutes under moderate light (15 lux in the center region). The latency to leave the starting arm, the total entries and the number of SAB were recorded. The sequence of entries in the 3 arms was recorded, considering the rat entered an arm when all four paws were inside the arm.

Alternation was quantified, and one alternation corresponded to successive entries of the three different arms. The number of alternations was then divided by the number of alternation opportunities namely corresponding to total arm entries minus one.

Open field (OF) was used to assay locomotor activity, anxiety and exploratory behavior of rats. This test was done in an open square with opaque black walls of dimensions 90x90x40cm, and the light intensity is set to 15 lux in the center of the OF. Rats' movement and rears were recorded by infrared beams during a session of 30min using the POLY_OPENFIELD software. After each trial, arena was cleaned with 50° ethanol to minimize olfactory cues. Speed and distance traveled were analyzed during 3-time sequences (0 to 10 min; 10 to 20 min and 20 to 30 min). We also recorded the time spent in each arena zone (center and peripheral).

Short-term spatial memory was assessed using the Novel Object Place Preference (NOP) task. This test is based in the innate tendency of rodents to spend more time exploring an object moved than another which was not moved (Ennaceur, Neave, et Aggleton 1997). This test was performed in two days: the first day corresponds to the habituation to the open field in which an allothetic symbol is placed (15 min of habituation). During the second day, two identical objects were presented to the rat during 3min; at the end of the presentation time, the animal returned to his cage after 5 minutes of retention. One of the objects was moved to a new position, and the rat was allowed to explore freely the objects for 3 min. The object moved was randomized between each rat to avoid location preference. Once the test phase was over, the arena and objects were cleaned with 50° ethanol before going to the next rat. Object exploration was manually scored and defined as the orientation of the nose to the object to a distance less than or equal to 2 cm. The percentage of time exploring the novel position vs the familiar position was calculated to assess spatial memory performance.

The Novel object recognition (NOR) test allows the assessment of the recognition memory. It is based on the innate tendency of rodents to explore novel objects over familiar ones (Ennaceur et Delacour 1988). This test was done in three steps in the same open field as the NOP task. Different protocols of NOR were used for rat models characterization, with different retention times and different objects number used: NOP with two objects and 1 hour of retention for Dp(11*Dyrk1a*)5 rats, NOR with two objects and 24 hours of retention for Del(*Dyrk1a*)4 and Dp(11*Dyrk1a*)5 rats and NOR with three objects and 24 hours of retention for Del(*Dyrk1a*)4 and Dp(11*Dyrk1a*)6 rats. In the first step, rats were habituated to the empty arena for 15 min. The second step, 24 hours later, corresponds to the memory acquisition

phase. At this step, two or three different objects are presented to the rats for 3 min. The third step corresponds to the retention test and was done with two retention times, either 1 hour or 24 hours after the phase of presentation. For this last session, one of the two or three objects was replaced by a novel object, and rats were free to explore the objects for 3 min. Different objects were used; the choice of objects and location of the novel object were randomized for each genotype to avoid object and location preference. Object exploration was manually scored and defined as the orientation of the nose to the object to a distance less than or equal to 2 cm. The percentage of time exploring familiar vs novel objects was calculated to assess recognition memory ability. Between each rat, the field and objects were cleaned with 50° ethanol between each rat to avoid object and location preference.

Long-term spatial learning and memory was analyzed with the Morris water maze (MWM). The water maze was a circular pool (diameter of 160cm and height of 80cm) filled with water maintained at 21±1°C, made opaque using a black paint (Gouache Redimix Noire #188039, Le Franc Bourgeois). The maze was split into 4 quadrants: South-East (SE), North-West (NW), North-East (NE) and South-West (SW). The escape platform (diameter of 10 cm) was submerged 3cm below the water's surface, so the rats were not able to see it. The light intensity of the test room was set to 70lux at the platform level. This experiment was performed to study reference memory through a spatial search strategy that involved finding a hidden platform in the maze using allothetic symbols placed on the walls around the pool. The acquisition phase of this test consisted of a 5-day learning phase with four 60 second trials per day. Each trial started with rats facing the interior wall of the pool and ended when they climbed onto the platform located on the NE quadrant or after a maximum searching time of 60 sec. The starting position was changed pseudo-randomly between trials. 24 hours after the last day of acquisition, rats were given a 60 sec probe test in which the platform had been removed. The distance traveled in each quadrant (NW, NE, SW and SE) was recorded to quantify the time spent in the target quadrant. Finally, 24 hours after the probe test, an index platform test (cue) was carried out to highlight potential visual or motivational problems. The platform was indicated by attaching a metal rod with a black and white polystyrene ball at its end. Each rat performed 4 tests, with a maximum duration of 60s. The sequence of release points, identical for all rats, was as follows: NE – SO – NO – SE. For the acquisition and index platform session, the distance travelled, velocity and latency to reach the platform were estimated with video tracking software (Ethovision, Wageningen, Netherlands).

Since rodents are social animals accustomed to living in groups, the social interaction test makes it possible to highlight alterations in sociability in our rat models. The test was carried out in the same device as the open field test (15 lux of room intensity). Two rats from different home cages and with the same genotype were placed in the arena. The test lasts 10 minutes and the arena was cleaned with 50° ethanol between each session. Using software (Ethovision, Wageningen, Netherlands) the number of times a social interaction occurred, and the duration of each interaction was quantified. The different interactions studied were following, pawing and sniffing head/head and head/posterior.

Statistical analysis of behavioral results

The statistical analyses were carried out with GraphPad Prism version 8.0.0 for Windows (GraphPad Software, Boston, Massachusetts USA), and a summary of all statistical results was included in Supplementary table 1. All data were expressed as mean group value ± standard error of the mean (SEM). The normal distribution of the data was checked by the Agostino-Pearson test and homogeneity of variances by the Brown-Forsythe test. Statistical difference between groups was analyzed with one way-ANOVA (open field) or two-way ANOVA (Circadian activity, MWM and NOP with 2 or 3 objects). In lack of normal data distribution or homogeneity of variances a Kruskal-Wallis non-parametric test was performed. The post hoc test (Sidak or Tukey) was conducted only if the F value in ANOVA achieved 0.05 level. For the Y-maze, OPP and NOR (with 2 or 3 objects), we performed a one-sample *t*-test on the percentage of novel object/position sniffing time or on the percentage of spontaneous alternation versus 50% (Y-maze, NOP, NOR with 2 objects) or 33% (NOR with 3 objects). A Student *t*-test was performed to compare rat models to controls (molecular analysis, circadian activity, open field and social interaction test). The significance threshold was set at $p<0.05$.

Optical coherence tomography (OCT)

After pupil dilatation with a topical application of tropicamide 0.5% (Mydriaticum, Théa pharma, France), rats were anesthetized using isoflurane (4% for induction and maintenance in a 0.4 L/min flow of 50%-50% mix of air and O_2) and placed on the stage of a Bioptigen R2200 spectral domain OCT (Bioptigen) with a heating pad. Cornea was kept moisturized with a thin layer of ocular gel (Ocry-gel, TVM) applied with surgical eye spears. For each eye, a rectangular

scan was obtained, corresponding to a region of 1.4 × 1.4 mm centered on the optic nerve. The thicknesses of the whole retina (including the pigmentary epithelium), the segments, the outer nuclear layer (ONL), the inner nuclear layer (INL), and the inner plexiform layer (IPL) for a given eye were calculated as the average of 2 measures at 0.5 mm from the optic nerve center using the Bioptigen InVivoVue 2.4.33 software.

RNA preparation

Hippocampus from adult Del(11*Dyrk1a*)4 or Dp(11*Dyrk1a*)6 male rats with their littermate controls (N=5 per group) were isolated and flash frozen in liquid nitrogen. Total RNA extraction was done using RNA extraction kit (Quiagen, Venlo, The Netherlands) according to the manufacturer's instruction. Total RNA quality was checked using an Agilent 2100 Bioanalyzer (Agilent Technologies, Santa Clara, CA, USA). cDNA synthesis was performed using the SuperScript® VILO™ cDNA Synthesis Kit (Invitrogen, Carlsbad, CA).

Transcriptomic analysis

The Transcriptome profile of the rat hippocampus isolated from Del(11*Dyrk1a*)4 and Dp(11Dyrk1a)6 rats models was analyzed with a specific bioinformatics pipeline and controlled for quality prior to and after data pre-processing and normalization (for more information, see (Duchon et al. 2021). The differential expressed genes (DEG) were identified using a method based on fold-change (FC) rank-ordering statistics (FCROS) (Dembélé 2019). In the FCROS method, *k* pairs of test/control samples were used to compute FC which ranked in increasing order and ranks obtained were associated with genes. Then, *k* ranks of each gene were used to calculate a statistic and resulting probability (*f*-value). After fixing the error level at 5% false discovery rate (FDR) the *f*-value allowed to identify the DEGs after. Functional differential analysis using GAGE was performed (Luo et al. 2009) and detail of this analysis could be found in a previous publication from our lab (Duchon et al. 2021).

Results

Generation and validation of new Del(*Dyrk1a*)4and Dup(*Dyrk1a*) rat models

A segmental deletion and a segmental duplication (11:34842454-34963976, Ensembl 91 database, GRCh38.p10) of 121.5 kb were generated by CRISPR-Cas9 to produce the Del(11*Dyrk1a*)4 and Dp(11*Dyrk1a*)5 rat models respectively. The DNA segment included the *Dyrk1a* gene and some non-coding region (Fig. 1A). *Dyrk1a* gene copy number was validated using ddPCR with one copy found in the Del(11*Dyrk1a*)4 model and three copies in the Dp(11*Dyrk1a*)5 model relative to two copies in the disomic control (wild type, wt) (Fig. 1B). In order to validate the amount of DYRK1A protein expressed in the two rat models, a western blot analysis was performed on hippocampal tissues of adult rats. A decrease of 42% in the expression level of DYRK1A was found in the Del(11*Dyrk1a*)4 model. However, the quantity of DYRK1A protein was not increased in Dp(11*Dyrk1a*)5 rats compared to disomic controls (Fig. 1C). We supposed that this might be due to absence in the duplicated region of some *Dyrk1a* regulatory sequences. We therefore generated a new model named Dp(11*Dyrk1a*)6 with a larger non-coding region around *Dyrk1a*, up to the next neighboring genes, *Dscr3* and *KcnJ6* (232 kb; 11:34791993-35024196, Ensembl 91 database, GRCh38.p10) (Fig. 1A). After validation of the presence of three copies of *Dyrk1a* in the Dp(11*Dyrk1a*)6 model (Fig. 1B), we showed that the amount of DYRK1A protein was increased in the hippocampus of Dp(11*Dyrk1a*)6 animals (Fig. 1C). To verify that the duplication in the Dp(11*Dyrk1a*)6 model did not impact the expression of genes on both sides of the duplication, we analyzed the mRNA expression of the *Dscr3* and *Kcnj6* genes present on either side of *Dyrk1a* in the hippocampus by quantitative RT-PCR. Results showed that duplication of *Dyrk1a* does not impact the expression of *Dscr3* and *Kcnj6* while Dyrk1a expression is increased (Fig. 1D). Thus, DYRK1A is overexpressed from the Dp(11*Dyrk1a*)6 allele without affecting the neighboring genes *Dscr3* and *Kcnj6*. Moreover, to validate the impact of the deletion of *Dyrk1a* in Del(11*Dyrk1a*)4 dosage of this activity was measured in brain extracts (Fig. 1E). As expected, a decrease of *Dyrk1a* activity was found in the brain of Del(11*Dyrk1a*)4 compared to disomic rats.

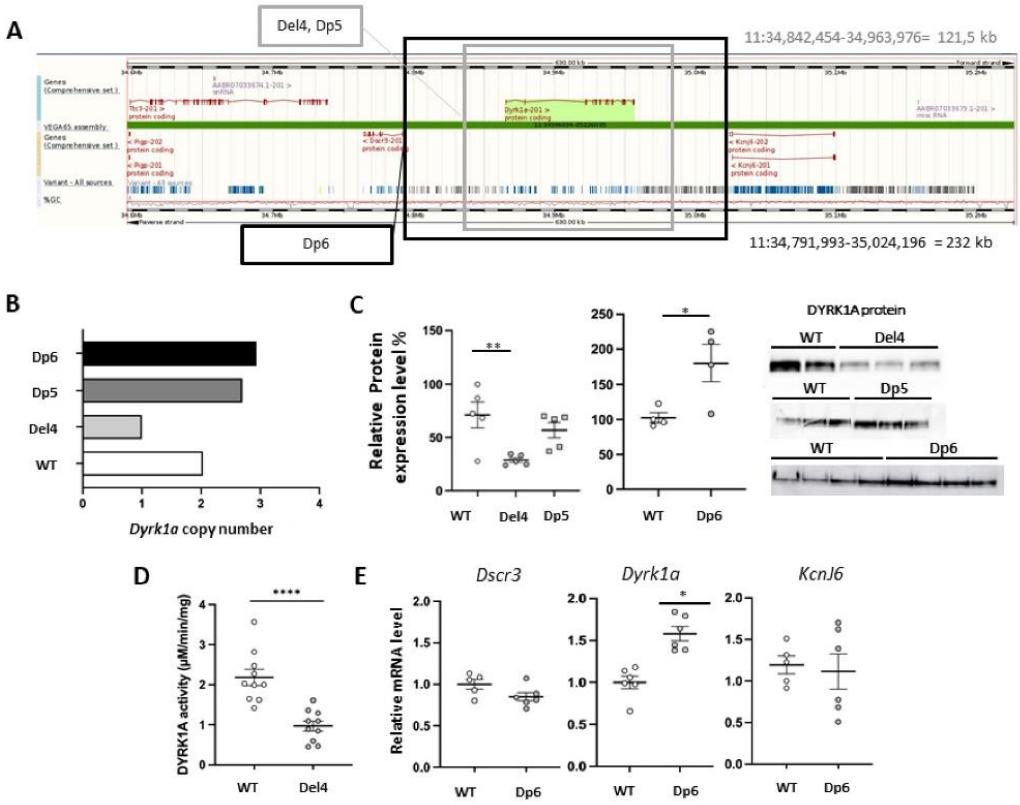

Fig. 1: Validation of the construction of the Del(11*Dyrk1a*)4, Dp(11*Dyrk1a*)5 and Dp(11*Dyrk1a*)6 rat models noted here Del4, Dp5 and Dp6. **(A)** The 121.5 kb (grey rectangle) deleted and duplicated region in the Del4 and in the Dp5 models respectively and the 219 kb (black rectangle) duplicated region in the Dp(11Dyrk1a)6 model, shown on a capture derived from the UCSC genome browser (http://genome.ucsc.edu/). **(B)** Analyse of *Dyrk1a* copy number by ddPCR in the three rat lines. Results show one copy of *Dyrk1a* in Del4 and three copies in Dp5 and Dp6 lines. **(C)** Quantification of immunoblots of DYRK1A protein in the hippocampus of the different rat models relative to control disomic rats showed a decrease of DYRK1A expression in Del4 compared to disomic rat controls (One-way ANOVA: $F_{2,12}$=6.740; ** p<0.01) but no difference of protein expression was detected in Dp5 rats compared to. Increase of DYRK1A protein expression is observed in Dp6 (Student's t-test: * p<0.05). Representative immunoblot detection shown on the right side. Data are presented as point plots with mean±SEM (n=5 rats for Del4 and Dp5 and n=4 rats for Dp6. **(D)** DYRK1A kinase activity in Del4 rat model. Kinase assay was realized on brain extract. Results show a decrease of DYRK1A activity in Del4 compared to the wild type (Student's t-test: **** p<0.0001, n=10 per group). **(E)** Relative mRNA level expression of *Dscr3*, *Kcnj6* and *Dyrk1a* genes in Dp6 to control disomic rats. No difference of mRNA levels for *Dscr3* and *Kcnj6* was observed in Dp6 compared to disomic rats while a 50%

increase in *Dyrk1a* mRNA expression is observed in Dp6 compared to controls (Student's *t*-test: * $p<0.05$). Data represent the mean±SEM (n=5 wild type and n=6 Dp6).

Dyrk1a deletion in rat model leads to impaired viability, locomotor and spatial memory deficit

First, when we generated the cohort the transmission rate of Del(11*Dyrk1a*)4/+ individuals was lower with 42% compared to controls (58%, n= 176 littermates; Chi2 test P=0,03). Thus, as in the mouse, *Dyrk1a* gene haploinsufficiency has an effect on the viability. Then we checked the body weight, at the beginning of the behavioral pipeline (aged 9 weeks). A significative decrease of Del(11*Dyrk1a*)4 rats body weight (n=15 390+/-10g) was observed compared to control animals (n=15, 456+/-6g; Student t test P=7,3 10^{-07}). After post-mortem analysis at 14 to 16 weeks, we also found that the brain weight was reduced in mutant individuals (n=15 per genotype, control 2,31g+/-0,03 and mutant 1,48+/-0,03; Student t test P= 1,3 10^{-09}). Then, we determined the impact of *Dyrk1a* on rat cognition and behavior. The circadian activity and open field tests were used to evaluate the locomotor activity of rats. Locomotor activity during the circadian test was recorded during 46 hours from day 1, 11:00 am until day 3, 11:00 am. The diurnal activity was analyzed by grouping together data from the two diurnal phases (from 5 to 12 respectively from the first and second day) and the nocturnal activity (12 hours by night) – without habituation phase – by grouping data from the two nocturnal phases. A decrease of Del4 rats mean locomotor activity was noticed only during nocturnal session (Fig. 2A). In addition, a decrease in the number of rears throughout the test was observed in Del4rats compared to controls (Fig. 2A). Exploratory activity was analyzed in the open field. Del4 rats exhibited a decrease in locomotor activity with a reduction of the total distance traveled compared to the control (Suppl. Fig. 1B). This was due to a decreased activity during the first 10 minutes of exploration of the arena, reflecting hypoactivity in those animals (Fig. 2B, *left*). The distance travelled by Del4 rat was reduced at the periphery and not in the center of the arena (Fig. 2B *right*).

Subsequently, cognitive abilities were evaluated with Y-maze (working memory), Novel Object Place Preference (NOP= with 5 minutes of retention (short-term spatial memory), Novel Object Recognition (NOR) with two objects with 1h or 24h of retention and three objects (recognition memory) and Morris Water Maze (MWM, long-term spatial learning and memory) in 9-12-week-old males. Y-maze results reveal no difference between Del(11*Dyrk1a*)4 rats and disomic rats for the percentage of spontaneous alternation (Fig. 2C). The deletion of *Dyrk1a* in rats,

therefore, did not induce a deficit in working memory. The OPP test with 5 min retention revealed that, unlike controls, Del(11*Dyrk1a*)4 rats were not able to discriminate the new position from the familiar one (Fig. 2D). These results showed an alteration of the short-term spatial memory in Del(11*Dyrk1a*)4. The NOR test with 2 objects highlighted that Del(11*Dyrk1a*)4 rats, like the controls, were able to differentiate the novel object (No) versus from the familiar object (Fo) after 1h or 24h of retention (Fig. 2E). The lack of deficit of the Del(11*Dyrk1a*)4 rats in this test, opposite to the *Dyrk1a*$^{+/-}$ mouse model, might be due to the fact that this test is too simple for the rats compared to mice (Arqué et al. 2008). Hence, we decided to choose a more complex NOR test by going through the presentation of 3 different objects. For this test, Del(11*Dyrk1a*)4 rats like control rats, spent more than 33% on the No object (Fig. 2F). As a result, Del(11*Dyrk1a*)4 rats did not have a deficit in recognition memory. In the MWM, during the learning phase with the hidden platform, the distance travelled by two genotypes to find the platform decreased during the five days of acquisition, reflecting a platform localization learning (Fig. 2G, *left*). However, Del(11*Dyrk1a*)4 rats traveled a greater distance to find the platform than control rats during this phase, with a significant difference on days 2 and 3. These results highlighted that the learning capacity, although still present, was decreased in Del(11*Dyrk1a*)4 rats. During the probe test, both genotypes presented a significant preference for the targeted quadrant compared to hazard (25%) indicating no long-term spatial deficit (Fig. 2G, *right*).

Haploinsufficiency of DYRK1A caused a syndrome with autism spectrum disorder. Therefore, we checked social interaction, looking at different behaviors in a defined environment between two stranger rats with the same genotype. Analyzing the percentage of time each pair of animals spent having social interactions, the duration of social interactions was decreased in Del(11*Dyrk1a*)4 rats compared to controls (Fig. 2H, *left*). More precisely, a reduction of the time spent "following" and "pawing" was observed among Del(11*Dyrk1a*)4 compared to control animals (Fig. 2H, *right*), unraveling an alteration of Del(11*Dyrk1a*)4 model in social interaction abilities.

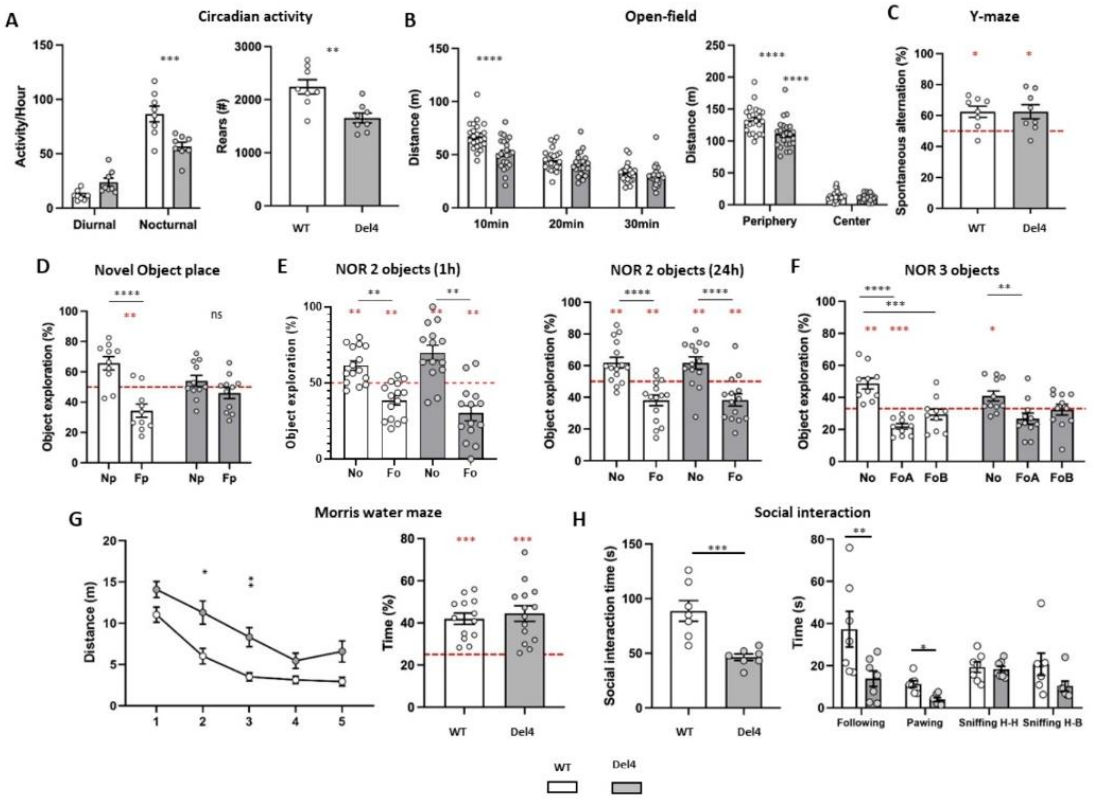

Fig. 2: Impact of *Dyrk1a* deletion in the Del(11*Dyrk1a*)4 rat model on behaviour and cognition

Del(11*Dyrk1a*)4 (Del4) rats shown in grey and disomic control rats are in white. **(A)** Circadian locomotor activity per hour during the diurnal and nocturnal phases of the test (*left*) and the total number of rears during the whole recording (*right*). Data show a decrease in the mean locomotor activity of Del4 during the nocturnal phase (two-way ANOVA: $F_{1,14}$=38.84; Šídák post-hoc: n=8 per group). Number of rears is decreased in Del4 compared to controls (Student *t*-test; n=8 per group). **(B)** Analysis of the distance traveled in a new environment recorded in the OF by increments of 10 minutes (*left*) and by zone (periphery and center; *right*). The distance traveled during the first 10 minutes was significantly lower in Del4 compared to disomic rats (two-way ANOVA: F1,44=9.074; Šídák post-hoc). Del4 travelled less distance at the periphery than control rats (two-way ANOVA: $F_{1,44}$=9.330; Šídák post-hoc, n = 23 per group). **(C)** Percentage of spontaneous alternation in Y-maze. One sample *t*-test vs 50% (hazard) show Del4 and disomic rats performed in the test (n=8 per genotype) **(D)** NOP test with 5 minutes of retention. Results are presented as the percentage of exploration time of the object with the new position (Np) and the object which was not moved (Familiar position, Fp). One sample *t*-test vs 50% (hazard) showed Del4 failed to recognize Np object (n=10 wild type and n=11 Del4). **(E)** NOR with two objects and 1h or 24 hours of retention or **(F)** with three objects (*right*). Results show the percentage of exploration time of Novel object (No) and Familiar objects (Fo, FoA, FoB). For NOR with two objects, Del4 rats discriminate the No from the Fo

after 1h or 24h of retention (one sample *t*-test: n=15 per genotype). For NOR with three objects, on sample *t*-test *vs* hazard indicated that control and Del4 rats explored more time than 33% the No (n=10 control and n=11 Del4)). **(G)** Mean of the distance traveled during the four trials for each day of acquisition session (left) and percentage of time spent on the target quadrant (NE) during the probe test session (*right*) in MWM. Two-way repeated measures ANOVA (Genotype x Day) show a significative decrease of distance traveled between day 1 and day 5 for two genotypes reflecting (Day effect $F_{2.810,75.67}$=39.10; Tukey post-hoc: p<0.0001 D1 *vs* D5 for control, p<0.01 D4 *vs* D5 for Del4). During the second and third days of acquisition Del4 travelled more distance than disomic rats ($F_{2.810,75.67}$= 39.10; Šídák post-hoc: *p<0.05 control *vs* Del4 for D2, p<0.01 Del4 *vs* control for D3). For the probe test, one sample *t*-test *vs* 25% (hazard) show that two genotypes spend more time in the target quadrant (n=14 per group). **(G)** Total time spent having different social interactions (*left*) and the duration of each different social behaviour (*right*): following, pawing, sniffing head-head and sniffing head-back. Results indicate a decrease of total social interaction time (*left*) and a reduction of following behaviour (*right*) in Del4 compared to disomic rats (n=7 per group, Student *t*-test; ns = non significative, * p<0.05, ** p<0.01, *** p<0.001; in black between groups and in red versus hazard).

Overexpression of *Dyrk1a* induced cognitive deficits in rat models

For the phenotyping characterization of the Dp(11*Dyrk1a*)5 rat model, locomotor activity was evaluated with the OF test, cognitive skills were measured with a two-object recognition test, with 1h and 24h of retention, and the MWM for spatial long-term learning. No behavior alterations could be detected in the Dp(11*Dyrk1a*)5 rats compared to controls, as expected from the absence of DYRK1A overexpression in this model (Fig. S1).

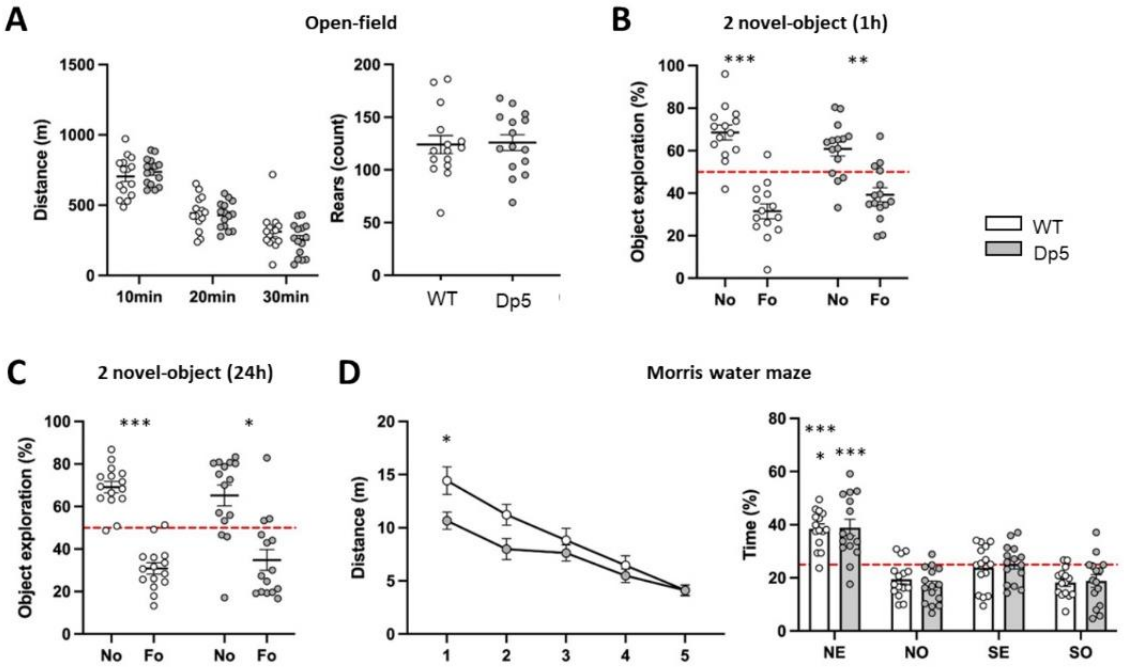

Fig. S1: The Dp(11*Dyrk1a*)5 rat model displays normal behaviour and cognition

Cohorts of n=16 individuals carrying D(11*Dyrk1a*)5 (Dp5) mouse models (shown in grey), and n=16 disomic control rats were analysed between 9 and 12 weeks of age. **(A)** The distance traveled and rearing activities in Dp5 individuals in the open field was similar to control littermates (n=16). **(B and C)** The percentage of exploration of objects in the NOR with two objects after respectively 1h or 24 hours of retention was similar in carrier and control animals. **(D)** The mean of the distance travelled during the four trials for each day of acquisition session (left) and percentage of time spent on the target quadrant (NE) during the probe test session (*right*) in MWM, showed normal pattern of spatial learning and memory (Two-way repeated measures ANOVA).

Then we analyzed the Dp(11*Dyrk1a*)6 that displayed and increase in *Dyrk1a* expression. First, transmission and body weight were similar between Dp(11*Dyrk1a*)6 rats and control animals at 9 weeks age (Fig. S2). Then, to characterize Dp(11*Dyrk1a*)6 rat model, a detailed behavioral pipeline was used. As previously, we first focused our attention on the locomotor activity. The circadian activity test (Fig. 3A) showed a decrease in locomotor activity in *Dyrk1a* trisomic rats during the nocturnal phase with no specific effect during the habituation, and the two diurnal and nocturnal phases (Fig. S2). Moreover, no difference was found between the two genotypes for the number of rears throughout the test (Fig. S2). Like Del(*Dyrk1a*)4rats, trisomic rats for *Dyrk1a* have a hypoactivity during the circadian test, but only for the nocturnal phase. However, contrary to Del(*Dyrk1a*), an increase in distance travelled by Dp(11*Dyrk1a*)6 rats was noticed

during the 10 first minutes of exploration of the open field (Fig. 3B). This hyperactivity was not seen in the total distance travelled during the 30 minutes of the test (Fig. S2). In addition, Dp(11*Dyrk1a*)6rats did not present any difference with control animals in the number of rears during the circadian monitoring or in the open-field (Fig. S2B-C). No difference between Dp(11*Dyrk1a*)6 and control rats was detected for distance travelled at the periphery or center of the arena (Fig. 4B), suggesting that Dp(11*Dyrk1a*)6do did not present alteration of anxiety.

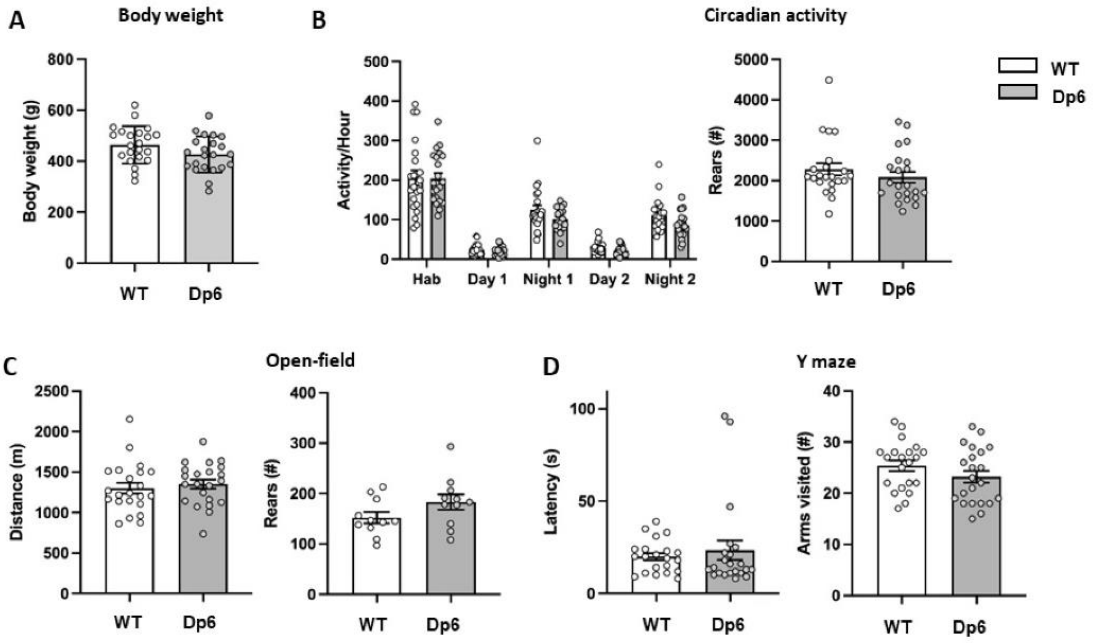

Fig S2: Normal behavior parameter in the Dp(11*Dyrk1a*)6 rat models.

Grey and white represent Dp(11*Dyrk1a*)6 (Dp6) and disomic control male rats (n=22 per genotype), respectively The body weight, the activity and nb of rears during the circadian activity, the total distance travelled and number of rears in the open field with the latency to escape from the first arm ant the number of arms visited in the Y maze did not show any statistical significance using Student t test when comparing the Dp(11*Dyrk1a*)6 with their control littermates.

Then, we evaluated different types of memory: the working memory, position recognition memory, object recognition memory and long-term spatial learning and memory. Unlike mice transgenic for the *Dyrk1a* gene, Dp(11*Dyrk1a*)6 rats did not have a spontaneous alternation deficit in the Y maze test (Fig. 4C), suggesting that they have normal working memory. Moreover, no difference between genotype was found in the number of arms visited or the exit latency of the starting arm (Fig. S2). The results of the NOP test (Fig. 4D) showed an

alteration of short-term spatial memory in Dp(11*Dyrk1a*)6 rats. In addition, in the 3-object novel object recognitiont, even if Dp(11*Dyrk1a*)6rats spent more than hazard (33%) exploring the novel object (No), they did not spent significantly more time exploring the No from the familiar ones, reflecting an alteration of their recognition memory (Fig. 4E). Finally, the MWM test shows that Dp(11*Dyrk1a*)6 animals did not have a deficit in learning and long-term spatial memory (Fig. 4F).

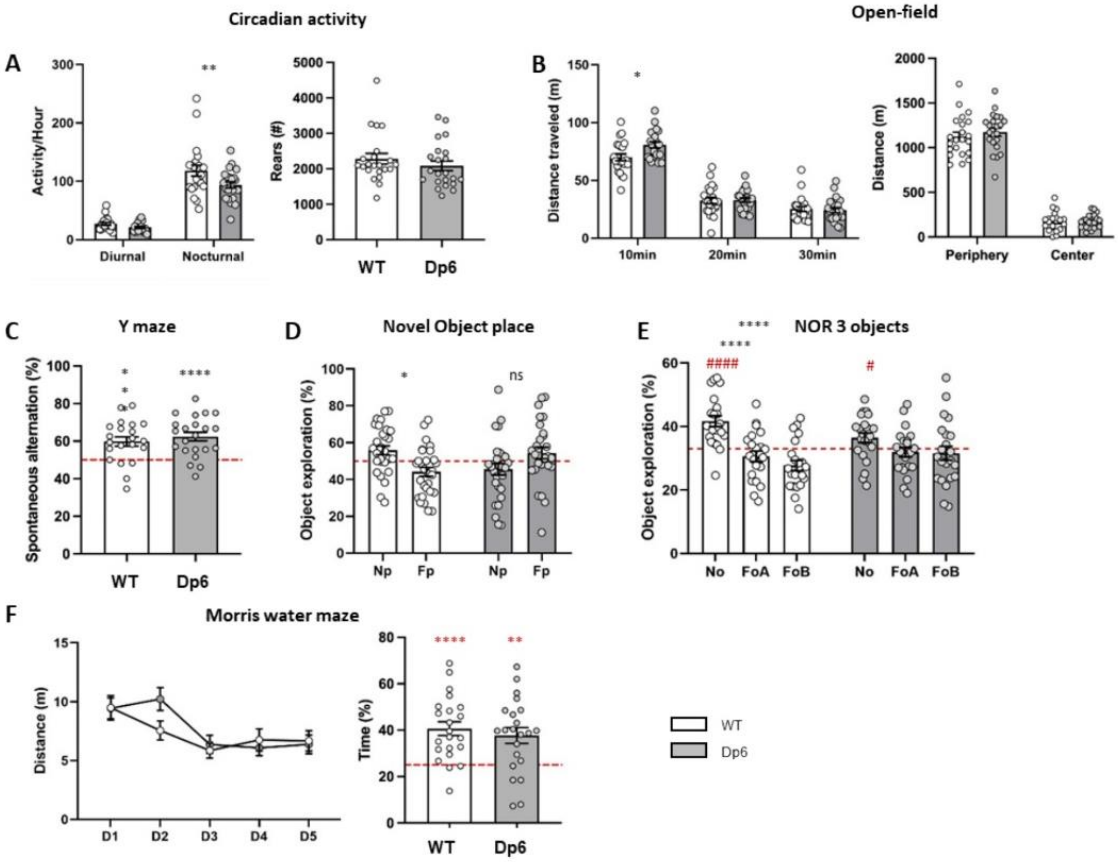

Fig. 3: Behavioural phenotyping of the Dp(11*Dyrk1a*)6rat line unravelled cognitive deficits.

Grey and white represent respectively Dp(11*Dyrk1a*)6 and disomic control male rats. **(A)** Mean locomotor activity per hour during diurnal and nocturnal phases of the circadian activity test. Dp(11*Dyrk1a*)6 activity was decreased during nocturnal phase of the test (two-way ANOVA, $F_{1,45}$=5.755; Šídák post-hoc: * p<0.05 Dp(11*Dyrk1a*)6 *vs* control rats; n=22 per group). **(B)** Distance travelled in the open field showed an increase during the 10 first minutes of the test when comparing Dp(11*Dyrk1a*)6 to control littermates (two-way ANOVA, $F_{2,84}$=4,647; Šídák post-hoc: *p<0.05). No difference was observed between the two genotypes for distance traveled in different zone of arena (two-way ANOVA: $F_{1,42}$=0.8462; n=22 per group). **(C)** Percentage of spontaneous alternation. One sample *t*-test vs 50% (hazard) showed Dup2(*Dyrk1a*), like wild type, performed in the test (*** p<0.001, **** p<0.0001; n=21

controls and n=22 Dup2(*Dyrk1a*)). **(D)** Object Place Recognition test with 5 minutes of retention. The analysis of the mean exploration time of objects in percentage with the new position (Np) and of the familiar object (Fp) using a sample *t*-test vs 50% (hazard) highlighted that Dp(11*Dyrk1a*)6failed to recognize the Np (ns = non-significant, ** $p<0.01$, n=29 per group). **(E)** Novel Object Recognition test with 24 hours of retention and three objects showed the percentage of exploration time of the Novel object (No) and Familiar objects A and B (FoA, FoB). Dp(11*Dyrk1a*)6 rats failed to discriminate No from FoA and FoB (two-way ANOVA, $F_{2,126}=3,725$, **** $p<0.0001$; one sample t-test compared to 33%: # $p<0.05$, #### $p<0.0001$; n=22 per group). **(F)** Acquisition session (*left*) and probe test session (*right*) in the Morris water maze. Results are presented with the mean ±SEM of the distance travelled during the 5 days of acquisition (*left*) and the percentage of time spent in the target quadrant (*right*). No difference in the distance travelled during the acquisition days was observed between wild type and Dp(11Dyrk1a)6 rats. In the probe test, both wild-type and Dp(11*Dyrk1a*)6 rats spend more time in the target quadrant (One sample *t*-test vs 25% (hazard), ** $p<0.01$, **** $p<0.0001$; n=22 per group).

Craniofacial changes associated with Dyrk1a dosage in rat models

Using a morphometric analysis as described previously (Ahumada et al., BIORXIV/2024/612914), we found that the Del(*Dyrk1a*)4 model showed significant changes in the form and shape matrix of the skull. In more detail, voxel-based analysis showed that changes in shape correspond to a reduction in the dimensions of the neurocranium (microcephaly) with an increase in the dimensions of the midface (Fig. 5). In the mandible, there is a tendency to be wider, but shorter.

In the case of Dp(*Dyrk1a*)6, the skull showed no change in head dimensions Voxel-based analysis shows that the changes in shape correspond to a reduction in the dimensions of the frontal bone, nasal bone and zygomatic arch, and an increase in the dimensions of the neurocranium, mimicking the Down syndrome brachycephaly. In the mandible, there was a reduction in the width of all structures that are smaller. Overall, these results showed that the dosage of *Dyrk1a* regulates the shape of the neurocranium, with one copy leading to microcephaly and 3 copies to brachycephaly typically found in Down syndrome. In addition, the face and the mandible were larger in the Del(*Dyrk1a*)4 model, and tended to be smaller in the Dp(*Dyrk1a*)6.

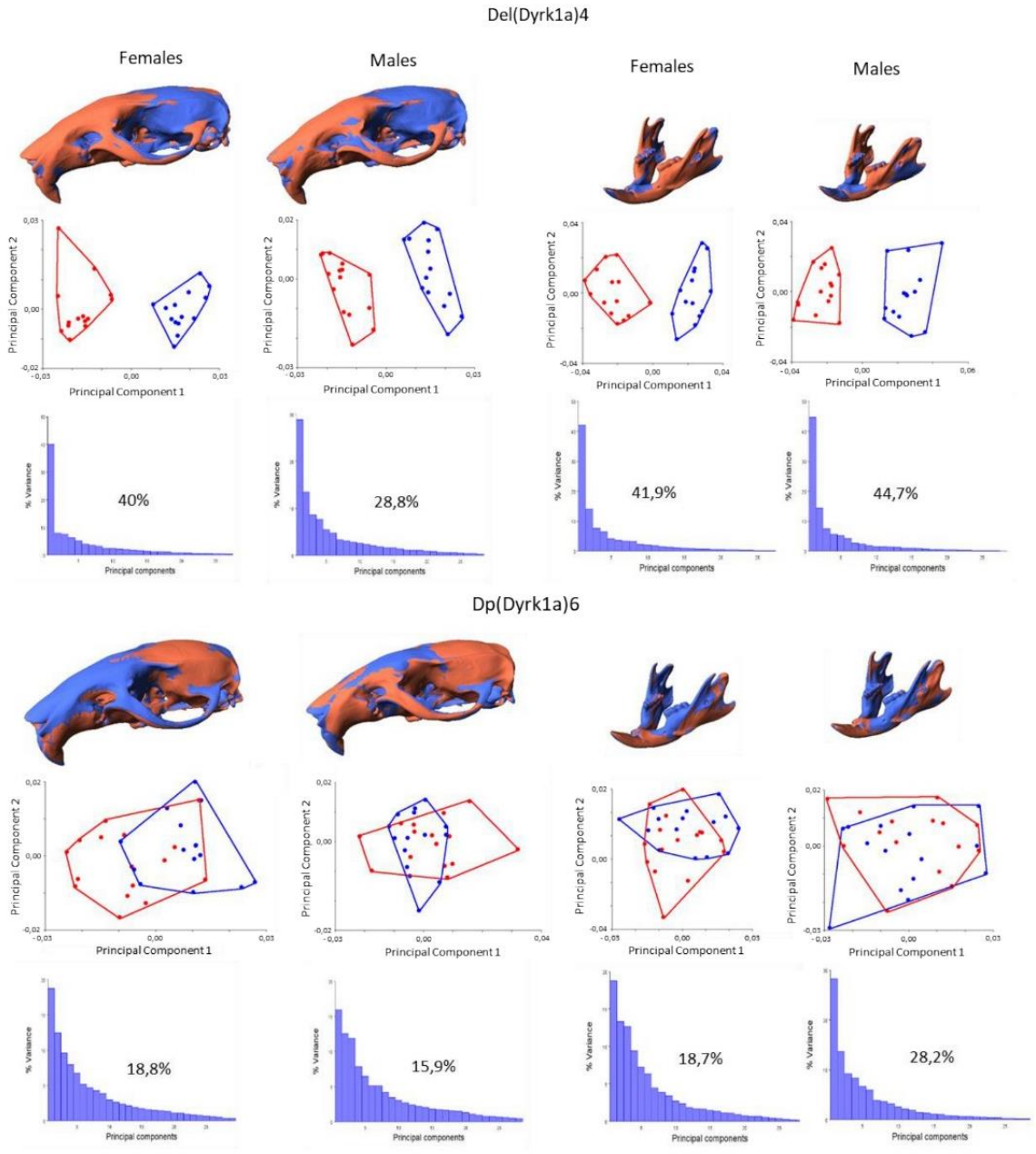

Fig 4: Morphometric analysis of the skull (left) and mandible (right) of the Del(11*Dyrk1a*)4 and Dp(11*Dyrk1a*)6 rat models. N=14-15 individuals per genotype and sex were analysed for shape difference. For each model, the skull and mandible are shown separately by sexes. The first picture highlights 1) the warping observed comparing wild-type and mutant within blue, the bones with decreased dimensions in *Dyrk1a* models, and in red, the bones with increased dimensions; 2) PC1 and PC2 graphs to show the separation of mutant and control samples (red for Del or Dup and blue for control); 3) the percentage of variance for the PCA dimension shown in blue.

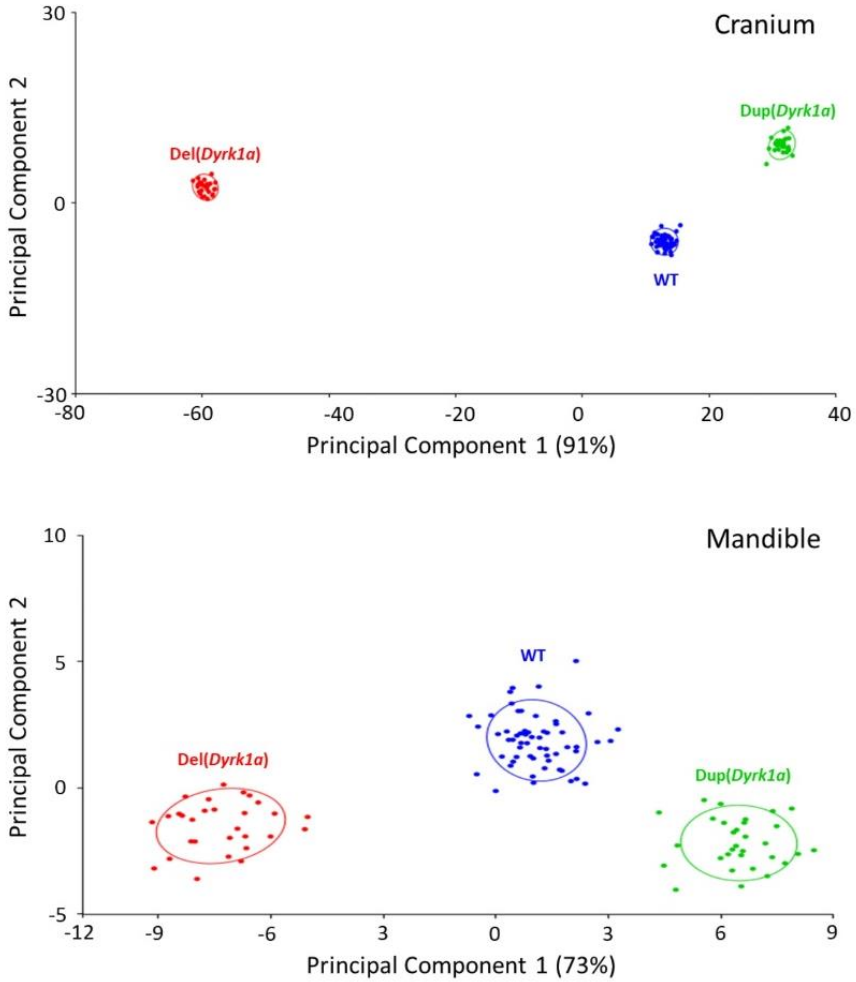

Fig 5. Integrative multivariate analysis Del(11*Dyrk1a*)4 and Dp(11*Dyrk1a*)6

All the craniofacial data from the models and their control littermate were collected to carry a principal component analysis (PCA). *Dyrk1a* models showed significant differences compared with the wild-type controls in the first two dimensions of the PCA and were separated into three main groups for the cranium and mandible. The group of Del(11*Dyrk1a*)4 located on an opposite direction on PC1 (that accounts for 91% in the cranium and 73% in the mandible of the variance) compared to Dp(11*Dyrk1a*)6 individuals and the WT control groups was found in between, closer to the duplication as expected from the phenotype analysis. (n= 57 WT, n=56 Del(11*Dyrk1a*)4 and 61 Dp(11*Dyrk1a*)6 balanced for the sex).

Impact of *Dyrk1a* deletion on adult rat transcriptome profile

A transcriptomic analysis was performed on adult hippocampi and compared to control littermates to highlight the impact of a Dyrk1a gene monosomy on the adult rat transcriptome.

We identified 723 differential expressed genes corresponding to 65 % protein-coding genes and 25% non-coding genes involved in 222 de-regulated pathways, identified by GAGE (Generally applicable gene set enrichment for pathway analysis)(Luo et al. 2009). From the 222 altered pathways the analysis highlighted the most affected groups (**Fig. 6A**) with the metabolism encompassing 31% of the total pathway, enzymes activity 24%, synapse 17% and transcription & epigenomic regulation 15 % (**Fig. 6B**). Of particular interest, synaptic function was common to 39 of those pathways. Synaptic function pathways were upregulated and linked to learning and memory, axons and dendrites morphogenesis, synapse assembly, modulation of synapse transmission, post-synapse density and specialization. These results unraveled a high impact of *Dyrk1a* haploinsufficiency over a large range of molecular functions and biological processes and pathways. They pointed at the impact of *Dyrk1a* in key pathways for learning and memory deficits, observed in this model.

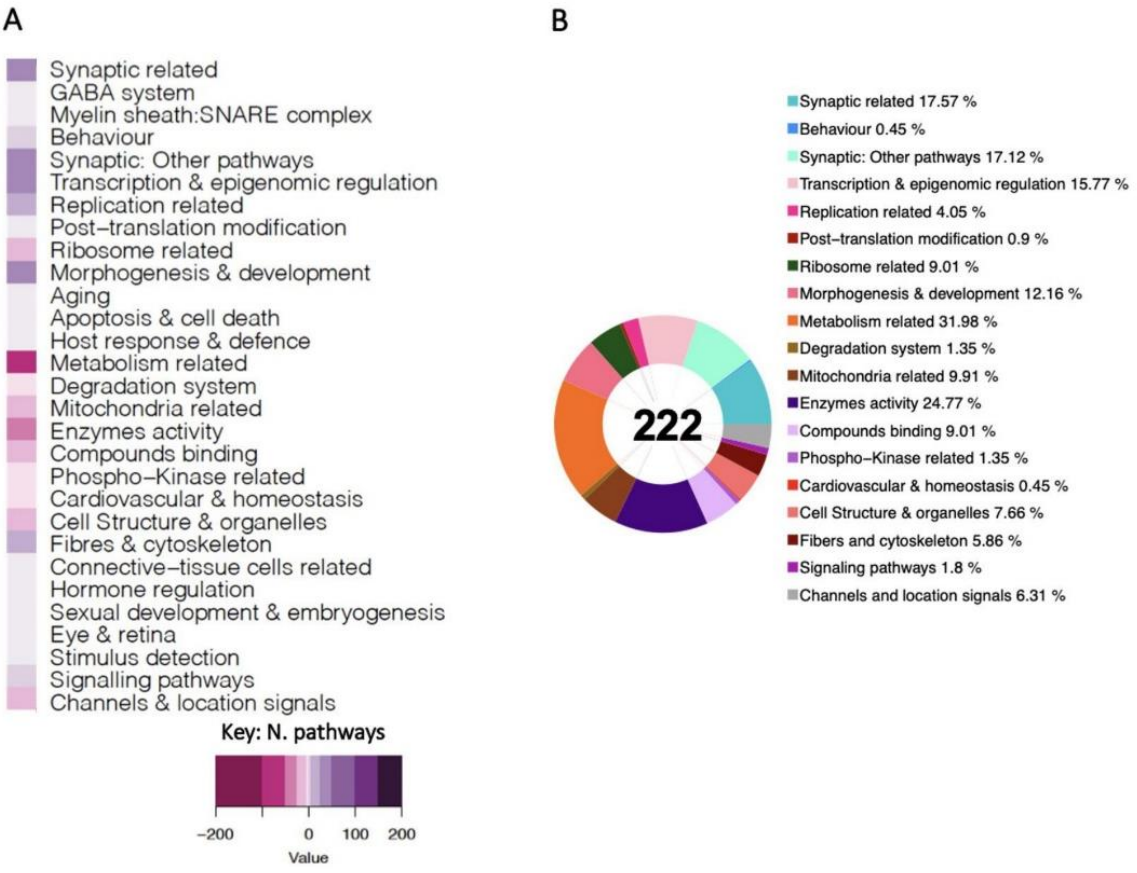

Figure 6: Introducing the adult rat Del(*Dyrk1a*)4 in the *Dyrk1a* dosage analysis.

(A) Heatmap representation of the number and regulation sense of the pathways altered due to *Dyrk1a* gene dosage in Del(*Dyrk1a*)4 rats using the genome expression for each model identified by GAGE (Luo et al. 2009) R package and filtered by q- value cut off < 0.1. On the *left* the average number of pathways, on the *right* instead, divided by regulatory sense, only upregulated pathways (purple) and only downregulated (pink). Grouped in the categories shown on the computer such as synaptic related, transcription & epigenomics regulation and replication related. The synaptic related group was divided in 4 subgroups: GABA system, myelin sheath and SNARE complex formation, behavior and others. The color key breaks represent the number of pathways within the categories Breaks (-200,-100,-50,-25,-5,-0.5,+0.5,+5,+25,+50,+100,+150,200). The minus or pink color represents down regulated pathways, the white color represents no pathway found in the category and the purple or positive numbers stands for up regulated pathways respectively. **(B)** Percentage of pathways on each defined group de-regulated on the adult Del(*Dyrk1a*)4 rat deficit model by RNA-Seq from 222 pathways found altered by GAGE.

Discussion

The rat model for *Dyrk1a* haploinsufficiency displays phenotypes similar to the mouse *Dyrk1a*$^{+/-}$ model and relevant for human MRD7

The Del(*Dyrk1a*)4 allele is similar to deletion of *Dyrk1a* observed in MRD7 and induce several features related to the disease. First the decrease in spontaneous activity in rats was observed in the circadian activity test during the habituation and nocturnal sessions, reflecting an alteration in their intrinsic activity during their activity phase. Furthermore, a reduction in the locomotor activity of Del(*Dyrk1a*)4 rats was also observed by the decrease in the number of rearing during the same test, but also by a decrease in the total distance covered in the arena during the open field test. Moreover, hypoactivity in this test is also associated with the habituation phase, showing an impact on the behavior of exploring a new environment. The Del(*Dyrk1a*)4 rats showed an alteration when exposed to novel, non-stressful environments. A similar hypoactivity phenotype has also been reported in *Dyrk1a* heterozygous mice with a decrease in the number of righting as well as distance traveled in the open field test (Fotaki et al. 2004; Raveau et al. 2018). Similarly to the mouse, no change in anxiety level was detected in the Del(Dyrk1a)4 rats compared with control animals (Raveau et al. 2018).

The learning and memory deficits in Del(*Dyrk1a*)4 rats are comparable to those found in mice, carrying a deletion of *Dyrk1a*. For example, an absence of working memory deficits is highlighted by the Y-maze test in Del(*Dyrk1a*) rats, as has been found in *Dyrk1a*$^{tm1.2Ics}$ mice (Brault et al. 2021). Del(*Dyrk1a*)4 rats show no deficit in long-term spatial memory, but learning of platform location and hence spatial learning is impaired in the Morris pool task, as in another *Dyrk1a*$^{tm1Mla/+}$ mice (Arqué et al. 2008). Short-term spatial memory, which is highly dependent on the hippocampus, was measured using the PPO test. This memory is clearly impaired in Del(*Dyrk1a*)4 rats. This type of memory has never been studied in *Dyrk1a* mutant allele in mouse. While impaired recognition memory was shown in *Dyrk1a*$^{tm1Ml/+}$ mice with the two-object NOR (Arqué et al. 2008), no deficits in the two- or three-object NOP have been observed in Del(*Dyrk1a*)4 rats. This difference may be explained by the fact that the two- and three-object NOP tests are too simple to reveal an object recognition deficit in rats. Another hypothesis is that *Dyrk1a* haploinsufficiency in rats simply does not lead to impaired recognition memory. MRD7 is an autism spectrum disorder syndrome and the Del(*Dyrk1a*)4 model showed a decrease in social interactions was found in *Dyrk1a*^{em1Kzy} mice whose catalytic domain has been truncated (Raveau et al. 2018). Overall the Del(*Dyrk1a*)4 rat model is relevant for modeling MRD7 which encompasses not only point mutations but a series of deletions including *DYRK1A* (van Bon et al. 2011; Bronicki et al. 2015; Ji et al. 2015; Evers et al. 2017; Courraud et al. 2021). Individuals with MRD7 present with growth retardation, microcephaly, facial dysmorphia, ataxic gait, eating disorder, speech impediment, autism spectrum disorder and intellectual disability (Møller, Rubolini, et Lehikoinen 2008; Courraud et al. 2021). The Del(11*Dyrk1a*)4 rat model reproduces cognitive function abnormalities with impaired short-term spatial memory and spatial learning. The model also displays microcephaly and craniofacial changes. While we showed that Del(*Dyrk1a*) rats also exhibit hypoactivity, it would be interesting to better characterize the motor functions of Del(11*Dyrk1a*)4 rats by assessing the animals' motor coordination and balance. The results will enable us to verify whether *Dyrk1a* haploinsufficiency in rats better reproduces the ataxia observed in patients with MRD7 syndrome. In addition, numerous studies highlight that the *Dyrk1a* gene is involved in regulating the excitation/inhibition balance between the glutamatergic and GABAergic neuronal system (Souchet et al. 2014; 2015). Deregulation of the balance can lead to epilepsies, which are precisely observed in people with MRD7 syndrome (Møller, Rubolini, et Lehikoinen 2008; Courcet et al. 2012). Therefore, an epilepsy susceptibility test should be carried out by

injection of the pro-convulsant agent pentylenetetrazol. This would increase the spectrum of features replicated in the Del(11*Dyrk1a*)4 model to study the MRD7 syndrome.

The duplication of the *Dyrk1a* locus in rats required a larger non-coding region than in mice

To generate rat models with single or three copies of the *Dyrk1a* gene, the CrispR-Cas9 gene-editing system was used to generate the duplication of a 121.7 kb fragment in the Dp(11Dyrk1a)5, containing the complete sequence of the *Dyrk1a* gene. This fragment corresponds to the sequence present in the BAC that was integrated into the genome of the Tg(*Dyrk1a*)189N3Yah model (Guedj et al. 2012). The Dp(11*Dyrk1a*)6 model carries a duplication of a larger 219 kb-long fragment, also containing the complete sequence of *Dyrk1a*, but with all the intergenic regions upstream and downstream of the gene. While in the Dp(11*Dyrk1a*)5 no *Dyrk1a* overexpression and no behaviour and cognitive phenotypes was detected, the Dp(11*Dyrk1a*)6 displayed *Dyrk1a* overexpression and very specific and related learning and cognitive phenotypes similar to the Tg(*Dyrk1a*)189N3Yah (Guedj et al. 2012) and relevant for Down syndrome. Thus, to induce an increase in DYRK1A expression, a larger non-coding region is apparently required in the rat model. We can envisage that non-coding regions duplicated in the Dp(11*Dyrk1a*)6 model are likely to contain regulatory sequences required for *Dyrk1a* transcription according to dosage. These results underpin a genome difference between mouse and rat species, as the 121.7 kb sequence is sufficient to induce an increase in DYRK1A protein expression in Tg(*Dyrk1a*) mice (Guedj et al. 2012). Due to the increased size of the duplicated region, we verified that the expression of the *Dscr3* and *Kcnj6* genes were not altered. As no disruption of *Dscr3* and *Kcnj6* RNA expression was observed in the Dp(11*Dyrk1a*)6 model, the phenotypes observed and discussed are the sole should be the consequence of the sole duplication of *Dyrk1a*.

Impact of *Dyrk1a* haploinsufficiency on the adult rat transcriptome in the hippocampus

Transcriptomic analysis of adult Del(*Dyrk1a*) rats revealed altered regulation of synaptic signalling pathways, including those involved in learning and memory processes, synapsis and axon and dendrite morphogenesis. These results are in line with behavioural analysis, which has shown memory deficits, as in the PPO test. The results obtained in Del(*Dyrk1a*) rats will then have to be compared with those obtained in Dup2(*Dyrk1a*) rats. However, transcriptomic analyses carried out by Dr. Muniz-Moreno on *Dyrk1a*+/- mice also revealed 93% deregulation

of synaptic signalling pathways (Muñiz Moreno 2019, Doctoral dissertation, University of Strasbourg). These pathways are involved in pre- and post-synaptic membranes and axons. Synaptic pathways affected include GABAergic, serotonergic, glutamatergic and cholinergic pathways. These results are similar to those of Del(*Dyrk1a*) rats, and it therefore seems important to identify key genes involved in synaptic signalling that are deregulated in both rat models, and to validate their expression by another technique, notably RT-qPCR.

The duplication of *Dyrk1a* in the Dp(11*Dyrk1a*)6 allele model mirrors the phenotypes observed in mouse models overexpressing *Dyrk1a* and in Down syndrome.

DYRK1A is a major driver gene whose overdosage contribute to the Down syndrome phenotypes in mouse models (Atas-Ozcan et al. 2021). In the Dp(11*Dyrk1a*)6, we observed hypoactivity during the circadian activity test but a hyperactivity at the start of the open field test, whereas Del(11*Dyrk1a*)4 rats showed hypoactivity in the open field. Probably, spontaneous locomotor activity for rat in a new environment is controlled in a dose-dependent manner by the *Dyrk1a* gene activity. This contrast was also observed in mouse models. Tg(*Dyrk1a*)189N3Yah mice showed hyperactivity, while two heterozygous knock-out of *Dyrk1a* mouse models are hypoactive (Fotaki et al. 2004; Duchon et al. 2021). Regarding the learning and memory, the Dp(11*Dyrk1a*)6 rat models showed no impairment of working memory in the Y-maze test, opposite to the the Tg(*Dyrk1a*)189N3Yah mouse model (Duchon et al. 2021). It would be interesting to assess short-term memory with a more complex test than the Y maze, particularly with the arm maze test, which measures working memory and reference memory (Olton, Collison, et Werz 1977). Although there are similarities in the overexpression of *Dyrk1a* between the mouse and rat models, there are also differences that could be investigated.

The Morris water maze, on the other hand, revealed no alteration in the acquisition and recall phases of the test for the Dp(11*Dyrk1a*)6 model. Therefore, no impairment of their spatial memory and learning abilities is observed contrary to th.e Tg(*Dyrk1a*)189N3Yah mice, which perform worse than controls (Souchet et al. 2014). This may be explained by the fact that rats are generally more competent and less stressed by the Morris water maze test. Consequently, it is possible that the mouse cognitive deficit is reinforced by stress in the mice and not observed in the rat models (Ellenbroek et Youn 2016). Another test, such as the Barnes maze, could be used to validate the absence of impaired learning and spatial memory in

Dp(11*Dyrk1a*)6 rats. Indeed, Dp2(11*Dyrk1a*)6 rats displayed impaired spatial memory in the NOP test with 5 min retention. In Tg(*Dyrk1a*)189N3Yah mice, a similar deficit in the NOP with 24 hours of retention was also reported (Nguyen et al. 2018). Thus, an increase in *Dyrk1a* dosage triggers slightly different cognitive alterations in mouse and rat models. In mice overexpressing *Dyrk1a*, a deficit in long-term spatial memory is observed, whereas in rats, a deficit in short-term memory is detected. An impairment of long-term object recognition memory assessed with the three-object NOR was demonstrated in Dp(11*Dyrk1a*)6 rats. These results are not equivalent to the long-term recognition memory deficit observed in Tg(*Dyrk1a*)189N3Yah transgenic mice, where the NOR is based on two objects (Nguyen et al. 2018; Duchon et al. 2021). Thus, we probably must adapt the test to the organism model. When considering replicating a disease in a given species, we must consider a more ethological perspective, looking at the normal behaviour of the species and adapting our test.

Nevertheless, we validated a new *Dyrk1a*-overexpressing rat model, showing impaired cognitive functions and craniofacial changes relevant to Down syndrome. This rat model will permit analysing the impact of DYRK1A overexpression in a second species and understanding better the common molecular mechanisms underlying Down syndrome features. In addition, numerous studies have demonstrated that inhibition of DYRK1A kinase activity - in models overexpressing *Dyrk1a* – rescues the memory functions of these animals (Stensen et al. 2021; Atas-Ozcan et al. 2021). This Dp(11*Dyrk1a*)6 rat model could, therefore, be used to confirm the reproducibility and the efficacy of drug treatments in correcting memory function by inhibiting DYRK1A activity in a model other than the mouse.

References

Ahn, Kyoung-Jin, Hey Kyeong Jeong, Han-Saem Choi, Soo-Ryoon Ryoo, Yeon Ju Kim, Jun-Seo Goo, Se-Young Choi, Jung-Soo Han, Ilho Ha, et Woo-Joo Song. 2006. « DYRK1A BAC Transgenic Mice Show Altered Synaptic Plasticity with Learning and Memory Defects ». *Neurobiology of Disease* 22 (3): 463‑72. https://doi.org/10.1016/j.nbd.2005.12.006.

Altafaj, X., M. Dierssen, C. Baamonde, E. Martí, J. Visa, J. Guimerà, M. Oset, et al. 2001. « Neurodevelopmental Delay, Motor Abnormalities and Cognitive Deficits in Transgenic Mice Overexpressing Dyrk1A (Minibrain), a Murine Model of Down's Syndrome ». *Human Molecular Genetics* 10 (18): 1915‑23. https://doi.org/10.1093/hmg/10.18.1915.

Altafaj, Xavier, Eduardo D. Martín, Jon Ortiz-Abalia, Aitana Valderrama, Cristina Lao-Peregrín, Mara Dierssen, et Cristina Fillat. 2013. « Normalization of Dyrk1A Expression by AAV2/1-

shDyrk1A Attenuates Hippocampal-Dependent Defects in the Ts65Dn Mouse Model of Down Syndrome ». *Neurobiology of Disease* 52 (avril):117‑27. https://doi.org/10.1016/j.nbd.2012.11.017.

Arqué, Glòria, Vassiliki Fotaki, David Fernández, María Martínez de Lagrán, Maria L. Arbonés, et Mara Dierssen. 2008. « Impaired Spatial Learning Strategies and Novel Object Recognition in Mice Haploinsufficient for the Dual Specificity Tyrosine-Regulated Kinase-1A (Dyrk1A) ». *PloS One* 3 (7): e2575. https://doi.org/10.1371/journal.pone.0002575.

Atas-Ozcan, Helin, Véronique Brault, Arnaud Duchon, et Yann Herault. 2021. « Dyrk1a from Gene Function in Development and Physiology to Dosage Correction across Life Span in Down Syndrome ». *Genes* 12 (11): 1833. https://doi.org/10.3390/genes12111833.

Birling, Marie-Christine, Laurence Schaeffer, Philippe André, Loic Lindner, Damien Maréchal, Abdel Ayadi, Tania Sorg, Guillaume Pavlovic, et Yann Hérault. 2017. « Efficient and Rapid Generation of Large Genomic Variants in Rats and Mice Using CRISMERE ». *Scientific Reports* 7 (mars):43331. https://doi.org/10.1038/srep43331.

Bon, B. W. M. van, A. Hoischen, J. Hehir-Kwa, A. P. M. de Brouwer, C. Ruivenkamp, A. C. J. Gijsbers, C. L. Marcelis, et al. 2011. « Intragenic Deletion in DYRK1A Leads to Mental Retardation and Primary Microcephaly ». *Clinical Genetics* 79 (3): 296‑99. https://doi.org/10.1111/j.1399-0004.2010.01544.x.

Brault, Véronique, Thu Lan Nguyen, Javier Flores-Gutiérrez, Giovanni Iacono, Marie-Christine Birling, Valérie Lalanne, Hamid Meziane, et al. 2021. « Dyrk1a Gene Dosage in Glutamatergic Neurons Has Key Effects in Cognitive Deficits Observed in Mouse Models of MRD7 and Down Syndrome ». *PLoS Genetics* 17 (9): e1009777. https://doi.org/10.1371/journal.pgen.1009777.

Bronicki, Lucas M., Claire Redin, Severine Drunat, Amélie Piton, Michael Lyons, Sandrine Passemard, Clarisse Baumann, et al. 2015. « Ten New Cases Further Delineate the Syndromic Intellectual Disability Phenotype Caused by Mutations in DYRK1A ». *European Journal of Human Genetics: EJHG* 23 (11): 1482‑87. https://doi.org/10.1038/ejhg.2015.29.

Bui, Linh C., Laure Tabouy, Florent Busi, Jean-Marie Dupret, Nathalie Janel, Chris Planque, Jean-Maurice Delabar, Fernando Rodrigues-Lima, et Julien Dairou. 2014. « A High-Performance Liquid Chromatography Assay for Dyrk1a, a Down Syndrome-Associated Kinase ». *Analytical Biochemistry* 449 (mars):172‑78. https://doi.org/10.1016/j.ab.2013.12.024.

Cieuta-Walti, Cécile, Aida Cuenca-Royo, Klaus Langohr, Claire Rakic, Ma Ángeles López-Vílchez, Julián Lirio, Domingo González-Lamuño Leguina, et al. 2022. « Safety and Preliminary Efficacy on Cognitive Performance and Adaptive Functionality of Epigallocatechin Gallate (EGCG) in Children with Down Syndrome. A Randomized Phase Ib Clinical Trial (PERSEUS Study) ». *Genetics in Medicine: Official Journal of the American College of Medical Genetics* 24 (10): 2004‑13. https://doi.org/10.1016/j.gim.2022.06.011.

Courcet, Jean-Benoît, Laurence Faivre, Perrine Malzac, Alice Masurel-Paulet, Estelle Lopez, Patrick Callier, Laetitia Lambert, et al. 2012. « The DYRK1A Gene Is a Cause of Syndromic Intellectual Disability with Severe Microcephaly and Epilepsy ». *Journal of Medical Genetics* 49 (12): 731‑36. https://doi.org/10.1136/jmedgenet-2012-101251.

Courraud, Jérémie, Eric Chater-Diehl, Benjamin Durand, Marie Vincent, Maria Del Mar Muniz Moreno, Imene Boujelbene, Nathalie Drouot, et al. 2021. « Integrative Approach to Interpret DYRK1A Variants, Leading to a Frequent Neurodevelopmental Disorder ».

Genetics in Medicine: Official Journal of the American College of Medical Genetics 23 (11): 2150-59. https://doi.org/10.1038/s41436-021-01263-1.

Dang, T., W. Y. Duan, B. Yu, D. L. Tong, C. Cheng, Y. F. Zhang, W. Wu, et al. 2018. « Autism-Associated Dyrk1a Truncation Mutants Impair Neuronal Dendritic and Spine Growth and Interfere with Postnatal Cortical Development ». *Molecular Psychiatry* 23 (3): 747-58. https://doi.org/10.1038/mp.2016.253.

Dembélé, Doulaye. 2019. « Analysis of High-Throughput Biological Data Using Their Rank Values ». *Statistical Methods in Medical Research* 28 (8): 2276-91. https://doi.org/10.1177/0962280218764187.

Do Carmo, Sonia, et A. Claudio Cuello. 2013. « Modeling Alzheimer's disease in transgenic rats ». *Molecular Neurodegeneration* 8 (1): 37. https://doi.org/10.1186/1750-1326-8-37.

Drummond, Eleanor, et Thomas Wisniewski. 2017. « Alzheimer's Disease: Experimental Models and Reality ». *Acta Neuropathologica* 133 (2): 155-75. https://doi.org/10.1007/s00401-016-1662-x.

Duchon, Arnaud, et Yann Herault. 2016. « DYRK1A, a Dosage-Sensitive Gene Involved in Neurodevelopmental Disorders, Is a Target for Drug Development in Down Syndrome ». *Frontiers in Behavioral Neuroscience* 10:104. https://doi.org/10.3389/fnbeh.2016.00104.

Duchon, Arnaud, Maria del Mar Muniz Moreno, Sandra Martin Lorenzo, Marcia Priscilla Silva de Souza, Claire Chevalier, Valérie Nalesso, Hamid Meziane, et al. 2021. « Multi-influential genetic interactions alter behaviour and cognition through six main biological cascades in Down syndrome mouse models ». *Human Molecular Genetics* 30 (9): 771-88. https://doi.org/10.1093/hmg/ddab012.

Earl, Rachel K., Tychele N. Turner, Heather C. Mefford, Caitlin M. Hudac, Jennifer Gerdts, Evan E. Eichler, et Raphael A. Bernier. 2017. « Clinical phenotype of ASD-associated DYRK1A haploinsufficiency ». *Molecular Autism* 8 (octobre):54. https://doi.org/10.1186/s13229-017-0173-5.

Ellenbroek, Bart, et Jiun Youn. 2016. « Rodent Models in Neuroscience Research: Is It a Rat Race? » *Disease Models & Mechanisms* 9 (10): 1079-87. https://doi.org/10.1242/dmm.026120.

Ennaceur, A., et J. Delacour. 1988. « A New One-Trial Test for Neurobiological Studies of Memory in Rats. 1: Behavioral Data ». *Behavioural Brain Research* 31 (1): 47-59. https://doi.org/10.1016/0166-4328(88)90157-x.

Ennaceur, A., N. Neave, et J. P. Aggleton. 1997. « Spontaneous Object Recognition and Object Location Memory in Rats: The Effects of Lesions in the Cingulate Cortices, the Medial Prefrontal Cortex, the Cingulum Bundle and the Fornix ». *Experimental Brain Research* 113 (3): 509-19. https://doi.org/10.1007/pl00005603.

Evers, Jochem M.G., Roman A. Laskowski, Marta Bertolli, Jill Clayton-Smith, Charu Deshpande, Jacqueline Eason, Frances Elmslie, et al. 2017. « Structural analysis of pathogenic mutations in the DYRK1A gene in patients with developmental disorders ». *Human Molecular Genetics* 26 (3): 519-26. https://doi.org/10.1093/hmg/ddw409.

Fotaki, V., M. Martínez de Lagrán, X. Estivill, M. Arbonés, et M. Dierssen. 2004. « Haploinsufficiency of Dyrk1A in Mice Leads to Specific Alterations in the Development and Regulation of Motor Activity ». *Behavioral Neuroscience* 118:815-21. https://doi.org/10.1037/0735-7044.118.4.815.

Fotaki, Vassiliki, Mara Dierssen, Soledad Alcántara, Salvador Martínez, Eulàlia Martí, Caty Casas, Joana Visa, Eduardo Soriano, Xavier Estivill, et Maria L. Arbonés. 2002. « Dyrk1A Haploinsufficiency Affects Viability and Causes Developmental Delay and Abnormal Brain Morphology in Mice ». *Molecular and Cellular Biology* 22 (18): 6636-47. https://doi.org/10.1128/MCB.22.18.6636-6647.2002.

García-Cerro, Susana, Noemí Rueda, Verónica Vidal, Sara Lantigua, et Carmen Martínez-Cué. 2017. « Normalizing the Gene Dosage of Dyrk1A in a Mouse Model of Down Syndrome Rescues Several Alzheimer's Disease Phenotypes ». *Neurobiology of Disease* 106 (octobre):76-88. https://doi.org/10.1016/j.nbd.2017.06.010.

Grau, Cristina, Krisztina Arató, José M. Fernández-Fernández, Aitana Valderrama, Carlos Sindreu, Cristina Fillat, Isidre Ferrer, Susana de la Luna, et Xavier Altafaj. 2014. « DYRK1A-Mediated Phosphorylation of GluN2A at Ser1048 Regulates the Surface Expression and Channel Activity of GluN1/GluN2A Receptors ». *Frontiers in Cellular Neuroscience* 8 (octobre). https://doi.org/10.3389/fncel.2014.00331.

Guedj, Fayçal, Patricia Lopes Pereira, Sonia Najas, Maria-Jose Barallobre, Caroline Chabert, Benoit Souchet, Catherine Sebrie, et al. 2012. « DYRK1A: A master regulatory protein controlling brain growth ». *Neurobiology of Disease* 46 (1): 190-203. https://doi.org/10.1016/j.nbd.2012.01.007.

Hämmerle, Barbara, Edgar Ulin, Jordi Guimera, Walter Becker, François Guillemot, et Francisco J. Tejedor. 2011. « Transient Expression of Mnb/Dyrk1a Couples Cell Cycle Exit and Differentiation of Neuronal Precursors by Inducing p27KIP1 Expression and Suppressing NOTCH Signaling ». *Development (Cambridge, England)* 138 (12): 2543-54. https://doi.org/10.1242/dev.066167.

Himpel, S., P. Panzer, K. Eirmbter, H. Czajkowska, M. Sayed, L. C. Packman, T. Blundell, et al. 2001. « Identification of the Autophosphorylation Sites and Characterization of Their Effects in the Protein Kinase DYRK1A ». *The Biochemical Journal* 359 (Pt 3): 497-505. https://doi.org/10.1042/0264-6021:3590497.

Ji, Jianling, Hane Lee, Bob Argiropoulos, Naghmeh Dorrani, John Mann, Julian A. Martinez-Agosto, Natalia Gomez-Ospina, et al. 2015. « DYRK1A Haploinsufficiency Causes a New Recognizable Syndrome with Microcephaly, Intellectual Disability, Speech Impairment, and Distinct Facies ». *European Journal of Human Genetics* 23 (11): 1473-81. https://doi.org/10.1038/ejhg.2015.71.

Jinek, Martin, Krzysztof Chylinski, Ines Fonfara, Michael Hauer, Jennifer A. Doudna, et Emmanuelle Charpentier. 2012. « A Programmable Dual-RNA-Guided DNA Endonuclease in Adaptive Bacterial Immunity ». *Science (New York, N.Y.)* 337 (6096): 816-21. https://doi.org/10.1126/science.1225829.

Kraeuter, Ann-Katrin, Paul C. Guest, et Zoltán Sarnyai. 2019. « The Y-Maze for Assessment of Spatial Working and Reference Memory in Mice ». *Methods in Molecular Biology (Clifton, N.J.)* 1916:105-11. https://doi.org/10.1007/978-1-4939-8994-2_10.

Leder, Susanne, Yvonne Weber, Xavier Altafaj, Xavier Estivill, Hans-Georg Joost, et Walter Becker. 1999. « Cloning and Characterization of DYRK1B, a Novel Member of the DYRK Family of Protein Kinases ». *Biochemical and Biophysical Research Communications* 254 (2): 474-79. https://doi.org/10.1006/bbrc.1998.9967.

Li, Zhongyou, Tao Yu, Masae Morishima, Annie Pao, Jeffrey LaDuca, Jeffrey Conroy, Norma Nowak, Sei-Ichi Matsui, Isao Shiraishi, et Y. Eugene Yu. 2007. « Duplication of the Entire 22.9 Mb Human Chromosome 21 Syntenic Region on Mouse Chromosome 16 Causes

Cardiovascular and Gastrointestinal Abnormalities ». *Human Molecular Genetics* 16 (11): 1359-66. https://doi.org/10.1093/hmg/ddm086.

Lindner, Loic, Pauline Cayrou, Sylvie Jacquot, Marie-Christine Birling, Yann Herault, et Guillaume Pavlovic. 2021. « Reliable and Robust Droplet Digital PCR (ddPCR) and RT-ddPCR Protocols for Mouse Studies ». *Methods (San Diego, Calif.)* 191 (juillet):95-106. https://doi.org/10.1016/j.ymeth.2020.07.004.

Luco, Stephanie M., Daniela Pohl, Erick Sell, Justin D. Wagner, David A. Dyment, et Hussein Daoud. 2016. « Case report of novel DYRK1A mutations in 2 individuals with syndromic intellectual disability and a review of the literature ». *BMC Medical Genetics* 17 (1): 15. https://doi.org/10.1186/s12881-016-0276-4.

Luo, Weijun, Michael S. Friedman, Kerby Shedden, Kurt D. Hankenson, et Peter J. Woolf. 2009. « GAGE: generally applicable gene set enrichment for pathway analysis ». *BMC Bioinformatics* 10 (1): 161. https://doi.org/10.1186/1471-2105-10-161.

Møller, Anders Pape, Diego Rubolini, et Esa Lehikoinen. 2008. « Populations of Migratory Bird Species That Did Not Show a Phenological Response to Climate Change Are Declining ». *Proceedings of the National Academy of Sciences of the United States of America* 105 (42): 16195-200. https://doi.org/10.1073/pnas.0803825105.

Muñiz Moreno, Maria del Mar. 2019. « Characterization of genes, pathways and biological cascades involved in brain dysfunction observed in Down Syndrome and Mental retardation Disease 7 ». These de doctorat, Strasbourg. https://theses.fr/2019STRAJ122.

Nguyen, Thu Lan, Arnaud Duchon, Antigoni Manousopoulou, Nadège Loaëc, Benoît Villiers, Guillaume Pani, Meltem Karatas, et al. 2018. « Correction of Cognitive Deficits in Mouse Models of Down Syndrome by a Pharmacological Inhibitor of DYRK1A ». *Disease Models & Mechanisms* 11 (9): dmm035634. https://doi.org/10.1242/dmm.035634.

Olton, David S., Christine Collison, et Mary Ann Werz. 1977. « Spatial memory and radial arm maze performance of rats ». *Learning and Motivation* 8 (3): 289-314. https://doi.org/10.1016/0023-9690(77)90054-6.

Ori-McKenney, Kassandra M., Richard J. McKenney, Hector H. Huang, Tun Li, Shan Meltzer, Lily Yeh Jan, Ronald D. Vale, Arun P. Wiita, et Yuh Nung Jan. 2016. « Phosphorylation of β-Tubulin by the Down Syndrome Kinase, Minibrain/DYRK1a, Regulates Microtubule Dynamics and Dendrite Morphogenesis ». *Neuron* 90 (3): 551-63. https://doi.org/10.1016/j.neuron.2016.03.027.

Park, Joongkyu, Jee Young Sung, Joohyun Park, Woo-Joo Song, Sunghoe Chang, et Kwang Chul Chung. 2012. « Dyrk1A Negatively Regulates the Actin Cytoskeleton through Threonine Phosphorylation of N-WASP ». *Journal of Cell Science* 125 (Pt 1): 67-80. https://doi.org/10.1242/jcs.086124.

Raveau, Matthieu, Atsushi Shimohata, Kenji Amano, Hiroyuki Miyamoto, et Kazuhiro Yamakawa. 2018. « DYRK1A-Haploinsufficiency in Mice Causes Autistic-like Features and Febrile Seizures ». *Neurobiology of Disease* 110 (février):180-91. https://doi.org/10.1016/j.nbd.2017.12.003.

Song, W. J., S. H. Chung, et D. M. Kurnit. 1997. « The Murine Dyrk Protein Maps to Chromosome 16, Localizes to the Nucleus, and Can Form Multimers ». *Biochemical and Biophysical Research Communications* 231 (3): 640-44. https://doi.org/10.1006/bbrc.1997.6154.

Soppa, Ulf, Julian Schumacher, Victoria Florencio Ortiz, Tobias Pasqualon, Francisco J. Tejedor, et Walter Becker. 2014. « The Down Syndrome-Related Protein Kinase DYRK1A Phosphorylates P27(Kip1) and Cyclin D1 and Induces Cell Cycle Exit and Neuronal

Differentiation ». *Cell Cycle (Georgetown, Tex.)* 13 (13): 2084-2100. https://doi.org/10.4161/cc.29104.

Souchet, Benoit, Fayçal Guedj, Zsuza Penke-Verdier, Fabrice Daubigney, Arnaud Duchon, Yann Herault, Jean-Charles Bizot, et al. 2015. « Pharmacological Correction of Excitation/Inhibition Imbalance in Down Syndrome Mouse Models ». *Frontiers in Behavioral Neuroscience* 9:267. https://doi.org/10.3389/fnbeh.2015.00267.

Souchet, Benoit, Fayçal Guedj, Ignasi Sahún, Arnaud Duchon, Fabrice Daubigney, Anne Badel, Yuchio Yanagawa, et al. 2014. « Excitation/Inhibition Balance and Learning Are Modified by Dyrk1a Gene Dosage ». *Neurobiology of Disease* 69 (septembre):65-75. https://doi.org/10.1016/j.nbd.2014.04.016.

Soundararajan, Meera, Annette K. Roos, Pavel Savitsky, Panagis Filippakopoulos, Arminja N. Kettenbach, Jesper V. Olsen, Scott A. Gerber, Jeyanthy Eswaran, Stefan Knapp, et Jonathan M. Elkins. 2013. « Structures of Down Syndrome Kinases, DYRKs, Reveal Mechanisms of Kinase Activation and Substrate Recognition ». *Structure (London, England: 1993)* 21 (6): 986-96. https://doi.org/10.1016/j.str.2013.03.012.

Stensen, Wenche, Ulli Rothweiler, Richard Alan Engh, Melissa R. Stasko, Ilya Bederman, Alberto C. S. Costa, Anders Fugelli, et John S. Mjøen Svendsen. 2021. « Novel DYRK1A Inhibitor Rescues Learning and Memory Deficits in a Mouse Model of Down Syndrome ». *Pharmaceuticals (Basel, Switzerland)* 14 (11): 1170. https://doi.org/10.3390/ph14111170.

Tejedor, F., X. R. Zhu, E. Kaltenbach, A. Ackermann, A. Baumann, I. Canal, M. Heisenberg, K. F. Fischbach, et O. Pongs. 1995. « Minibrain: A New Protein Kinase Family Involved in Postembryonic Neurogenesis in Drosophila ». *Neuron* 14 (2): 287-301. https://doi.org/10.1016/0896-6273(95)90286-4.

Thomazeau, Aurore, Olivier Lassalle, Jillian Iafrati, Benoit Souchet, Fayçal Guedj, Nathalie Janel, Pascale Chavis, Jean Delabar, et Olivier J. Manzoni. 2014. « Prefrontal Deficits in a Murine Model Overexpressing the down Syndrome Candidate Gene Dyrk1a ». *The Journal of Neuroscience: The Official Journal of the Society for Neuroscience* 34 (4): 1138-47. https://doi.org/10.1523/JNEUROSCI.2852-13.2014.

Yu, Tao, Zhongyou Li, Zhengping Jia, Steven J. Clapcote, Chunhong Liu, Shaomin Li, Suhail Asrar, et al. 2010. « A Mouse Model of Down Syndrome Trisomic for All Human Chromosome 21 Syntenic Regions ». *Human Molecular Genetics* 19 (14): 2780-91. https://doi.org/10.1093/hmg/ddq179.

Discussion, conclusions and perspectives

Rodent models in Down syndrome research

The main objective in understanding the pathology of DS has been to determine the genotype-phenotype correlations. The prevailing hypothesis for the genetic causes underlying DS pathology is that individual phenotypes are caused by an extra copy of one or more of the ~310 genes present on HSA21 (« Chromosome 21: 1-46,709,983 - Chromosome summary - Homo_sapiens - Ensembl genome browser 112 », s. d.). Such genes are described as being dosage sensitive. It is expected that the discovery of these genes would lead to the understanding of the molecular pathways that cause the various DS phenotypes, and consequently, to the identification of more efficient treatment options (Lana-Elola et al. 2011).

Initially, the search for these dosage-sensitive genetic culprits took advantage of human partial trisomies of HSA21 (Delabar et al. 1993; Korenberg et al. 1994; Korbel et al. 2009; Lyle et al. 2009), but their use was limited by the rarity of them, the heterogeneity of the specific phenotypes, and the genetic variation between individuals (Lana-Elola et al. 2011). An essential way to solve this was throught the creation of rodent models replicating the clinical characteristics of DS. New technologies have simplified the creation of those rodent models with desired segmental duplications.

Mice are the most used animal model for studying the pathophysiology of human diseases. Indeed, mice are biologically very similar to humans: 90% of human and mouse genome regions have comparable synteny (Chinwalla et al. 2002). In the case of HSA21, the orthologous genes are found on three different mouse chromosomes: Mmu10, Mmu16, and Mmu17. The majority of HSA21 genes, including the *Dyrk1a* gene, are located on Mmu16 (102 genes) between *Lipi* and *Zbtb21*. Over the years, researchers have generated numerous mouse models of DS to better understand its pathophysiology and identify genotype-phenotype correlations, with the goal of identifying target genes for DS therapies (Herault et al. 2017).

Rat models represent as well an optimal animal model; reproducing a majority of the phenotypes observed in DS, as in the transchromosomal rat model TcHsa21 (Kazuki et al. 2020). This model shows learning and spatial memory deficits, increased anxiety, and hyperactivity.

Cerebral volume is smaller, with a reduced cerebellar size. Besides, the craniofacial morphology and cardiac development of TcHsa21 rats are impaired (Kazuki et al. 2022) like in DS. Also, the rat models allow us to better explore behavior, cognition, memory and social interactions. Compared to mice, they are socially more active and competent and less stressed by cognitive tests such as the Morris maze (Ellenbroek et Youn 2016).

The objectives of this PhD were to investigate through different rodent models the molecular genetics underlying the DS-CF phenotype and discover new dosage-sensitive genes.

Briefly, Chapter 1 (Article#1) describes how we mapped a new chromosomic region. Using the Dp(16)1Yey mouse model as a reference, we achieved a genetic dissection of the Mmu16 with a new panel of mouse models developed in our laboratory (IGBMC-ICS). Thanks to this, we were able to define a shorter chromosomic region and postulate new candidate genes responsible for the DS-CF phenotype and to understand the fundamental molecular basis underlying this phenotype. Additionally, we have generated a new mouse model that allowed us to perform a phenotypic shape rescue of the midface hypoplasia, a crucial characteristic of the DS-CF phenotype. This article will help us gain a better knowledge of the genetic links that led to the development of this phenotype. This will support further research developing new and more precise models to identify the phenotypical CF recovery, with the objective of finding interceptive treatments in the future.

Chapter 2 is focused on the validation of new DS rat models, defining their specific phenotype and identifying a new chromosomic region of interest for the DS-CF phenotype. Furthermore, a complete trisomic rat model will aid in understanding the genetic relationships that enhance the expression of different phenotypes. Our findings will benefit future studies in the craniofacial field, not only for DS but also for other rare diseases with craniofacial dysmorphism.

Dissection of the *Lipi-Zbtb21* region and its contribution to DS craniofacial DS-CF phenotype, using a new panel of mouse models

In DS individuals, craniofacial dysmorphism is almost 100% penetrant, but the contributive genetic and developmental factors are unclear. As previously described, different DS mouse models have been used to study this specific phenotype, as Ts65Dn (Olson et al. 2004), Ts66Yah (Duchon et al. 2022), Ts1Cje (Sago et al. 1998) and Dp(16)1Yey (Li et al. 2007), with different segmental duplications in Mmu16 and presenting the DS-CF phenotype. However, these models haven't been sufficient to completely dissect and propose new candidates' genes. In contrast, Dp1Rhr (Olson et al. 2007), a DS model with a duplication of the 33 genes that compound the Down Syndrome critical region (DSCR), a small region located at 21q22 believed to be the responsible for most of the phenotypic traits associated with DS (Delabar et al. 1993), showed that this region was not enough to develop all the phenotypes found in DS, in the case of the CF phenotype, this model shows a macrocephaly and an inverse phenotype to DS (Deitz et Roper 2011).

The DS-CF phenotype in mouse typically encompasses microcephaly, a small midface, a reduced mediolateral orbital region, reduced bizygomatic breadth, a small maxilla, brachycephaly (relatively wide neurocranium), and a small mandible (Olson et al. 2004). To study this characteristic phenotype, we analyzed the Dp(16)1Yey model (Article #1), taking advantage that this model carries a complete duplication of Mmu16 (*Lipi-Zbtb21* region) (Li et al. 2007) and has a previously been well described for the DS-like craniofacial phenotype (Starbuck et al. 2014).

Our results replicate the same findings of Starbuck et al. (2014). Using a standard craniofacial analysis plus a new voxel analysis, we achieved to observe the principals changes in the skull and mandibles in 3D. A decrease in the dimensions of the midface (midface hypoplasia) with a short nasal region and an increase of dimensions in the neurocranium width, with a reduction in the occipital bone that leads to a shortening of the anteroposterior axis (brachycephaly). In the mandible, we found a decrease in the width of the ramus, body, incisor alveolus, and molar alveolus, and increased lateral dimension in coronoid and condylar process, which is expected

due the skull brachycephaly. Besides, skeletal staining showed a defect in intramembranous ossification. The analysis at different embryonic stages allowed us to hypothesize that the changes observed at E18.5 correspond to a delay and not to a continuous defect in intramembranous ossification. This defect could be related to a problem in the differentiation of mesenchymal cells into osteoblasts or in osteoblast proliferation with a subsequent attenuated osteoblast function (Thomas et al. 2021). Here, we demonstrate that the craniofacial dysmorphism found in Dp(16)1Yey correlates with the human DS-CF phenotype, making it a good model to study DS-CF phenotype.

We mapped the *Lipi-Zbtb21* region using a new panel of DS mouse models, with specific CF phenotypes for each one, to reduce the chromosomic region and find dosage-sensitives genes responsible for the DS-CF phenotype. As shown in the integrative multivariate analysis in Chapter 1, we observed that the DS strains show significant differences compared with their wild-type controls, explaining the contribution of each of the regions to the different characteristics of the CF phenotype in four main groups. [1] Dp(16)1Yey, Dp(16)1Yey/Ripply3tm1b with strong brachycephaly and midface hypoplasia; [2] Dp(16)12Yah and Dp(16)9Yah with stronger midface hypoplasia and brachycephaly; [3] Dp(16)10Yah, Dp(16)13Yah and Dp(16)8Yah with less significative changes; [4] Dp(16)11Yah and Dp(16)7Yah close to the wild-type and inverse dimension in the principal component 1, while the Ts66Yah, the Tg(Dyrk1a) are on the same side of the DS models. These four main groups are translated in 3 different chromosomic regions of Mmu16 (CF1, CF2 and CF3), as can be seen in Figure 21.

We excluded a region compound between *Tmprss15-Grik1*, triplicated in Dp(16)11Yah alone, with almost no effect on CF form and shape, similar to the results found in Redhead et al. (Redhead et al. 2023) and their model Dp(16)9Tyb, that doesn't present a DS-CF phenotype. Nevertheless, we found the contribution of the most centromeric part CF3 involved in cranium enlargement as new. It could be slightly artificial as this effect was not seen in the Dp(16)1Yey, but could also be due to an effect specific to this region while not triplicated with CF2 and CF3. More detailed investigations with new models would allow to discriminate the genetic interaction of the 3 CF regions.

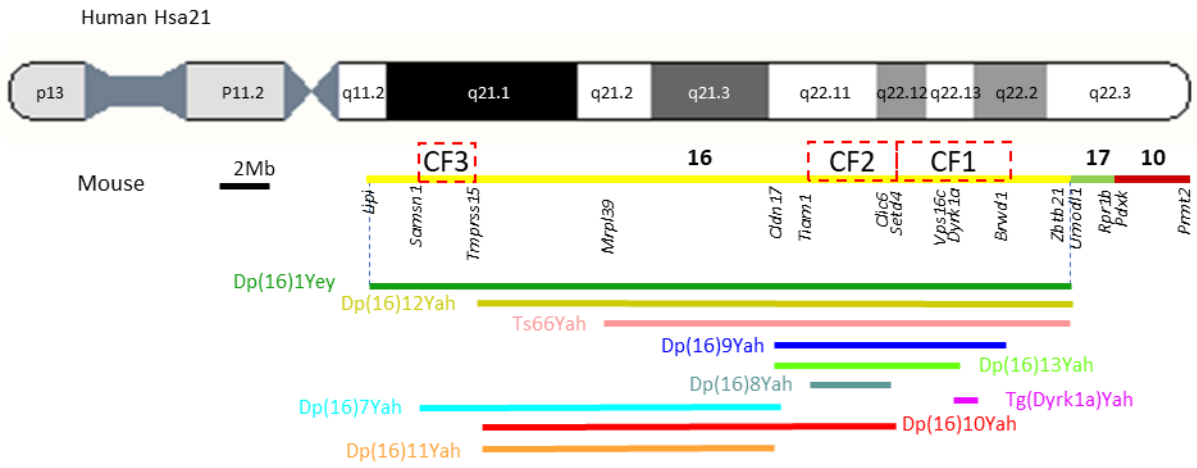

Figure 21. Relative position of the new 3 different chromosomic regions on Mmu16. CF1, CF2 and CF3 in red squares.

Searching for new candidates genes for the DS-CF phenotype and considering the strong DS-like phenotype found in Dp(16)9Yah and Dp(16)12Yah, we focused in the region CF1, specifically in the region compound between *Setd4-Dyrk1a*. Inside this region, using the data set "Temporal analysis of ectoderm and mesenchyme gene expression in the developing mouse facial prominences" from the FaceBase Consortium (Hong Li 2017), we identified a set of candidate genes. Among these genes, *Dyrk1a* (Dual Specificity Tyrosine Phosphorylation Regulated Kinase 1A) and *Ripply3* (*Ripply* Transcriptional Repressor 3) seemed promising targets for CF in DS.

Role of *Dyrk1a* in the DS-CF mouse phenotype

The *DYRK1A* gene encodes a member of the dual-specificity tyrosine phosphorylation-regulated kinase (DYRK) family (van Bon et al. 2011). It is located between *DSCR3* and *KCNJ6*, on the DSCR of human chromosome 21 and in the syntenic region of mouse chromosome 16 (Galceran et al. 2003). It plays a role in major developmental steps of brain development, controlling the proliferation of neural progenitors, the migration of neurons, their dendritogenesis and the function of the synapse (Atas-Ozcan et al. 2021) and recently has been identified as one of the genes required in three copies to cause CF dysmorphology in mouse models of DS (Redhead et al. 2023).

Considering this information, in Article #1, we hypothesized that in mice the DS-CF phenotype is related to the overexpression of *Dyrk1a*. Interestingly, we found that *Dyrk1a* could be responsible for brachycephaly in DS. We confirmed this hypothesis analyzing the Tg(*Dyrk1a*) mouse line, where we found as well mice with brachycephaly. The new model Dp(16)13Yah, where *Dyrk1a* is found in two copies, has lost the strong brachycephaly.

We demonstrated that 3 copies of *Dyrk1a* are necessary to induce the brachycephaly found in DS. This is correlated with the findings in Dp(16)1Tyb by Redhead et al. (Redhead et al. 2023), where *Dyrk1a* was crucial to generate complete DS-CF phenotypes, and the use of DYRK1A inhibitors or genetic knockout of *DYRK1A* has been shown to rescue the skull and jaw malformations (McElyea et al. 2016; Redhead et al. 2023).

However, Johnson et al. in 2024 showed that a decrease in *Dyrk1a* in *Xenopus* resulted in craniofacial malformations, altered expression of critical craniofacial regulators as *Pax3* and *Sox9* fundamental for cranial neural crest development, and presented altered retinoic acid, hedgehog, nuclear factor of activated T cells (NFAT), Notch and WNT signaling pathways. These results indicate that DYRK1A function is critical for early craniofacial development and must properly regulate the expression of specific craniofacial regulators in the branchial arches (Johnson et al. 2024). Therefore, we decided to analyze the levels of expression of *Dyrk1a* in craniofacial precursors tissues. In mouse models of DS, brain levels of DYRK1A are increased by a factor of around 1.5, demonstrating that expression of this protein is dose dependent. In adult mice, *Dyrk1a* is highly expressed in the olfactory bulb, entorhinal cortex, hippocampus, cerebellar cortex and gray matter (Martí et al. 2003). In the rat, *Dyrk1a* is abundantly expressed during embryonic development in the cerebral cortex, hippocampus, hypothalamus, midbrain and spinal cord. In adult rats, *Dyrk1a* levels are stable and ubiquitous in the brain, heart, liver, kidneys and lungs (Okui et al. 1999). In Article #1, we showed that, in the DS mouse model Dp(16)1Yey and in the DS rat model Dup(RNO11), at early embryonic stage (E11.5 and E12.5 respectively), there is a high level of expression (x1.4) of *Dyrk1a* in the frontonasal process, maxillary process, mandibular process, lateral and medial nasal process, and first pharyngeal arch, precursors tissues of the craniofacial complex. It is known that the gain of function of *Dyrk1a* induce proliferation arrest, and the loss of function caused over proliferation and cell

death and has a regulatory role in cell cycle exit of vertebrate (Hammerle et al. 2011). For this reason we evaluated the proliferation and mitotic index in Dp(16)1Yey; we detected defects in the first branchial arch, precursor of various craniofacial structures.

In conclusion, in DS *Dyrk1a* overdosage is essential and sufficient for the brachycephaly seen in DS, but other genes are responsible for the mandibular phenotypes observed in DS. Its high expression in the craniofacial precursor tissues, demonstrates that it plays a major role in craniofacial development, which can be explained by the defect in proliferation and mitosis index, in addition to the defects in NCC migration described by Redhead et al. (Redhead et al. 2023). Also this is correlated with the results obtained in Chapter 2, with the analysis of the rat models Dp(11*Dyrk1a*)6Yah and Del(11*Dyrk1a*)4Yah.

Role of *Ripply3* in the mouse midface shortening

Ripply3, also known as Down syndrome critical region 6 (Dscr6), is a transcriptional corepressor that acts as a negative regulator of the transcriptional activity of *Tbx1* playing a role in the developing pharyngeal apparatus. It is observed in endoderm and ectoderm cells in the pouches and in the caudal pharyngeal region, suggesting a specific role in these cells (Okubo et al. 2011). In *Ripply3*$^{-/-}$ mouse models, phenotypic abnormalities were first identified in the pharyngeal pouches forming posterior to the second arch. Also, in *Ripply3*$^{-/-}$ embryos were described with a loss of the third and fourth pharyngal arches, causing abnormal development of the vascular system, including deletion of the aortic arch and misshapen major blood vessels. This defects lead to cardiovascular defects, as abnormality in heart development, hypotrophy of the aorta and incomplete formation of the ventricular septum (Okubo et al. 2011; 2021).

In Article#1, we focused on the role of *Ripply3* as negative regulator of the transcriptional activity of *Tbx1* in the developing first pharyngeal arch, structure that is giving rise to the midface components as the maxillary prominence (becomes the future maxilla, zygomatic bone and part of the temporal bone) and mandibular prominence that becomes the future mandible (Frisdal et Trainor 2014). *Tbx1* Is the first dosage-sensitive gene identified in the DiGeorge syndrome (DGS)/velocardiofacial syndrome (VCFS), a congenital disorder characterized by

neural-crest-related developmental defects. In human and DGS models, *TBX1* haploinsufficiency causes craniofacial anomalies (Lindsay et al. 2001) and contributes to heart defects (Merscher et al. 2001). More precisely, the phenotype observed in the mutant mice for the T-box gene, *Tbx1*$^{+/-}$, encompasses abnormal development of the skeletal structures derived from the first and second pharyngeal arches, with reduced dimension of the midface (Jerome et Papaioannou 2001); a similar situation found in the DS mouse models. In our article (Article#1), we could demonstrate that in Dp(16)1Yey at an early stage (E11.5) and in the rat model Dup(RNO11) at E12.5, *Ripply3* is overexpressed, and consecutively, *Tbx1* is downregulated in the midface precursor tissues. These results are correlated with some DS models, such as Ts1Rhr and Ts1Cje, where the expression of the *Tbx1* gene was found to be significantly downregulated in the brain structures. Furthermore, *Tbx1* might be involved in delayed fetal brain development and postnatal psychiatric phenotypes observed in DS (Shimizu et al. 2021). Still, we also detected a defect in cell proliferation of the NCC derivates in the first branchial arch, which also demonstrated a contribution to the midface shortening.

In addition, to confirm this role, we generated a new mouse model: Dp(16)1Yey/*Ripply3*^{tm1b}, with a phenotypic rescue of the DS midface phenotype. We demonstrated an increased shape dimension in the structures corresponding to the midface compared to Dp(16)1Yey. In the multivariate analysis of all the models was possible to found the Dp(16)1Yey/*Ripply3*^{tm1b} model close to Dp(16)1Yey, was located in the main group and dimension of the models that present a strong brachycephaly, but displaced in PC2 from the group where a strong midface hypoplasia predominates (Dp(16)9Yah and Dp(16)12Yah).

In conclusion, we hypothesized that the overexpression of *Ripply3* in DS mouse models will lead to a downregulation of *Tbx1*, explaining the midface shortening in DS, but also in other DS organs and tissues, leading to additional changes. Some of these changes are related to DS heart defects, such as the tetralogy of Fallot observed in some individuals, that may be related to *Ripply3*-dependent downregulation of *Tbx1*, while in DGS, they are caused by the direct *Tbx1* haploinsufficiency (Merscher et al. 2001). Consequently, investigating treatment for DGS to reestablish a normal TBX1 function will also be of interest for Down syndrome, not only for the craniofacial phenotype but also for the brain and the heart function.

New rat models recapitulate the human DS-CF phenotype

Over the last years, numerous mouse models of DS were developed (Herault et al. 2017). In mice, the syntenic regions to the HSA21 are found on three different chromosomes: 10, 16, and 17. Most of these models carry partial or complete duplication of one of these chromosomic regions, with some carrying a duplication of one specific gene playing an important role in the development of DS-related phenotypes (Davisson, Schmidt, et Akeson 1990; Davisson et al. 1993; Reeves et al. 1995). The study of these models helped us to identify DS dosage-sensitive genes. However, since the syntenic regions are split on the different chromosomes in mice, it makes difficult to create a full trisomic model, although not impossible (Y. Li et al. 2021). Rat models have proven to be an effective solution to this problem. Indeed, rats only split the syntenic regions to the HSA21 on two chromosomes, 11 and 20, simplifying the process of creating a complete trisomic model. Moreover, the development of the CRISPR/Cas9 technique has made it possible to modify the rat genome easily and rapidly (Birling et al. 2017).

The project, as detailed in Chapter 2, allowed the characterization of various new DS rat models (Figure 13). Dup(Rno20), Dup(Rno11), and Dup(Rno11-20) models display different DS phenotypes. The behavioral studies revealed a major role for the Rno11 region in the development of cognitive deficits such as short-term spatial memory, long-term spatial memory, spatial learning deficit, working memory deficit, hypoactivity, and anxiety. There was also a reduction in body mass in Dup(Rno11), as well as an increase in locomotor activity. These defects are mirrored in the complete trisomy model, Dup(Rno11-20), for which additional phenotypes are observed. This underlines the importance of interactions between these 2 regions, which are necessary for the appearance of certain phenotypes or the accentuation of others.

The CF phenotype found in these models reveals a confirmed role of the Rno11 (*Lipi* to *Zbtb21* region) with an influence of the Rno20 (*Umodl1-Prmt2* region) on craniofacial changes. We observed significant form and shape changes in the models carrying a duplication of the chromosome 11, as microcephaly, shortening of the midface, smaller mandible and brachycephaly. Furthermore, when combined both models, Dup(Rno11-20) led to the addition

of significant landmarks located in premaxilla and frontal bones showing an influence of the overdosage of Rno20 region.

These results can be correlated with the ones described by Kazuki et al. (2022) in the TcHSA21 rat, a transchromosomic model of DS with a complete trisomy, which contains a freely segregating, EGFP-inserted, human chromosome 21 (Kazuki et al. 2022). They found a smaller craniofacial skeleton compared to WT controls, with significant reduction in linear distances between landmarks concentrated on the facial skeleton, and additional increased dimensions on the cranial vault. An antero-posteriorly retracted face associated with a supero-inferiorly "raised" cranial vault was also described (Kazuki et al. 2022), similar to the phenotype found in our new models.

Besides, it is possible to compare these results with the Dp(16)1Yey mouse model that involves a duplication on mouse chromosome 16 between the *Lipi* and *Zbtb21* genes, identical to the duplication in Dup(Rno11) model (Li et al. 2007). In Dp(16)1Yey, the CF phenotype corresponds to a reduced dimension of the maxillary and palate, brachycephaly, and reduced mandibular size (Li et al. 2007; Yu et al. 2010; Starbuck et al. 2014). Moreover, it is also possible to find other defects as working memory deficit, locomotor activity deficient, delay in learning in Dp(16)1Yey, but the difference between the study types makes it more difficult to compare directly with Dup(RNO11) (Goodliffe et al. 2016; Duchon et al. 2021).

When we compare these results with the phenotype observed in DS human individuals, we found that the DS-CF phenotype corresponds to an overall reduction in head dimensions (microcephaly), brachycephaly (relatively wide neurocranium), small midface, reduced mediolaterally orbital region, reduced bizygomatic breadth, small maxilla, small mandible and increased individual variability (Fink, Madaus, et Walker 1975; Farkas, Kolar, et Munro 1985; Allanson 1993; Frostad, Cleall, et Melosky 1971; Farkas, Posnick, et Hreczko 1991; Richtsmeier, Baxter, et Reeves 2000), features also seen in Dup(RNO11) and Dup(RNO11-20), validating the use of these models for further CF studies.

On the other hand, given that *Dyrk1a* is an important candidate gene for the development of the DS-CF phenotype (Redhead et al. 2023), we analyzed other new rat models linked to DS and

Mental Retardation autosomal Dominant 7 syndrome (MRD7), Dp(11*Dyrk1a*)6Yah and Del(11*Dyrk1a*)4Yah (Birling et al. 2017). Using the same morphometric technique, we showed that Del(11*Dyrk1a*)4Yah model exhibits a microcephaly. We found a reduction in the dimensions of the neurocranium and an increase in the dimensions of the midface. Results correlated with the MRD7 patients phenotype, who display microcephaly and facial dysmorphia (Ji et al. 2015; Courraud et al. 2021). Beyond the craniofacial aspect, this model also recapitulates different cognitive MDR7 phenotypes found in patients, as abnormalities in the impaired short-term spatial memory, spatial learning, hypoactivity, epilepsies and ataxia (Møller, Rubolini, et Lehikoinen 2008). In the case of Dp(11*Dyrk1a*)6Yah, skull analysis shows a significative increase of dimensions in the neurocranium presenting a brachycephaly. Our results are in line with recent publications confirming that *Dyrk1a* plays an important role in the DS-CF phenotype in mice (Redhead et al. 2023; Johnson et al. 2024).

In summary, in Chapter 2 we hypothesized that rat models carrying the duplication of Rno11 display the DS-CF phenotype, defining the chromosomal region comprised between the genes *Lipi* and *Zbtb21* as responsible, thus addressing the second objective of this thesis.

We also demonstrated that *Dyrk1a* is required in 3 copies to generate the brachycephaly in DS rat models, as shown in Dp(11*Dyrk1a*)6Yah model. This was also confirmed with the *Dyrk1a* haploinsufficiency model [Del(11*Dyrk1a*)4Yah], where a single copy of *Dyrk1a* led to a decrease in the shape and size of the neurocranium, inverse phenotype to that found in Dp(11*Dyrk1a*)6Yah. Beyond the craniofacial aspect, these results allow validating these rat models for future studies, opening new avenues for potential targeted treatment to soften craniofacial dysmorphism in Down syndrome, but also of other syndromes with craniofacial manifestations involving genes within this chromosomal region.

This doctoral thesis work was possible thanks to the following funding:

Interdisciplinary Thematic Institute IMCBio, as part of the ITI 2021-2028 program of the University of Strasbourg, CNRS and Inserm, was supported by IdEx Unistra (ANR-10-IDEX-0002), SFRI-STRAT'US project (ANR 20-SFRI-0012), INBS PHENOMIN (ANR-10-INBS-07) and EUR IMCBio

(ANR-17-EURE-0023) under the framework of the French Investments for the Future Program, and European Union's Horizon 2020 research and innovation programme GO-DS21 under grant agreement No 848077.

I received funding from the National Agency for Research and Development (ANID)/Scholarship Program/DOCTORADO BECAS CHILE/2020-72210028.

Future work will be based on continuous collaborations between the Institute of Genetics, Molecular and Cellular Biology, CNRS- UMR7104, INSERM U1258 (IGBMC), the Faculté de Chirurgie Dentaire Robert Frank de l'Université de Strasbourg and the reference center for rare oral an dental diseases, CRMR O-Rares, Hôpitaux Universitaires de Strasbourg.

Résumé de la thèse en français

Introduction

Les altérations les plus courantes et caractéristiques de la Trisomie 21 (T21) sont les troubles de l'apprentissage ainsi que la dysmorphie crâniofaciale (Lana-Elola et al. 2011). La sévérité des caractéristiques crâniofaciales distinctives chez les individus porteurs de T21 (Kisling 1966) varie d'un individu à l'autre (Roper et Reeves 2006) et inclut divers symptômes tels que la microcéphalie, la brachycéphalie, une réduction du tiers moyen de la face, de la région orbitale médiolatérale, de l'os maxillaire, de la largeur bizygomatique et de la mandibule (Fink, Madaus, et Walker 1975; Farkas, Kolar, et Munro 1985; Allanson 1993; Baxter et al. 2000; Richtsmeier, Baxter, et Reeves 2000). Les individus présentent également une faible masse osseuse associée à une réduction de l'activité des ostéoblastes et du renouvellement osseux (McKelvey et al. 2013). Selon l'hypothèse actuelle, la diversité des phénotypes observés dans la T21 serait due à une perturbation de l'homéostasie des protéines, causée par la présence d'une copie supplémentaire d'un ou de plusieurs des 310 gènes du chromosome 21 (HSA21). Certains de ces gènes sont sensibles à la dose, ce qui implique qu'une augmentation du nombre de copies entraîne une activité accrue des protéines associées (Zhu et al. 2019; Duchon et Herault 2016).

A ce jour, les gènes candidats associés aux phénotypes crâniofaciaux identifiés dans les modèles de T21 incluent *Dyrk1a*, *Rcan1* (*SDcr1*) et *Ets2*. Le gène *DYRK1A* est impliqué dans plusieurs phénotypes de la T21, y compris la déficience intellectuelle, l'altération des fonctions motrices et les anomalies crâniofaciales (Hämmerle et al. 2011; Arron et al. 2006; Atas-Ozcan et al. 2021). Cependant, les mécanismes exacts par lesquels le déséquilibre du dosage des gènes du HSA21 affecte la morphogenèse demeurent encore mal compris (Starbuck et al. 2017).

Plusieurs études chez la souris et l'homme ont tenté d'identifier des gènes candidats qui pourraient, individuellement ou collectivement, expliquer chacune des caractéristiques cliniques (Korbel et al. 2009; McCormick et al. 1989). Sachant que le HSA21 présente une synergie conservée avec des régions orthologues sur trois chromosomes murins (Mmu), à savoir les Mmu10, Mmu16 et Mmu17 (Reeves et al. 1995; Sago et al. 1998) et grâce aux avancées rapides dans le domaine du génie génétique ces dernières années, de nombreux modèles de souris pour la T21 ont été générés (Dierssen, Herault, et Estivill 2009).

Les études crâniofaciales n'ont été réalisées que sur quelques modèles murins de la T21. Le modèle Ts65Dn, largement étudié, montre un certain isomorphisme, reflétant une similarité avec les phénotypes observés chez les personnes atteintes de T21. (Olson et al. 2004). Il s'agit d'un modèle dans lequel une région du Mmu16 a été transloquée sur le court segment du Mmu17, ce qui la rend donc trisomique pour 104 gènes Mmu16 orthologues du HSA21 entre *Mrpl39* et *Zbtb21* (Olson et al. 2004; Gardiner et al. 2003; Muñiz Moreno et al. 2020).

Le modèle Ts65Dn présente une faible masse osseuse, due à des défauts cellulaires intrinsèques dans la différenciation des ostéoblastes, ce qui réduit la formation osseuse. De plus, la résorption osseuse, médiée par les ostéoclastes, est également diminuée, mais insuffisamment pour compenser le faible taux de formation osseuse (Parsons et al. 2007; Thomas et al. 2021). Ces souris présentent également de nombreux phénotypes cognitifs et comportementaux comparables à ceux des personnes atteintes de T21, ainsi que des caractéristiques squelettiques, crâniofaciales, cardiovasculaires et de mégacaryocytopoïèse (McKelvey et al. 2013). S'y ajoute une brachycéphalie, une réduction des dimensions de la face et de la voûte crânienne (Richtsmeier, Baxter, et Reeves 2000), ainsi qu'une diminution du volume du cervelet et de la densité des cellules granuleuses du gyrus denté (Baxter et al. 2000).

Un autre modèle de souris important est le Ts1Cje qui présente une duplication d'une région plus restreinte incluant 81 gènes orthologues au HSA21. Ce modèle a été utilisé pour affiner la recherche de gènes sensibles à l'effet dose (Sago et al. 1998). Certaines caractéristiques de la T21 sont retrouvées, notamment des troubles de l'apprentissage et des troubles de l'humeur, une réduction généralisée des régions crâniofaciale et une microcéphalie (Richtsmeier et al. 2002).

Des caractéristiques crâniofaciales similaires ont été rapportées dans notre nouveau modèle Ts66Yah (Duchon et al. 2022) démontrant une contribution majeure des gènes en surdosage (entre *Mrpl39* à *Zbtb21*) aux phénotypes crâniofaciaux.

Le modèle Dp(16Cbr1-Fam3b)1Rhr (noté ici Dp1Rhr), trisomique pour 33 gènes (Olson et al. 2007) présente une taille globale accrue ainsi que des altérations crâniofaciales, dont une mandibule plus grande et morphologiquement distincte de celle observée chez les souris

Ts65Dn et les individus atteints de T21 (Deitz et Roper 2011). D'autres études sur les souris Dp1Rhr ont montré des différences dans la taille du cervelet et du cerveau, ainsi que dans la potentialisation neuronale à long terme et les performances aux tests comportementaux de mémoire et d'apprentissage (Olson et al. 2007).

Ces dernières années, la technologie Cre-loxP a rendu possible la duplication plus précise de certaines régions orthologues au HSA21. Le modèle murin Dp(16)1Yey se caractérise par une duplication directe de 22,9 Mb de la totalité de la région Mmu16, en synténie conservée avec le HSA21, abritant environ 113 gènes orthologues (Z. Li et al. 2007). Parmi les phénotypes observés dans ce modèle, on note des caractéristiques crâniofaciales spécifiques, telles que des modifications dans le taille de l'os maxillaire, de la mandibule et du palais, ainsi qu'une brachycéphalie. De plus, le crâne présente également une variabilité accrue par rapport aux congénères euploïdes pour certaines distances linéaires spécifiques (Li et al. 2007; Yu et al. 2010; Starbuck et al. 2014).

En 2023, grâce à une analyse morphométrique du modèle de souris Dp1Tyb et à un panel de cartographie génétique associé, Redhead et al. (Redhead et al. 2023) ont révélé que la présence en trois copies du gène *Dyrk1a* induit une dysmorphie crâniofaciale chez les souris Dp1Tyb. La souche de souris porte une duplication de 23 Mb de Mmu16, la plus grande des régions orthologues au HSA21, qui contient 145 gènes codants et représentant environ 62 % du HSA21 (Lana-Elola et al. 2016). L'étude des souris Dp1Tyb a mis en évidence de nombreux traits phénotypiques caractéristiques de la T21 humaine, notamment des malformations cardiaques congénitales, une densité osseuse réduite et des déficits au niveau de la mémoire, de la locomotion, de l'audition et du sommeil (Chang et al. 2020; Lana-Elola et al. 2011; 2016; Thomas et al. 2020; Watson-Scales et al. 2018).

Il est crucial de comprendre la complexité génétique et les processus biologiques adaptatifs qui sous-tendent le développement des structures crâniofaciales. Étant donné la conservation de nombreux gènes chez les mammifères, il est probable que les programmes génétiques responsables de phénotypes spécifiques soient également conservés. Par conséquent, l'étude

de modèles animaux peut s'avérer particulièrement utile et pertinente pour éclairer les découvertes génétiques chez l'homme (Richtsmeier, Baxter, et Reeves 2000).

Comme l'on montré les différents modèles étudiés, une trisomie partielle a permis de cartographier les zones du HSA21 contribuant aux anomalies crâniofaciales, mais aucune région spécifique n'a encore été identifiée (Lyle et al. 2009; Korbel et al. 2009). Identifier les gènes sensibles à l'effet dose qui contribuent à chaque composant du phénotype de la T21 serait une avancée majeure pour comprendre les mécanismes moléculaires sous-jacents aux différents symptômes et pour développer des pistes thérapeutiques plus ciblées (Antonarakis 2017; Antonarakis et al. 2020). C'est précisément cet objectif que cette thèse vise à atteindre.

Chapitre 1 : Nouveaux modèles de souris pour le syndrome de Down

Pour répondre à cette problématique, des nouveaux modèles de souris ont été développés avec des duplications segmentaires dans le Mmu16. Pour Dp(*16Samsn1-Cldn17*)7Yah (Dp(16)7Yah), nous avons dupliqué le segment entre *Samsn1* et *Cldn17*. Dp(*16Tiam1-Clic6*))8Yah (Dp(16)8Yah) présente une duplication entre *Tiam1* et *Clic6*. Dp(*16Cldn17-Brwd1*))9Yah (Dp(16)9Yah) présente une duplication dans l'intervalle entre *Cldn17* et *Brwd1*. Dp(*16Tmprss15-Setd4*)10Yah (Dp(16)10Yah) présente une duplication du segment entre *Tmprss15* et *Setd4*, similaire à Dp(*16Tmprss15-Grik1*)11Yah (Dp(16)11Yah), mais ce modèle présente une région dupliquée jusqu'à *Grik1.* Dp(*16Tmprss15-Zbtb21*)12Yah (Dp(16)12Yah) présente la région dupliquée de *Tmprss15* à *Zfp295*, et Dp(*16Cldn17-Vps26c*(*Dyrk1aKO*))13Yah (Dp(16)13Yah) de *Cldn17* à *Vps26c*, jusqu'à la séquence de *Dyrk1a* qui est inactivée. Toutes les lignées ont été maintenues sur un fond génétique C57BL/6J.

Dans ce projet de thèse, nous avons utilisé ces nouveaux modèles de souris améliorés ainsi que des modèles déjà établis tels que Dp(16)1Yey et Tg(*Dyrk1a*), afin d'établir des corrélations entre le phénotype/génotype des souris et ceux des hommes. Notre objectif était de comprendre l'impact potentiel de la duplication de différentes régions chromosomiques sur les caractéristiques crâniofaciales, en menant une analyse morphométrique des modèles animaux.

Cette démarche nous a permis d'orienter nos recherches vers des régions chromosomiques spécifiques et les gènes candidats associés, responsables du phénotype crâniofacial.

Etude de la contribution des sous-régions de l'intervalle *Lipi-Zbtb21* aux caractéristiques crâniofaciales de la T21 en utilisant Dp(16)1Yey contre un nouveau panel de modèles de souris.

Nous avons tiré parti d'un modèle de souris connu, Dp(16)1Yey (qui porte une trisomie complète du Mmu16) (Li et al. 2007) comme référence par rapport au nouveau panel de modèles de souris (Dp7Yah, Dp8Yah, Dp9Yah, Dp10Yah, Dp11Yah, Dp12Yah and Dp13Yah) qui sont porteurs de différentes duplications du Mmu16, pour cartographier l'emplacement des gènes sensibles au dosage qui causent cette dysmorphie. 10 animaux par génotype (n=180) âgés de 14 semaines ont été utilisés.

Brièvement, à l'aide de l'imagerie volumetrique par faisceau conique (CBCT), tecnique de tomodensitometrie permetant de produire une radiographie numerisé, nous avons modélisé une reconstruction tridimensionelle du crâne et de la mandibule pour les 9 différents modèles de souris : Dp(16)1Yey, Dp7Yah, Dp8Yah, Dp9Yah, Dp10Yah, Dp11Yah, Dp12Yah, Dp13Yah, Tg(Dyrk1) et souris sauvage (WT) des mêmes portées. Ensuite, nous avons placé manuellement 61 points de repères anatomiques, 39 dans le crâne et 22 dans la mâchoire. Une fois tous les points de repères crâniofaciaux placés, nous avons extrait leurs coordonnées 3D et nous avons effectué l'analyse matricielle de la distance euclidienne (EDMA) en effectuant deux tests différents : Form difference matrix (FDM) et Shape difference matrix (SDM). Pour une étude multivariable, nous avons utilisé l'analyse en composantes principales (ACP). Nous avons également tiré parti de l'analyse générale de Procrustes, une méthode qui place plusieurs spécimens individuels dans le même espace de forme en mettant à l'échelle, en translatant et en faisant pivoter les coordonnées des points de repères autour du centroïde de chaque échantillon (Rohlf et Slice 1990) en utilisant un nouveau logiciel, Stratovan Checkpoint, qui nous a permis de créer des modèles moyens de populations et d'effectuer une analyse des voxels.

Les résultats trouvés chez les souris Dp(16)1yey avec l'analyse morphométrique standard en plus de la nouvelle analyse de voxel confirment le phénotype crâniofacial précédemment publié

(Starbuck et al. 2014) qui montre une dimension réduite du maxillaire et du palais, une brachycéphalie et une taille réduite de la mandibule. Les résultats des modèles avec des duplications génomiques plus courtes (Dp9Yah et Dp12Yah) ont montré des changements significatifs et un phénotype crâniofacial caractéristique de la T21, identique à celui que nous avons trouvé pour les Dp(16)1Yey. Dans le cas de Dp13Yah, des changements significatifs ont été observés, mais pas la brachycéphalie. Un phénotype inverse a été constaté chez Dp(16)7Yah et Dp(16)11Yah par rapport au Dp(16)1Yey. Le Dp(16)10Yah présentait une réduction globale des dimensions de la tête, partiellement observée chez le Dp(16)8Yah avec une partie médiane de la face plus importante. Cependant, une augmentation de la taille du prémaxillaire et de l'os occipital, entraînant un allongement de l'axe antéropostérieur chez Dp(16)10Yah, a également été observée chez Dp(16)13Yah. Ces résultats nous permettent de proposer 3 régions chromosomiques différentes qui génèrent des changements significatifs dans la morphologie crâniofaciale. Ainsi, nous avons ciblé une région précise comme étant responsable du phénotype crâniofacial de la T21, ce qui nous a permis de proposer des nouveaux gènes candidats : *Dyrk1a* et *Ripply3*.

En outre, considérant l'étude de McKelvey et al. en 2013, où les auteurs ont montré que les individus atteints de T21 ont également une faible masse osseuse associée à une réduction de l'activité des ostéoblastes et du renouvellement osseux, nous avons proposé d'étudier les défauts d'ossification en effectuant une coloration du squelette avec du rouge alizarine et du bleu alcian, dans un modèle représentatif de souris T21, le Dp(16)1Yey. Nous avons analysé le développement de l'os crânien à E18,5 et P2 en utilisant la coloration du squelette au bleu alcian/rouge alizarine sur n= 5 échantillons par génotype. La coloration du squelette entier « whole amount » permet d'évaluer la forme et la taille des éléments qui le compose (Rigueur et Lyons 2014). Nous avons ainsi pu détecter des changements dans l'ossification endomembraneuse de ce modèle T21 par rapport au WT. A E18,5, nous avons trouvé une diminution de l'ossification dans les os à ossification endomembraneuse, mais, à P2, aucun changement significatif n’a été observé. Ces résultats indiquent un retard dans le processus d'ossification endomembraneuse chez les modèles de souris T21.

Rôle du surdosage en *Dyrk1a* dans l'augmentation des dimensions du neurocrâne (brachycéphalie) sur les modèles de souris SD.

Dyrk1a est impliqué dans plusieurs phénotypes de la T21 et les anomalies crâniofaciales (Guedj et al. 2012; McElyea et al. 2016; Llambrich et al. 2022; Redhead et al. 2023). Au cours de la dernière décennie, il est devenu l'un des principaux gènes candidats à l'intervention thérapeutique dans la T21 (De la Torre et al. 2014; Atas-Ozcan et al. 2021). Ici, nous avons tiré parti du modèle Tg(*Dyrk1a*), un modèle avec 3 copies de *Dyrk1a* (Guedj et al. 2012) et des résultats du nouveau modèle Dp13Yah, pour confirmer le rôle de *Dyrk1a* dans le développement du phénotype crâniofacial caractéristique de la T21. Les résultats ont montré la présence d'une brachycéphalie, une augmentation des dimensions du neurocrâne chez les souris Tg(*Dyrk1a*), ainsi qu'une réduction du tiers moyen de la face. Les souris Dp13Yah présentaient une diminution des dimensions du tiers moyen de la face mais pas de brachycéphalie, ce qui peut s'expliquer par le fait que ce modèle ne porte que 2 copies de *Dyrk1a*.

Ces résultats nous permettent de confirmer notre hypothèse selon laquelle *Dyrk1a* est responsable de la brachycéphalie observée dans le neurocrâne, ainsi que du développement de la partie médiane de la face. Les deux modèles présentent des changements dans cette zone et l'on sait que ces structures osseuses ont la même origine embryonnaire, les cellules de la crête neurale (NCC) (Richtsmeier et Flaherty 2013). Cette observation suggère que le surdosage en *Dyrk1a* pourrait affecter la prolifération/migration des NCC au cours du développement crâniofacial. Pour ce faire, nous avons évalué la prolifération des NCC avec de la 5-Ethynyl-2'-désoxyuridine (EdU), un analogue de la thymidine qui peut s'incorporer dans l'ADN au cours de la réplication (Tucker et al. 2010). 4 femelles Dp(16)1Yey gestantes ont été utilisées afin d'obtenir 5 embryons de chaque génotype Dp(16)1Yey/WT. L'EdU a été injecté par voie intrapéritonéale dans les femelles gestantes et les embryons ont été collectés 24h après, après la migration des NCC (E9.5). Une analyse immunohistologique a été réalisée pour détecter la prolifération des dérivés des NCC dans le premier arc branchial des embryons, ainsi que des analyses quantitatives (Harris, Zalucki, et Piper 2018) pour définir l'indice de prolifération et de

mitose. Les résultats obtenus détectent des défauts de prolifération et un indice mitotique réduit dans le premier arc branchial confirmant la relation de Dyrk1a/NCC et le phénotype.

***Ripply3*, un gène candidat pour le phénotype de raccourcissement du visage dans les modèles de souris du syndrome de Down**

Ripply3 (Ripply Transcriptional Repressor 3) est un corépresseur transcriptionnel, agissant comme régulateur négatif de l'activité transcriptionnelle de *Tbx1* et jouant un rôle dans le développement de l'appareil pharyngé et de ses dérivés (Okubo et al. 2011). Tbx1 est le premier gène sensible à la dose identifié dans la région del22q11/DGS et est lié au syndrome de DiGeorge (DGS), ou syndrome vélo-cardiofacial (VCFS), une maladie congénitale caractérisée par des défauts de développement liés à la crête neurale. Chez l'homme, l'haploinsuffisance de *TBX1* provoque des anomalies crâniofaciales (Lindsay et al. 2001). Dans le modèle murin du syndrome de DiGeorge, les souris mutantes pour le gène T-box (*Tbx1*+/-) présentent un développement anormal des structures squelettiques dérivées de premier et deuxième arcs pharyngés, avec une réduction de la partie médiane de la face (Jerome et Papaioannou 2001), de facon similaire à ce qui est observé dans les modèles de souris T21. Compte tenu de ces informations, nous postulons que la surexpression de *Ripply3* dans les modèles de souris T21 conduira à une régulation négative de *Tbx1*, à l'origine du phénotype de la diminution du tiers médian de la face que l'on retrouve dans la T21.

Nous avons effectué une analyse d'expression génique par le « Droplet Digital PCR (ddPCR) ». Cette analyse permet de réaliser des PCR digitales basées sur la génération de gouttelettes pour obtenir une quantification absolue des ADN ou ARN (Lindner et al. 2021). Le résultat a confirmé la surexpression de *Ripply3* et la régulation negative de *Tbx1* dans le modèle murin Dp(16)1Yey comparativement aux WT. Suite à cette observation, nous avons souhaité confirmer le rôle de *Ripply3* en créant un nouveau modèle murin issu du croisement en Dp(16)1Yey et Ripply3 ^{tmb1}, donnant lieu à un modèle qui porte 3 copies de tous les gènes situés dans le Mmu16 mais avec seulement 2 copies fonctionnelles de *Ripply3*. Dans ce cas, l'analyse morphométrique comparant le nouveau modèle Dp(16)1Yey/Ripply3^{tmb1} au modèle Dp(16)1Yey a permis de sauver le phénotype, avec une augmentation significative des structures qui composent la

region du face médiane. Cette observation confirme l'effet du surdosage de *Ripply3* dans le raccourcissement de la face médiane, attribuable à la régulation négative de *Tbx1*.

Chapitre 2 : Modèles de rats atteints du syndrome de Down

Notre équipe, sous la direction du Dr. Yann Hérault à l'IGBMC, a développé de nouveaux modèles de rats en utilisant les technologies LoxP/Cre et CrispR/Cas9, avec le soutien de l'Institut Clinique de la Souris (ICS) à Illkirch-Graffenstaden. Ces modèles sont porteurs d'une duplication de différentes régions des chromosomes homologues au HSA21 (Muñiz Moreno et al. 2020; Duchon et al. 2022).

Dans le génome du rat, les régions homologues au HSA21 englobent 213 gènes trouvés sur le chromosome 11 du rat (Rno11), comprenant 24,4Mb entre *Lipi* et *Zbtb21*, et sur Rno20 pour la partie la plus télomérique de 3,6Mb entre *Umodl1* et *Prmt2* (Muñiz Moreno et al. 2020). Nous avons généré des duplications segmentaires pour chaque intervalle, à savoir Dp(11*Lipi-Zbtb21*)Yahlcs et Dp(20*Umodl1-Prmt2*)Yahlcs, nommés ici Dup(Rno11) et Dup(Rno20) respectivement.

En tenant compte du fait que *Dyrk1a* est un gène candidat majeur pour le développement des phénotypes caniofaciaux associés à la T21, nous avons étudié de nouveaux modèles de rats liés à la T21 et au retard mental autosomique dominant 7, créés à l'aide de la stratégie « CRISpr-Mediated Rearrangement mechanism » (CRISMERE). Les modèles Dp(11*Dyrk1a*)6Yah et Del(11*Dyrk1a*)4Yah ont été générés à l'aide des paires de gRNA ciblant la région autour de la position chr11 :34,842,454-34,963,976 (génome de rat RGSC 6.0/rn6), couvrant un intervalle de 121.7 kb. Deux autres paires de sgRNA, l'une située en amont et l'autre en aval de *Dyrk1a*, ont été utilisées pour dupliquer une région de 219 kb englobant ainsi toute la région génétique située entre *Dscr3* et *Kcnj6*, correspondant à l'intervalle en position chr11:34,791,993-35,011,015 (Birling et al. 2017).

L'analyse du modèle de rat T21 complet a confirmé le rôle de la région de *Lipi* à *Zbtb21* avec une influence de la région *Umodl1-Prmt2* sur les changements craniofaciaux.

Tout d'abord, nous avons réalisé des analyses morphométriques pour étudier les trois modèles de rats porteurs chacun d'un génotype différent : Dup(Rno11), Dup(Rno20) et la combinaison de ces deux modèles Dup(Rno11-20), par rapport aux souris WT issues des mêmes portées. 15 animaux par génotype et par sexe (n=120) âgés de 14 semaines ont été utilisés. Nous avons appliqué la même méthodologie rigoureuse que celle utilisée chez les modèles murins pour analyser les repères crâniométriques (Duchon et al. 2022; Qiu et al. 2019).

Des changements de forme significatifs sont observés dans les modèles porteurs d'une duplication du chromosome 11, tels que la microcéphalie, le raccourcissement de la partie médiane du visage et une mandibule plus petite. Pour suivre les landmarks ayant subi un changement significatif et comprendre où ils se situaient dans la structure crânio-faciale, l'analyse de « EDMA FORM ou SHAPE Influence landmarks » a été effectuée. Le modèle Dup(Rno11) présentait les repères anatomiques les plus influents au niveau des os maxillaires, des os temporaux (avec la partie squamosale) et de la mandibule tandis que la combinaison Dup(Rno11-20) a conduit à l'ajout de landmarks situés dans le prémaxillaire et les os frontaux, ce qui montre une influence du surdosage de la région Rno20 chez le rat.

Dans le crâne et la mandibule, l'ACP entre Dup(Rno20) et WT ne montrait pas de différence contrairement aux rats Dup(Rno11) et Dup(Rno11-20) qui présentaient une différence significative des dimensions par rapport au groupe WT. Aussi, les résultats de l'analyse voxel ont montré que les modèles Dup(Rno11) et Dup(Rno11-20) présentent des traits dysmorphiques tels que la brachycéphalie et une diminution de la taille du tiers moyen de la face et des mandibules plus petites.

En conclusion, nous pouvons dire que 1) les modèles porteurs de la duplication du chromosome 11 présentent le phénotype CF-SD et 2) le dosage de la région du chromosome 20 modifie le résultat en renforçant ces phénotypes.

L'analyse des modèles de rats Del(11*Dyrk1a*)4Yah et Dp(11*Dyrk1a*)6Yah confirme le rôle de *Dyrk1a* dans la brachycéphalie de la T21.

En utilisant la même analyse morphométrique décrite ci-dessus, nous avons trouvé que le modèle Del(11*Dyrk1a*)4Yah présente des changements significatifs dans la FDM et la SDM du crâne, montrant une diminution générale de la taille de la tête, appelée microcéphalie. Dans le cas de la mandibule, seule la FDM montrait des modifications significatives. Dans l'analyse de composantes principales (ACP), une variation d'environ 40 % a été démontrée à la fois dans le crâne et dans la mandibule. Plus en détail, l'analyse des voxels montre que les changements de forme correspondent à une réduction des dimensions du neurocrâne et à une augmentation des dimensions de la partie médiane de la face. Finalement, la mandibule montre un élargissement de toutes les structures.

Dans le modèle Dp(11*Dyrk1a*)6Yah, le crâne présentait des changements significatifs dans la SDM, mais pas dans la FDM, ce qui indique que la taille globale de la tête ne change pas, mais que sa forme est modifiée. En revanche, la mandibule montrait des changements significatifs tant dans la FDM que dans la SDM. L'ACP a révélé une variation d'environ 18 % à la fois dans le crâne et dans la mandibule. L'analyse des voxels a montré que ces changements de forme incluent une réduction des dimensions de l'os frontal, l'os nasal et l'arcade zygomatique, ainsi qu'une augmentation des dimensions du neurocrâne (Brachycéphalie). Concernant la mandibule, nous avons observé une réduction de la largeur de toutes les structures.

Ces résultats ont montré que 1) *Dyrk1a* est nécessaire en 3 copies pour générer la brachycéphalie typique de la T21, comme le démontre l'analyse des voxels du modèle Dp(11*Dyrk1a*)6Yah. 2) Cette conclusion est également corroborée par les obervations faites avec le modèle Del(11*Dyrk1a*)4Yah, où une seule copie de *Dyrk1a* entraîne un phénotype inverse à celui de Dp(11*Dyrk1a*)6Yah, caractérisé par une diminution de la forme et de la taille du neurocrâne.

Conclusion

En conclusion, nous avons une compréhension approfondie des principales caractéristiques associées à la T21. Cette pathologie offre une opportunité précieuse pour découvrir des mécanismes communs ou nouveaux, étant donné qu'elle est souvent associée à une fréquence accrue de divers troubles physiques et mentaux. Nous avons identifié et validé une nouvelle région chromosomique responsable du phénotype crâniofacial caractéristique de la T21. Grâce à un nouveau panel de modèles de rongeurs, nous avons pu proposer et confirmer de nouveaux gènes candidats, *Dyrk1a* et *Ripply3*. Nous avons confirmé le rôle de *Dyrk1a* dans la brachycéphalie du neurocrâne et identifié le rôle du surdosage du facteur de transcription *Ripply3* dans le raccourcissement de la zone mèdiane de la face, par la régulation négative de *Tbx1*, un autre facteur de transcription impliqué dans un phénotype similaire trouvé dans le syndrome de DiGeorge. Ce syndrome se manifeste lors du développement des arcs branchiaux, avec une réduction de la prolifération cellulaire et de l'index mitotique.

Dans l'ensemble, nous avons identifié un nouveau gène sensible à la dose, responsable des malformations crâniofaciales associées à la T21. Nous proposons également de nouveaux modèles dans lesquels nous pensons pouvoir restaurer l'ensemble du phénotype crâniofacial typiques de la T21. Ces avancées pourraient également offrir une meilleure compréhension des autres phénotypes spécifiques observés chez les mutants *Tbx1* et les modèles de T21.

References

Al-Ani, Azza Husam, Joseph Safwat Antoun, William Murray Thomson, Tony Raymond Merriman, et Mauro Farella. 2017. « Hypodontia: An Update on Its Etiology, Classification, and Clinical Management ». *BioMed Research International* 2017:9378325. https://doi.org/10.1155/2017/9378325.

Alesi, Marianna, Giusppe Battaglia, Annamaria Pepi, Antonino Bianco, et Antonio Palma. 2018. « Gross Motor Proficiency and Intellectual Functioning: A Comparison among Children with Down Syndrome, Children with Borderline Intellectual Functioning, and Typically Developing Children ». *Medicine* 97 (41): e12737. https://doi.org/10.1097/MD.0000000000012737.

Alio, Juan J., Jose Lorenzo, et Carmen Iglesias. 2008. « Cranial base growth in patients with Down syndrome: A longitudinal study ». *American Journal of Orthodontics and Dentofacial Orthopedics* 133 (5): 729-37. https://doi.org/10.1016/j.ajodo.2006.03.036.

Alió, Juan, José Lorenzo, M. Carmen Iglesias, Francisco J. Manso, et Eva M. Ramírez. 2011. « Longitudinal maxillary growth in Down syndrome patients ». *The Angle Orthodontist* 81 (2): 253-59. https://doi.org/10.2319/040510-189.1.

Allanson, Judith. 1993. « Anthropometric craniofacial pattern profiles in Down syndrome ». *American Journal of Medical Genetics*, janvier. https://www.academia.edu/14410045/Anthropometric_craniofacial_pattern_profiles_in_Down_syndrome.

Alvarez, N., et L. Rubin. 1986. « Atlantoaxial Instability in Adults with Down Syndrome: A Clinical and Radiological Survey ». *Applied Research in Mental Retardation* 7 (1): 67-78. https://doi.org/10.1016/0270-3092(86)90019-6.

Amano, A., T. Kishima, S. Akiyama, I. Nakagawa, S. Hamada, et I. Morisaki. 2001. « Relationship of Periodontopathic Bacteria with Early-Onset Periodontitis in Down's Syndrome ». *Journal of Periodontology* 72 (3): 368-73. https://doi.org/10.1902/jop.2001.72.3.368.

American College of Obstetricians and Gynecologists' Committee on Practice Bulletins—Obstetrics, Committee on Genetics, et Society for Maternal-Fetal Medicine. 2020. « Screening for Fetal Chromosomal Abnormalities: ACOG Practice Bulletin, Number 226 ». *Obstetrics and Gynecology* 136 (4): e48-69. https://doi.org/10.1097/AOG.0000000000004084.

Andersson, Els-Marie M., Stefan Axelsson, Marit E. Austeng, Britt Øverland, Ingrid E. Valen, Terese A. Jensen, et Harriet Akre. 2014. « Bilateral Hypodontia Is More Common than Unilateral Hypodontia in Children with Down Syndrome: A Prospective Population-Based Study ». *European Journal of Orthodontics* 36 (4): 414-18. https://doi.org/10.1093/ejo/cjt063.

Antonarakis, S. E., M. B. Petersen, M. G. McInnis, P. A. Adelsberger, A. A. Schinzel, F. Binkert, C. Pangalos, O. Raoul, S. A. Slaugenhaupt, et M. Hafez. 1992. « The Meiotic Stage of Nondisjunction in Trisomy 21: Determination by Using DNA Polymorphisms ». *American Journal of Human Genetics* 50 (3): 544-50.

Antonarakis, Stylianos E. 2017. « Down Syndrome and the Complexity of Genome Dosage Imbalance ». *Nature Reviews Genetics* 18 (3): 147-63. https://doi.org/10.1038/nrg.2016.154.

Antonarakis, Stylianos E., Robert Lyle, Emmanouil T. Dermitzakis, Alexandre Reymond, et Samuel Deutsch. 2004. « Chromosome 21 and down Syndrome: From Genomics to Pathophysiology ». *Nature Reviews. Genetics* 5 (10): 725-38. https://doi.org/10.1038/nrg1448.

Antonarakis, Stylianos E., Brian G. Skotko, Michael S. Rafii, Andre Strydom, Sarah E. Pape, Diana W. Bianchi, Stephanie L. Sherman, et Roger H. Reeves. 2020. « Down syndrome ». *Nature reviews. Disease primers* 6 (1): 9. https://doi.org/10.1038/s41572-019-0143-7.

Araya, Paula, Katherine A. Waugh, Kelly D. Sullivan, Nicolás G. Núñez, Emiliano Roselli, Keith P. Smith, Ross E. Granrath, et al. 2019. « Trisomy 21 Dysregulates T Cell Lineages toward an Autoimmunity-Prone State Associated with Interferon Hyperactivity ». *Proceedings of the National Academy of Sciences of the United States of America* 116 (48): 24231-41. https://doi.org/10.1073/pnas.1908129116.

Areias, Cristina, Benedita Sampaio-Maia, Viviana Macho, Leal I, Paulo Melo, et David Andrade. 2013. « Does the chemistry in the saliva of Down syndrome children explain their low caries prevalence? » *European Journal of Paediatric Dentistry. Official Journal of the Italian Society of Paediatric Dentistry*. 2013 Mar;14(1):23-6. (mars):23-26.

Armitage, G. C. 1999. « Development of a Classification System for Periodontal Diseases and Conditions ». *Annals of Periodontology* 4 (1): 1-6. https://doi.org/10.1902/annals.1999.4.1.1.

Arron, Joseph R., Monte M. Winslow, Alberto Polleri, Ching-Pin Chang, Hai Wu, Xin Gao, Joel R. Neilson, et al. 2006. « NFAT Dysregulation by Increased Dosage of DSCR1 and DYRK1A on Chromosome 21 ». *Nature* 441 (7093): 595-600. https://doi.org/10.1038/nature04678.

Atas-Ozcan, Helin, Véronique Brault, Arnaud Duchon, et Yann Herault. 2021. « Dyrk1a from Gene Function in Development and Physiology to Dosage Correction across Life Span in Down Syndrome ». *Genes* 12 (11): 1833. https://doi.org/10.3390/genes12111833.

Bagić, Ivana, et Zeljko Verzak. 2003. « Craniofacial Anthropometric Analysis in Down's Syndrome Patients ». *Collegium Antropologicum* 27 Suppl 2:23-30.

Baruchel, André, Jean-Pierre Bourquin, John Crispino, Sergi Cuartero, Henrik Hasle, Johann Hitzler, Jan-Henning Klusmann, et al. 2023. « Down syndrome and leukemia: from basic mechanisms to clinical advances ». *Haematologica* 108 (10): 2570-81. https://doi.org/10.3324/haematol.2023.283225.

Bauer, Danielle, Carla A. Evans, Ellen A. Begole, et Larry Salzmann. 2012. « Severity of Occlusal Disharmonies in down Syndrome ». *International Journal of Dentistry* 2012:872367. https://doi.org/10.1155/2012/872367.

Benhaourech, Sanaa, Abdenasser Drighil, et Ayoub El Hammiri. 2016. « Congenital Heart Disease and Down Syndrome: Various Aspects of a Confirmed Association ». *Cardiovascular Journal of Africa* 27 (5): 287-90. https://doi.org/10.5830/CVJA-2016-019.

Bermudez, Beatriz E. B. V., Camila M. de Oliveira, Mônica N. de Lima Cat, Neiva I. R. Magdalena, et Adriane Celli. 2019. « Gastrointestinal Disorders in Down Syndrome ». *American Journal of Medical Genetics Part A* 179 (8): 1426-31. https://doi.org/10.1002/ajmg.a.61258.

Bertapelli, Fabio, Ken Pitetti, Stamatis Agiovlasitis, et Gil Guerra-Junior. 2016. « Overweight and Obesity in Children and Adolescents with Down Syndrome-Prevalence, Determinants, Consequences, and Interventions: A Literature Review ». *Research in Developmental Disabilities* 57 (octobre):181-92. https://doi.org/10.1016/j.ridd.2016.06.018.

Bhowate, Rahul, et A. Dubey. 2005. « Dentofacial Changes and Oral Health Status in Mentally Challenged Children ». *Journal of the Indian Society of Pedodontics and Preventive Dentistry* 23 (2): 71-73. https://doi.org/10.4103/0970-4388.16445.

Bimstein, E., W. Wignall, D. Cohen, et J. Katz. 2008. « Root Surface Characteristics of Children Teeth with Periodontal Diseases ». *The Journal of Clinical Pediatric Dentistry* 32 (2): 101-4. https://doi.org/10.17796/jcpd.32.2.b6423rj156864l18.

Birling, Marie-Christine, Laurence Schaeffer, Philippe André, Loic Lindner, Damien Maréchal, Abdel Ayadi, Tania Sorg, Guillaume Pavlovic, et Yann Hérault. 2017. « Efficient and Rapid Generation of Large Genomic Variants in Rats and Mice Using CRISMERE ». *Scientific Reports* 7 (1): 43331. https://doi.org/10.1038/srep43331.

Bon, B. W. M. van, A. Hoischen, J. Hehir-Kwa, A. P. M. de Brouwer, C. Ruivenkamp, A. C. J. Gijsbers, C. L. Marcelis, et al. 2011. « Intragenic Deletion in DYRK1A Leads to Mental Retardation and Primary Microcephaly ». *Clinical Genetics* 79 (3): 296-99. https://doi.org/10.1111/j.1399-0004.2010.01544.x.

Carlson, Laura M., et Neeta L. Vora. 2017. « Prenatal Diagnosis: Screening and Diagnostic Tools ». *Obstetrics and Gynecology Clinics of North America* 44 (2): 245-56. https://doi.org/10.1016/j.ogc.2017.02.004.

Carrada, Camila Faria, Flávia Almeida Ribeiro Scalioni, Dionéia Evangelista Cesar, Karina Lopes Devito, Luiz Cláudio Ribeiro, et Rosangela Almeida Ribeiro. 2016. « Salivary Periodontopathic Bacteria in Children and Adolescents with Down Syndrome ». *PLOS ONE* 11 (10): e0162988. https://doi.org/10.1371/journal.pone.0162988.

CDC. 2024. « Down Syndrome ». Birth Defects. 22 mai 2024. https://www.cdc.gov/birth-defects/about/down-syndrome.html.

Chang, Pishan, Daniel Bush, Stephanie Schorge, Mark Good, Tara Canonica, Nathanael Shing, Suzanna Noy, et al. 2020. « Altered Hippocampal-Prefrontal Neural Dynamics in Mouse Models of Down Syndrome ». *Cell Reports* 30 (4): 1152-1163.e4. https://doi.org/10.1016/j.celrep.2019.12.065.

Chinwalla, Asif T., Lisa L. Cook, Kimberly D. Delehaunty, Ginger A. Fewell, Lucinda A. Fulton, Robert S. Fulton, Tina A. Graves, et al. 2002. « Initial Sequencing and Comparative Analysis of the Mouse Genome ». *Nature* 420 (6915): 520-62. https://doi.org/10.1038/nature01262.

« Chromosome 21: 1-46,709,983 - Chromosome summary - Homo_sapiens - Ensembl genome browser 112 ». s. d. Consulté le 28 août 2024. http://www.ensembl.org/Homo_sapiens/Location/Chromosome?r=21:1-46709983.

Churchill, Shervin S., Gail M. Kieckhefer, Carol A. Landis, et Teresa M. Ward. 2012. « Sleep Measurement and Monitoring in Children with Down Syndrome: A Review of the Literature, 1960-2010 ». *Sleep Medicine Reviews* 16 (5): 477-88. https://doi.org/10.1016/j.smrv.2011.10.003.

Cichon, P., L. Crawford, et W. D. Grimm. 1998. « Early-Onset Periodontitis Associated with Down's Syndrome--Clinical Interventional Study ». *Annals of Periodontology* 3 (1): 370-80. https://doi.org/10.1902/annals.1998.3.1.370.

Cohen, M. M., R. A. Winer, S. Schwartz, et G. Shklar. 1961. « Oral Aspects of Mongolism. I. Periodontal Disease in Mongolism ». *Oral Surgery, Oral Medicine, and Oral Pathology* 14 (janvier):92-107. https://doi.org/10.1016/0030-4220(61)90478-9.

Courraud, Jérémie, Eric Chater-Diehl, Benjamin Durand, Marie Vincent, Maria Del Mar Muniz Moreno, Imene Boujelbene, Nathalie Drouot, et al. 2021. « Integrative Approach to Interpret DYRK1A Variants, Leading to a Frequent Neurodevelopmental Disorder ». *Genetics in Medicine: Official Journal of the American College of Medical Genetics* 23 (11): 2150-59. https://doi.org/10.1038/s41436-021-01263-1.

Cruz, Narlito V., Sanaa A. Mahmoud, Harold Chen, Mary Lowery-Nordberg, Kristin Berlin, et Sami L. Bahna. 2009. « Follow-up Study of Immune Defects in Patients with Dysmorphic Disorders ». *Annals of Allergy, Asthma & Immunology* 102 (5): 426-31. https://doi.org/10.1016/S1081-1206(10)60516-9.

Cuoghi, Osmar Aparecido, Francielle Topolski, Lorraine Perciliano de Faria, Carla Machado Occhiena, Nancy Dos Santos Pinto Ferreira, Camila Ribeiro Ferlin, et Marcos Rogério de Mendonça. 2016. « Prevalence of Dental Anomalies in Permanent Dentition of Brazilian Individuals with Down Syndrome ». *The Open Dentistry Journal* 10:469-73. https://doi.org/10.2174/1874210601610010469.

Cutress, T. W. 1971. « Periodontal Disease and Oral Hygiene in Trisomy 21 ». *Archives of Oral Biology* 16 (11): 1345-55. https://doi.org/10.1016/0003-9969(71)90036-7.

Davisson, M. T., C. Schmidt, et E. C. Akeson. 1990. « Segmental Trisomy of Murine Chromosome 16: A New Model System for Studying Down Syndrome ». *Progress in Clinical and Biological Research* 360:263-80.

Davisson, M. T., C. Schmidt, R. H. Reeves, N. G. Irving, E. C. Akeson, B. S. Harris, et R. T. Bronson. 1993. « Segmental Trisomy as a Mouse Model for Down Syndrome ». *Progress in Clinical and Biological Research* 384:117-33.

Deitz, Samantha L., et Randall J. Roper. 2011. « Trisomic and Allelic Differences Influence Phenotypic Variability during Development of Down Syndrome Mice ». *Genetics* 189 (4): 1487-95. https://doi.org/10.1534/genetics.111.131391.

Delabar, J. M., D. Theophile, Z. Rahmani, Z. Chettouh, J. L. Blouin, M. Prieur, B. Noel, et P. M. Sinet. 1993. « Molecular Mapping of Twenty-Four Features of Down Syndrome on Chromosome 21 ». *European Journal of Human Genetics: EJHG* 1 (2): 114-24. https://doi.org/10.1159/000472398.

Desai, S. S. 1997. « Down Syndrome: A Review of the Literature ». *Oral Surgery, Oral Medicine, Oral Pathology, Oral Radiology, and Endodontics* 84 (3): 279-85. https://doi.org/10.1016/s1079-2104(97)90343-7.

Desingu, Vanathy, Amrutha Adapa, et Shantha Devi. 2019. « Dental Anomalies in Down Syndrome Individuals: A Review ». *Journal of Scientific Dentistry* 9 (1): 6-8. https://doi.org/10.5005/jp-journals-10083-0902.

Dierssen, Mara, Yann Herault, et Xavier Estivill. 2009. « Aneuploidy: From a Physiological Mechanism of Variance to Down Syndrome ». *Physiological Reviews* 89 (3): 887-920. https://doi.org/10.1152/physrev.00032.2007.

Down, J. L. 1995. « Observations on an Ethnic Classification of Idiots. 1866 ». *Mental Retardation* 33 (1): 54-56.

Driscoll Deborah A. et Gross Susan. 2009. « Prenatal Screening for Aneuploidy ». *New England Journal of Medicine* 360 (24): 2556-62. https://doi.org/10.1056/NEJMcp0900134.

Duchon, Arnaud, Maria Del Mar Muñiz Moreno, Claire Chevalier, Valérie Nalesso, Philippe Andre, Marta Fructuoso-Castellar, Mary Mondino, et al. 2022. « Ts66Yah, a Mouse Model of Down Syndrome with Improved Construct and Face Validity ». *Disease Models & Mechanisms* 15 (12): dmm049721. https://doi.org/10.1242/dmm.049721.

Duchon, Arnaud, et Yann Herault. 2016. « DYRK1A, a Dosage-Sensitive Gene Involved in Neurodevelopmental Disorders, Is a Target for Drug Development in Down Syndrome ». *Frontiers in Behavioral Neuroscience* 10 (juin):104. https://doi.org/10.3389/fnbeh.2016.00104.

Duchon, Arnaud, Maria del Mar Muniz Moreno, Sandra Martin Lorenzo, Marcia Priscilla Silva de Souza, Claire Chevalier, Valérie Nalesso, Hamid Meziane, et al. 2021. « Multi-influential genetic interactions alter behaviour and cognition through six main biological cascades in Down syndrome mouse models ». *Human Molecular Genetics* 30 (9): 771-88. https://doi.org/10.1093/hmg/ddab012.

Ellenbroek, Bart, et Jiun Youn. 2016. « Rodent Models in Neuroscience Research: Is It a Rat Race? » *Disease Models & Mechanisms* 9 (10): 1079-87. https://doi.org/10.1242/dmm.026120.

Esbensen, A. J., E. K. Hoffman, E. Stansberry, et R. Shaffer. 2018. « Convergent Validity of Actigraphy with Polysomnography and Parent Reports When Measuring Sleep in Children with Down Syndrome ». *Journal of Intellectual Disability Research: JIDR* 62 (4): 281-91. https://doi.org/10.1111/jir.12464.

« European Platform on Rare Disease Registration ». s. d. Consulté le 10 avril 2024. https://eu-rd-platform.jrc.ec.europa.eu.

Farkas, L. G., M. J. Katic, C. R. Forrest, et L. Litsas. 2001. « Surface Anatomy of the Face in Down's Syndrome: Linear and Angular Measurements in the Craniofacial Regions ». *The Journal of Craniofacial Surgery* 12 (4): 373-79; discussion 380. https://doi.org/10.1097/00001665-200107000-00011.

Farkas, L. G., J. C. Posnick, et T. Hreczko. 1991. « Anthropometry of the Head and Face in 95 Down Syndrome Patients ». *Progress in Clinical and Biological Research* 373:53-97.

Farkas, Leslie G., Marko J. Katic, et Christopher R. Forrest. 2002a. « Age-Related Changes in Anthropometric Measurements in the Craniofacial Regions and in Height in Down's Syndrome ». *The Journal of Craniofacial Surgery* 13 (5): 614-22. https://doi.org/10.1097/00001665-200209000-00004.

———. 2002b. « Surface Anatomy of the Face in Down's Syndrome: Age-Related Changes of Anthropometric Proportion Indices in the Craniofacial Regions ». *The Journal of Craniofacial Surgery* 13 (3): 368-74. https://doi.org/10.1097/00001665-200205000-00002.

Farkas, Leslie G., John C. Kolar, et Ian R. Munro. 1985. « Craniofacial Disproportions in Apert's Syndrome: An Anthropometric Study ». *The Cleft Palate Journal* 22 (4): 253-65.

Faulks, D., M.-N. Mazille, V. Collado, J.-L. Veyrune, et M. Hennequin. 2008. « Masticatory Dysfunction in Persons with Down's Syndrome. Part 2: Management ». *Journal of Oral Rehabilitation* 35 (11): 863-69. https://doi.org/10.1111/j.1365-2842.2008.01878.x.

Ferrari, Marta, et Stefano Stagi. 2021. « Autoimmunity and Genetic Syndromes: A Focus on Down Syndrome ». *Genes* 12 (2): 268. https://doi.org/10.3390/genes12020268.

Ferrario, Virgilio F., Claudia Dellavia, Anna Colombo, et Chiarella Sforza. 2004. « Three-Dimensional Assessment of Nose and Lip Morphology in Subjects with down Syndrome ». *Annals of Plastic Surgery* 53 (6): 577-83. https://doi.org/10.1097/01.sap.0000130702.51499.6b.

Fink, G. B., W. K. Madaus, et G. F. Walker. 1975. « A Quantitative Study of the Face in Down's Syndrome ». *American Journal of Orthodontics* 67 (5): 540-53. https://doi.org/10.1016/0002-9416(75)90299-7.

Frisdal, Aude, et Paul A Trainor. 2014. « Development and Evolution of the Pharyngeal Apparatus ». *Wiley interdisciplinary reviews. Developmental biology* 3 (6): 403-18. https://doi.org/10.1002/wdev.147.

Frostad, W. A., J. F. Cleall, et L. C. Melosky. 1971. « Craniofacial Complex in the Trisomy 21 Syndrome (Down's Syndrome) ». *Archives of Oral Biology* 16 (7): 707-22. https://doi.org/10.1016/0003-9969(71)90116-6.

Frydman, Alon, et Hessam Nowzari. 2012. « Down Syndrome-Associated Periodontitis: A Critical Review of the Literature ». *Compendium of Continuing Education in Dentistry (Jamesburg, N.J.: 1995)* 33 (5): 356-61.

Fung, Karen, Herenia Lawrence, et Paul Allison. 2008. « A Paired Analysis of Correlates of Dental Restorative Care in Siblings with and without Down Syndrome ». *Special Care in Dentistry: Official Publication of the American Association of Hospital Dentists, the Academy of Dentistry for the Handicapped, and the American Society for Geriatric Dentistry* 28 (3): 85-91. https://doi.org/10.1111/j.1754-4505.2008.00018.x.

Galceran, J., K. de Graaf, F. J. Tejedor, et W. Becker. 2003. « The MNB/DYRK1A Protein Kinase: Genetic and Biochemical Properties ». In *Advances in Down Syndrome Research*, édité par G. Lubec, 139-48. Vienna: Springer. https://doi.org/10.1007/978-3-7091-6721-2_12.

Gallo, Claudio, Irene Pastore, Marta Beghetto, et Carla Mucignat-Caretta. 2019. « Symmetry of dental agenesis in Down Syndrome children ». *Journal of Dental Sciences* 14 (1): 61-65. https://doi.org/10.1016/j.jds.2018.04.003.

Gameren-Oosterom, Helma B. M. van, Minne Fekkes, Simone E. Buitendijk, Ashna D. Mohangoo, Jeanet Bruil, et Jacobus P. Van Wouwe. 2011. « Development, Problem Behavior, and Quality of Life in a Population Based Sample of Eight-Year-Old Children with Down Syndrome ». *PloS One* 6 (7): e21879. https://doi.org/10.1371/journal.pone.0021879.

Gardiner, Katheleen, Andrew Fortna, Lawrence Bechtel, et Muriel T Davisson. 2003. « Mouse Models of Down Syndrome: How Useful Can They Be? Comparison of the Gene Content of Human Chromosome 21 with Orthologous Mouse Genomic Regions ». *Gene* 318 (octobre):137-47. https://doi.org/10.1016/S0378-1119(03)00769-8.

Ghaith, Batool, Manal Al Halabi, et Mawlood Kowash. 2017. « Dental Implications of Down Syndrome (DS): Review of the Oral and Dental Characteristics ». *JSM Dentistry*, mai. https://www.jscimedcentral.com/article/Dental-Implications-of-Down-Syndrome-%28DS%29%3A-Review-of-the-Oral--and-Dental-Characteristics.

Goffinski, Alida, Maria A. Stanley, Nicole Shepherd, Nichole Duvall, Sandra B. Jenkinson, Charlene Davis, Marilyn J. Bull, et Randall J. Roper. 2015. « Obstructive Sleep Apnea in Young Infants with Down Syndrome Evaluated in a Down Syndrome Specialty Clinic ». *American Journal of Medical Genetics. Part A* 167A (2): 324-30. https://doi.org/10.1002/ajmg.a.36903.

Goodliffe, Joseph W., Jose Luis Olmos-Serrano, Nadine M. Aziz, Jeroen L. A. Pennings, Faycal Guedj, Diana W. Bianchi, et Tarik F. Haydar. 2016. « Absence of Prenatal Forebrain Defects in the Dp(16)1Yey/+ Mouse Model of Down Syndrome ». *The Journal of Neuroscience: The Official Journal of the Society for Neuroscience* 36 (10): 2926-44. https://doi.org/10.1523/JNEUROSCI.2513-15.2016.

Guimaraes, Carolina V. A., Lane F. Donnelly, Sally R. Shott, Raouf S. Amin, et Maninder Kalra. 2008. « Relative Rather than Absolute Macroglossia in Patients with Down Syndrome: Implications for Treatment of Obstructive Sleep Apnea ». *Pediatric Radiology* 38 (10): 1062-67. https://doi.org/10.1007/s00247-008-0941-7.

Hall, Bertil. 1966. « Mongolism in Newborn Infants: An Examination of the Criteria for Recognition and Some Speculations on the Pathogenic Activity of the Chromosomal Abnormality ». *Clinical Pediatrics* 5 (1): 4-12. https://doi.org/10.1177/000992286600500102.

Hallgrimsson, Benedikt, Christopher J. Percival, Rebecca Green, Nathan M. Young, Washington Mio, et Ralph Marcucio. 2015. « Chapter Twenty - Morphometrics, 3D Imaging, and Craniofacial Development ». In *Current Topics in Developmental Biology*, édité par Yang Chai, 115:561-97. Craniofacial Development. Academic Press. https://doi.org/10.1016/bs.ctdb.2015.09.003.

Hämmerle, B., C. Elizalde, J. Galceran, W. Becker, et F. J. Tejedor. 2003. « The MNB/DYRK1A Protein Kinase: Neurobiological Functions and Down Syndrome Implications ». *Journal of Neural Transmission. Supplementum*, nº 67, 129-37. https://doi.org/10.1007/978-3-7091-6721-2_11.

Hasle, H., I. H. Clemmensen, et M. Mikkelsen. 2000. « Risks of Leukaemia and Solid Tumours in Individuals with Down's Syndrome ». *Lancet (London, England)* 355 (9199): 165-69. https://doi.org/10.1016/S0140-6736(99)05264-2.

Hasle, Henrik, Jan M. Friedman, Jørgen H. Olsen, et Sonja A. Rasmussen. 2016. « Low Risk of Solid Tumors in Persons with Down Syndrome ». *Genetics in Medicine: Official Journal of the American College of Medical Genetics* 18 (11): 1151-57. https://doi.org/10.1038/gim.2016.23.

Hattori, M., A. Fujiyama, T. D. Taylor, H. Watanabe, T. Yada, H. S. Park, A. Toyoda, et al. 2000. « The DNA Sequence of Human Chromosome 21 ». *Nature* 405 (6784): 311-19. https://doi.org/10.1038/35012518.

Heinke, Dominique, Jennifer L. Isenburg, Erin B. Stallings, Tyiesha D. Short, Mimi Le, Sarah Fisher, Xiaoyi Shan, et al. 2021. « Prevalence of Structural Birth Defects among Infants with Down

Syndrome, 2013-2017: A US Population-Based Study ». *Birth Defects Research* 113 (2): 189-202. https://doi.org/10.1002/bdr2.1854.

Hennequin, Martine, D. Faulks, et J. L. Veyrune. 2000. « Le syndrome bucco-facial affectant les personnes porteuses d une trisomie-21. » https://docplayer.fr/20945468-Le-syndrome-bucco-facial-affectant-les-personnes-porteuses-d-une-trisomie-21.html.

Herault, Yann, Jean M. Delabar, Elizabeth M. C. Fisher, Victor L. J. Tybulewicz, Eugene Yu, et Veronique Brault. 2017. « Rodent Models in Down Syndrome Research: Impact and Future Opportunities ». *Disease Models & Mechanisms* 10 (10): 1165-86. https://doi.org/10.1242/dmm.029728.

Hong Li, Kenneth Jones., Joan Hooper, Trevor Williams. 2017. « Temporal analysis of ectoderm and mesenchyme gene expression in the developing mouse facial prominences. » *FaceBase Consortium*. https://doi.org/10.25550/TJA.

Huang, T. T., M. Yasunami, E. J. Carlson, A. M. Gillespie, A. G. Reaume, E. K. Hoffman, P. H. Chan, R. W. Scott, et C. J. Epstein. 1997. « Superoxide-Mediated Cytotoxicity in Superoxide Dismutase-Deficient Fetal Fibroblasts ». *Archives of Biochemistry and Biophysics* 344 (2): 424-32. https://doi.org/10.1006/abbi.1997.0237.

Huggard, Dean, Derek G. Doherty, et Eleanor J. Molloy. 2020. « Immune Dysregulation in Children With Down Syndrome ». *Frontiers in Pediatrics* 8:73. https://doi.org/10.3389/fped.2020.00073.

Hyett, J. A., M. Perdu, G. K. Sharland, R. S. Snijders, et K. H. Nicolaides. 1997. « Increased Nuchal Translucency at 10-14 Weeks of Gestation as a Marker for Major Cardiac Defects ». *Ultrasound in Obstetrics & Gynecology: The Official Journal of the International Society of Ultrasound in Obstetrics and Gynecology* 10 (4): 242-46. https://doi.org/10.1046/j.1469-0705.1997.10040242.x.

Izumi, Y., S. Sugiyama, O. Shinozuka, T. Yamazaki, T. Ohyama, et I. Ishikawa. 1989. « Defective Neutrophil Chemotaxis in Down's Syndrome Patients and Its Relationship to Periodontal Destruction ». *Journal of Periodontology* 60 (5): 238-42. https://doi.org/10.1902/jop.1989.60.5.238.

Jain, Preyal D., Akshatha Nayak, Shreekanth D. Karnad, et Kaiorisa N. Doctor. 2022. « Gross Motor Dysfunction and Balance Impairments in Children and Adolescents with Down Syndrome: A Systematic Review ». *Clinical and Experimental Pediatrics* 65 (3): 142-49. https://doi.org/10.3345/cep.2021.00479.

Jensen, G. M., J. F. Cleall, et A. S. Yip. 1973. « Dentoalveolar Morphology and Developmental Changes in Down's Syndrome (Trisomy 21) ». *American Journal of Orthodontics* 64 (6): 607-18. https://doi.org/10.1016/0002-9416(73)90291-1.

Jerome, L. A., et V. E. Papaioannou. 2001. « DiGeorge Syndrome Phenotype in Mice Mutant for the T-Box Gene, Tbx1 ». *Nature Genetics* 27 (3): 286-91. https://doi.org/10.1038/85845.

Jesuino, Flávia Aline Silva, et José Valladares-Neto. 2013. « Craniofacial morphological differences between Down syndrome and maxillary deficiency children ». *European Journal of Orthodontics* 35 (1): 124-30. https://doi.org/10.1093/ejo/cjr105.

Ji, Jianling, Hane Lee, Bob Argiropoulos, Naghmeh Dorrani, John Mann, Julian A. Martinez-Agosto, Natalia Gomez-Ospina, et al. 2015. « DYRK1A Haploinsufficiency Causes a New

Recognizable Syndrome with Microcephaly, Intellectual Disability, Speech Impairment, and Distinct Facies ». *European Journal of Human Genetics* 23 (11): 1473-81. https://doi.org/10.1038/ejhg.2015.71.

Johnson, H. Katherine, Stacey E. Wahl, Fatmata Sesay, Larisa Litovchick, et Amanda JG. Dickinson. 2024. « Dyrk1a is required for craniofacial development in *Xenopus laevis*. » *Developmental Biology*, avril. https://doi.org/10.1016/j.ydbio.2024.04.004.

Kazuki, Yasuhiro, Feng J Gao, Yicong Li, Anna J Moyer, Benjamin Devenney, Kei Hiramatsu, Sachiko Miyagawa-Tomita, et al. 2020. « A non-mosaic transchromosomic mouse model of Down syndrome carrying the long arm of human chromosome 21 ». Édité par Susan L Ackerman, Huda Y Zoghbi, Yann Herault, William Mobley, et Tarik Haydar. *eLife* 9 (juin):e56223. https://doi.org/10.7554/eLife.56223.

Kazuki, Yasuhiro, Feng J. Gao, Miho Yamakawa, Masumi Hirabayashi, Kanako Kazuki, Naoyo Kajitani, Sachiko Miyagawa-Tomita, et al. 2022. « A Transchromosomic Rat Model with Human Chromosome 21 Shows Robust Down Syndrome Features ». *American Journal of Human Genetics* 109 (2): 328-44. https://doi.org/10.1016/j.ajhg.2021.12.015.

Khurana, Sonam, Ayman R. Khalifa, Nader N. Rezallah, Scott Lozanoff, et Ahmed Z. Abdelkarim. 2024. « Craniofacial and Airway Morphology in Down Syndrome: A Cone Beam Computed Tomography Case Series Evaluation ». *Journal of Clinical Medicine* 13 (13): 3908. https://doi.org/10.3390/jcm13133908.

Kisling, Erik. 1966. « Cranial Morphology in Down's Syndrome: A Comparative Roentgencephalometric Study in Adult Males ». Copenhagen: Munksgaard.

Klingel, Daniel, Ariane Hohoff, Robert Kwiecien, Dirk Wiechmann, et Thomas Stamm. 2017. « Growth of the hard palate in infants with Down syndrome compared with healthy infants—A retrospective case control study ». *PLoS ONE* 12 (8): e0182728. https://doi.org/10.1371/journal.pone.0182728.

Klingenberg, Christian Peter. 2011. « MorphoJ: An Integrated Software Package for Geometric Morphometrics ». *Molecular Ecology Resources* 11 (2): 353-57. https://doi.org/10.1111/j.1755-0998.2010.02924.x.

Korayem, Mohammed A., et Eman A. AlKofide. 2014. « Characteristics of Down Syndrome Subjects in a Saudi Sample ». *The Angle Orthodontist* 84 (1): 30-37. https://doi.org/10.2319/030813-195.1.

Korbel, Jan O., Tal Tirosh-Wagner, Alexander Eckehart Urban, Xiao-Ning Chen, Maya Kasowski, Li Dai, Fabian Grubert, et al. 2009. « The Genetic Architecture of Down Syndrome Phenotypes Revealed by High-Resolution Analysis of Human Segmental Trisomies ». *Proceedings of the National Academy of Sciences of the United States of America* 106 (29): 12031-36. https://doi.org/10.1073/pnas.0813248106.

Korenberg, J. R., X. N. Chen, R. Schipper, Z. Sun, R. Gonsky, S. Gerwehr, N. Carpenter, C. Daumer, P. Dignan, et C. Disteche. 1994. « Down Syndrome Phenotypes: The Consequences of Chromosomal Imbalance ». *Proceedings of the National Academy of Sciences of the United States of America* 91 (11): 4997-5001. https://doi.org/10.1073/pnas.91.11.4997.

Korenberg, J. R., H. Kawashima, S. M. Pulst, T. Ikeuchi, N. Ogasawara, K. Yamamoto, S. A. Schonberg, R. West, L. Allen, et E. Magenis. 1990. « Molecular Definition of a Region of

Chromosome 21 That Causes Features of the Down Syndrome Phenotype ». *American Journal of Human Genetics* 47 (2): 236-46.

Lana-Elola, Eva, Sheona D. Watson-Scales, Elizabeth M. C. Fisher, et Victor L. J. Tybulewicz. 2011. « Down syndrome: searching for the genetic culprits ». *Disease Models & Mechanisms* 4 (5): 586-95. https://doi.org/10.1242/dmm.008078.

Latham, R. A. 1972. « The Sella Point and Postnatal Growth of the Human Cranial Base ». *American Journal of Orthodontics* 61 (2): 156-62. https://doi.org/10.1016/0002-9416(72)90093-0.

Lejeune, J., M. Gautier, et R. Turpin. 1959. « [Study of somatic chromosomes from 9 mongoloid children] ». *Comptes Rendus Hebdomadaires Des Seances De l'Academie Des Sciences* 248 (11): 1721-22.

Lele, S., et J. T. Richtsmeier. 1991. « Euclidean Distance Matrix Analysis: A Coordinate-Free Approach for Comparing Biological Shapes Using Landmark Data ». *American Journal of Physical Anthropology* 86 (3): 415-27. https://doi.org/10.1002/ajpa.1330860307.

Lele, Subhash R., et Joan T. Richtsmeier. 2001. *An Invariant Approach to Statistical Analysis of Shapes*. CRC Press.

Li, Yichen, Zhuo Xing, Tao Yu, Annie Pao, Marcel Daadi, et Y. Eugene Yu. 2021. « Coat Color-Facilitated Efficient Generation and Analysis of a Mouse Model of Down Syndrome Triplicated for All Human Chromosome 21 Orthologous Regions ». *Genes* 12 (8): 1215. https://doi.org/10.3390/genes12081215.

Li, Zhongyou, Tao Yu, Masae Morishima, Annie Pao, Jeffrey LaDuca, Jeffrey Conroy, Norma Nowak, Sei-Ichi Matsui, Isao Shiraishi, et Y. Eugene Yu. 2007. « Duplication of the Entire 22.9 Mb Human Chromosome 21 Syntenic Region on Mouse Chromosome 16 Causes Cardiovascular and Gastrointestinal Abnormalities ». *Human Molecular Genetics* 16 (11): 1359-66. https://doi.org/10.1093/hmg/ddm086.

Linden, M. S. van der, S. Vucic, D. J. F. van Marrewijk, et E. M. Ongkosuwito. 2017. « Dental Development in Down Syndrome and Healthy Children: A Comparative Study Using the Demirjian Method ». *Orthodontics & Craniofacial Research* 20 (2): 65-70. https://doi.org/10.1111/ocr.12139.

Lindner, Loic, Pauline Cayrou, Sylvie Jacquot, Marie-Christine Birling, Yann Herault, et Guillaume Pavlovic. 2021. « Reliable and Robust Droplet Digital PCR (ddPCR) and RT-ddPCR Protocols for Mouse Studies ». *Methods*, Methods of genome engineering and model validation, 191 (juillet):95-106. https://doi.org/10.1016/j.ymeth.2020.07.004.

Lindsay, Elizabeth A., Francesca Vitelli, Hong Su, Masae Morishima, Tuong Huynh, Tiziano Pramparo, Vesna Jurecic, et al. 2001. « Tbx1 Haploinsufficiency in the DiGeorge Syndrome Region Causes Aortic Arch Defects in Mice ». *Nature* 410 (6824): 97-101. https://doi.org/10.1038/35065105.

Loane, Maria, Joan K. Morris, Marie-Claude Addor, Larraitz Arriola, Judith Budd, Berenice Doray, Ester Garne, et al. 2013. « Twenty-Year Trends in the Prevalence of Down Syndrome and Other Trisomies in Europe: Impact of Maternal Age and Prenatal Screening ». *European Journal of Human Genetics: EJHG* 21 (1): 27-33. https://doi.org/10.1038/ejhg.2012.94.

Lyle, Robert, Frédérique Béna, Sarantis Gagos, Corinne Gehrig, Gipsy Lopez, Albert Schinzel, James Lespinasse, et al. 2009. « Genotype-Phenotype Correlations in Down Syndrome Identified by Array CGH in 30 Cases of Partial Trisomy and Partial Monosomy Chromosome 21 ». *European Journal of Human Genetics: EJHG* 17 (4): 454-66. https://doi.org/10.1038/ejhg.2008.214.

Macho, V., A. Coelho, C. Areias, P. Macedo, et D. Andrade. 2014. « Craniofacial Features and Specific Oral Characteristics of Down Syndrome Children ». *Oral Health and Dental Management* 13 (2): 408-11.

Macho, Viviana, Miguel Palha, Ana Paula Macedo, Orquídea Ribeiro, et Casimiro Andrade. 2013. « Comparative Study between Dental Caries Prevalence of Down Syndrome Children and Their Siblings ». *Special Care in Dentistry: Official Publication of the American Association of Hospital Dentists, the Academy of Dentistry for the Handicapped, and the American Society for Geriatric Dentistry* 33 (1): 2-7. https://doi.org/10.1111/j.1754-4505.2012.00297.x.

Malak, Roksana, Anna Kostiukow, Agnieszka Krawczyk-Wasielewska, Ewa Mojs, et Włodzimierz Samborski. 2015. « Delays in Motor Development in Children with Down Syndrome ». *Medical Science Monitor: International Medical Journal of Experimental and Clinical Research* 21 (juillet):1904-10. https://doi.org/10.12659/MSM.893377.

Malt, Eva Albertsen, Renate Charlotte Dahl, Trine Marie Haugsand, Ingebjørg H. Ulvestad, Nina Merete Emilsen, Børre Hansen, Yon Eduin Galezo Cardenas, Rolf Olof Skøld, Anne Tove Berge Thorsen, et Eva Merete Male Davidsen. 2013. « Health and Disease in Adults with Down Syndrome ». *Tidsskrift for Den Norske Laegeforening: Tidsskrift for Praktisk Medicin, Ny Raekke* 133 (3): 290-94. https://doi.org/10.4045/tidsskr.12.0390.

Martí, Eulàlia, Xavier Altafaj, Mara Dierssen, Susana de la Luna, Vassiliki Fotaki, Mónica Alvarez, Mercè Pérez-Riba, Isidro Ferrer, et Xavier Estivill. 2003. « Dyrk1A Expression Pattern Supports Specific Roles of This Kinase in the Adult Central Nervous System ». *Brain Research* 964 (2): 250-63. https://doi.org/10.1016/s0006-8993(02)04069-6.

Mastrorosa, F. Kumara, Allison N. Rozanski, William T. Harvey, Jordan Knuth, Gage Garcia, Katherine M. Munson, Kendra Hoekzema, Glennis A. Logsdon, et Evan E. Eichler. 2024. « Complete chromosome 21 centromere sequences from a Down syndrome family reveal size asymmetry and differences in kinetochore attachment ». *bioRxiv*, février, 2024.02.25.581464. https://doi.org/10.1101/2024.02.25.581464.

Mattos, Marlon Fraga, Patrícia Matos Biselli-Chicote, Joice Matos Biselli, Thiago Luís da Silva Assembleia, Eny Maria Goloni-Bertollo, et Érika Cristina Pavarino. 2018. « Interleukin 6 and 10 Serum Levels and Genetic Polymorphisms in Children with Down Syndrome ». *Mediators of Inflammation* 2018:6539548. https://doi.org/10.1155/2018/6539548.

McCormick, Mary Kay, Albert Schinzel, Michael B. Petersen, Gail Stetten, Daniel J. Driscoll, Eduardo S. Cantu, Lisbeth Tranebjaerg, Margareta Mikkelsen, Paul C. Watkins, et Stylianos E. Antonarakis. 1989. « Molecular Genetic Approach to the Characterization of the “Down Syndrome Region” of Chromosome 21 ». *Genomics* 5 (2): 325-31. https://doi.org/10.1016/0888-7543(89)90065-7.

McElyea, Samantha D., John M. Starbuck, Danika M. Tumbleson-Brink, Emily Harrington, Joshua D. Blazek, Ahmed Ghoneima, Katherine Kula, et Randall J. Roper. 2016. « Influence of Prenatal EGCG Treatment and Dyrk1a Dosage Reduction on Craniofacial Features

Associated with Down Syndrome ». *Human Molecular Genetics* 25 (22): 4856-69. https://doi.org/10.1093/hmg/ddw309.

McKelvey, K. D., T. W. Fowler, N. S. Akel, J. A. Kelsay, D. Gaddy, G. R. Wenger, et L. J. Suva. 2013. « Low bone turnover and low bone density in a cohort of adults with Down syndrome ». *Osteoporosis international : a journal established as result of cooperation between the European Foundation for Osteoporosis and the National Osteoporosis Foundation of the USA* 24 (4): 1333-38. https://doi.org/10.1007/s00198-012-2109-4.

Melyn, M. A., et D. T. White. 1973. « Mental and Developmental Milestones of Noninstitutionalized Down's Syndrome Children ». *Pediatrics* 52 (4): 542-45.

Merscher, S., B. Funke, J. A. Epstein, J. Heyer, A. Puech, M. M. Lu, R. J. Xavier, et al. 2001. « TBX1 Is Responsible for Cardiovascular Defects in Velo-Cardio-Facial/DiGeorge Syndrome ». *Cell* 104 (4): 619-29. https://doi.org/10.1016/s0092-8674(01)00247-1.

Miamoto, Cristina Batista, Luciano José Pereira, Maria Letícia Ramos-Jorge, et Leandro Silva Marques. 2011. « Prevalence and Predictive Factors of Sleep Bruxism in Children with and without Cognitive Impairment ». *Brazilian Oral Research* 25 (5): 439-45. https://doi.org/10.1590/s1806-83242011000500011.

Michejda, M., et F. J. Menolascino. 1975. « Skull Base Abnormalities in down's Syndrome ». *Mental Retardation* 13 (1): 24-26.

Miguel-Díez, Javier de, José R. Villa-Asensi, et José L. Alvarez-Sala. 2003. « Prevalence of Sleep-Disordered Breathing in Children with Down Syndrome: Polygraphic Findings in 108 Children ». *Sleep* 26 (8): 1006-9. https://doi.org/10.1093/sleep/26.8.1006.

Modéer, T., M. Barr, et G. Dahllöf. 1990. « Periodontal Disease in Children with Down's Syndrome ». *Scandinavian Journal of Dental Research* 98 (3): 228-34. https://doi.org/10.1111/j.1600-0722.1990.tb00966.x.

Møller, Anders Pape, Diego Rubolini, et Esa Lehikoinen. 2008. « Populations of Migratory Bird Species That Did Not Show a Phenological Response to Climate Change Are Declining ». *Proceedings of the National Academy of Sciences of the United States of America* 105 (42): 16195-200. https://doi.org/10.1073/pnas.0803825105.

Moraes, Mari Eli Leonelli de, Luiz Cesar de Moraes, Gustavo Nogara Dotto, Patrícia Pasquali Dotto, et Luis Roque de Araújo dos Santos. 2007. « Dental Anomalies in Patients with Down Syndrome ». *Brazilian Dental Journal* 18 (4): 346-50. https://doi.org/10.1590/s0103-64402007000400014.

Morgan, James. 2007. « Why Is Periodontal Disease More Prevalent and More Severe in People with Down Syndrome? » *Special Care in Dentistry: Official Publication of the American Association of Hospital Dentists, the Academy of Dentistry for the Handicapped, and the American Society for Geriatric Dentistry* 27 (5): 196-201. https://doi.org/10.1111/j.1754-4505.2007.tb00346.x.

Muñiz Moreno, Maria del Mar, Véronique Brault, Marie-Christine Birling, Guillaume Pavlovic, et Yann Herault. 2020. « Chapter 4 - Modeling Down Syndrome in Animals from the Early Stage to the 4.0 Models and Next ». In *Progress in Brain Research*, édité par Mara Dierssen, 251:91-143. Preclinical Research in Down Syndrome: Insights for Pathophysiology and Treatments. Elsevier. https://doi.org/10.1016/bs.pbr.2019.08.001.

Naerland, T., K. A. Bakke, S. Storvik, G. Warner, et P. Howlin. 2017. « Age and Gender-Related Differences in Emotional and Behavioural Problems and Autistic Features in Children and Adolescents with Down Syndrome: A Survey-Based Study of 674 Individuals ». *Journal of Intellectual Disability Research: JIDR* 61 (6): 594-603. https://doi.org/10.1111/jir.12342.

Ng, D. K., H. N. Hui, C. H. Chan, K. L. Kwok, P. Y. Chow, J. M. Cheung, et S. Y. Leung. 2006. « Obstructive Sleep Apnoea in Children with Down Syndrome ». *Singapore Medical Journal* 47 (9): 774-79.

Nicolaides, K. H., G. Azar, D. Byrne, C. Mansur, et K. Marks. 1992. « Fetal Nuchal Translucency: Ultrasound Screening for Chromosomal Defects in First Trimester of Pregnancy ». *BMJ (Clinical Research Ed.)* 304 (6831): 867-69. https://doi.org/10.1136/bmj.304.6831.867.

Nieminen, Pekka. 2009. « Genetic Basis of Tooth Agenesis ». *Journal of Experimental Zoology. Part B, Molecular and Developmental Evolution* 312B (4): 320-42. https://doi.org/10.1002/jez.b.21277.

Nikopensius, T., T. Annilo, T. Jagomägi, C. Gilissen, M. Kals, K. Krjutškov, R. Mägi, et al. 2013. « Non-Syndromic Tooth Agenesis Associated with a Nonsense Mutation in Ectodysplasin-A (EDA) ». *Journal of Dental Research* 92 (6): 507-11. https://doi.org/10.1177/0022034513487210.

Okubo, Tadashi, Keiko Hara, Sadahiro Azuma, et Shinji Takada. 2021. « Effect of Retinoic Acid Signaling on *Ripply3* Expression and Pharyngeal Arch Morphogenesis in Mouse Embryos ». *Developmental Dynamics* 250 (7): 1036-50. https://doi.org/10.1002/dvdy.301.

Okubo, Tadashi, Akinori Kawamura, Jun Takahashi, Hisato Yagi, Masae Morishima, Rumiko Matsuoka, et Shinji Takada. 2011. « Ripply3, a Tbx1 repressor, is required for development of the pharyngeal apparatus and its derivatives in mice ». *Development* 138 (2): 339-48. https://doi.org/10.1242/dev.054056.

Okui, M., T. Ide, K. Morita, E. Funakoshi, F. Ito, K. Ogita, Y. Yoneda, J. Kudoh, et N. Shimizu. 1999. « High-Level Expression of the Mnb/Dyrk1A Gene in Brain and Heart during Rat Early Development ». *Genomics* 62 (2): 165-71. https://doi.org/10.1006/geno.1999.5998.

Oliveira, Ana Cristina Borges, Saul Martins Paiva, Mônica Rodrigues Campos, et Dina Czeresnia. 2008. « Factors Associated with Malocclusions in Children and Adolescents with Down Syndrome ». *American Journal of Orthodontics and Dentofacial Orthopedics: Official Publication of the American Association of Orthodontists, Its Constituent Societies, and the American Board of Orthodontics* 133 (4): 489.e1-8. https://doi.org/10.1016/j.ajodo.2007.09.014.

Olson, L, Joan Richtsmeier, J Leszl, et Roger Reeves. 2004. « Olson, LE, Richtsmeier, JT, Leszl, J and Reeves, RH. A chromosome 21 critical region does not cause specific Down syndrome phenotypes. Science 306: 687-690 ». *Science (New York, N.Y.)* 306 (novembre):687-90. https://doi.org/10.1126/science.1098992.

Olson, Lisa E., Randall J. Roper, Crystal L. Sengstaken, Elizabeth A. Peterson, Veronica Aquino, Zygmunt Galdzicki, Richard Siarey, Mikhail Pletnikov, Timothy H. Moran, et Roger H. Reeves. 2007. « Trisomy for the Down syndrome 'critical region' is necessary but not sufficient for brain phenotypes of trisomic mice ». *Human Molecular Genetics* 16 (7): 774-82. https://doi.org/10.1093/hmg/ddm022.

O'Riordan, M. W., et G. F. Walker. 1978. « Dimensional and Proportional Characteristics of the Face in Down's Syndrome ». *Journal of Dentistry for the Handicapped* 4 (1): 6-9.

Orner, G. 1976. « Periodontal Disease among Children with Down's Syndrome and Their Siblings ». *Journal of Dental Research* 55 (5): 778-82. https://doi.org/10.1177/00220345760550051101.

Parsons, Trish, Timothy M. Ryan, Roger H. Reeves, et Joan T. Richtsmeier. 2007. « Microstructure of Trabecular Bone in a Mouse Model for down Syndrome ». *The Anatomical Record* 290 (4): 414-21. https://doi.org/10.1002/ar.20494.

Plaiasu, Vasilica. 2017. « Down Syndrome - Genetics and Cardiogenetics ». *Maedica* 12 (3): 208-13.

Pueschel, Siegfried M. 2001. *A Parent's Guide to Down Syndrome: Toward a Brighter Future*. Paul H. Brookes Publishing Company.

« Rare Diseases - European Commission ». 2024. 8 mars 2024. https://health.ec.europa.eu/european-reference-networks/rare-diseases_en.

Redhead, Yushi, Dorota Gibbins, Eva Lana-Elola, Sheona Watson-Scales, Lisa Dobson, Matthias Krause, Karen J. Liu, Elizabeth M. C. Fisher, Jeremy B. A. Green, et Victor L. J. Tybulewicz. 2023. « Craniofacial dysmorphology in Down syndrome is caused by increased dosage of Dyrk1a and at least three other genes ». *Development* 150 (8): dev201077. https://doi.org/10.1242/dev.201077.

Reeves, R. H., N. G. Irving, T. H. Moran, A. Wohn, C. Kitt, S. S. Sisodia, C. Schmidt, R. T. Bronson, et M. T. Davisson. 1995. « A Mouse Model for Down Syndrome Exhibits Learning and Behaviour Deficits ». *Nature Genetics* 11 (2): 177-84. https://doi.org/10.1038/ng1095-177.

Reuland-Bosma, W., W. A. van der Reijden, et A. J. van Winkelhoff. 2001. « Absence of a Specific Subgingival Microflora in Adults with Down's Syndrome ». *Journal of Clinical Periodontology* 28 (11): 1004-9. https://doi.org/10.1034/j.1600-051x.2001.281103.x.

Richtsmeier, J. T., L. L. Baxter, et R. H. Reeves. 2000. « Parallels of Craniofacial Maldevelopment in Down Syndrome and Ts65Dn Mice ». *Developmental Dynamics: An Official Publication of the American Association of Anatomists* 217 (2): 137-45. https://doi.org/10.1002/(SICI)1097-0177(200002)217:2<137::AID-DVDY1>3.0.CO;2-N.

Richtsmeier, Joan T., Ann Zumwalt, Elaine J. Carlson, Charles J. Epstein, et Roger H. Reeves. 2002. « Craniofacial Phenotypes in Segmentally Trisomic Mouse Models for Down Syndrome ». *American Journal of Medical Genetics* 107 (4): 317-24. https://doi.org/10.1002/ajmg.10175.

Roizen, Nancy J., et David Patterson. 2003. « Down's Syndrome ». *Lancet (London, England)* 361 (9365): 1281-89. https://doi.org/10.1016/S0140-6736(03)12987-X.

Roper, Randall J., et Roger H. Reeves. 2006. « Understanding the Basis for Down Syndrome Phenotypes ». *PLoS Genetics* 2 (3): e50. https://doi.org/10.1371/journal.pgen.0020050.

Rueda, N., J. Flórez, et C. Martínez-Cué. 2008. « Chronic Pentylenetetrazole but Not Donepezil Treatment Rescues Spatial Cognition in Ts65Dn Mice, a Model for Down Syndrome ». *Neuroscience Letters* 433 (1): 22-27. https://doi.org/10.1016/j.neulet.2007.12.039.

Russell, B. G., et I. Kjaer. 1995. « Tooth Agenesis in Down Syndrome ». *American Journal of Medical Genetics* 55 (4): 466-71. https://doi.org/10.1002/ajmg.1320550415.

Sago, Haruhiko, Elaine J. Carlson, Desmond J. Smith, Joshua Kilbridge, Edward M. Rubin, William C. Mobley, Charles J. Epstein, et Ting-Ting Huang. 1998. « Ts1Cje, a Partial Trisomy 16 Mouse Model for Down Syndrome, Exhibits Learning and Behavioral Abnormalities ». *Proceedings of the National Academy of Sciences* 95 (11): 6256-61. https://doi.org/10.1073/pnas.95.11.6256.

Sasaki, Y., Y. Sumi, Y. Miyazaki, T. Hamachi, et M. Nakata. 2004. « Periodontal Management of an Adolescent with Down's Syndrome--a Case Report ». *International Journal of Paediatric Dentistry* 14 (2): 127-35. https://doi.org/10.1111/j.1365-263x.2004.00529.x.

Saxén, L., S. Aula, et T. Westermarck. 1977. « Periodontal Disease Associated with Down's Syndrome: An Orthopantomographic Evaluation ». *Journal of Periodontology* 48 (6): 337-40. https://doi.org/10.1902/jop.1977.48.6.337.

Schott, Nadja, Benjamin Holfelder, et Orania Mousouli. 2014. « Motor Skill Assessment in Children with Down Syndrome: Relationship between Performance-Based and Teacher-Report Measures ». *Research in Developmental Disabilities* 35 (12): 3299-3312. https://doi.org/10.1016/j.ridd.2014.08.001.

Sforza, Chiarella, Claudia Dellavia, Claudia Dolci, Elena Donetti, et Virgilio F. Ferrario. 2005. « A Quantitative Three-Dimensional Assessment of Abnormal Variations in the Facial Soft Tissues of Individuals with Down Syndrome ». *The Cleft Palate-Craniofacial Journal: Official Publication of the American Cleft Palate-Craniofacial Association* 42 (4): 410-16. https://doi.org/10.1597/04-005.1.

Shapira, Joseph, Stella Chaushu, et Adrian Becker. 2000. « Prevalence of Tooth Transposition, Third Molar Agenesis, and Maxillary Canine Impaction in Individuals with Down Syndrome ». *The Angle Orthodontist* 70 (4): 290-96. https://doi.org/10.1043/0003-3219(2000)070<0290:POTTTM>2.0.CO;2.

Shapiro, B. L. 1975. « Amplified Developmental Instability in Down's Syndrome ». *Annals of Human Genetics* 38 (4): 429-37. https://doi.org/10.1111/j.1469-1809.1975.tb00632.x.

Shapiro, B. L., R. J. Gorlin, R. S. Redman, et H. H. Bruhl. 1967. « The Palate and Down's Syndrome ». *The New England Journal of Medicine* 276 (26): 1460-63. https://doi.org/10.1056/NEJM196706292762603.

Shimizu, Ryohei, Keiichi Ishihara, Eri Kawashita, Haruhiko Sago, Kazuhiro Yamakawa, Ken-Ichi Mizutani, et Satoshi Akiba. 2021. « Decrease in the T-Box1 Gene Expression in Embryonic Brain and Adult Hippocampus of down Syndrome Mouse Models ». *Biochemical and Biophysical Research Communications* 535 (janvier):87-92. https://doi.org/10.1016/j.bbrc.2020.12.026.

Shukla, Deepika, Deepika Bablani, Aman Chowdhry, Raveena Thapar, Puneet Gupta, et Shashwat Mishra. 2014. « Dentofacial and Cranial Changes in Down Syndrome ». *Osong Public Health and Research Perspectives* 5 (6): 339-44. https://doi.org/10.1016/j.phrp.2014.09.004.

Sixou, J. L. 2008. « Aspects bucco-dentaires de la trisomie 21 chez l'enfant ». *Archives de Pédiatrie* 15 (5): 852-54. https://doi.org/10.1016/S0929-693X(08)71939-0.

Soares, Karinn de Araújo, Regina Ferraz Mendes, Raimundo Rosendo Prado Júnior, Laylla Campelo Rosa, et Karoenna Cardoso de Araújo Costa. 2009. « Prevalência de maloclusão em portadores de Síndrome de Down na cidade de Teresina-PI ». *RGO (Porto Alegre)*, 187-91.

Starbuck, John M., Tara Dutka, Tabetha S. Ratliff, Roger H. Reeves, et Joan T. Richtsmeier. 2014. « Overlapping Trisomies for Human Chromosome 21 Orthologs Produce Similar Effects on Skull and Brain Morphology of Dp(16)1Yey and Ts65Dn Mice ». *American journal of medical genetics. Part A* 164 (8): 1981-90. https://doi.org/10.1002/ajmg.a.36594.

Startin, Carla M., Hana D'Souza, George Ball, Sarah Hamburg, Rosalyn Hithersay, Kate M. O. Hughes, Esha Massand, et al. 2020. « Health Comorbidities and Cognitive Abilities across the Lifespan in Down Syndrome ». *Journal of Neurodevelopmental Disorders* 12 (1): 4. https://doi.org/10.1186/s11689-019-9306-9.

Tang, Ying, Qiaojin Tang, Haiyan Luo, Xuehui Zhang, Qiuyu Chen, Wenying Tang, Ting Wang, Lihua Yang, et Hongwu Liao. 2022. « Research Progress in Isolation and Enrichment of Fetal Cells from Maternal Blood ». *Journal of Chemistry* 2022 (1): 7131241. https://doi.org/10.1155/2022/7131241.

Thomas, Jared R., Jonathan LaCombe, Rachel Long, Eva Lana-Elola, Sheona Watson-Scales, Joseph M. Wallace, Elizabeth M. C. Fisher, Victor L. J. Tybulewicz, et Randall J. Roper. 2020. « Interaction of sexual dimorphism and gene dosage imbalance in skeletal deficits associated with Down syndrome ». *Bone* 136 (juillet):115367. https://doi.org/10.1016/j.bone.2020.115367.

Thomas, Jared R., Kourtney Sloan, Kelsey Cave, Joseph M. Wallace, et Randall J. Roper. 2021. « Skeletal Deficits in Male and Female down Syndrome Model Mice Arise Independent of Normalized Dyrk1a Expression in Osteoblasts ». *Genes* 12 (11): 1729. https://doi.org/10.3390/genes12111729.

Vicari, Stefano. 2006. « Motor Development and Neuropsychological Patterns in Persons with Down Syndrome ». *Behavior Genetics* 36 (3): 355-64. https://doi.org/10.1007/s10519-006-9057-8.

Vicari, Stefano, Elisabeth Bates, Maria Cristina Caselli, Patrizio Pasqualetti, Chiara Gagliardi, Francesca Tonucci, et Virginia Volterra. 2004. « Neuropsychological Profile of Italians with Williams Syndrome: An Example of a Dissociation between Language and Cognition? » *Journal of the International Neuropsychological Society: JINS* 10 (6): 862-76. https://doi.org/10.1017/s1355617704106073.

Vicente, Ascensión, Luis-Alberto Bravo-González, Ana López-Romero, Clara Serna Muñoz, et Julio Sánchez-Meca. 2020. « Craniofacial Morphology in down Syndrome: A Systematic Review and Meta-Analysis ». *Scientific Reports* 10 (1): 19895. https://doi.org/10.1038/s41598-020-76984-5.

Watson-Scales, Sheona. 2018. « Analysis of Motor Dysfunction in Down Syndrome Reveals Motor Neuron Degeneration. », mai.

Wilson, M. D. 1994. « Special Considerations ... for the Dental Professional for Patients with Down's Syndrome ». *Journal - Oklahoma Dental Association* 84 (3): 24-26.

Wiseman, Frances K., Tamara Al-Janabi, John Hardy, Annette Karmiloff-Smith, Dean Nizetic, Victor L. J. Tybulewicz, Elizabeth M. C. Fisher, et André Strydom. 2015. « A Genetic Cause

of Alzheimer Disease: Mechanistic Insights from Down Syndrome ». *Nature Reviews. Neuroscience* 16 (9): 564-74. https://doi.org/10.1038/nrn3983.

Yoshihara, Toshihiro, Takanobu Morinushi, Sachiko Kinjyo, et Youichi Yamasaki. 2005. « Effect of Periodic Preventive Care on the Progression of Periodontal Disease in Young Adults with Down's Syndrome ». *Journal of Clinical Periodontology* 32 (6): 556-60. https://doi.org/10.1111/j.1600-051X.2005.00712.x.

Yu, Tao, Zhongyou Li, Zhengping Jia, Steven J. Clapcote, Chunhong Liu, Shaomin Li, Suhail Asrar, et al. 2010. « A Mouse Model of Down Syndrome Trisomic for All Human Chromosome 21 Syntenic Regions ». *Human Molecular Genetics* 19 (14): 2780-91. https://doi.org/10.1093/hmg/ddq179.

Zhu, Ping Jun, Sanjeev Khatiwada, Ya Cui, Lucas C. Reineke, Sean W. Dooling, Jean J. Kim, Wei Li, Peter Walter, et Mauro Costa-Mattioli. 2019. « Activation of the ISR Mediates the Behavioral and Neurophysiological Abnormalities in Down Syndrome ». *Science (New York, N.Y.)* 366 (6467): 843-49. https://doi.org/10.1126/science.aaw5185.

Université de Strasbourg

José Tomás AHUMADA SAAVEDRA

École Doctorale des Sciences de la Vie et de la Santé STRASBOURG

Analyse crâniofaciale des modèles de rongeurs du syndrome de Down

Résumé

Les altérations les plus fréquentes et les plus caractéristiques du syndrome de Down (SD) sont les troubles de l'apprentissage et la dysmorphie crâniofaciale (CF). Le phénotype CF comprend des dimensions réduites de la tête, une brachycéphalie, une région orbitale médio-latérale réduite, une largeur bizygomatique réduite, un petit maxillaire, une petite mandibule et une variabilité individuelle accrue. Jusqu'à présent, les mécanismes cellulaires et moléculaires qui sous-tendent ce phénotype CF restent inconnus. Cette thèse, utilisant un nouveau panel de modèles de rats et de souris, a proposé de nouveaux gènes candidats pour le phénotype SD-CF. Nous avons confirmé le rôle de *Dyrk1a* dans la brachycéphalie du neurocrâne et identifié le surdosage du facteur de transcription *Ripply3* pour le raccourcissement de la face médiane par la sous-régulation de *Tbx1*, un autre facteur de transcription impliqué dans des phénotypes similaires trouvés dans le syndrome de DiGeorge. Nous avons défini de nouveaux gènes sensibles au dosage responsables des malformations du SD-CF, et de nouveaux modèles ont été proposés pour sauver le phénotype SD-CF. Ces nouvelles connaissances pourraient également permettre de mieux comprendre les phénotypes cérébraux et cardiovasculaires spécifiques observés chez les mutants *Tbx1* et les modèles de DS.

Mots-clés : Trisomie 21, syndrome de Down, crâniofacial SD dysmorphie, modèles murins du SD, gènes sensibles au dosage, *Dyrk1a*, *Ripply3*, *Tbx1*, Syndrome de DiGeorge.

Abstract

The most frequent and distinctive alterations found in Down syndrome (DS) are learning disability and craniofacial (CF) dysmorphism. The CF phenotype includes reduced head dimensions, brachycephaly, reduced mediolateral orbital region, reduced bizygomatic breadth, small maxilla, small mandible, and increased individual variability. Until now, the cellular and molecular mechanisms underlying this CF phenotype remain unknown. This thesis, using a new panel of rats and mice models proposed new candidate genes for the DS-CF phenotype. We confirmed the role of *Dyrk1a* in neurocranium brachycephaly and identified the overdosage of the transcription factor *Ripply3* for midface shortening through the downregulation of *Tbx1*, another transcription factor involved in similar phenotypes was found in Di George Syndrome. We defined new dosage-sensitive genes responsible for DS-CF malformations, and new models were proposed to rescue the DS-CF phenotype. This new knowledge may also lead to insights for specific brain and cardiovascular phenotypes observed in *Tbx1* mutants and DS models.

Keywords: Trisomy 21, Down syndrome, DS craniofacial dysmorphism, DS rodent models, dosage-sensitive genes, *Dyrk1a*, *Ripply3*, *Tbx1*, DiGeorge syndrome.